Finite Element Prediction of Deformation Mechanics in Incremental Forming Processes

by

Khamis Essa Ali Essa

A thesis submitted to
the University of Birmingham
for the degree of

DOCTOR OF PHILOSOPHY

School of Mechanical Engineering
The University of Birmingham
Edgbaston, B15 2TT, UK

JUNE 2011

ABSTRACT

Sheet metal forming that incorporates an incremental approach has demonstrated a great potential to form a wide range of industrial products. This thesis deals with two examples of incremental metal forming; one a very traditional process, conventional spinning, and the other a more modern development, single point incremental forming (SPIF). The thesis presents new insights into gaps in the knowledge of these two processes through numerical modelling of their deformation mechanics and geometrical accuracy.

The deformation mechanics of conventional spinning is investigated by constructing finite element (FE) models of a cylindrical cup using both single and dual roller passes. In dual-pass conventional spinning, a variety of roller-traces is applied to provide a better understanding of the stress and strain distributions that develop in subsequent passes. A design of experiments (DOE) technique is used to generate an experimental plan based on all the relevant process parameters, followed by an analysis of variance (ANOVA) approach which is then used to determine the most critical parameters. A second DOE based only on the latter is used to generate another experimental plan to study their effect on the final product quality and determine the optimal setting of these parameters that leads to a defect-free product. The results indicated that the deformation mechanics in dual-pass spinning is more complex, and the area in which most of the plastic deformation is taking place changes during the subsequent passes. The use of the statistical and optimisation methods results in an additional improvement in the final product quality by more than 22%.

The deformation mechanics of SPIF is investigated by constructing a novel dual-level finite element model of the forming of a truncated cone. The first-level FE model is validated against experimental data and is used to explore the principal characteristics of the deformation, normal strains and the final product geometries. The second level FE model is used to investigate the deformation modes through the sheet thickness. A Marciniak-Kuczynski model is used to show the effect of the through-thickness shear strain on the formability. DOE and ANOVA techniques are used to investigate the influence of the different process parameters on the predicted through-thickness shear. Simple strategies that include adding a backing plate, using a kinematic supporting tool and tool path modification are applied to reduce the geometrical errors without affecting the process flexibility. The results of the second-level FE model indicated that shear, both perpendicular to and parallel to, the tool plane is an important component in the deformation mechanism in SPIF and that it has a significant influence on increasing the necking limit and hence improving formability. The applied strategies result in a significant reduction in the geometrical errors, enhancing the possibility of using the process in critical applications.

DEDICATION

To the soul of my grandfather and grandmother,

my parents,

my beloved wife and my lovely children:

Nour Eldeen, Nouraan and Nizar

ACKNOWLEDGMENTS

No words can adequately express my great gratitude to **Dr. Peter Hartley** for his encouragement, assistance, inspiration, guidance on the all aspects and interest shown in the work. He never declined from offering help. It is the greatest honour to work under his supervision. I would like also to thank **Dr. Robert Cripps** for his co-supervision.

I am deeply indebted to **Dr. Julian Allwood** and **Omer Music**, Department of Engineering Cambridge University, for providing the truncated cone test sample and the experimental force data. I am very grateful for their valuable ideas and comments in developing the FE model described in this thesis.

I would like to thank **Dr. Philip Eyckens**, Department MTM, Faculty of Engineering, Katholieke Universiteit Leuven, Belgium, for his support with the development and running of the Marciniak–Kuczynski model.

I gratefully acknowledge the UK ORSAS scheme and the School of Mechanical Engineering for providing a studentship which financially supported this research.

I would like also to express my deep and special appreciation to technicians in our group, particularly **Mr. Alan Saywell** and **Mr. Andrew Loat** for their sincere help throughout my experimental work. Thanks to all staff members of the School of Mechanical Engineering, University of Birmingham who have supported me and to my colleagues who have offered all the help I needed.

At last, but not least, I would like to express my sincere thanks to **My Parents**, for their support, cooperation and their understanding all along the road. Deepest special thanks for **My Wife**, for her endurance, serenity, love and support in every possible way during my PhD study.

PUBLICATIONS

The material in this thesis has been published as following;

Journal Publications

Essa, K. and Hartley, P., 2011. *An evaluation of shear deformation mechanisms in single point incremental forming using a dual-level finite-element model.* CIRP Journal of Manufacturing Science and Technology, *under review*.

Essa, K. and Hartley, P., 2010. Investigation on the effects of process parameters on the through-thickness shear strain in single point incremental forming using dual level FE modelling and statistical analysis. Computer Methods in Materials Science CMMS. 10(4): pp. 1-11.

Essa, K. and Hartley, P., 2010. An assessment of various process strategies for improving precision in single point incremental forming. International Journal of Material Forming, DOI 10.1007/s12289-010-1004-9.

Essa, K. and Hartley, P., 2010. Optimization of conventional spinning process parameters by means of numerical simulation and statistical analysis. Proceedings of the Institution of Mechanical Engineers, Part B: Journal of Engineering Manufacture. 224(11): pp. 1691-1705.

Essa, K. and Hartley, P., 2009. Numerical simulation of single and dual pass conventional spinning processes. International Journal of Material Forming. 2(4): pp. 271-281.

Essa, K. and Hartley, P., 2009. Numerical investigation on the effect of roller-trace in dual pass cup spinning. Journal for Technology of Plasticity. 34(2009): pp. 15-25.

Conference Publications

Essa, K., 2009. Investigation on the forward tube spinning process by numerical simulation. BlueBEAR user forum, University of Birmingham, UK.

TABLE OF CONTENTS

LIST OF FIGURES

LIST OF TABLES

LIST OF ABBREVIATIONS

AISF	Asymmetric Incremental Sheet Forming
ANOVA	Analysis of Variance
CAD/CAM	Computer Aided Design/ Computer Aided Manufacturing
CMMs	Coordinate Measuring Machine
CNC	Computer Numerically Controlled
FE	Finite Element
FLC	Forming Limit Curve
FLD	Forming Limit Diagram
ISF	Incremental Sheet Forming
PVC	Polyvinyl chloride
QC	Quality Characteristic
SPIF	Single Point Incremental Forming
TPIF	Two Point Incremental Forming

CHAPTER 1:

INTRODUCTION

1.1 Background

Although there are many types of manufacturing processes, the common target is to produce semi finished products such as sheets, plates and rods or specific finished products with high quality and low cost. Metal forming is a manufacturing process in which a metal workpiece or a sheet blank is deformed plastically by dies or tools, often without subsequent extensive metal removal. It has the capability to produce parts that have superior mechanical properties, an excellent surface finish and dimensional accuracy with minimum material waste. Therefore, it has a very important position among manufacturing processes.

In many forming processes, such as forging, the entire workpiece may be deformed plastically, while in others the plastic region is localised in a smaller region of the material. In processes such as forward extrusion and plate or bar rolling, a local volume of plastically deforming material is established between the forming dies or rolls. While the material continuously moves the location between the tools that imparts plastic deformation is fixed, and these are referred to as steady-state processes. Alternatively, non-steady state processes are those in which both the tool location and the local region of plastic deformation are changing throughout the process. Processes such as this in sheet forming are usually referred to as incremental sheet forming (ISF) processes, and are quite common in the metal forming industry. These processes have a common feature in which at any time, there is a small localised deformation, and that region of

local deformation moves over the entire workpiece during the course of the process. The incremental nature that results from plastically deforming a small volume of the workpiece reduces the peak power required and consequently the forming forces are reduced, which allows a smaller machine frame. In addition, the life of the forming tools is usually much longer compared with that in conventional processes.

As a result of advances in manufacturing technology, particularly the development of computer numerically controlled (CNC) machinery, and a growing interest in customisation, modern incremental forming techniques have been developed that have high flexibility and require low capital and running costs. In the late 1980's, customer demands for small batch production over an increasing range of products enhanced the importance of greater flexibility in manufacturing processes. More recently, new techniques have been developed called asymmetric incremental sheet forming (AISF), which are capable of meeting these requirements. AISF generally refers to a die-less forming process which can be used to form complex shapes using simple tools. The process has received increasing attention due to its high flexibility and low cost. In AISF, a simple tool moves over the sheet surface and produces highly localised plastic deformation. Thus, a variety of complex 3-D shapes can be formed through the tool movement along correctly designed and controlled paths without using a dedicated die.

1.2 Scope and Aim of the Thesis

The aim of this thesis is to investigate gaps that exist in the knowledge of some incremental forming processes in order to obtain information that enables better control over process parameters to be obtained and accordingly, improve the quality of products

produced by these processes. This thesis will use a numerical modelling approach to examine the deformation mechanisms and process characteristics of two examples of incremental metal forming, one a very traditional process and the other a more modern development. Conventional spinning is used as an example of a traditional incremental sheet forming process. Despite its long history the operation of this process was until recently perceived as a 'black art', but now a more scientific approach is taken. The deformation mechanism for conventional spinning is not well understood because of its complexity. Conventional spinning will be numerically simulated through finite element (FE) modelling and the model validated against published experimental data. The objective is to determine the forces and strains generated during the deformation process and to investigate how they are affected by various process parameters. Additionally, to predict the process behaviour using subsequent roller passes with different roller geometries and a variety of roller-traces. To complement the numerical analysis, statistical tools will be engaged with the FE model to obtain the optimum combination of the working parameters that allow the production of a defect-free product. This will help to provide a clear background on the deformation behaviour of the process and to improve the final product quality.

Single point incremental forming (SPIF) is the more modern example of an incremental sheet forming process. The process is the subject of much current research and development, although some research on the analysis of the deformation mechanism is contradictory. Some investigations suggest that stretching and thinning are the only dominant modes of deformation, while other investigations indicate that high values of transverse shear are present through the sheet thickness. Since experimental observations of through-thickness phenomena are extremely difficult, FE modelling of

the SPIF processes is an essential tool. FE modelling, however, must be undertaken very carefully with a clear understanding of the limitations of the models. For example, models with one or two elements in the thickness direction will give good predictions of geometry but not of through-thickness shear. In order to provide clear information about through-thickness shear strains, a large number of elements through the thickness must be used. However, the large number of elements will result in unrealistic computational times. This problem can be treated by using a multi-level FE modelling technique. In this thesis, a dual-level approach will be developed in which a more detailed description of the deformation mechanics can be provided. The full, first-level FE model is validated against experimental data and used to explore the principal characteristics of the deformation, normal strains and the final product geometry. The second-level FE model is used to show the significance of assigning a sufficient number of elements on the shear deformation. A Marciniak-Kuczynski (MK) model is then used to show the effect of the through-thickness shear strain on the necking limit. The dual-level FE model will also be used in conjunction with a statistical approach to show the effect of different process parameters on the through-thickness shear strain components. Some strategies to improve the process precision will be investigated using the new FE model. The objective is to provide a more comprehensive study on shear effects in the SPIF process and hence improve the process behaviour. With the motivation of improving the geometrical accuracy, the possibility of using the process in critical application seems to be promising.

In general, the aim of the thesis is achieved through satisfying the following objectives:

- Examine the conventional spinning process by FE modelling and optimise the process parameters for a particular product design.

- Provide a clear understanding on the dominant modes of deformation in SPIF and analyse the influence of process parameters on the through-thickness shear strain.
- Investigate some process strategies through FE modelling to improve the level of accuracy of the SPIF process.

1.3 Structure of the Thesis

This thesis comprises eight chapters. Chapter 2 deals with brief definitions and a literature review of research conducted on incremental forming processes. Construction of the finite element models for conventional spinning is given in Chapter 3. An optimisation of conventional spinning by means of finite element modelling and statistical analysis is detailed in Chapter 4. Chapter 5 illustrates the procedure of constructing the dual-level-finite element model for SPIF in order to explore the through-thickness shear strains and its experimental validation. An investigation on the effect of process parameters on the through-thickness shear strains is explained in Chapter 6. Strategies to improve precision in single point incremental forming processes are discussed in Chapter 7. The conclusions from this work and recommendations for future work are given in Chapter 8.

CHAPTER 2:

LITERATURE REVIEW

2.1 Introduction

To provide a basis for the research presented in this thesis, this chapter gives a review of previous work carried out in two specific areas; metal spinning and asymmetric incremental sheet forming. A wide body of previous research on these two forming methods will be listed under the following sections; description, classification/configurations, advantages and applications, equipment, implementation procedure, methods of investigation and results of analyses. The chapter concludes with a brief summary to highlight some of the gaps in the knowledge identified in this review.

2.2 Sheet Metal Forming Processes with an Incremental Approach

Incremental sheet forming processes (ISF) is a general term used to define many processes including spinning, drawing, stretching, rolling, shot peen forming, laser forming and asymmetric incremental sheet forming. These processes have a common feature in which at any time, there is a small localised deformation (small compared to the size of the workpiece) taking place. The process usually results in the entire workpiece being deformed plastically, either by moving the workpiece over or through the forming tools, or, more often, moving the tools over the workpiece. The incremental nature that results from plastically deforming only a small volume of the workpiece reduces the required power and forming loads, which allows a smaller machine frame.

Sheet metal forming processes involving an incremental approach can be classified in terms of the applied technology and final product complexity into two categories; traditional methods (such as metal spinning, deep drawing, stretching and rolling) and modern developments (such as laser forming and asymmetric incremental sheet forming AISF). The traditional processes are usually limited to simple or symmetric products and are not capable of producing complex geometries. In the modern techniques, CAD/CAM applications are often used and thus, asymmetric products with a more complex geometry can be produced. Metal spinning with other traditional methods are considered to be the basis for the development of recent modern incremental sheet forming. As a result, it is important to clearly understand the mechanism of deformation in metal spinning in order to understand these modern methods. However, establishing the importance of spinning process parameters and improving product quality is still a major area of investigation and remains a demanding task. The following is an overview of the two incremental sheet forming technologies, one of the classical methods which is spinning and the other from the more recently developed methods, which is AISF.

2.3 Metal Spinning

Research in metal spinning has been mapped in five previous reviews over more than 30 years. In 1979 Slater [1] completed the first review of metal spinning. This review covered experimental and analytical models used to predict forming forces, wrinkling, forming limits and surface finish. In 1985, Lange [2] reviewed the German literature and this covered the principles, tools and spinning machines in more detail. In 2003, Hagan and Jeswiet [3] described the principles of conventional and shear spinning as the basis for a study of AISF processes. Also in 2003, Wong et al [4] completed a

review of conventional, shear and tube spinning processes. This gave a detailed history of their evolution and key results for rotary sheet forming processes. The most recent and extensive review was written by Music and Allwood [5] in 2009. This review covered the configurations and deformation mechanics of conventional spinning and shear forming.

Metal spinning refers to a group of some of the oldest forming processes that allow production of hollow, axially symmetric sheet metal components. The basic technique of spinning, consists of clamping a sheet metal blank against a mandrel on a spinning lathe, and gradually forming the blank onto the mandrel surface by a roller, either in a single pass or in a series of passes as shown in Figure 2.1

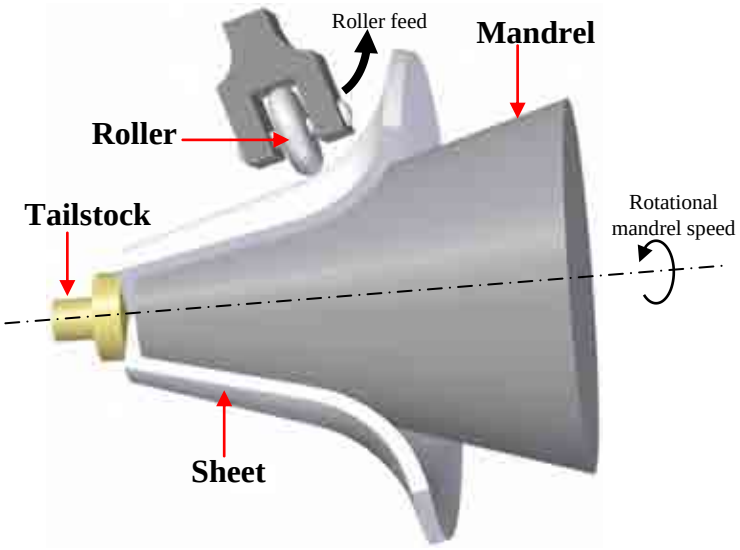

Figure 2.1: Common configuration of metal spinning.

History records evidence that metal spinning was known to ancient Egyptians where the process emerged from the art of potting clay using a potter wheel. It then travelled to China in the 10th century, then to England in the 14th century and eventually to the USA

in the 19th century [4]. Results of the craft appear in the histories of most countries since that time. At the beginning of the 20th century, spinning was considered an art rather than science, as it required operators with considerable experience and skill. At that time, spinning was employed mainly to produce domestic products such as cooking pots where the dimensional accuracy was not critical. Later in the mid 20th century, spun components of higher dimensional accuracy were required. This led to an increase in the scientific research in this area. The attention of research in sheet metal spinning has increased over recent years due to an increase the demand for parts in various industries, especially those associated with transport where new trends require parts with very high strength to weight ratios and low cost. Spinning processes are very efficient in producing such characteristics in addition to the flexibility that exists in the production and relative low cost of the forming tools.

2.3.1 General classification of metal spinning

Metal spinning is generally classified into three groups; conventional spinning, shear spinning and tube spinning. In conventional and shear spinning, the starting workpiece is a circular blank sheet while, in tube spinning the starting workpiece is a cup that is originally deformed by either conventional spinning or deep drawing. The main differences between conventional spinning and shear spinning are in the wall thickness and the diameter of the final product as shown in Figure 2.2. The wall thickness in conventional spinning remains nearly constant throughout the process, so the final wall thickness of the formed part is equal to the thickness of the blank. In contrast, during shear spinning, the wall thickness is reduced and dictated by the angle between the wall of the component and the axis of rotation. In shear spinning, the final diameter is equal

to the diameter of the blank while in conventional spinning the final diameter is determined by the mandrel profile. In tube spinning, the final thickness is defined by the increase in length of the workpiece. In conventional and tube spinning, parts can be formed in a single step or in a number of steps, while in shear spinning, forming is usually done in a single step.

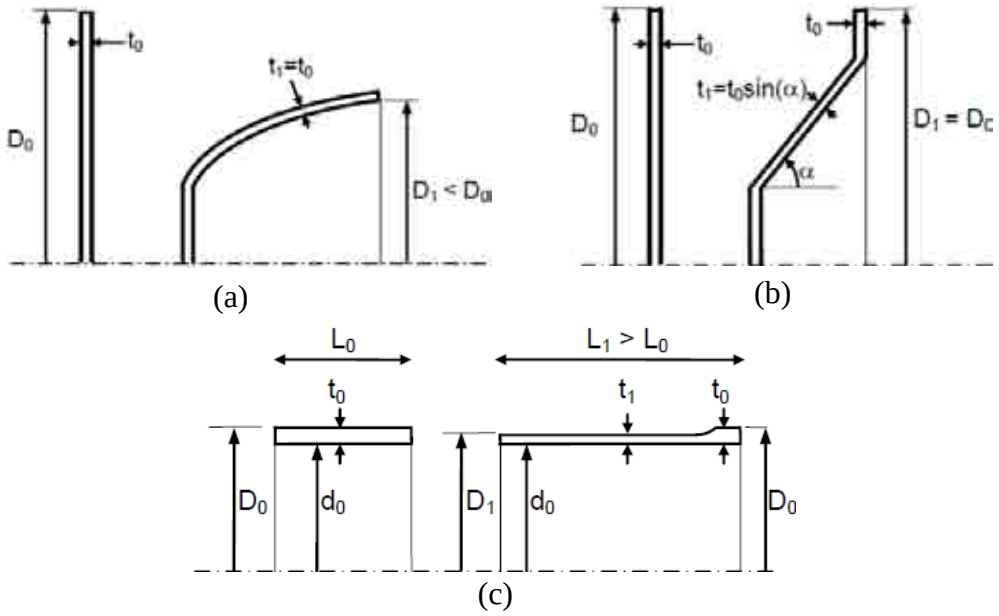

Figure 2.2: Classification of metal spinning: blank at left and product at right [5], (a) conventional spinning, (b) shear spinning, (c) tube spinning.

The classification of spinning into conventional spinning, shear spinning and tube spinning is widely accepted. However, the only formal standard classification is that of the German DIN Standard 8582. This classification based on the internal stresses generated in the material during the forming operation which cause material yielding. These stresses occur either as a combination of tensile/compression or solely as compression. The type of stress generated is determined by the technique applied to convert the blank to the required finished part. Based on the DIN standard 8582, in

conventional spinning the material is deformed plastically by a combination of tensile and compressive stresses. In shear spinning, the material is deformed plastically by compressive stresses only [4, 5]. This classification was followed by Lange [2] and Kalpakjian [6]. In contrast to the similarity between conventional and shear spinning, the mechanics of tube spinning are quite different, as pointed out by Gur and Tirosh [7] who treat tube spinning as a combination of extrusion and rolling.

2.3.2 Advantages and applications

Conventional spinning is an effective method for producing thin-wall axisymmetric parts and has the capability to produce parts which cannot be manufactured by competing processes such as deep drawing. The process has a number of advantages which include low tooling cost, small localised deformation under the roller that leads to low forces and energy consumption, high flexibility, capability for net shape forming, high surface quality of the final product and improvement of mechanical properties by increasing the strain hardening of the material as a cold working process [4, 5, 8]. The dimensional accuracy achieved by conventional spinning means that many components do not need further operations. Sheet metal spinning has a variety of applications including parts for the automotive and aerospace industries, musical instruments, art objects and kitchenware. Some typical examples of these parts are aircraft parts, radar reflectors, tank shells, satellite cones, tank heads and bottoms, barrel heads, funnels, reflectors, wheel rims, gas bottles, centrifuges, lighting reflectors, brake cylinders, spools, stainless steel sinks, kettles, and home utensils. The products produced by spinning have a diameter ranging from 0.003 to 10m and thicknesses ranging from 0.4 to 25mm [9]. Figure 2.3 shows typical examples for metal spinning products.

Figure 2.3: A wide range of products can be produced by conventional spinning [10-12].

2.3.3 Equipment for spinning processes

The main tools in spinning processes are the roller, mandrel, and tailstock. Figure 2.4 illustrates some examples of roller design. Spinning rollers are normally made from steel, the shape of the roller varying according to the application. Typical modern roller geometries are shown in Figure 2.4. Nowadays, the material used is a tool steel with 12% chrome content and a hardness of 60 to 62 HRC, particularly suited to resist the heat generated in the process [13]. No loss of hardness is experienced, even at temperatures up to 500^0C which can be generated by friction when "cold" forming.

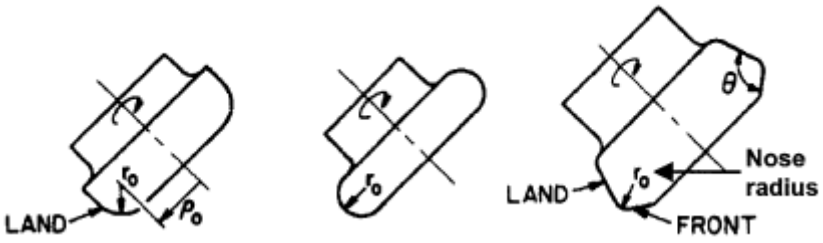

Figure 2.4: Some examples of roller design [4].

The mandrel refers to the rigid axisymmetric tool with the profile of the final component. It is used to support the sheet during deformation. Due to the high compressive load beneath the roller, the surface finish of the internal surface depends on the surface of the mandrel. The tailstock refers to the circular disk clamping the sheet to the mandrel. The tailstock may be flat or curved to fit over the mandrel and further support the sheet while it is being formed.

Industrial spinning processes became established in the 1950s' with the development of efficient spinning machines. Prior to that, manual spinning was the rule. Early metal spinners would move the spinning tool purely by hand. The spinner could produce whatever movements required in order to apply his knowledge to the behaviour of the metal. The only limitation was the available power of spinning machines. The first high-performance machines for mass production worked with copying controls. Directly dependent on a copying template, however, the range of possible movements was restricted. Due to the complexity of the spinning operation, developments in control systems over the last ten years have been established [13]. With the aid of these latest control systems, the potential to work the widest possible range of material can be exploited to the full. Only in this way has it become possible to produce various component configurations and to significantly expand the range of parts which can be formed. Tool magazines and tool changers of various designs reduce changeover and production times. The load sensors themselves cannot balance out load fluctuations inherent to the process. Full auto cycling is achieved with the addition of automatic feeders. Figure 2.5 shows an example of the actual spinning process.

blank ready to spin Spinning finished aluminium cover

Figure 2.5: A spinning process [14].

2.3.4 Implementation procedure

In spinning practice, a blank sheet is clamped between a rotating mandrel and supporting holder/tailstock and is gradually shaped over this rotating mandrel with a roller that produces a localised pressure. In general, the roller moves along both axial and radial directions of the mandrel. The roller could be used for single or for multiple passes until the sheet attains the geometry of the mandrel. Figure 2.6 shows the principle of conventional spinning. A disk blank (1) is concentrically clamped against the mandrel (3) by the tailstock-mounted pressure pad (4). Via the main spindle (7) this then starts to rotate. The blank is driven by frictional contact. The spinning roller (2) is powered in planes X-Z by a 2-axis compound slide (8) and progressively forms the blank until the metal lies on the mandrel. For conventional spinning, one or more roller passes are made along the contour of the workpiece to lay it tightly on the mandrel to obtain the final product (10). In the same set-up, it is possible to carry out a variety of secondary operations, for example, the edge of the part may be trimmed (6). Figure 2.7 shows typical geometries that can be obtained by conventional spinning.

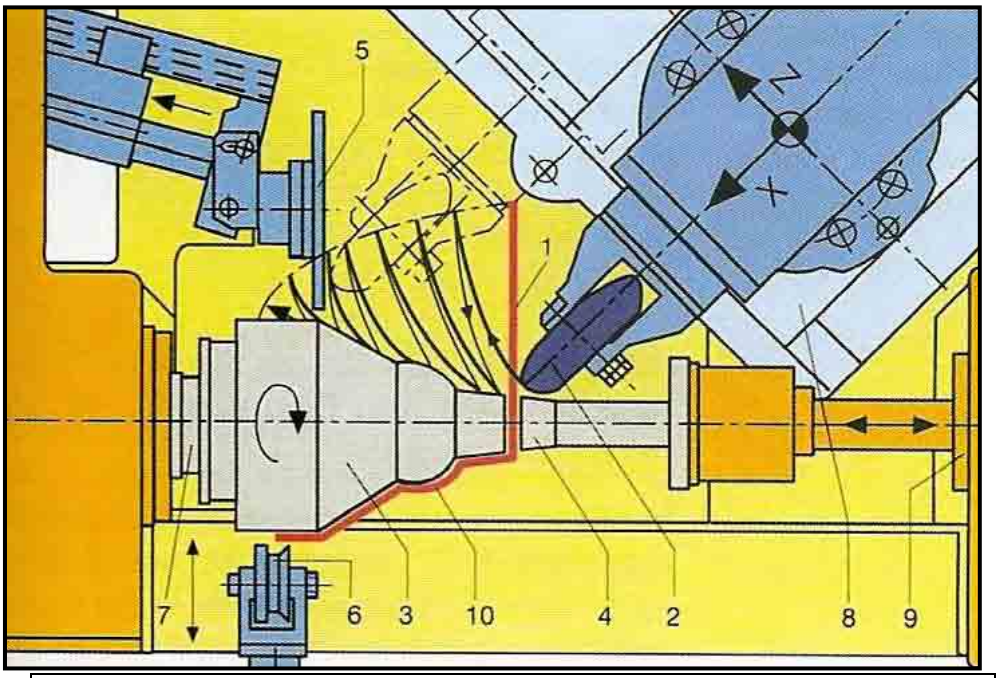

1 disc blank	4 tailstock pad	7 main spindle
2 roller	5 blank support unit	8 cross slide
3 mandrel	6 trimming unit	9 tail stock
		10 spun part

Figure 2.6: Conventional spinning process and elements involved [13].

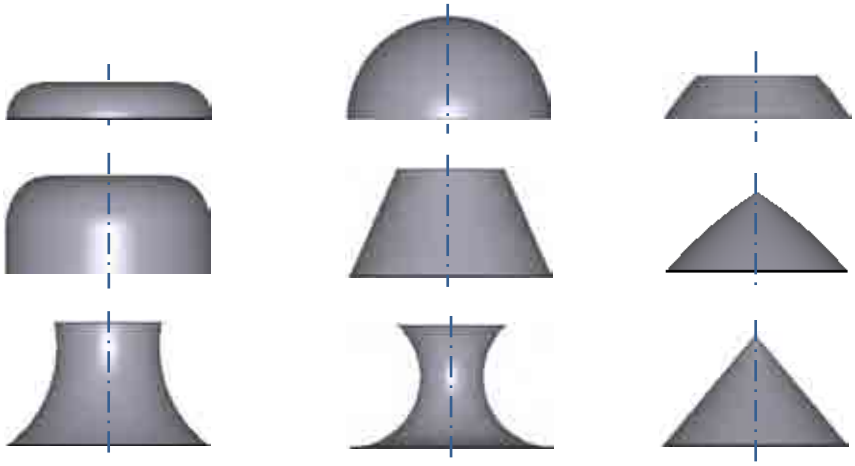

Figure 2.7: Examples of feasible geometries that can be produced by conventional and shear spinning.

2.3.5 Investigative approaches in spinning

Knowledge about the mechanics of conventional spinning has been developed by many systematic investigations of the process using both experimental and theoretical techniques. The theoretical techniques include analytical and numerical methods. In the present investigation, the finite element method will be used as the main investigation tool. This section presents a survey of all three techniques although with more detail for the numerical methods.

2.3.5.1 Experimental approaches

Experimental techniques such as the plugged hole method, grid line method and surface etching have been used to study the deformation mechanism and strain evolution in spinning. These approaches are illustrated in Figure 2.8. The plugged hole technique consists of drilling holes in a spiral pattern in the sheet blank and filling them with another material (see Figure 2.8a). After the sheet is spun, the holes are revealed by cutting the sheet, and examined to construct a three-dimensional picture of sheet deformation. The technique was proposed by Avitzur and Yang [15]. The grid line technique is slightly different in which the sheet blank is cut in two, grid lines are inscribed on the exposed surfaces and the two parts are soldered together (see Figure 2.8b). After spinning the sheet, the two parts are separated by melting the solder and the two surfaces cleaned to study deformation through the sheet thickness. This method was proposed by Kalpakcioglu [16]. The third approach is the surface etching technique in which the strains are measured by etching a pattern of circles of known size on the sheet surface before spinning (see Figure 2.8c). The deformed circles are measured after

spinning with an optical projector to determine surface strains. This technique was used by Quigley and Monaghan [17].

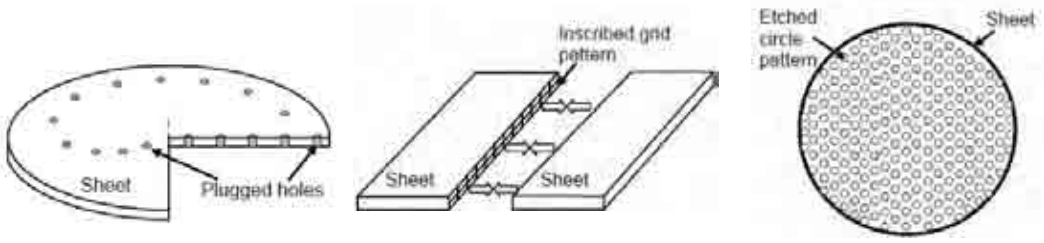

(a) (b) (c)

Figure 2.8: Experimental methods of studying deformation and strains in spinning [5], (a) Plugged holes method, (b) Grid line method, (c) Surface etching method.

2.3.5.2 Analytical approaches

Many analytical approaches such as the ideal work method and the upper bound method have been used to predict the forming forces and failure. The first ideal work model was developed by Avitzur and Yang in 1960 [15] to calculate the circumferential force in shear spinning by assuming that the deformation is pure shear. More recently, Kim et al [18] developed another analytical model assuming the deformation is a combination of bending and shear to calculate the tangential force. This model was modified by Kim et al [19] to include the prediction of axial and radial force components. The upper bound method was first used by Joorabchian and Slater in 1979 [20]. They assumed both axisymmetric deformation and plane strain deformation to make an estimate of the upper bound of a dimensionless tangential force in spinning. Despite this large number of models in shear spinning, only one analytical model for conventional spinning was developed by Quigley and Monaghan [17] to estimate the thickness, radial and

circumferential strain distributions. The results of this model showed that for conventional spinning the strains involved are much less than for shear forming.

2.3.5.3 Numerical approaches

Experimental and analytical techniques are useful tools allowing for the study of a number of parameters in spinning. However, for a more detailed analysis of the process, numerical methods such as finite element modelling are required. These methods can in principle enable the prediction of all the process deformation related parameters, thus enabling a prediction of product quality, which provides a means of designing the process and the operating schedule. The incremental nature of spinning with a small deformation zone and changing contact conditions requires numerical models with fine meshes and a large number of time increments. Thus numerical methods applied to spinning are plagued by having long solution times. A portion of the research in this area has therefore concentrated on reducing computational time by introducing simplifying assumptions.

The first numerical model of spinning was developed by Alberti et al [21] in 1989, who used the simplifying assumption of axisymmetric deformation, in which the roller is modelled as a ring of growing diameter. This assumption is based on the fact that the ratio of roller feed to sheet rotational speed, i.e. feed ratio is low in spinning. As this was the first publication on numerical modelling of spinning, its importance lies in the fact that it demonstrated the ability of a numerical model to predict geometry, strains and loads in spinning, although no validation of these values is provided by the authors. This technique is rarely used, although a very similar approach with an axisymmetric

elasto-plastic model was developed by Liu et al in 2002 [22] to study the effect of various roller-traces on strains and stresses in conventional spinning.

Three-dimensional numerical models of spinning aim to give increased accuracy, but require significantly longer computational times. Nine three-dimensional models have been identified in the literature. The differences between these models come from material models (rigid plastic and elastic plastic) and solution algorithms (implicit and explicit). There are three implicit models in the literature. The first implicit model of conventional spinning is that of Quigley and Monaghan in 2001 [23] who used an implicit solution algorithm with an elastic-plastic material model. In this model, roller friction is taken as zero, to represent the low rolling friction coefficient between the sheet and the roller. They have attempted both adaptive meshing and parallel processing to reduce the computational time. In their adaptive meshing scheme, the finite element mesh is automatically refined as it comes into contact with the roller, while the rest of the mesh is unrefined to reduce the total number of elements. They also applied parallel processing without remeshing and report that using 4 CPUs reduces the solution time by a factor of over 4, and also state that the network connection capacity severely limits the number of CPUs that can be used for parallel processing (see Figure 2.9). They further stress the importance of accurate modelling of the relative clearance (the distance between the roller and mandrel, as a percentage of the initial sheet thickness). They demonstrate that a small change in this parameter has a profound effect on the stresses developed under the roller. Quigley and Monaghan [24] further investigated the effect of parallel processing together with multi-domain FE modelling with remeshing to reduce the simulation time and reported that the modelling of multi-pass spinning processes within a feasible simulation time is possible.

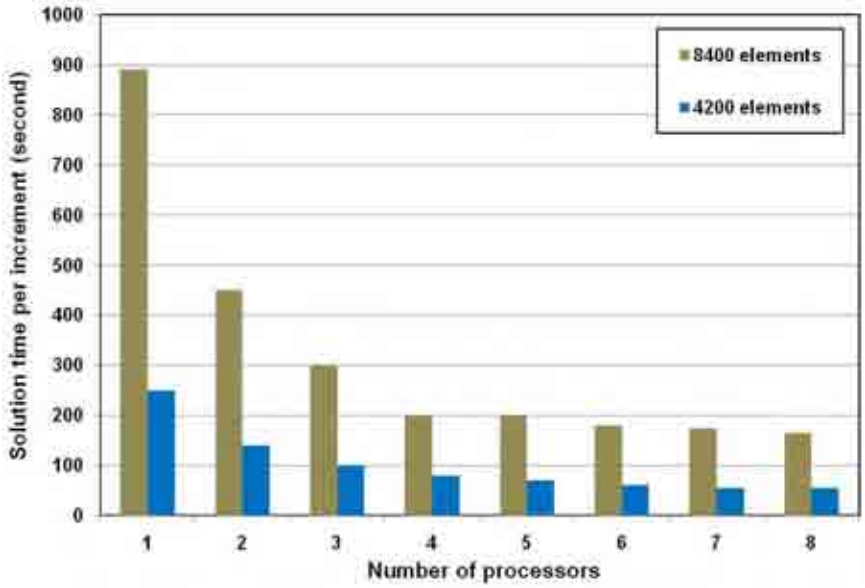

Figure 2.9: Effect of increasing the number of processors on the simulation time [23].

The second implicit model, for laser-assisted hot shear spinning, was established by Klocke and Wehrmeister in 2003 [25] to optimise the location of the laser and the heated zone. Their analysis was decoupled, with the thermal and mechanical models analysed separately in ABAQUS and DEFORM, respectively. An elastic-plastic implicit model was later applied to hot shear spinning by Lu et al in 2006 [26] to study flange bending in shear spinning.

Explicit models of forming process are generally faster than implicit formulations and therefore, they are recommended for modelling spinning (because of the simple tool path compared with other IF processes) as reported by Alberti et al [27]. Six explicit, elastic-plastic FE models for the first forming pass were developed by Kleiner et al in 2002 [28] and Klimmek et al in 2003 [29] to study stresses and wrinkling in conventional spinning. Based on experimental observations, they reported that stresses, and eventually, failure by wrinkling relate to both static and dynamic effects so spinning

should be modelled with explicit methods to take account of the latter. The model proposed by Kleiner et al [28] was developed with the commercial FE code PamStamp and the model proposed by Klimmek et al [29] developed with LS-Dyna. Zhan et al [30] developed an explicit elastic-plastic model of shear spinning to study stress, strain and thickness distributions. Zhan et al in 2007 [31] extended the FE model to predict the effect of feed ratio on tool forces and geometrical tolerances of produced parts. It has been reported that the maximum error in geometry predicted by the model agrees well with the experiments. They reported that in order for the explicit finite element model to be reliable, maximum kinetic energy and maximum artificial strain energy must be less than 10% of maximum internal energy. Sebastiani et al [32] confirmed that dynamic effects will have a major influence on the stresses generated in the sheet and therefore on wrinkling. Liu [33] simulated multi-pass and die-less conventional spinning processes by applying the dynamic explicit LS-DYNA finite element software. It was concluded that the element size of the sheet must be less than that in the tools in order to ensure a reasonable model of contact between them. Long and Hamilton in 2008 [34] developed an explicit FE model for single-pass conventional spinning of cylindrical cups to present the strain distributions in the thickness, hoop and radial directions. Hamilton and Long [35] extended their model to study the effect of load rate scaling and mass scaling factors on the simulation time of the explicit FE model as shown in Table 2.1.

Table 2.1: Effect of mass scaling and load rate scaling on the simulation time [35].

	Speed up technique and factor	Average stable increment	CPU time hour:min:sec
Model 1	Mass scaling x 5	6.57E-07	21:24:06
Model 2	Load rate scaling x 5	2.06E-07	13:18:59
Model 3	Load rate scaling x 21	2.42E-07	10:37:59

From the literature survey by Music and Allwood [5], it is suggested that only a qualitative prediction of the influence of process parameters on product geometry is available. Accurate prediction of product geometry requires the development of faster and more reliable numerical models. However, these models have not yet been developed and require further improvement.

2.3.6 Results of analysis of spinning

Having reviewed the experimental and theoretical techniques used to investigate spinning, this section presents an overview of the results of analysis of spinning processes in general and specifically conventional spinning.

2.3.6.1 Applicable material and sheet thickness

Materials used in metal spinning include light and regular gauge sheet steels [27, 36-39], stainless steels [13, 25, 31], pure and alloys of aluminium [8, 39], brass [13, 36], non-ferrous heavy metals such as copper [13]. With some materials, e.g. titanium or stainless steel, an intermediate annealing operation is required [40]. In other cases, materials may be formed by partial heating to reduce the forming forces and increase

the ductility, e.g. titanium, stainless steel or nickel [25] or to eliminate casting defects, e.g. cast aluminum alloys [41]. Generally, sheet thicknesses may range from 0.4 to 25mm and workpiece diameters from 0.003 to 10m [9].

2.3.6.2 Surface finish

Investigations on the effects of process parameters on the surface finish have concentrated on shear spinning more than conventional spinning. In shear spinning, Hayama in 1971 [42] concluded that low surface roughness can be achieved by using a low rotational mandrel speed, small roller diameter and low viscosity lubricant. It was also concluded that it is possible to obtain high surface quality without using a lubricant, but only for low feed rates and mandrel speeds. Joorabchian and Slater in 1979 [20] investigated the effects of process parameters; mandrel speed, feed rate and wall angle, on surface roughness in aluminium and brass. They concluded that for both brass and aluminium, for a given wall angle and feed rate, lower feed rates give lower surface roughness. Chen et al in 2005 [43] investigated the effect of mandrel speed, feed rate, thickness, roller nose radius and over-spinning on both outer and inner surface of aluminium cones. They concluded that a lower roller feed with a large roller nose radius and high over-spinning results in a lower surface roughness for the inner surface. In conventional spinning, Elkhabeery et al in 1991 [44] also concluded that low surface roughness can be achieved by using low feed rates and a larger roller nose radius. In the experimental and numerical investigation by Groche et al in 2003 [45], a correlation between surface roughness and contact pressure was developed. A considerable reduction in surface roughness is observed as a result of increasing the contact pressure.

The results showed that the contact pressure increases by decreasing the sheet thickness and roller nose radius.

2.3.6.3 Tool forces

In spinning processes, three mutually perpendicular components may be defined: tangential, radial and axial. Early studies of tool forces have concentrated mostly on the prediction of the tangential force. Recent studies have also included the axial and radial components of force, which are important in assessing the rigidity of spinning equipment. The effect of the process parameters such as feed ratio, mandrel rotational speed, sheet thickness, roller nose radius on tool force in shear spinning has been investigated. In the experimental studies by Avitzur and Yang [15] and Kalpakcioglu [16] and analytical models by Kim et al [18, 19], it was reported that tangential force increases as a result of increasing the feed rate. The axial and radial forces show the same trend, as shown by Joorabchian and Slater [20]. Joorabchian and Slater [20] and Chen et al [46] both report that there is a mandrel rotational speed at which the tangential force is a minimum. In contrast, the influence of rotational speed on the variation of axial and radial forces is negligible, as also pointed out by Hayama et al [47]. For sheet thickness, experimental and analytical studies by Avitzur and Yang [15], Kim et al [18], Kim et al [19] and Huang et al [48] have indicated that a directly proportional linear relationship exists between thickness and all three tool force components. Kim et al [18] reported that the axial and radial force increases with an increase in sheet thickness. An increase in the spinning force and moment was observed by Liang et al [49] as a result of increasing the mechanical properties such as modulus of elasticity, yield stress and strain hardening exponent.

Compared to shear spinning, forces in conventional spinning have not received as much attention. Early studies by Dröge in 1954 [36] showed that the tangential forming force is only a few percent of the axial force and that it increases with spinning ratio and thickness, but drops with an increase in roller nose radius. Hayama and Murota in 1963 [50] showed that there exist two peaks in the radial force, one at the beginning of the process, and one towards the end, as a result of the different deformation modes in the beginning and end of the process. Wang et al in 1989 [51] measured the forces experimentally under a variety of working parameters and observed the trend of forces increasing with thickness and roller nose radius, while the rotational mandrel speed has a negligible effect on forming forces. In the experimental study conducted by Xia et al [39] in 2005, the effect of feed rate, spinning ratio and relative clearance on radial and axial forces in conventional spinning are measured. They reported that as feed rate and spinning ratio increase, the radial and axial forces increase. Increasing the relative clearance between the roller and mandrel leads to a decrease in the axial and radial forces. Similar findings are also reported by Quigley et al [24]. Quigley et al [52] also reported that control of forces could be achieved by keeping a constant distance between the roller and blank in order to limit the force applied to the sheet.

Although these studies have some value in practice for the design or selection of spinning equipment, the insights into process mechanics provided by these studies is limited. The evolution of forces, stresses and strains during multi-pass conventional spinning should be evaluated numerically to provide better understanding of the processes mechanics under subsequent roller passes.

2.3.6.4 Deformation mechanics

The deformation mechanism of shear spinning is shown in Figure 2.10. In this process, the final sheet thickness t_f is calculated from the initial sheet thickness t_0 and the wall angle α, ($t_f = t_0 \sin \alpha$). The idealised deformation mechanism of shear spinning was proposed by Kalpakcioglu in 1961 [16] whereby the disc blank is visualised as consisting of concentric thin cylinders axially sliding over each other and forming a cone while at the same time fulfilling the sine law, as shown in Figure 2.10. The experimental results showed that the axial grid lines remain axial and confirmed that the concentric cylindrical surfaces in the original blank remain cylindrical in the deformed cone and their radial distance from the axis of symmetry remains unchanged. This demonstrates that the deformation process is one of pure shear with plane strain in the plane parallel to the undeformed sheet. In the axial direction, the undeformed section of the blank retains its original dimensions.

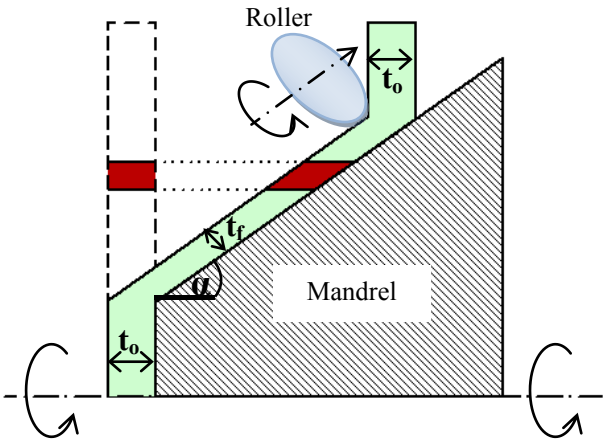

Figure 2.10: Idealised shear forming process.

For conventional spinning, in the work zone, the pattern of the generated stresses differs according to the direction of movement of the roller, which is either towards the edge of the blank, or towards the mandrel. When the roller moves toward the open end as shown

in Figure 2.11(a), the sheet is plastically deformed through two internal stresses. First, the tensile radial stress component which causes thinning of the sheet. However, this thinning is compensated by thickening caused by the circumferential compressive stress leading to a stress state similar to pure shear which therefore maintains a nearly constant thickness. When the roller moves towards the tailstock as shown in Figure 2.11(b), material builds up in front of the roller, generating compressive radial and circumferential stresses [2, 5, 13].

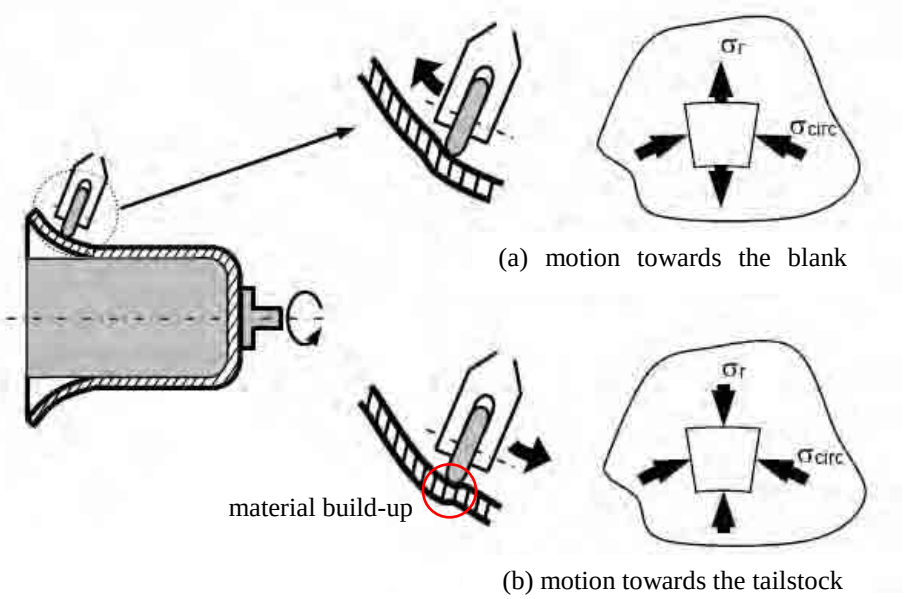

Figure 2.11: Development of work zone and material stress during conventional spinning [5], (a) Forward direction (b) Reverse direction.

2.3.6.5 Common defects and prediction of failure

There are three common defects in spinning which are wrinkling, circumferential cracks and radial cracks as illustrated in Figure 2.12. Wrinkling occurs due to the excessive compressive circumferential stresses, e.g. as a result of using very small sheet thickness [39], or a too large feed rate [35]. As mentioned in the previous section (Section 2.3.6.4), the process can be undertaken by inducing circumferential compressive stress

in the material. As a consequence, the material is compressed in the tangential direction, particularly towards the edge of the blank. As the load increases, the resistance to buckling is overcome, leading to the formation of wrinkles. In this case, it is necessary to apply a gradual combination of tensile radial stress and compressive circumferential stress through several roller passes [2, 5, 13]. Additionally, to avoid wrinkling, an increase of initial thickness must be associated with an increase in mandrel diameter for a constant sheet diameter [4, 5].

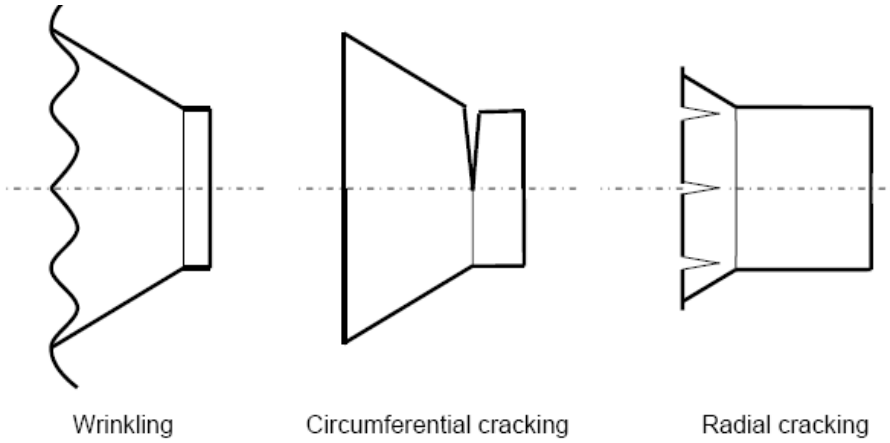

Figure 2.12: Common defects in metal spinning [5].

Circumferential cracks occur due to high tensile radial stress [5]. When the roller moves toward the edge of the blank, the material is stressed in the radial direction. The magnitude of this tensile load depends mainly on the roller nose radius. A small nose radius tends to produce high stresses. If the stresses are too great, the material to be formed is no longer sufficient to transmit the load. This leads to circumferential splitting/cracks, mainly in the area close the mandrel [13]. Radial cracks may form in two different cases; due to high circumferential tensile stresses or a combination of

circumferential compressive and bending stresses, which occur when existing wrinkles are being acted [5]. This usually happens as a result of severe wrinkling.

The prediction of fracture in shear spinning has been developed through studies of 'spinnability', defined as the maximum percent reduction in thickness a material can undergo before fracture. Kalpakcioglu in 1961 [53] examined the effect of process parameters on spinnability and reported that the roller nose radius, roller angle, feed rate and mandrel rotational speed do not have any influence. However, any deviation from the sine-law thickness and wall angle will strongly affect shear-spinnability. Spinnability increases with increasing over-spinning i.e., over-reduction where $t_f < t_0 \sin \alpha$, as observed by Kegg [54]. Kalpakcioglu [53] investigated theoretically the work zone under the roller and showed that over-spinning imposes an additional compressive stress on the material, thus increasing the ability of material to deform without fracture. Recently, in a study of the hot shear spinning process, Mori et al in 2009 [41] point out that over-spinning prevents surface cracks, due to the extra compressive stress being applied.

The first study on wrinkling in conventional spinning was performed by Kobayashi [55] in 1963 who developed an analytical model by modifying the theory of instability in deep drawing. It was reported that for a fixed initial sheet diameter, an increase in thickness of the blank must be followed by a corresponding increase in initial mandrel diameter to prevent wrinkling. In the experimental and theoretical investigations of Kleiner et al [28] to understand the mechanism of wrinkling, it was reported that decreases in the sheet thickness and increases in the blank diameter will make wrinkling more likely. Also, feed ratio, mandrel speed, tool and material have a significant

influence on wrinkling, with feed ratio being the most important. Another extensive study of wrinkling was performed by Xia et al [39], who report on single-pass conventional spinning of cups. Their experimental findings showed that thin sheets and higher feed ratios promote wrinkling, which supports the previous studies of Kleiner et al [28] and Klimmek et al [29]. Xia et al in 2005 [39] also report on the effect of spinning and feed ratios; for high spinning ratios, necking and fracture at the tailstock edge occur, at lower spinning ratios, wrinkling prevails.

Several attempts have been made to understand the mechanism of failure and its prediction. There is scope for the development of numerical models that can predict failure under a variety of working parameters and hence prevent it by obtaining an appropriate setting of these parameters. However, these models have not yet been established.

2.3.6.6 Geometric accuracy

Product geometry in spinning is defined by the variation of the part diameter and wall thickness along the product axis. Kalpakcioglu in 1961 [53] observed that the blank diameter has a significant influence on the final wall thickness. Elkhabeery et al in 1991 [44] studied the effects of feed rate and roller nose radius on thickness distribution and roundness tolerance in conventional spinning. They report that low feed rates and large roller nose radii, result in uniform thickness distribution and a better roundness tolerance. In a numerical study of shear spinning by Zhan et al [30, 31] it was reported that a high feed ratio produces more uniform thickness distributions, but at the same time results in a deviation of wall angle from the desired value. Sebastiani et al [38]

predicted, with an FE model, that sheet thinning takes place at the onset of wrinkling. Bai et al [8] studied the springback effect of thin-walled an aluminium alloy shell and used the change in one of the product dimensions, the half apex angle, to represent the amount of springback. They concluded that the elastic deformation during the process cannot be neglected and it plays an important role in springback effects.

It appears that at present only a qualitative prediction of the influence of process parameters on product geometry is possible. Accurate prediction of product geometry depends on the future development of fast, reliable numerical models. However, these models have not yet been established.

2.3.6.7 Roller-trace

The roller-trace refers to the profile of the pass that the roller follows during spinning. It has a significant effect on the product quality and surface finish. A careful choice and design of the roller-trace leads to a high quality, wrinkle-and crack-free product. In metal spinning, there are many profiles for roller pass that are used including linear, quadratic and involute curves (see Figure 2.13), however, the involute roller-trace is widely used in conventional spinning [4, 5, 22]. Many attempts were conducted to evaluate the effects of roller-trace on the stress and strain distributions during spinning [22, 56-59]. Hayama et al in 1970 [56] compared linear, quadratic and involute roller-traces and concluded that an involute roller-trace gives the best results, obtaining a maximum spinning ratio of up to 2.5, compared to 2 for quadratic and 1.7 for linear. This is supported by Liu et al [22] who also compared linear, quadratic and involute roller-traces and showed that an involute roller-trace will generate the lowest radial and

tangential strains and stresses in the sheet. Both Liu et al [22] and Kang et al [57] further point out that the design of the first pass in conventional spinning plays a decisive role in determining the final wall thickness distribution. Kawai et al [59] reported that the thinning phenomenon of the wall in shear spinning can be prevented by the use of a non-linear roller-trace, e.g. involute or quadratic to allow a gradual change in the wall thickness from the initial to the final value.

From the literature, it seems that the design of roller-trace still remains an art obtained by practice. Many investigations were conducted to understand the effects of the different roller-traces on the deformation behaviour. However, these investigations focused only on the first pass and ignored the accumulation effects of using subsequent passes of different roller-trace.

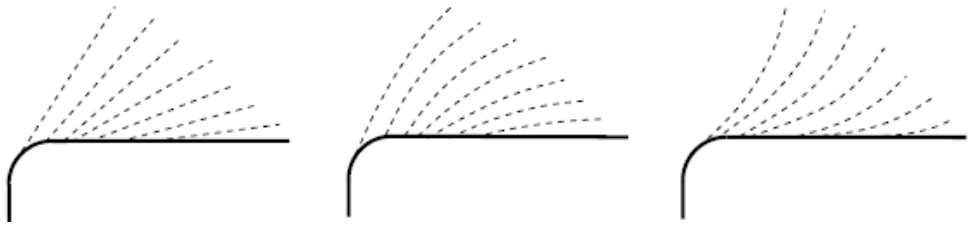

Figure 2.13: Roller-trace designs in conventional spinning, (a) linear, (b) quadratic curve, (c) involute curve [5].

2.4 Asymmetric Incremental Sheet Forming (AISF)

Research in modern incremental sheet forming has been mapped in four reviews over the last ten years. In 2001, Shima [60] completed the first review of modern ISF, which described the main variations in equipment and experimental configurations. In 2003, Hagan and Jeswiet [3] published the second review, this started with a short background of symmetric ISF (such as conventional and shear spinning) followed by a detailed description of AISF processes. In 2005, Jeswiet et al [61] provided a broader review of modern ISF. This included equipment configurations, tool path design procedures and the main results in terms of accuracy, forming limits and surface finish. More recently, Jeswiet et in 2008 [62] discussed the development of the metal forming processes including AISF since 2000.

Asymmetric incremental sheet forming AISF generally refers to a die-less forming process which can be used to form complex shapes using simple tools. The process has received increasing attention due to its high flexibility and low cost. The die less nature of the process, the freedom of the forming tool to move in three dimensions under CNC control and its capability for producing both symmetric and asymmetric shapes are the main differences between AISF and other ISF processes. In AISF, a simple tool moves over the sheet surface and produces a highly localised plastic deformation. Thus, a variety of complex 3-D shapes can be formed through the tool movement along correctly designed and controlled paths without using a dedicated die.

2.4.1 Configurations of AISF

As defined by Jeswiet et al [61], the two most common forms of ISF are single point incremental forming (SPIF) and two-point incremental forming (TPIF). SPIF, also known as negative die-less incremental forming, involves forming a clamped workpiece with a single tool as shown in Figure 2.14 (a). TPIF took its name because the sheet metal blank is pressed at two points simultaneously. The first point pushes into the sheet causing plastic deformation while tracing the outline of the shape to be produced. The second point works as a static supporting post that creates an upward counter force on the sheet metal blank as shown in Figure 2.14 (b). TPIF has been used in four different configurations: with a central support post, with a partial positive die support and with a full positive or negative die support. TPIF has the disadvantage of requiring specialised tooling for all configurations and is therefore not a fully flexible process.

(a) (b)

Figure 2.14: (a) SPIF and (b) TPIF.

2.4.2 Advantages and applications

The most important advantages of AISF are the possibility for rapid prototyping of industrial sheet metal forming before mass production, high flexibility, homogenous deformation, strong customer orientation and low costs. The process has many

industrial applications which include rapid prototypes for automotive industries and light weight components with reflexive surfaces such as vehicle headlights and automotive heat/noise shields [63, 64] (see Figure 2.15a) and for non-automotive applications such as solar ovens, motorbike seats and motorbike gas tanks [65] (see Figure 2.15b). In addition, the process has potential in medical applications. It can be used to produce customised ankle supports [66] and dental plates [67] as shown in Figure 2.16.

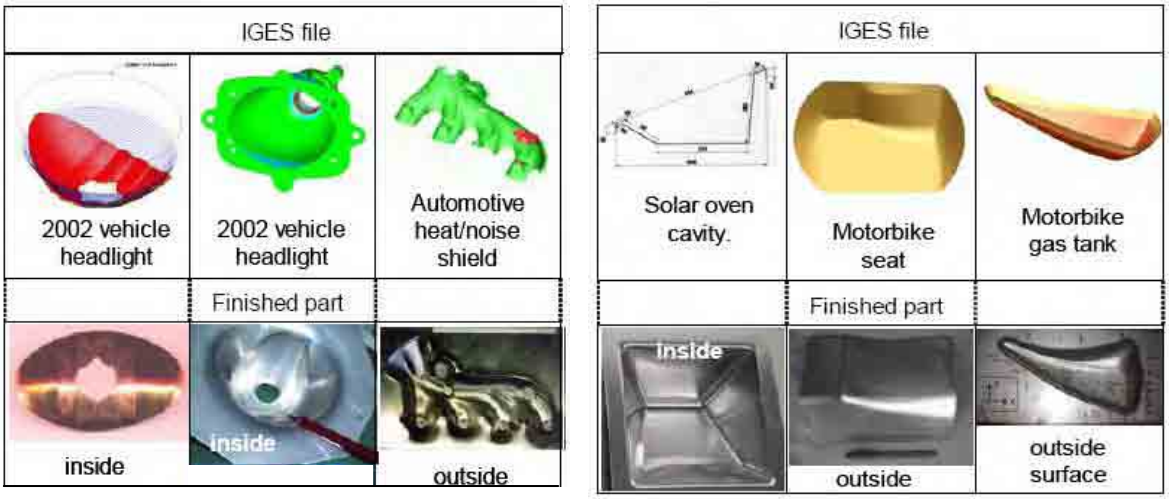

(a) (b)

Figure 2.15: Rapid prototype for (a) automotive industries [63, 64] and (b) non-automotive industries [65].

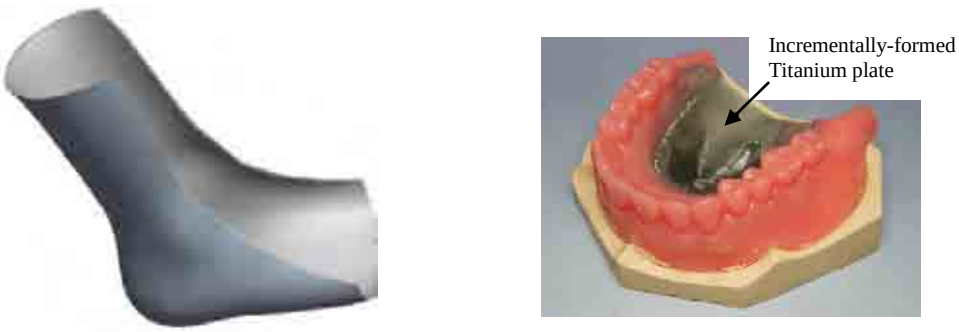

Figure 2.16: Medical applications (a) ankle support [66] and (b) dental plate [67].

AISF could also be used to produce inexpensive die surfaces and moulds [68]. Smith et al [69] proposed a new hybrid process that combines thin part machining and SPIF. The new process enabled the creation of various geometries (such as thin wall with multiple bends and hourglass domed thin floor) that would be very difficult to obtain using any other processes. Additionally, SPIF showed its capability to successfully form sheets produced by friction stir welding (FSW) [70].

2.4.3 Equipment for AISF

There are three basic elements required for AISF including the blank holder, forming tool and machine for driving the tool, in addition to the sheet metal blank. Clamping of the workpiece in both SPIF and TPIF has almost always involved using a continuous frame to rigidly clamp around the edge of the workpiece. The forming tool for AISF consists of a working head which applies a localised force to the sheet to cause the deformation. The most common design of forming head used for AISF is a sphere or spherical section because it is able to turn corners or roll across the surface whilst maintaining a smooth contact with the sheet for a good surface finish, as well as being able to form the sheet from a wide range of angles. In some investigations, other types of tool such as shot peening [71] and water jet [72] have been successfully used to deform the blank sheet. For very large wall angles e.g. 90^{o}, a small tool shank must be used to avoid the contact between the tool shank and deformed sheet. The tool head is usually made of tool steel which is suitable for most applications. To avoid tool wear, the tool head can be coated by cemented carbide [73] (see Figure 2.17). The most common tool diameters range from 6 to 30mm.

Figure 2.17: Cemented carbide tools with diameters of 6, 10 and 30mm [73].

The machinery which supports and drives the forming tool in AISF has a significant influence on the process capabilities because it determines the allowable tool speed, positioning accuracy, complexity of tool path programming, limiting tool forces and degrees of freedom of movement. Many investigations used a three-axis CNC milling machine for AISF research due to its computerised tool path programming. However, excessive wear on the bearings due to high tool forces in AISF compared to conventional milling processes was reported. A further limitation is that a CNC milling machine is not possible for all TPIF configurations. With the aim of overcoming some of these limitations, specialised AISF machines have been developed by a number of research groups. The first specialised rig was built by Iseki in 1992 [74] followed by a more advanced custom-built NC machine built by Amino as described by Maki [75] and shown in Figure 2.18 (a). A specialised rig for SPIF was commissioned at the University of Cambridge in October 2004, developed by Allwood et al [76] as shown in Figure 2.18 (b). Robot arms have been used in research as a tool driving mechanism in order to increase the number of degrees of freedom and allow a greater range of movement in comparison to the machines described, used first by Meier et al in 2005 [77] and later by Lamminen et al [78], Maidagan et al [79], Callegari et al [80] and Vihtonen et al [81].

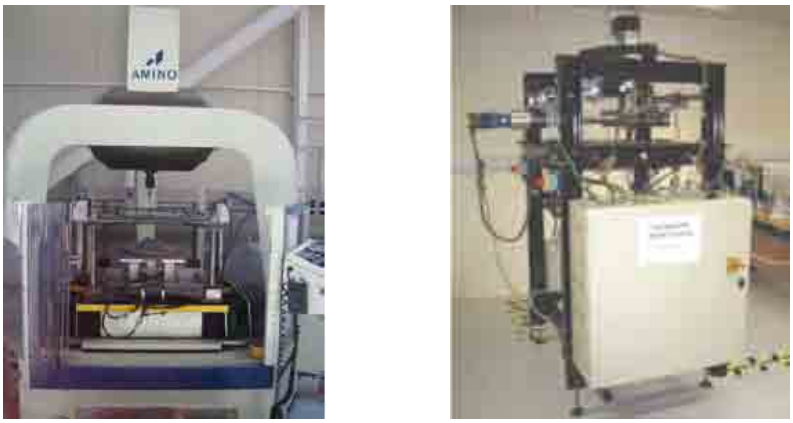

(a) (b)

Figure 2.18: Specialized AISF built (a) by Amino [75] and (b) Allwood [76].

2.4.4 Implementation procedure

The implementation procedure of AISF processes usually starts with a CAD drawing of the required product. For customised products as in medical applications, the CAD drawing can be generated by a reverse engineering approach where a laser scans an object of the required finished shape as demonstrated by Ambrogio et al [66]. The next step is to obtain the tool path that will produce an approximation to the required geometry, this may be generated by CAD/CAM software such as Pro/Engineer, Unigraphics, Mechanical Desktop, MasterCam and Matlab. The tool path progresses inwards and downwards around a concave profile of the product geometry for SPIF and outwards and downwards around a convex profile of the product geometry for TPIF. The next step is the selection of the process variables. The product quality characteristics are affected by the process variables and therefore, they should be chosen carefully. The variables include tool diameter, feed, rotation speed and lubrication. The implementation procedure for AISF process is shown in Figure 2.19.

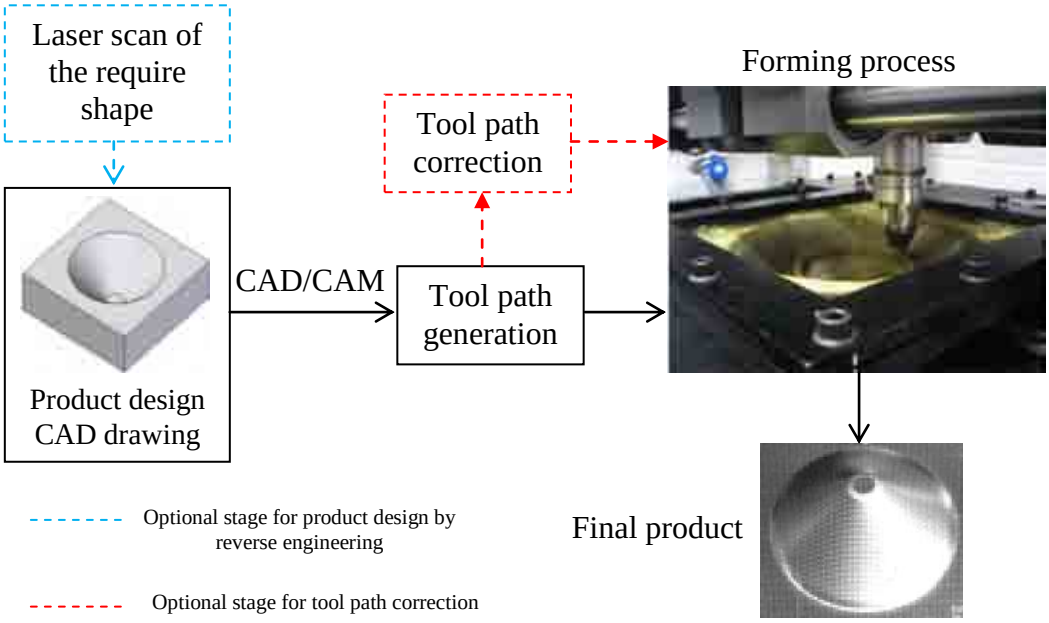

Figure 2.19: Implementation procedure for AISF process.

In some cases, the tool path needs some correction before forming the required product through an optional step. The reasons for tool path correction could be for an improvement of geometric accuracy [82-86], avoidance of rupture [63, 87-91] or an improvement in the uniformity of the wall thickness [92-96]. The assessment of the tool path and any corrections required could be done by; using finite element modelling as demonstrated by Filice et al [87]; deriving an equation for predicting forming limits based on the material parameters as demonstrated by Fratini et al [97]; using a multi-pass forming strategy as used by Jeswiet et al [63], Iseki [88], Hirt et al [90] and Ceretti et al [98]; or in-process control as demonstrated by Ambrogio et al [99]. In the last approach, an integrated on-line measuring system, composed of a digital inspection and computer numerically controlled (CNC) open program, was employed to minimize profile errors. This system collected data on the geometry in specific steps, and the subsequent tool path was modified to compensate for the geometrical errors. In the

numerical simulation of AISF, the tool path can be defined manually (for simple geometry) or exported directly from the CAM software through Matlab or any subroutine function (for complex geometry) as used by Robert et al [100] and Nguyen et al [101].

2.4.5 Investigative approaches in AISF

Experimental, analytical and numerical methods have been used to measure the process characteristics and evaluate the mechanics of AISF processes. The different investigation techniques are reviewed below, whilst the results of the investigations are reported later in Section 2.4.6.

2.4.5.1 Experimental approaches

Experimental methods have been used in AISF processes to measure the process characteristics such as geometry, strains, tool force, thickness and surface finish. Measurements of geometry and geometric accuracy of sheets formed by AISF have been carried out by three principal methods. These methods use coordinate measuring machines (CMMs); laser scanners; and 3D stereovision systems. Coordinate measuring machines are used to measure the geometry of the sheet after unclamping by taking point-by-point measurements as used by Meier et al [77] and Hirt et al [83]. Laser scanners or stereovision systems are suitable for geometry measurement whilst the sheet is still clamped. However, a problem that can be encountered is that the sheet surface can be partly obscured whilst it is mounted in the machine, and hence the full surface may not be measurable. Laser scanners measure the geometry of a sheet by scanning across it in a line as used by Ambrogio et al [84] and Duflou et al [86]. A stereovision

system offers the advantage over a laser scanner of imaging of the entire surface simultaneously and thus a scan is not required. This method has been used by Hirt et al [83] and Watzeels et al [102].

In AISF processes, two methods have been used for measurement of strains on the sheet surface which are strain gauges and grids applied to the surface. Strain gauges are the simplest technique and used to measure the strains developed at discrete points on the sheet surface throughout the forming process, as used by Kitazawa [103]. However, being difficult to attach and measure the strain at discrete points only demonstrates the limitations to this technique. An alternative technique for strain measurement is by comparing the size of circles on a grid applied to the sheet surface before forming to their size after forming. The grid pattern must be applied to the surface that is not contacted by the tool to avoid damage. The grid can be applied easily by several methods such as impressing the grid onto the sheet surface, Filice et al [87], silk-screen printing, Jeswiet et al [91], a photographic technique, Kitazawa [103] and Iseki [104], electro-chemical etching, Shim and Park [105] or scribing the grid onto the surface manually, Kim and Park [106]. Whatever the method, the major and minor diameters of the distorted ellipses of the grid after forming are measured and used to calculate the major and minor surface strains.

The techniques used for measuring tool force in AISF include the measurement of reaction forces on the workpiece support with a force dynamometer, Duflou et al [107, 108] and Bologa et al [109]; measurement of forces on the tool post using strain gauges, Jeswiet et al [110]; and measurement of reaction forces on the workpiece support with load cells. The last method is used in the purpose-built machine designed by Allwood et

al [76]. Automatic measurement of sheet thickness in AISF is difficult because points need to be measured accurately on opposing surfaces, where usually only one side is accessible to scanners or CMM's. The thickness can manually be measured using a micrometer after cutting the sheet as used by Bambach et al [96]. Alternatively, a CMM can be used to measure the positions of points on opposite sides of the sheet and hence the sheet thickness can be calculated, as used by Ambrogio et al [95, 111]. Recently, an online thickness measurement system based in ultrasonic technology integrated into the forming tool was developed by Dejardin et al [112]. Surface roughness has been measured for a variety of process parameters as demonstrated by Hagan et al [113] using white light interferometry.

2.4.5.2 Analytical approaches

Analytical methods are not commonly used in the analysis of AISF. A few examples included are based on a membrane analysis method; Martins et al in 2008 [114] presented the different modes of deformation commonly found in SPIF. Silva et al [115, 116] constructed an analytical model based on the same approach to address the influence of the process parameters and explain the enhanced formability of SPIF. The Marciniak-Kuczynski (MK) model framework first proposed in 1967 [117] is a commonly used analytical tool to predict the limit of sheet formability due to the onset of localised necking. The model assumes an imperfection (groove b) in an otherwise perfectly homogeneous sheet (matrix a) and the initial groove orientation, determined by Φ_0, changes during deformation due to matrix straining as shown in Figure 2.20. A monotonic deformation is imposed onto the matrix a, in terms of a constant velocity gradient L^a. Through assumptions of incompressibility, force equilibrium and geometric

compatibility components of the groove velocity gradient L^b can be determined. They generally evolve during deformation, so an incremental procedure is applied. For each initial groove orientation Φ_0, there is a certain major in-plane strain in the matrix, at which deformation becomes localised within the groove (called the necking strain ε_{11}). The forming limit strain is found as the minimum of all necking strains [118, 119].

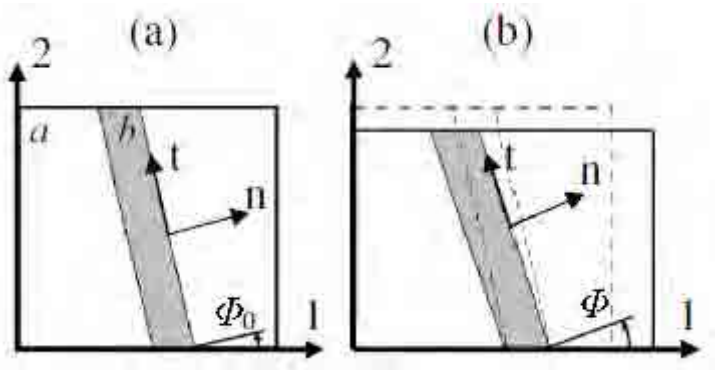

Figure 2.20: MK model (a) undeformed state and (b) deformed state. The 1-2 axes represent the major and minor in-plane directions. The n-t axes are fixed for the groove b. The 3-axes i.e. sheet thickness, is perpendicular to the sketch plane [119].

Recently, an extension to the MK model framework was proposed by Allwood et al [118] and Eyckens et al [119, 120] in order to explicitly account for through-thickness shear, which is usually disregarded in MK analyses. The extended MK model shows that through-thickness shear increases the forming limit and delays the onset of localised necking as shown in Figure 2.21. The forming limits shown in Figure 2.21 are obtained from a paddle forming process where through-thickness shear is taking place.

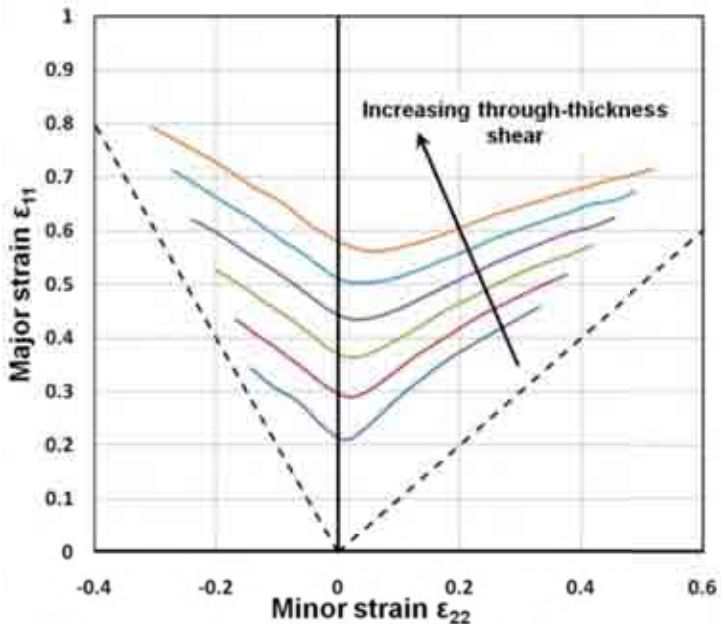

Figure 2.21: Effect of through-thickness shear on the forming limit as predicted through an extended MK model by Allwood et [118].

2.4.5.3 Numerical approaches

Numerical methods, for example FE modelling, permit a detailed study of complex deformation behaviour as in AISF and as experimental observations of through-thickness phenomena are extremely difficult, modelling of the AISF processes becomes an essential tool. Numerical modelling of AISF has been used for three main purposes: prediction of tool forces for safe design of machines; prediction of stresses and strains through the sheet and throughout the process; and prediction of the deformation in order to improve geometric accuracy. The simulations in AISF are time consuming because the tool paths are inherently long and require a large number of time steps to model the continually changing contact conditions and because the mesh size under the indenter needs to be fine to simulate accurately the localised deformation. Therefore, in the literature, many investigations have focused on reducing the simulation time in AISF without compromising accuracy.

Explicit and Implicit codes have been used in the simulation of AISF. The implicit method involves the solution of non-linear equations through an iterative procedure while the explicit method is based on dynamic equilibrium and requires the solution of a set of linear independent equations at each step of the deformation path [121]. Mass and speed scaling used in explicit models can allow a faster solution time than implicit models of the same process. Bambach et al [89, 96], Ambrogio et al [95, 111, 122], Hirt et al [123], Qin et al [124], He et al [125] and Decultot et al [126] all used explicit code for the simulation of parts formed by AISF (such as a simple cone and a truncated pyramid) and they found that explicit models using mass or speed scaling had a solution time that was much less than that of an equivalent implicit model. However, the explicit method is only practical on the condition that the time step is small and the tool path is simple. The increase in mass scaling or the tool speed scaling can cause artificial inertia effects which degrade the numerical results, hence a continuous check of the ratio of kinetic energy to deformation energy is often employed, as used for example by Ambrogio et al [84]. Bambach et al [127] conducted a comparative study of implicit and explicit methods to evaluate their effects on the predicted geometry of a truncated cone made by SPIF. One implicit and two explicit FE models, M1 and M2, are used. Explicit-M1 was simulated using a higher mass scaling than explicit-M2. The maximum distance $d_{(max)}$ and average distance $d_{(av)}$ between the experimental profile and the FE profile was used as a measure of the quality of the predicted geometry. The results indicated that the implicit method provides more accurate results compared with the explicit method although it requires a relatively large number of increments. The high mass scaling used in explicit-M1 will reduce the simulation time however, it will increase the deviation from the experimental data as shown in Table 2.2.

Table 2.2: Performance of Implicit and Explicit FE Analysis [127]

Method	Time step	$d_{(max)}$, mm	$d_{(av)}$, mm	CPU time, hrs
Implicit	4.0E-3	1.09	0.59	7.32
Explicit-M1	1.0E-4	1.82	1.19	0.58
Explicit-M2	1.0E-5	1.67	1.13	3.1

Ambrogio et al [95] and He et al [125] found that an explicit model was unsuitable for the prediction of wall thickness in SPIF due to numerical stability problems. They reported that an implicit model of the same process gave a stable solution with minimum error. Bambach et al [128] also reported that the greatest deviation between implicit and explicit predictions of geometry occurred where the tool path was not smooth, e.g. where the tool incremented downwards. They suggested that this was a result of the high kinetic energy transmitted downwards. The simulation time of implicit analysis can be reduced by using a refinement-derefinement (RD) strategy or the combined Newton-Raphson and condensed linearised elastic (CNRCLE) method as used by Hadoush and Boogaard [129, 130]. Shell and solid elements are both used in the FE modelling of AISF. Robert et al [100] introduced an elasto-plastic material definition implemented through a VUMAT user subroutine with shell elements to minimize the FE simulation time using Abaqus/Explicit. The objective was to implement the incremental deformation theory of plasticity. They concluded that this approach can improve the efficiency of the modelling process and reduce the computational time. Lasunon and Knight [131] have conducted numerical investigation on both single point and two point incremental forming processes. The FE models used shell elements to simulate and study the effects of process variables on the formed profiles and thickness variations for both processes. For the same purpose, Dejardin et al [132] constructed finite element models, also using shell elements for SPIF. Eyckens

et al [133] constructed a partial FE model, using linear brick elements with Abaqus/Implicit, of a conical shape produced by SPIF, to predict the forming limit of the process. In this model, three elements were assigned through the sheet thickness in order to identify the strain path. Tanaka et al [134] also constructed a partial model of an SPIF cone forming process to assess residual stress, although this single-level model consisted of a regular hexahedral segment with no influence of prior process deformation. Ma and Mo [135] constructed full and simplified 3-D FE models for single point incremental forming to simulate the deformation of a truncated cone and a truncated pyramid. Both models used only one linear brick element through the thickness. They reported that although brick elements are much better than shell elements, the simulation time is much longer.

From the literature survey, it can be concluded that, although insights into AISF have been gained through FE simulations, two major challenges to this approach are that the simulations are extremely time consuming to implement and that details of through-thickness phenomena are limited. The latter are limited because shell elements are often chosen for simulations of the full sheet because the sheet is thin. A focus of model development is therefore required to reduce processing times without compromising accuracy. Additionally, the implicit method is more suitable for the simulation of AISF processes than explicit method.

2.4.6 Results of analysis of AISF

Results of previous analyses of AISF using the experimental, analytical and numerical methods above can be summarised into the following areas: applicable materials and

sheet thickness; surface finish; tool forces; the deformation mechanics, forming limit and geometric accuracy. The extent of current knowledge of the process in each of these areas is reviewed below.

2.4.6.1 Applicable material and sheet thickness

The small plastic zone and incremental nature of the process contributes to increased formability, making it easier to deform low formability materials. Therefore, AISF processes are applicable to a wide range of elastic-plastic materials. However, research in AISF so far has been mainly applied to metals such as aluminium, stainless steels and mild steels [61], due to their high ductility, but there are a few examples of its use in more difficult to form materials. The AISF processes have been applied successfully to the forming of brass [97], copper [97, 136], titanium[103, 136-138], gold [136], silver [136] and platinum [136]. Landert [139] showed the applicability of AISF to composite materials to form sandwich panels with metal faceplates and metal fibre or polymer cores. Some non-metallic materials have been considered, for example by Le et al [140] who investigated the applicability of SPIF to deform thermoplastic material. Recently, Franzen et al [141] and Martins et al [142] in 2009 carried out the first work on SPIF of PVC and polymers respectively. Allwood et al [143] found that most sheet metal products out of a range of 28 examples had a thickness between 0.4 and 3 mm. AISF has been applied to foils from 10μm to 100μm using a specialised micro forming apparatus designed by Tanaka et al [144]. The deformation has been successfully achieved using 5mm thick aluminium sheet as reported by Jyllilä [145]. However, the common sheet thickness used for research in AISF is in the range of 0.5 mm to 1.5 mm.

2.4.6.2 Surface finish

The surface finish of products formed by AISF can be characterised as a striated surface, i.e. large-scale waviness, due to the movement of the tool along overlapping contours [113]. This can either be an advantage or a disadvantage of AISF in comparison to pressing depending on the application. If surface finish is a critical requirement as for car body panels, pressing inherently will offer a smooth surface whereas AISF may not. This problem could be avoided by incrementally forming a car body panel with two sheets on top of each other and discarding the upper sheet. Alternatively, the surface finish can be improved by coating with paint or other substances to disguise the striations. On the other hand, the characteristic surface of AISF was an advantage for a bespoke light shade designed by Rachel Tomlinson of Cambridge University. The striated surface created a striking visual effect, which is a desirable feature of the product, which would not be possible to obtain with pressing (see Figure 2.22).

Figure 2.22: A bespoke light shade manufactured by AISF and designed by Rachel Tomlinson, University of Cambridge in 2005. The striated surface is a desirable feature of the product.

Allwood et al [76], Leach et al [82] and Junk et al [146] each have reported that surface roughness increases as step-down size increases. Hagan and Jeswiet [113] showed that roughness increases exponentially with step-down size in SPIF. Lubrication was found

to improve the surface finish as reported by Kim and Park [106]. Junk et al [146] found that surface roughness increases as wall angle and tool diameter increase in TPIF. Recently, Wang et al in 2010 [147] designed a double-head tool setup that showed a permissible improvement to the surface roughness of a truncated pyramid made by SPIF.

2.4.6.3 Tool forces

Tool force in AISF is an important topic due to the problem of excessive wear on the bearings of adapted CNC milling machines that were originally designed for machining. Experimental approaches have been used to measure the trend in tool forces throughout the process using simple geometries [107-110]. Analytical and numerical models have been developed for prediction of the influence of process parameters on tool force throughout the process [148-152].

The literature of AISF shows that there are three perpendicular force components normally examined, i.e. an axial force component, and components parallel and perpendicular to the tool travelling direction. Duflou et al in 2005 [107, 108] measured the forces for a square-based pyramid and a cone formed by SPIF and found that the force increases to a maximum over the first few contours before stabilising to a steady-state value. Similar trends in tool forces have been measured for square-based pyramids formed by TPIF by Jeswiet et al [110]. A quantitative comparison of perpendicular tool force components in SPIF has shown that the axial (vertical) tool force is the largest component, approximately twice the perpendicular tool force component, observed by Bologa et al [109] and Jeswiet et al [110].

Duflou et al [107, 108] investigated the effect of process parameters on tool force in SPIF. The results showed that the total tool force vector increases linearly with tool diameter and step-down size and by a quadratic relationship with wall angle and sheet thickness. It was found that step-down size has the least influence on tool force, and hence can be increased without a great penalty to reduce production times but it would have a detrimental effect on surface finish. Bologa et al in 2005 [109] investigated the influence of step-down size, sheet thickness and tool diameter on the three components of tool force in SPIF in order to derive an equation that relates the tool force with these process parameters. It was concluded that as any of these parameters increases the three force components increase and that sheet thickness has the strongest effect on tool force. Duflou et al in 2007 [150] carried out a set of experiments from which regression equations were derived to predict the tool forces as a function of step-down size, wall angle, tool diameter and thickness and found similar results. Durante et al in 2009 [152] investigated the effect of tool rotation on the forming forces and found that a decrease in forming force peaks is observed when the tool is set in rotation. Recently, Katajarinne et al in 2010 [153] reported that the use of an appropriate lubricant and tool coating result in reducing the forming forces.

2.4.6.4 Deformation mechanics

The complex nature of the deformation results from many factors such as the continually changing contact location, large plastic deformation and complex tool kinematics. Numerical methods, for example FE modelling, permit a detailed study of this behaviour and experimental observations of through-thickness phenomena are extremely difficult. Experimental approaches and FE methods have been used to

measure or predict the strains and displacements in order to evaluate the deformation mechanics. Although previous work has provided valuable information, this is limited and sometimes contradictory, and hence the deformation is not fully understood.

Both experimental measurements and numerical simulations have revealed uniaxial surface strains during the deformation process of both SPIF and TPIF. This means that stretching and thinning are the common modes of deformation. This was first measured for SPIF of circular and elliptical frustums by Iseki in 1993 [154] and later predicted through FE analysis by Shim and Park in 2001 [105], Bambach et al in 2003 [89] and Hirt et al in 2003 [155] (see Figure 2.23). Park and Kim [156] predicted a similar result for pyramids formed by both SPIF and TPIF with a central support post. Near to uniaxial surface strains were measured by Fratini et al in 2004 [97] for a truncated cone formed by SPIF from various materials and by Jeswiet and Young in 2005 [157] for various shapes formed by SPIF.

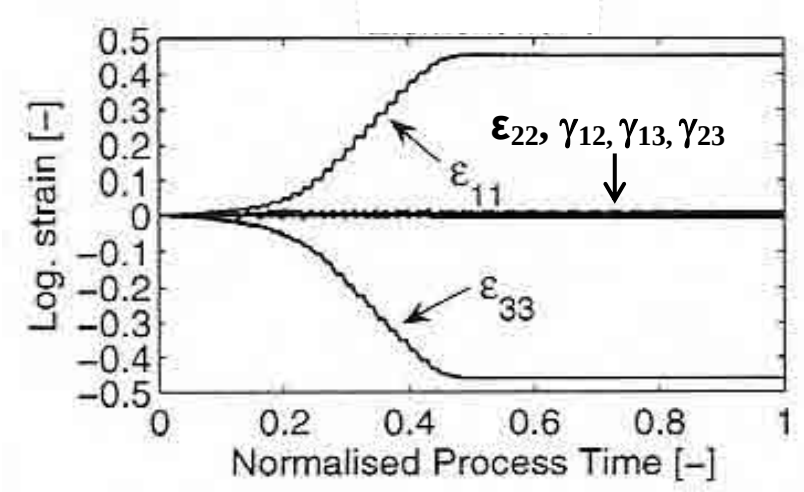

Figure 2.23: Strain history for an element deformed by SPIF as predicted through FE modelling by Bambach et al [89]: ε_{11} and ε_{33} represent sheet stretching and thinning respectively.

Although near to uniaxial surface strains have been most commonly observed in AISF, non-zero minor surface strains can be achieved under certain conditions. Shim and Park [105] found that near to equi-biaxial strains occurred at the corners of shapes with various angles, whilst uniaxial strains occurred along the flat sides. Filice et al [87] reported that minor surface strain could be increased by reducing the radius of curvature of the tool path. Achieving non-zero minor surface strains has been of particular interest for plotting forming limit diagrams over a range of ratios of major to minor surface strain as will be shown in the next section.

Following from the above result, it can be concluded that strains along straight sides are uniaxial and that material mainly displaces normal to the plane of the undeformed sheet. This follows a relationship between the wall thickness after forming (t_f) with the wall angle (α) and the initial sheet thickness (t_0) known as the sine law ($t_f = t_0 \sin \alpha$) used originally to predict the sheet thickness in shear spinning. Many investigations have been conducted to test the accuracy of the sine law for the prediction of wall thickness in SPIF or TPIF. The sine law showed an accurate prediction of wall thickness with various wall angles formed by TPIF as reported first by Matsubara in 1994 [158]. A detailed investigation of the accuracy of the sine law across the profile of cones of various wall angles formed by SPIF was carried out by Young and Jeswiet in 2004 [94], which showed a good prediction of the wall thickness. Similar results are reported by Ambrogio et al in 2005 [95] for cones formed by SPIF.

In the literature, the deformation mechanism of AISF has been linked with that derived from experimental measurements of shear spinning by Avitzur in 1960 [15] on which the derivation of the sine law is based. The deformation mechanism of shear spinning is

considered to be pure shear with plane strain in the plane parallel to the undeformed sheet, and is found to be similar to that in AISF. The deformation mechanism of AISF has been described as pure shear by Kim and Yang in 2000 [93] when experimentally investigating the formability of SPIF, in investigations of wall thickness variations in SPIF by Young and Jeswiet in 2004 [94], in investigations of incremental sheet forming by Shankar et al in 2005 [159] and in experimental and numerical investigations on SPIF and TPIF by Hirt et al [137, 160].

Contrary to the idealised deformation mechanisms described above, Allwood et al in 2007 [118] have shown by experimental measurement that significant shear deformation occurs in a plane normal to the sheet surface and parallel to the tool travelling direction; also, Jackson and Allwood in 2009 [161] measured high shear strains in a plane parallel to the tool movement and lower shear stains in a plane perpendicular to the tool movements for SPIF as shown in Figure 2.24. Bambach et al [89] predicted, using a 3D FE model, that whilst stretching and thinning are significant, all shear components are negligible as shown above in Figure 2.23. However, this is not necessarily a contradiction to the experimental measurements of Allwood et al [118] because the tool path used by Bambach et al [89] alternated in direction which would tend to cancel out any shear on successive laps as a result of friction, whereas the tool always moved in the same direction in the experiment by Allwood et al [118].

Overall the above have provided useful insight into the deformation mechanics. However, there are some gaps in the knowledge. In particular, there are contradictory results for the through-thickness deformation both parallel and perpendicular to the tool direction. Therefore, accurate FE models with a large number of elements through the

thickness are required to provide clear information about the deformation mechanisms and in particular, the through-thickness shear deformation.

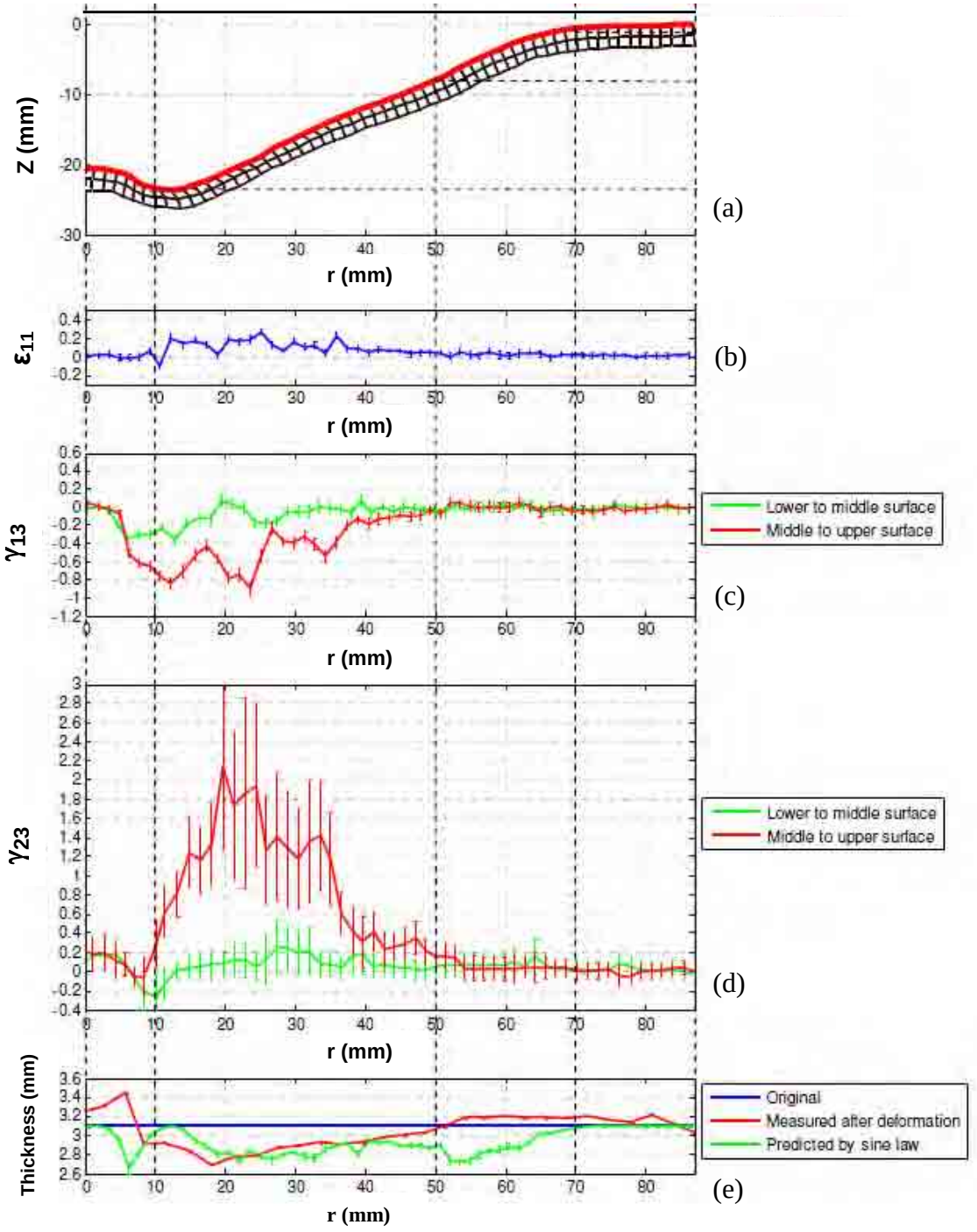

Figure 2.24: Measurements of plate formed by SPIF as experimentally measured by Jackson and Allwood [161]: (a) geometry, (b) sheet stretching ε_{11}, (c) shear perpendicular to tool direction γ_{13}, (d) shear parallel to tool direction γ_{23}, (e) thickness distribution.

2.4.6.5 Forming limit

Forming limits in AISF are found to be higher than those in traditional forming processes such as pressing. A range of theories have been presented for why this may be the case. The use of a forming limit diagram is a common method, in which the horizontal axis represents the minor surface strain (lowest strains) and the vertical axis represents the major surface strain (highest strains) at failure (as close as possible to a crack formation). Alternative measures of forming limit in SPIF and TPIF use the maximum major strain at zero minor strain (FLD_0) or the maximum wall angle at failure. Hussian et al [138, 162-165] proposed a method to test the formability in terms of the maximum achievable wall angle at failure by producing parts with a varying wall angle. This approach helped to minimise the required number of experiments to determine the forming limit of a sheet. It was concluded that the forming limit curve followed a straight line with a slope of -1 (see Figure 2.25) [87, 105, 154].

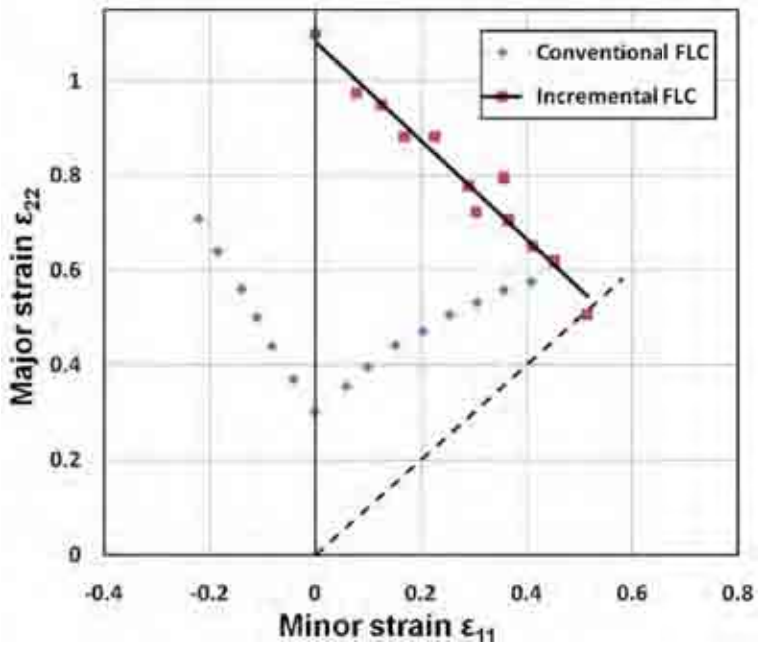

Figure 2.25: Experimental FLCs of AA1050 obtained from conventional test and SPIF test [87].

There are a number of process parameters that have a strong influence on the forming limit of SPIF and TPIF such as sheet material properties, step-down size, lubrication, tool diameter, and sheet thickness. Bambach et al [89] found that anisotropy had minor influence on a FE prediction of strains in SPIF of mild steel DC04. Fratini et al [97] found that the strain hardening coefficient had a significant effect of the formability where a higher strain hardening coefficient coincided with the greatest material formability. Ambrogio et al [95], Kitazawa [103], Kim and Park [106], Hirt et al [137] and Hussain et al [166, 167] all showed that formability increases as a result of decreasing step-down. With increasing the step-down size, the sheet undergoes heavier deformation conditions. Kim and Park [106] found that the formability increases as a result of using no lubrication and using a rotating ball instead of a hemispherical tool. Park et al [156], Hirt et al [137], Hussain et al [166, 167] and Ham and Jeswiet [168, 169] all found that decreasing the tool diameter results in increasing the forming limit. Jeswiet et al [170] found that the formability, in terms of the maximum wall angle, increases as a result of increasing the sheet thickness. Silva et al [115, 116] also reported that an increase in the sheet thickness will delay the onset of instability and fracture.

The forming limits of AISF have been compared to that of conventional forming limit tests first by Iseki in 1993 [154], Kitazawa [103], Shim and Park [105], Hirt et al [137] and later Lamminen in 2005 [78] who all reported that higher forming limits are achieved in AISF. Emmens et al [171] reviewed theories that have been proposed for the higher forming limits observed in ISF. Bambach et al in 2003 [89] reported that the increased forming limits observed in ISF are a result of the hydrostatic pressure suppressing damage. The same conclusion was reported later by Martins et al in 2008

[114]. Micari in 2005 [172] proposed that a further contributing factor to the increased forming limits in AISF is that the maximum principal stress is low in the actively yielding region which agreed with the results reported by Ambrogio et al [173]. Eyckens et al in 2007 [133] showed cyclic/serrated strain paths along the sheet thickness due to the sheet being repeatedly bent in the direction of tool movement and they concluded that cyclic effects can improve the formability. Emmens et al in 2008 [174] reported that bending-under-tension might be acting as a mechanism allowing large uniform straining in incremental sheet forming. Recently, Allwood et al in 2009 [175] proposed a model which predicted that through-thickness shear can increase the forming limits in comparison to pure stretching. Through-thickness shear was measured experimentally in SPIF by measuring the relative displacement of points marked on the upper and lower surfaces of sheets.

The validity of making a straight forward comparison of forming limits measured by AISF to those of the bulge formability test has recently been questioned, as well as the suitability of the forming limit curve for predicting forming limits in AISF. Allwood et al [118] reported that the conventional analysis used to predict forming limits in pressing is not applicable to AISF because it assumes that strain paths are proportional throughout the process and hence can be integrated. Landert [139], Allwood et al [118] and Bambach et al [176] all concluded that the forming limit curve is not an appropriate tool for predicting the feasibility of a given part design in AISF. Emmens [177] recently discussed how the major and minor surface strains in AISF are not the principal strains, due to through-thickness shear, whereas they are the principal strains in stretching.

From the literature reviewed above it can be concluded that the reason for the increased forming limits of AISF is not yet fully understood and cannot yet be predicted. Further work should be carried out to numerically predict the cause of increased forming limits in AISF. If the reason for increased forming limits is established, the process could be designed to take advantage of this to improve the forming limits. For example, if through-thickness shear is the cause, the process parameters could be set to increase shear, possibly by modifying the tool size or friction coefficient.

2.4.6.6 Geometric accuracy

One of the most important aspects for industrial processes is the geometrical accuracy of the formed product. However, the die-less nature of the process makes it difficult to achieve a high level of accuracy and typical geometrical errors arise from undesired rigid movement of regions of the sheet, elastic springback and sheet thinning [108, 132]. Fiorentino et al [178] reported that while the formability of SPIF is higher than that in TPIF, the low geometrical accuracy is still a problem in SPIF. Micari et al [179] defined geometrical error in SPIF as the distance between the profile obtained and the ideal one. Three typical forms of geometrical error that could be found on the final product are associated with sheet bending in the region of initial tool contact, sheet lifting near the base of the sheet so that the final depth is less than the designed one, i.e. springback, and a pillow effect at the centre of the final product. Springback that occurs during and after the forming operation is the main source of the process inaccuracy. This springback may consist of local springback (occurring during deformation), global springback (after unloading and removal of clamping) and springback due to trimming (if done) [131]. For AISF processes based on a simple contour or spiral tool path

following the product geometry, the error is typically of the order of millimetres. Leach et al in 2001 [82] found that asymmetric products could be incrementally formed to an accuracy of ±2 mm, Duflou et al in 2005 [86] measured errors between 1.8 mm and 5.4 mm on a scaled down model of a solar oven cavity with flat sides and Hirt et al [137] reported a geometric error of up to 3 mm for asymmetric demonstration products formed against a positive die.

Geometric accuracy has been improved through a number of techniques. These include tool path correction, tool path optimisation, multiple pass forming, process design modifications, and the application of dynamic local heating. A tool path correction algorithm based on geometric errors that are measured or numerically predicted for a product formed with a first guess of the tool path was used by Hirt et al [83, 180] and Ambrogio et al [85, 99]. Rauch et al [181] proposed an online monitoring system in SPIF that automatically adapts the tool path based on the online measurements of the force trends to avoid failure. A similar approach has been used by Filice et al [182] where the results of forming forces are used to correct the process parameters to prevent the sheet failure. The tool path could be optimised by obtaining a tool trajectory that minimised the geometrical errors. Bambach et al [96] used a path in which the tool alternates clockwise and anticlockwise. Attanasio et al [183, 184] used a tool path of variable step-down size i.e., constant scallop height. Bambach et al [185] used what they called “conical tool path strategy” in which, the tool movement starts at the centre of the part and opens up with increasing depth until the desired diameter at maximum depth is reached. The use of a tool path in which, in the first stage, the forming tool has a vertical movement followed by a trajectory which tries to cover formed surface was proposed by Oleksik et al [186]. The final deformation can be achieved through the use

of a number of forming stages to minimise the forming force and improve the geometrical accuracy as used by Duflou et al [86], Kim and Yang [93], Young and Jeswiet [94], Hirt et al [180], Duflou et al [187], Verbert et al [188], Skjoedt et al [189] and Bambach [190]. Franzen et al [191] described the use of an additional kinematic tool which moves on the bottom surface of the sheet in a synchronised motion with the forming tool in order to improve the geometrical accuracy. A different approach, implemented through the introduction of dynamic localised heat through a laser beam or electrical heating system, resulted in a reduction in stress levels and in the springback effect, which improved the accuracy, as demonstrated by Duflou et al [192, 193], Hino et al [194] and Ghiotti and Bruschi [195]. Simple methods used to improve the accuracy include, increasing the wall angle of the first few contours to reduce the bending in the undeformed area next to the sheet flange, Ambrogio et al [84], the use of statistical analysis to obtain empirical models based on the process parameters that can predict the geometrical errors and permit minimizing them, Ambrogio et al [196], and the application of an additional backdrawing phase, after the conventional negative deformation to minimise the final profile deviation, Filice et al [197], Ambrogio et al [198].

Although all of the above techniques have been used to successfully reduce the geometric error of products formed by AISF, there is a motivation for developing simple methods that are easy to implement and compensate the associated errors and to improve geometric accuracy without compromising the flexibility of the process.

2.5 Summary

The potential of metal forming which incorporates an incremental approach to produce a wide range of manufactured products has been clearly demonstrated. A wide range of experimental, analytical and numerical analyses have been performed, both on AISF and on its more traditional ISF forerunner, metal spinning. From the literature review, a number of areas in need of further investigation have been identified.

It can be seen that forces in conventional spinning have not received as much attention as for shear spinning. The majority of the previous research on spinning has focused on the first pass in conventional spinning, clearly, the effect of subsequent roller passes on the deformation mechanics needs more attention. Additionally, the effect of using a different roller-trace in subsequent passes on stress and strain distributions has not been the subject of much investigation. Statistical methods such as Design of Experiment (DOE) and Analysis of Variance ANOVA, which can be used to identify the most critical working parameters that affect the final product quality characteristics and their optimal setting, are rarely used in conventional spinning practice, but have great potential for this type of process.

Although SPIF and other AISF processes have potential application areas that include prototyping in the automotive industry and customised products in biomedical applications, the process is still not widely applied in industry. From the findings of the above review, there are many gaps in existing knowledge of the processes. An understanding of the process mechanics is limited. The higher formability associated with SPIF processes is an area where different ideas and explanations are given. Additionally, the geometrical accuracy resulting from SPIF is not good enough, and is

regarded as unacceptable for some applications. Techniques to improve geometric accuracy generally involve time consuming numerical analyses whose implementation is complex.

CHAPTER 3:

PROCESS MODELS FOR CONVENTIONAL SPINNING

3.1 Introduction and Scope of This Chapter

Due to the complex nature of sheet metal spinning processes, research is moving towards a greater use of numerical techniques. These, for example the finite element method, enable the study of parameters that cannot easily be measured directly, such as transient strains and stresses. Additionally, they permit a prediction of dynamic instabilities that may be used to control and achieve better product quality.

Despite the extensive use of numerical modelling techniques for the simulation of metal forming processes in general, it is used in sheet metal spinning much less than experimental investigations. This is most likely due to numerical complexities associated with the localised contact between the tool and workpiece and the need for a full three-dimensional model to simulate the process. These difficulties however, no longer present a major obstacle as modern commercial finite-element software and high-power computing facilities can overcome such problems. It is now possible to complete full three-dimensional simulations of the process, including the non-linear geometric and material effects, much more quickly than for an experimental assessment. The principal requirements of any numerical simulation are to ensure that the material data, tool motion, surface interaction and lubrication conditions are reproduced accurately in the model in order to provide process data that are realistic. A numerical

modelling approach can be a very efficient tool for reducing the cost of tool design and manufacturing development time by providing a detailed insight into the deformation characteristics of the sheet that is not obvious, or obtainable, from experimental observation. The computer models of the process permit a systematic study of the influence of important process parameters such as feed rate, tool design and workpiece material.

The aim of much of the previous finite element modelling work was to study the stresses and strains generated in the process and to investigate means of reducing the simulation time. Other investigations focussed on a specific spun product. In this chapter, a general dynamic explicit finite element model for single and dual pass conventional spinning is developed and used to study the effect of roller feed rate on the axial force, radial force and thickness strain during the spinning of cylindrical aluminium cups. Also, it shows the effect of using additional passes and different types of roller on the axial force and thickness strain, which has not previously been considered. The model developed for dual pass conventional spinning is used to study the effect of roller-traces on the cumulative strain distributions during the forming of cylindrical aluminium cups. The principal contributions of the research described here are:

- The development of FE models for the analysis of conventional spinning.
- An investigation on the effect of axial feed rate on the axial force, radial force and thickness strain.
- An investigation on the effect of using subsequent roller passes on the axial force and thickness strain.

- An investigation on the effect of roller geometry on the axial force and thickness strain.
- An investigation on the effect of introducing a combination of different roller-traces on sheet thinning.

3.2 FE Modelling of Conventional Spinning Processes

3.2.1 Explicit dynamic finite element modelling

The explicit method was originally developed, and is primarily used, to solve dynamic problems involving deformable bodies. A fully explicit procedure means that the state at time (t+Δt) is determined based on information at time (t). During each increment, the initial kinematic conditions are used to calculate the conditions for the next increment. The nodal acceleration ($\ddot{u}$) can be calculated at the beginning of the increment based on dynamic equilibrium through Equation 3-1[121], the superscripts refer to the time increment.

$$\ddot{u}^{(i)} = M^{-1}(F^{(i)} - I^{(i)}) \quad \text{(3-1)}$$

where (M) is the lumped mass matrix, (F) is the vector of externally applied forces and (I) is the vector of internal element forces. Since the explicit code uses a diagonal mass matrix, the acceleration at any nodal point is determined only through its mass and net acting force, without the need to solve simultaneous equations. Therefore each time increment is computationally inexpensive to solve. The term 'explicit' refers to the fact that the state of the analysis is advanced by assuming constant values for the velocities ($\dot{u}$) and the accelerations ($\ddot{u}$) across intervals of half the time step. From a knowledge

of the accelerations, the velocities ($\dot{u}$) and displacements (u) are advanced "explicitly" through each time increment (Δt) using the central difference rule, which is used in ABAQUS/Explicit code, as shown in Equations 3-2 and 3-3 [121]. The element strain increment dε is then computed from the strain rate ε̇, the stresses are computed from the constitutive equations as shown in Equation 3-4.

$$\dot{u}^{(i+\frac{1}{2})} = \dot{u}^{(i-\frac{1}{2})} + \frac{\Delta t^{(i+1)} + \Delta t^{(i)}}{2} \ddot{u}^{(i)} \quad \text{.....(3-2)}$$

$$u^{(i+1)} = u^{(i)} + \Delta t^{(i+1)} \dot{u}^{(i+\frac{1}{2})} \quad \text{.....(3-3)}$$

$$\sigma^{(i+1)} = \mathrm{f}(\sigma^{(i)}, \mathrm{d}\varepsilon) \quad \text{.....(3-4)}$$

In order to obtain accurate results, the time increment (Δt) must be quite small so that the accelerations are nearly constant during an increment. As the time increment decreases, the analysis will require an unacceptable number of increments and computational time. In order to reduce the computational time, either "load rate scaling" or "mass scaling" may be introduced. Both techniques show a significant reduction in the processing times with acceptable computational accuracy [8, 35, 37, 199, 200]. In conventional spinning, the load rate scaling reduces the simulation time by increasing the linear velocity of the roller and the rotational speed of the mandrel by the same factor in order to maintain the specified feed rate. Mass scaling reduces the simulation time by increasing the material density. Neither load rate scaling nor mass scaling must be set too large, which would cause the inertia forces to dominate and thus affect the computational accuracy.

3.2.2 Numerical model of conventional spinning processes

As described earlier, conventional spinning involves the forming of a circular sheet which is clamped between a rotating mandrel and supporting holder. The sheet is gradually shaped over this rotating mandrel through the action of a roller that produces a localised pressure and moves axially over the outer surface of the sheet**.** In the example here the mandrel has a diameter of 118 mm, a corner radius of 3mm and rotates with a constant rotational speed of 200 rpm. An aluminium sheet blank with an original diameter of 192 mm and thickness of 3 mm is attached to the mandrel. The holder has a diameter of 112 mm (see Figure 3.1).

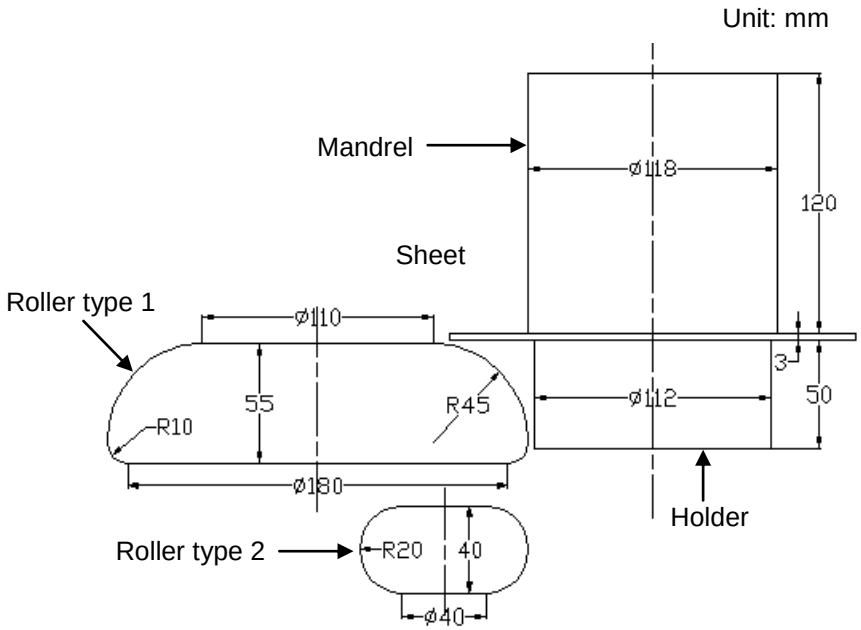

Figure 3.1: Geometries and dimensions of the models [33].

At the beginning of the FE simulation, the holder pushes the sheet forward to the mandrel with a small constant load of 100 KN in order to keep the sheet secure between the mandrel and the holder. Thus, the sheet and holder will rotate with the same mandrel speed. The sheet is spun into a cylindrical cup with an internal nominal diameter of 118

mm. The geometries and dimensions of the mandrel, sheet and type 1 roller are taken from Xia et al [39]. These conditions are also presented in two other investigations by Long and Hamilton [34] and Liu [33]. The dimensions of the type 2 roller are taken from Liu [33] and the holder dimensions are taken from Long and Hamilton [34]. These details are also shown in Figure 3.1.

The mandrel, holder and roller are modelled as rigid bodies, while the sheet is modelled as an elastic-plastic deformable body using the material properties of pure aluminium (A-1100-O). The stress strain curve for this aluminium is described by $\sigma = 148\varepsilon^{0.233}$ MPa, with an initial yield stress of 100 MPa and a mass density of 2700 kg/m^3. Isotropic elasticity is assumed with a Young's modulus of 70 GPa and Poisson's ratio 0.3 [34]. The material data are taken from Long and Hamilton [34], originally presented in Kalpakjian and Schmid [6]. Thermal and rate effects are not included in the present model. Coulomb friction is set with a friction coefficient of 0.2, 0.5 and 0.05 between the sheet and the mandrel, holder and roller respectively as assumed in [34]. Xia et al [39] did not indicate the lubrication used in their experimental study. The mass inertia of the roller is defined in order to allow the roller to rotate about its axis when contacting the sheet. Three-dimensional 8-node linear hexahedral elements (C3D8R) are used to mesh the sheet. The number of elements in an annular region in which the sheet will contact the round corner of the mandrel is increased as shown in Figure 3.2, in order to provide smooth contact between the mandrel and sheet and enhance the plastic bending deformation in this area.

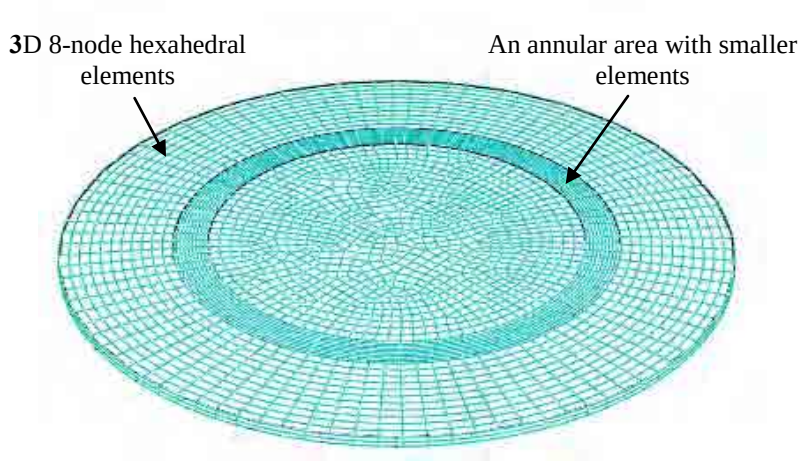

Figure 3.2: The finite element mesh used to represent the sheet.

The number of elements has been increased in several trials until merging of the results has been achieved. The mesh changed by increasing the number in the thickness direction taking into consideration the aspect ratio of the elements. Figure 3.3 shows the effect of the number of element through the sheet thickness on the history of the axial force. The number of elements in the thickness direction is two, this is the minimum number of elements required to properly reproduce the bending deformation around the mandrel corner without excessive element distortion and to get a good prediction of the maximum axial force with reasonable simulation time as shown in Figure 3.4. The total number of elements is 5968, with 9102 nodal points.

Figure 3.5 shows the finite element model and arrangement of components for the single-pass conventional spinning process. All simulations were performed on an Intel® Core™ Dual computer with a 3GHz CPU. Several values of load rate scaling were applied to reduce the simulation time. A maximum scaling factor of 21 was used, which provided a significant reduction in simulation time while maintaining a similar accuracy in the numerical results. The maximum deviation between the maximum axial force predicted by the FE model and that measured from Xia et al [39] is used to demonstrate

the accuracy of the numerical results. Using a load scale factor of 21, the simulation took 34 hours with a maximum deviation (e_f) in the maximum axial force of 3% as shown in Table 3.1.

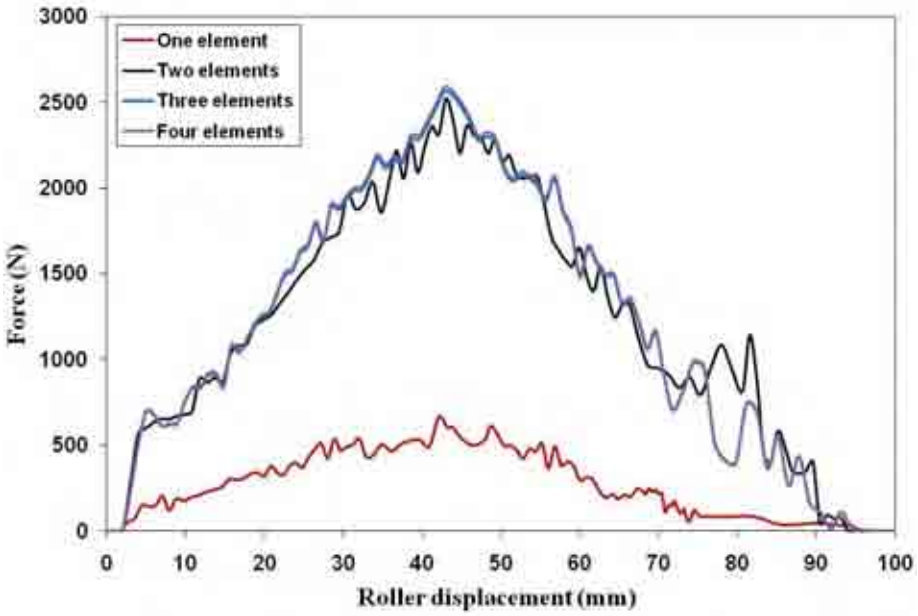

Figure 3.3: Effect of number of elements through the sheet thickness on the axial force history.

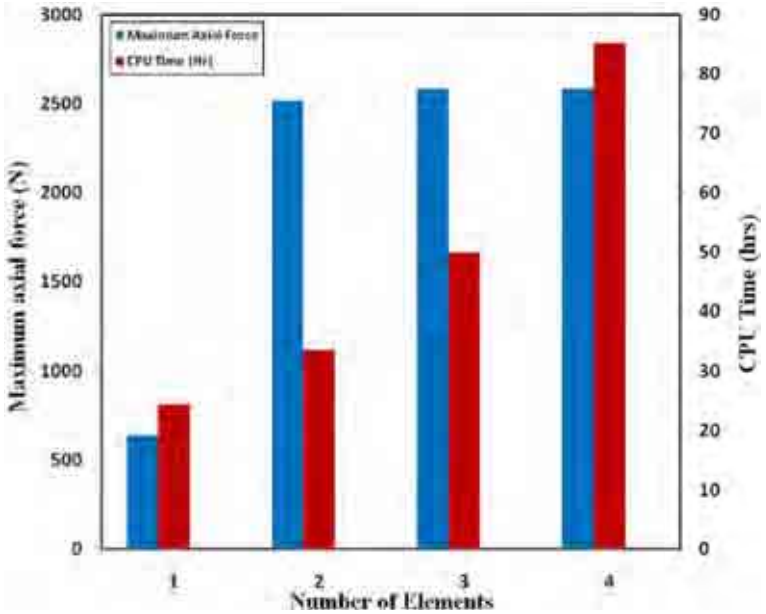

Figure 3.4: Effect of number of elements through the sheet thickness on the maximum axial force and simulation time.

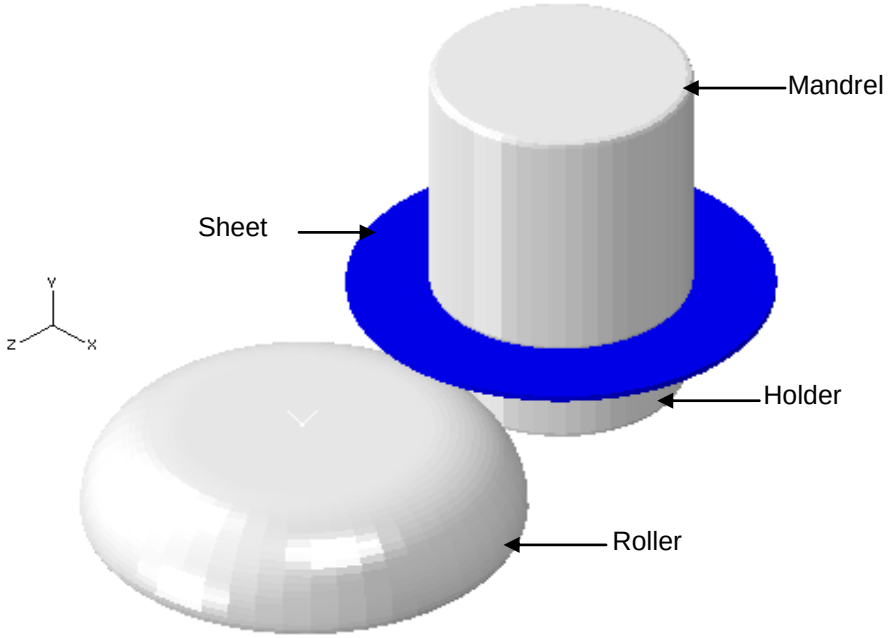

Figure 3.5: Finite element model of the single-pass conventional spinning process.

Table 3.1: Performance of the Explicit FE model under different load rate scale factors.

Performance / Scale factor	$e_{f(max)}$, %	CPU time, hrs
30	13.7	12
25	8.5	25
21	3	34
20	2.8	37

Three different cases (A, B, C) are to be simulated as shown in Table 3.2. Case A investigates the influence of feed rate in single pass spinning. Case B considers the effect of introducing a second pass in the process and case C examines the influence of changing the roller geometry in the second pass. For case B and case C, the number of passes is calculated from Equation 3-5 and Equation 3-6 [201].

$$i = \frac{h}{I_z} \quad \text{.....(3-5)}$$

$$I_z = 2 * R_r * K_t * K_\theta \quad \text{.....(3-6)}$$

Where,

h: total height of the workpiece.

I_z: Factor depends on the roller nose radius, sheet thickness and inner diameter of the final product.

R_r: roller nose radius.

K_t and K_θ are coefficients dependent on the material thickness and inner diameter of the workpiece respectively. These coefficients are calculated from Equation 3-7 and Equation 3-8 [201].

$$K_t = 0.3 + 0.23 * t_0 \quad \text{.....(3-7)}$$

$$K_\theta = 0.36 + 0.008 * d_i \quad \text{.....(3-8)}$$

Where,

t_0 is the sheet thickness and d_i is the inner diameter

By substituting the relevant values in equations 3-7 and 3-8, K_t and K_θ are found to be 0.99 and 1.304 respectively. Substituting these values in equation 3-5 and equation 3-6, gives the minimum number of roller passes as 1.93 ≈ 2. Therefore, case B and case C are dual-pass processes.

Table 3.2: The cases simulated and corresponding process conditions.

	Case		
Conditions	A	B	C
Roller type	1	1	2
No. of passes	1	2	2
Feed rate (mm/rev)	(0.5 – 1.0 – 2.0)	1.0	1.0
Rotational speed (rpm)	200	200	200

3.2.3 Validation of the finite element model

To determine the validity of the numerical models the single-pass conventional spinning process with a 1 mm/rev feed rate (case A) was selected and compared to the experimental results of Xia et al [39]. Figure 3.6 shows the progressive state of deformation and von Mises stress distribution for this case. It can be seen that for a roller displacement less than 20 mm, where there is no contact between the deforming sheet and the sides of the mandrel, the deformation state is essentially free bending. For roller displacements more than 20 mm and less 40 mm, the geometry developed during deformation closely resembles that in deep drawing. For roller displacements of more than 40 mm, the deformation state is a combination of compression and bending, where the sheet is compressed between the roller and mandrel which occurs simultaneously with the bending deformation around the mandrel corner.

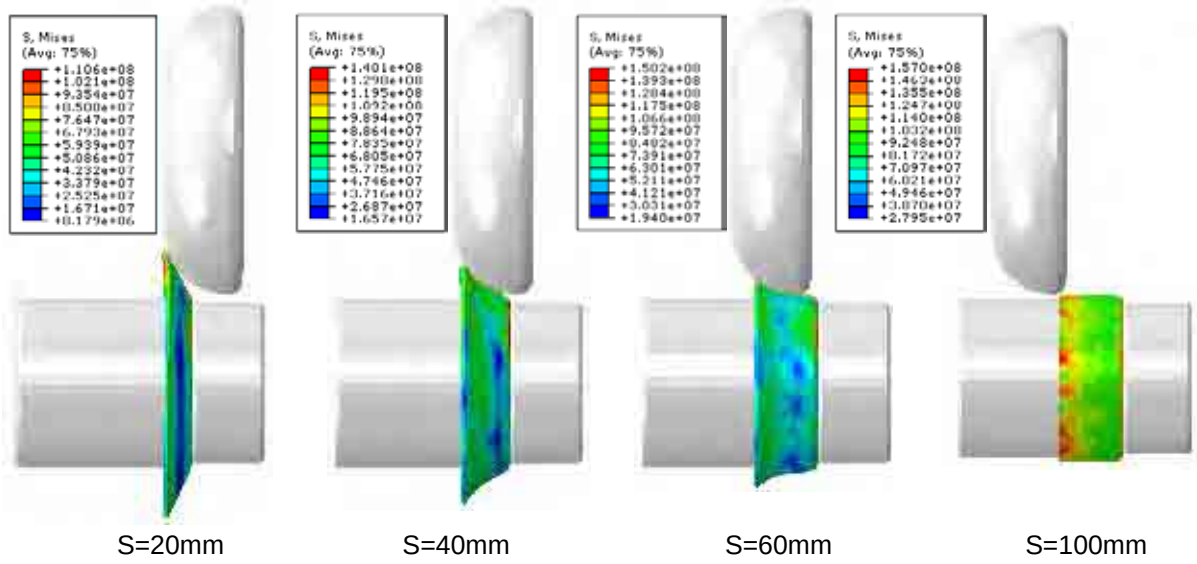

Figure 3.6: Deformation states during single-pass conventional spinning, case (A). S is the linear, axial displacement of the roller.

Figure 3.7(a) shows the shape of the fully deformed cup and Figure 3.7(b) shows a cross-section indicating the thickness distribution of the final cup. The local thinning in the corner region is evident. The distribution of von Mises stress shown in Figure 3.7(a) reveals a reasonably uniform level for much of the deformed wall of the cup, but with some variations, especially on the inner surface of the wall, towards the open end. Figure 3.7(b) shows a typical distribution of wall thickness variations in which the base of the cup held between the mandrel and holder is almost constant, while there is local thinning around the mandrel corner and slight thickening near the open end.

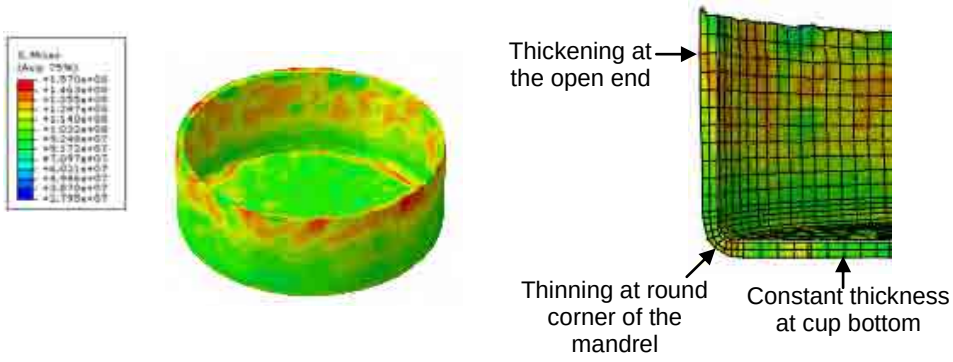

(a) (b)

Figure 3.7: (a) von Mises stress in the fully deformed cup, and (b) a section through the cup with the FE mesh superimposed revealing the local thinning.

Two assessments of the finite element results are required in order to ensure the validity of these models. Firstly, an assessment of the stability of the numerical solution must be undertaken to ensure that the solution is close to quasi-static conditions, followed by a comparison of the results to experimental data. Bai et al [8] and Liang et al [49] suggest that for the finite element model to be reliable, the maximum kinetic energy of the deformed material and the maximum artificial strain energy must both be less than 10% of the maximum internal energy. Also, the kinetic energy curve must be free of any sudden fluctuations. Figure 3.8 shows the history of internal energy, artificial strain energy and kinetic energy, and shows that the maximum kinetic energy is 7.9% of the internal energy and the maximum artificial strain energy is 9.5% of the internal energy. Therefore, the maximum values of both energy parameters are within the suggested limit.

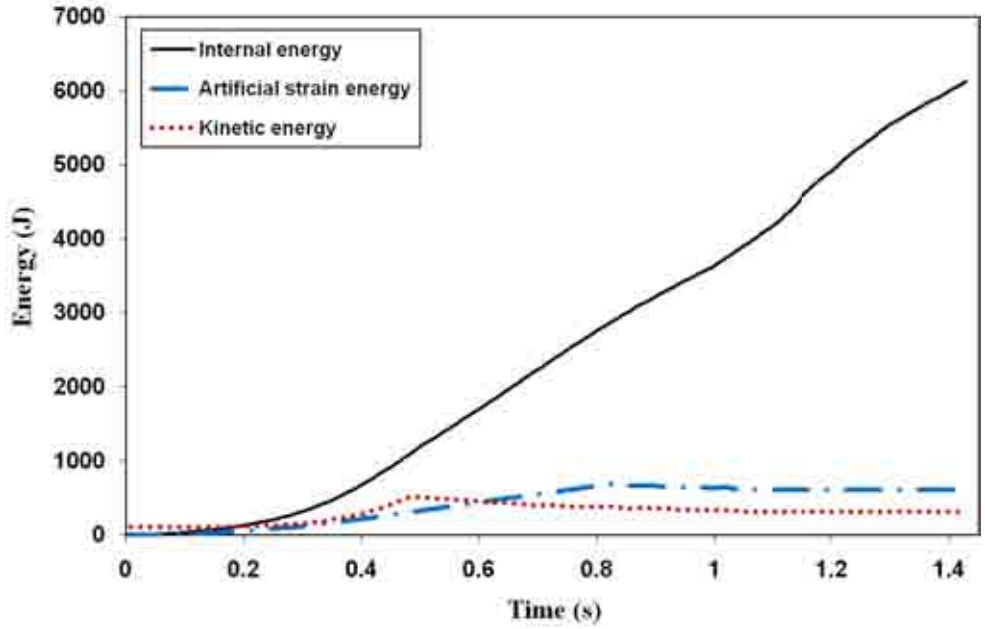

Figure 3.8: The energy history of the finite element solution.

Figure 3.9 and Figure 3.10 show the simulation results for the roller axial and radial forces compared to experimental results obtained by Xia et al [39] at 1 mm/rev feed rate for the single-pass conventional spinning process (Case A). Figure 3.9 displays the variation of axial force during the spinning process as the roller is moved axially from the initial position, at which point the roller starts to contact the sheet. As the plastic deformation increases, the axial force increases. The maximum axial force corresponds with the maximum plastic deformation that takes place near the round corner of the mandrel at approximately 45 mm roller displacement. At this stage, the deformation state is a combination of compression and bending. With further translation of the roller, the force decreases as necking occurs at the corner of the mandrel under large axial tensile stresses. This large axial tensile stress then decreases as the axial force decreases and necking does not continue. If the sheet thickness could not support the maximum axial force, fracture could take place at this region. The maximum axial force of the FE

model is approximately 2.51KN. The maximum error ratio is less than 19% and there is good agreement between the simulation and experimental force distribution.

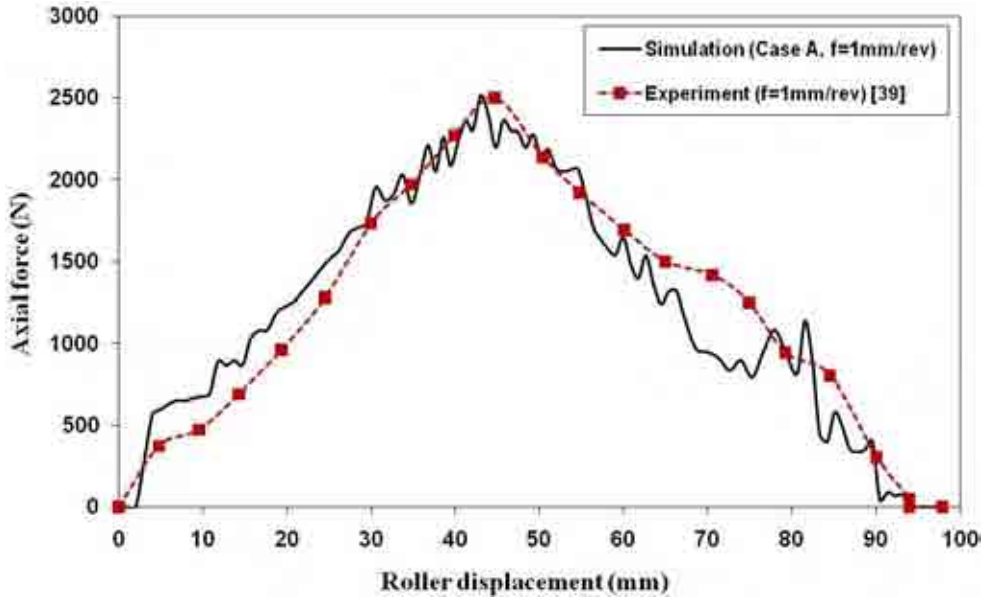

Figure 3.9: Experimental [39] and finite element axial force.

As shown in Figure 3.10, the rising trend of the radial force is similar to that shown by the axial force where the deformation state of the material is similar to free bending followed by deep drawing. The initial local maximum in the radial force at the displacement where the axial force reaches a peak is much greater, at approximately 5 kN, which is twice the value of the axial force. The FE data then suggests a reduction in the radial force followed by a further increase to a maximum of approximately 6 kN, after which there is a rapid drop as the roller reaches the end of the open cup. As a result of necking and thinning at the round corner of the mandrel due to a combination of tensile axial and circumferential compressive stresses, the material starts to flow in the radial direction, causing thickening that takes place toward the open end. This is associated with the increase in radial force after the initial local maximum. This agrees

with the findings reported by Jurković et al [202]. They concluded that the maximum radial force occurs at the end of the process. The FE model tends to over-estimate the radial force during the initial stages of deformation up to about 50 mm translation, which may be a result of not including the strain rate effect [33], but corresponds almost exactly thereafter. The maximum error ratio is about 25%.

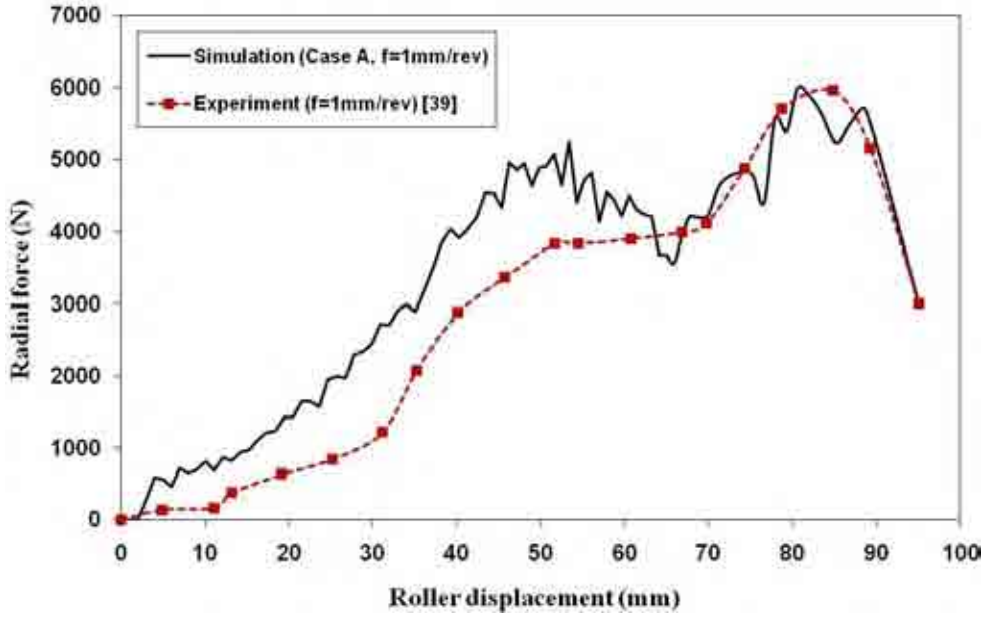

Figure 3.10: Experimental [39] and finite element radial force.

An important measure in terms of the geometric quality of the spun product is the variation in wall thickness and this is reflected in the distribution of thickness strain. Figure 3.11 shows the thickness strain along the depth of the fully formed cup measured from the cup bottom (closed end) compared to experimental results at 1 mm/rev feed rate for case A. It is clear that necking has occurred at the region contacting the round corner of the mandrel due to a large axial tensile stress in this sector, and both the FE and experimental data confirm this phenomenon. Due to the small radius of the mandrel corner and the friction (0.2) between the sheet and the mandrel, the inner layer of the

sheet in this sector is not able to slide easily around the corner resulting in compressive deformation in the bending direction. The outer layer of the sheet will have a large tensile deformation which leads to a large tensile bending stress and thinning in the sheet thickness in this sector. There is clearly excellent agreement between the FE and experimental data which, together with the assessment of axial and radial forces, provides sufficient confirmation of the validity of the FE model.

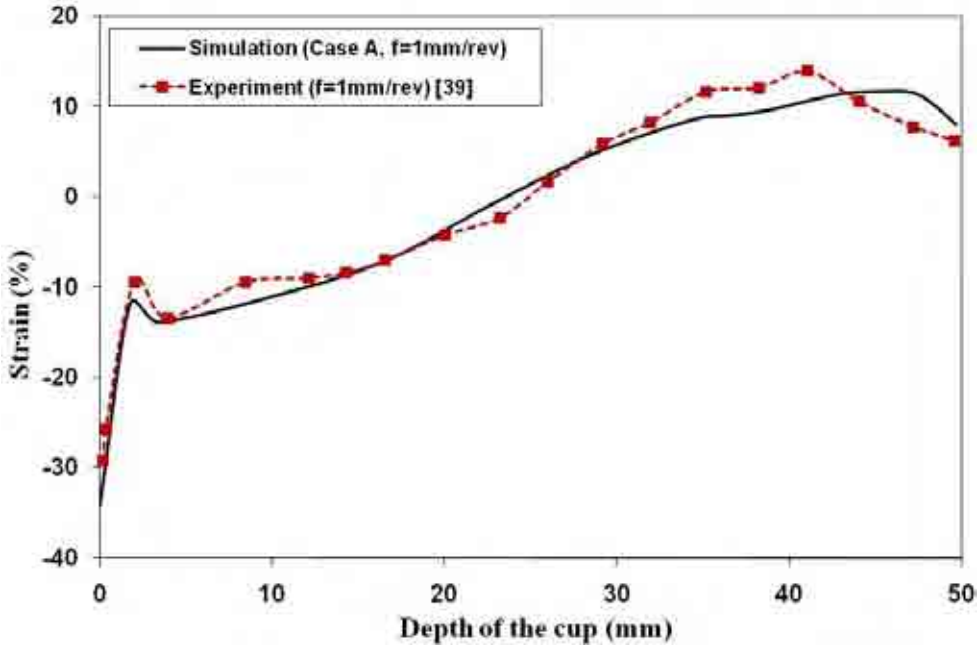

Figure 3.11: Experimental [39] and finite element thickness strain.

3.3 Numerical Investigation of Single and Dual Pass Conventional Spinning

The acceptable agreement between the FE and experimental results provides sufficient confidence to extend the numerical simulations to different processing conditions. Further work on Case A extends the assessment of the influence of the effect of feed rate on the axial force, radial force and thickness strain to include 0.5and 2.0 mm/rev, in

addition to the original case of 1.0 mm/rev. Cases B and C are models for two roller passes and for two different roller types respectively, at 1.0 mm/rev feed rate to assess the effect of roller pass and roller configuration on the axial force and thickness strain.

3.3.1 Effect of feed rate on the axial force and thickness strain

Figure 3.12and Figure 3.13 show the effect of different feed rates on the roller axial and radial forces for the single pass conventional spinning process. All three conditions show a similar variation in the force components as the roller translates along and deforms the sheet. In each case the maximum axial force occurred almost at the middle of the roller displacement while the maximum radial force occurred near to the open end at the end of the process. The general trend, that as the roller feed rate increases, the axial and radial forces increase, can be seen. Over much of the deformation process, for both force components, the relative increase in force when changing the feed rate from 0.5 to 1.0 mm/rev is much greater than the change from 1.0 to 2.0 mm/s, this is reflected in the maximum values of axial and radial forces as shown in Figure 3.14. The volume of the deformed material under the roller per unit time increases as a result of increasing feed rate. This leads to an increase in the power consumption required for the deformation and thus, the spinning forces will increase.

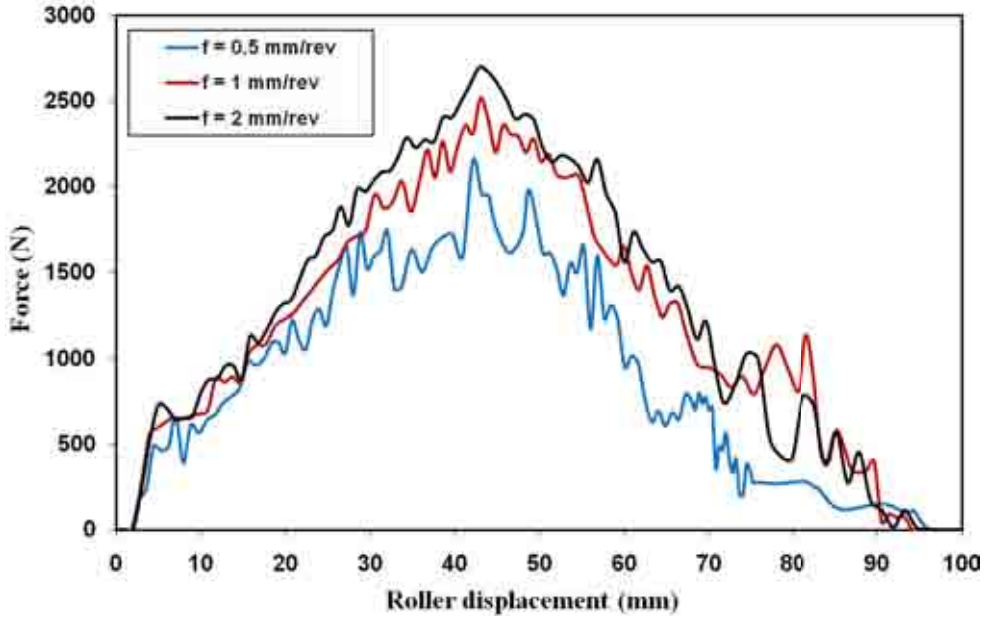

Figure 3.12: Effect of feed rate on the roller axial force for case A, (single pass roller type 1).

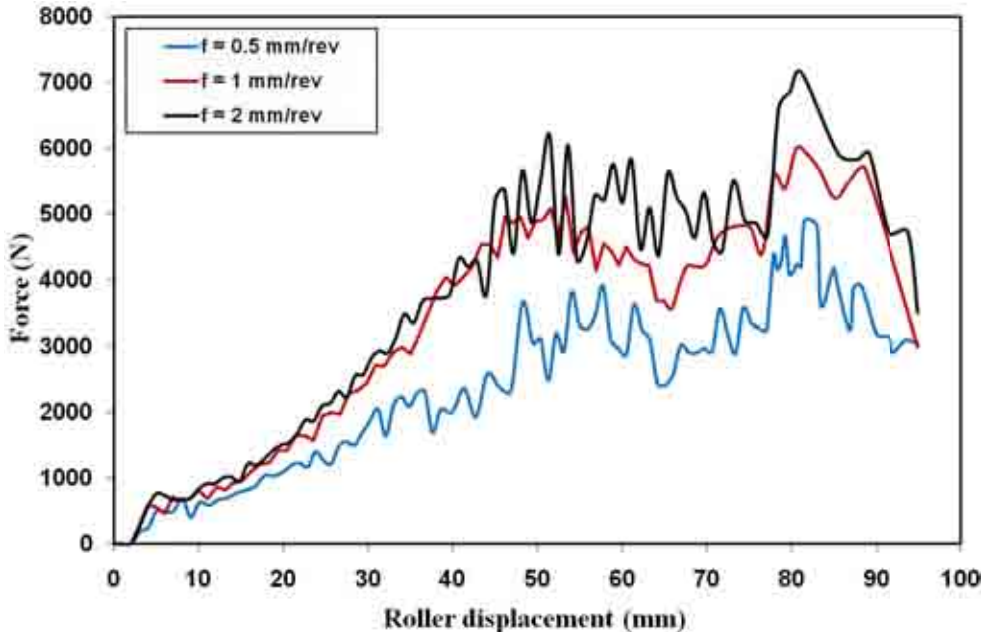

Figure 3.13: Effect of feed rate on the roller radial force for case A, (single pass roller type 1).

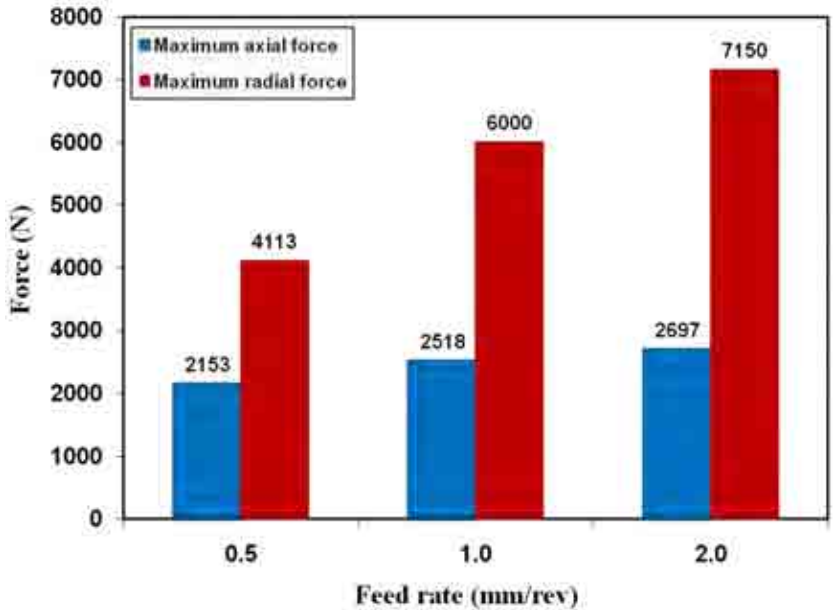

Figure 3.14: Effect of feed rate on the maximum axial and radial force for case A, (single pass roller type 1).

As shown in Figure 3.15, the thickness strain generally increases as a result of increasing the feed rate. As the roller moves toward the open end, the material is subjected to radial tensile stress and circumferential compressive stress. Additionally, as discussed before, increasing the feed rate will result in an increase in both axial and radial force. Therefore, as a result of increasing the axial and radial force, the compressive circumferential stress will increase and accordingly, the compressive circumferential deformation and thickness strain will increase. Over most of the deformation the change in thickness strain between 0.5 and 1.0 mm/rev is similar to the change between 1.0 and 2.0 mm/rev. All three curves show a drop in thickness strain, for the cases of 0.5 and 1.0 mm/rev this is quite localised near the mandrel corner, consistent with localised thinning. For the higher feed rate of 2.0 mm/rev the 'thinning' region is more diffuse, being spread over a region of about 10 mm further from the mandrel corner. This is a result of large build up of material in front of the roller, but instead, at lower feed rate, the roller tends to slide over the surface allowing material to

slide beneath the roller. This suggests that cups formed at high feed rates could be more susceptible to localised geometric defects.

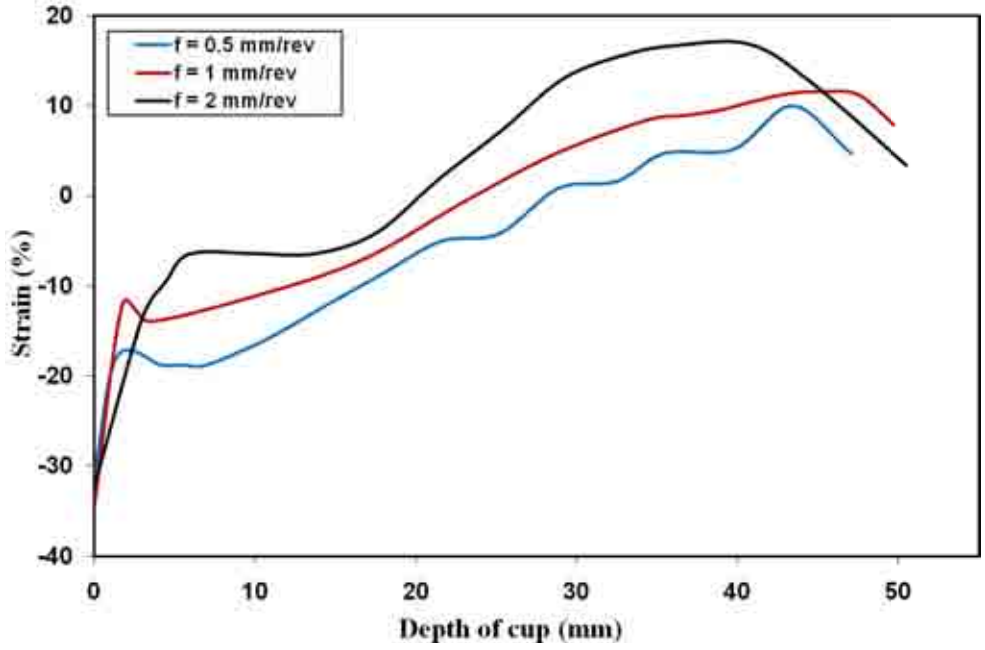

Figure 3.15: Effect of feed rate on the thickness strain for case A, (single pass roller type 1).

3.3.2 Effect of roller passes on the axial force and strain distribution

In order to improve the uniformity of the wall thickness, multi pass spinning is often recommended [17, 203]. During multi-pass spinning, a gradual combination of compressive tangential stress and tensile radial stress will be applied in the formed part and that leads to a more uniform thickness distribution. For the two dual pass spinning examples considered here, case B and case C, the axis of the roller is 45^{o} from the horizontal axis of the mandrel and sheet during the first pass, and parallel to the horizontal axis during the second pass (see Figure 3.16). Figure 3.16 shows the deformation states during the first and second passes for case B. After the second pass, the von Mises stress distribution is more uniform along the depth of the cup when

compared to the von Mises stress distribution resulting from single pass conventional spinning shown in Figure 3.7 (a).

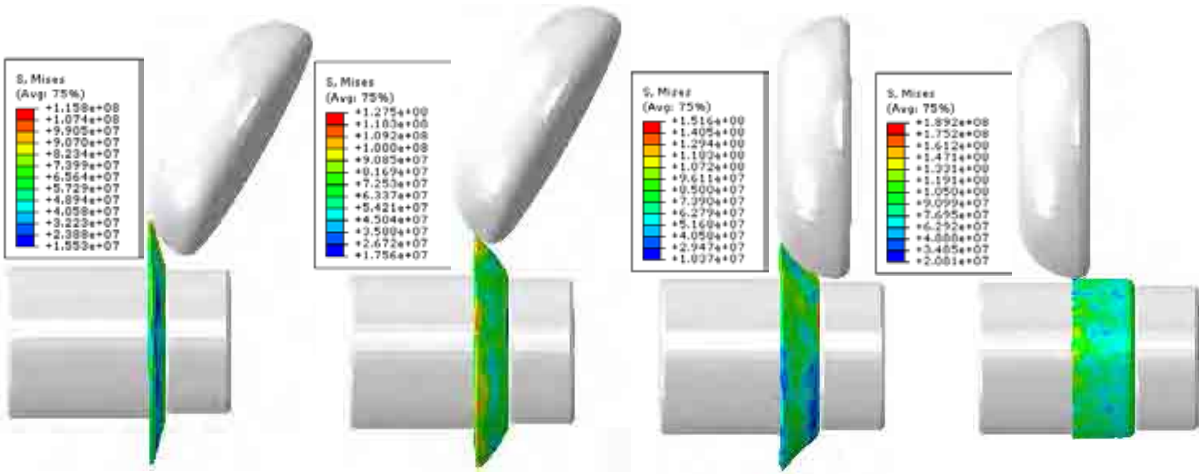

(a) First-Pass (b) Second-Pass

Figure 3.16: Deformation states during dual-pass conventional spinning with the same roller, case B, (roller type 1).

Figure 3.17 shows the axial force distribution for case A and case B. Due to the large plastic deformation and strain hardening effect, the maximum axial force in the second pass is larger than that in the first pass. During the first pass, the plastic deformation takes place around the round corner of the mandrel while during the second pass the plastic strain due to the local compression and bending deformation takes place toward the open end as shown in Figure 3.18. For the dual-pass conventional spinning example, there is some plastic deformation occurring during the first pass. Thus, the amount of plastic deformation during the second pass is not as large as the total plastic deformation required in a single pass process. Therefore, for case A and case B, it can be seen that the maximum axial force for dual-pass conventional spinning is slightly smaller than that for a single pass.

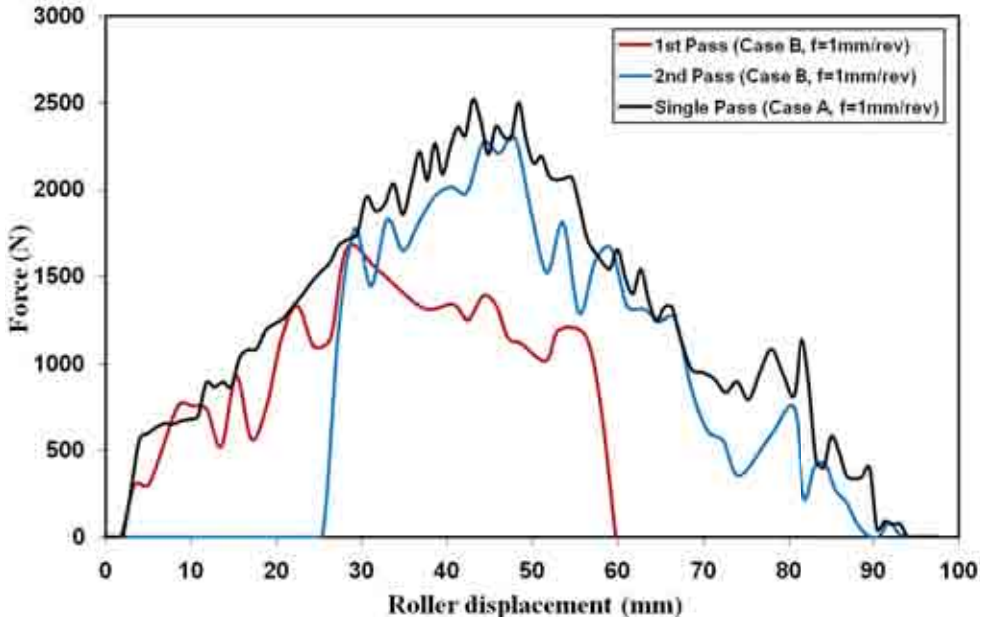

Figure 3.17: Effect of roller passes on the axial force for dual-pass conventional spinning with the same roller, (roller type 1).

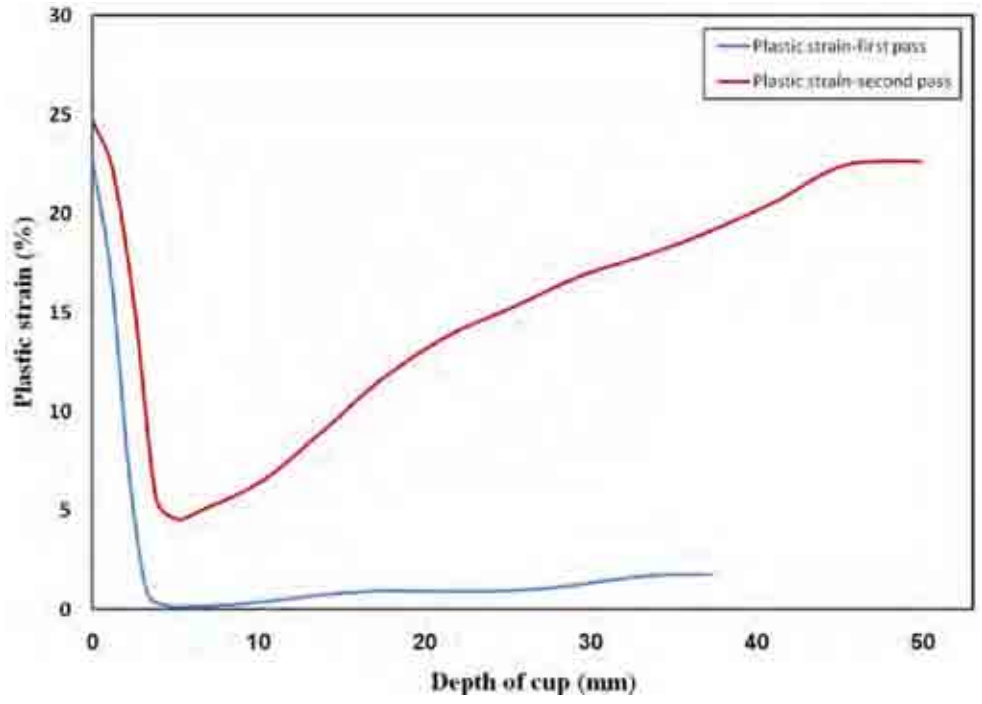

Figure 3.18: Maximum plastic strain distribution during first and second pass.

Case C is a dual-pass conventional spinning process using roller type 2. Figure 3.19 shows the deformation states and von Mises stress distribution during the first and

second pass. The roller geometry and dimensions are reproduced from Liu [4]. Figure 3.20 shows a comparison between case A and case C for the axial force. The maximum axial force in case C is about 4.6 kN and is much larger than that in case A. The large axial force is a result of using a roller with a smaller curvature and larger nose radius on the contacting surface (roller type 2), which gives a greater contact with the sheet.

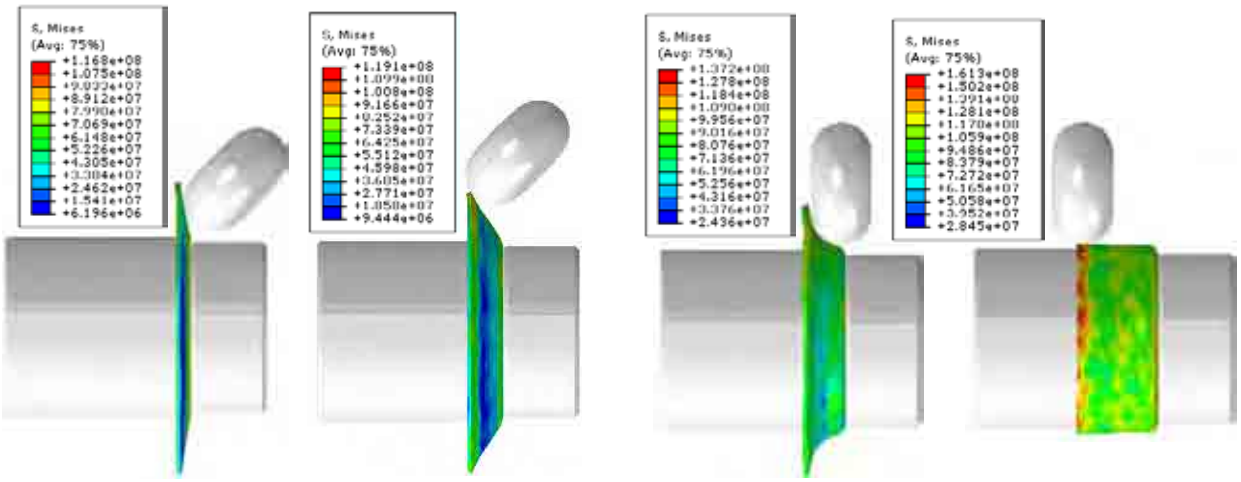

(a) First-Pass (b) Second-Passs

Figure 3.19: Deformation states during dual-pass conventional spinning with the same roller, case C (roller type 2).

This phenomenon becomes more obvious during the second pass as shown in Figure 3.19, where the deformation resembles that in ironing. Therefore, the maximum axial force during the first and second pass using roller type 2 is larger than that using roller type 1. The width of roller type 2 is smaller than that in roller type 1 and as a result, the roller nose radius in case C will contact the sheet earlier than that in case B. Therefore, the maximum force for case C during the first and second pass occurred earlier than that in case B. As the roller dimensions are decreased, it will lead to a decrease in the cost of

the tools, however, a more powerful spinning machine will be required. Therefore, selecting the optimum roller geometry and dimensions must be carefully considered.

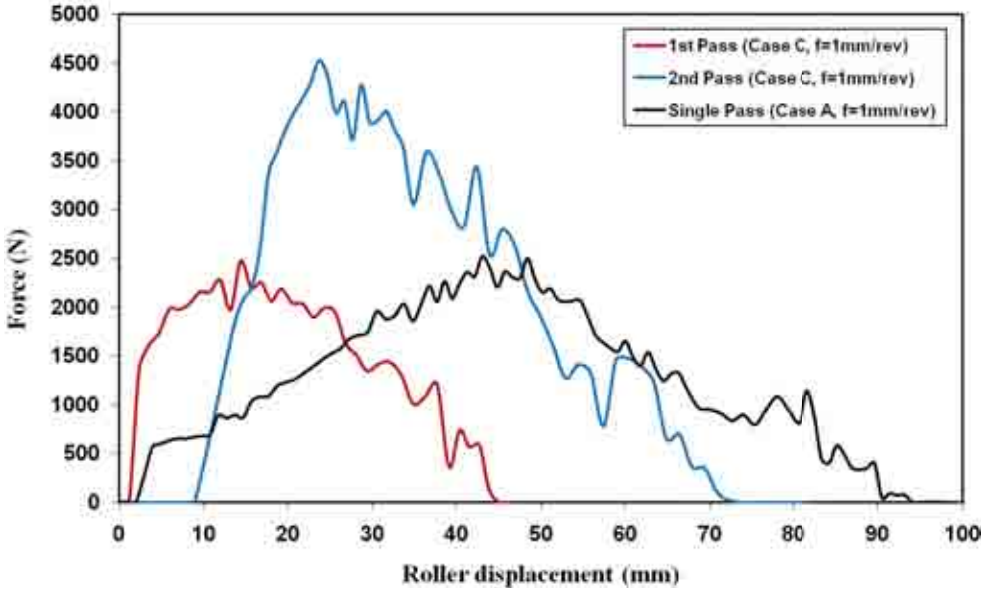

Figure 3.20: Effect of roller passes on the axial force for dual-pass conventional spinning with the same roller, Case C (roller type 2).

All three processes are compared in Figure 3.21. This shows the effect of roller profile and passes on the thickness strain. As the number of passes increases, a slightly more uniform thickness could be achieved. The thickness reduction at the region near the corner of the mandrel for case B is less than that for single pass. Although the thickness reduction is less localised for case C, the thinning is greater than that in case B due to the small roller dimensions. As a result, the thickening at the open end for dual pass cases is less than that for single pass case. Therefore, a multi-pass spinning process with suitable roller dimensions is recommended for obtaining a more uniform thickness distribution.

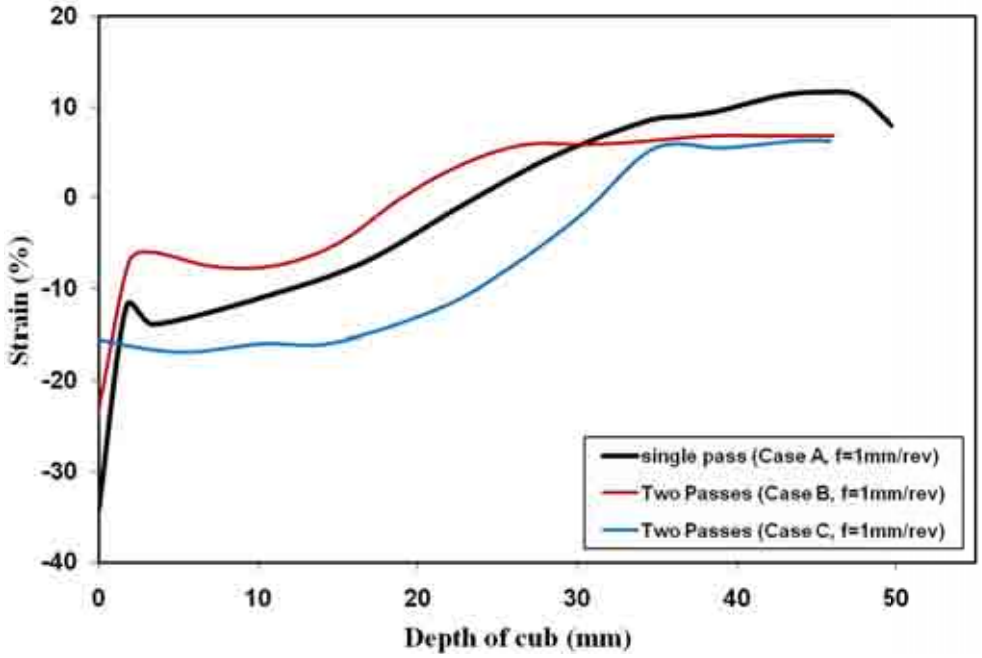

Figure 3.21: Effect of roller passes on the thickness strain.

The profile of roller type 1 is divided into two parts, these have radii of 45 mm and 10 mm as shown in Figure 3.1. The larger radius which contacts the sheet first, produces bending and deep drawing type deformation respectively when contacting the sheet. The smaller radius produces compressed bending when contacting the sheet as observed by Xia et al [39]. Therefore, it can be recognised that the strain distributions for case A and case B should display similar trends, as both cases are performed using the same roller type (roller type 1). The profile of roller type 2 has a single curvature with a 20 mm radius as shown in Figure 3.1. This profile produces bending when contacting the sheet in the first pass and ironing only when contacting the sheet in the second pass as shown in the deformation states in Figure 3.17. Therefore, as shown in Figure 3.21 for case C, the sheet thinning is greater and takes place at a further distance after the round corner of the mandrel. However, this thinning is less localised than that under roller type 1. This thinning is gradually decreased as a result of sheet thickening toward the open end.

3.4 Effect of Roller-trace in Dual-pass Cup Spinning

In cup spinning an important requirement is to control the uniformity of the wall thickness, and to do this multi pass spinning is recommended [17, 33, 203]. Multi pass spinning also leads to an improvement in both the surface roughness and forming limit [17]. During multi-pass spinning, a gradual combination of tensile radial stress and compressive circumferential stress is applied. This determines the required number of passes, the final shape and quality of the part. In conventional spinning processes, there are three main types of roller-trace paths, these are straight, concave and convex. Involute and quadratic curves are the most common types of concave and convex curves respectively.

3.4.1 Selection of roller-traces and working parameters

Many types of roller-traces could be selected, for this study the chosen roller traces are straight line, concave and convex curves. An example of a concave curve is an involute function and a suitable one for a convex curve is a quadratic function, as shown in Figure 3.22. It is important to note that the Y-axis as shown in Figure 3.22 represents the mandrel axis. In this investigation, three strategies for the process are to be simulated. In each case, during the first pass either a roller-trace of a straight line, involute curve or quadratic curve will be applied. In order to produce the final form of a cylindrical cup, the second roller-trace must, in each case, be a straight line. Therefore, during the second pass, the roller-trace for the three strategies is parallel to the mandrel axis. For accurate comparison, the initial and end points of the three roller-traces are the same along the first and second pass. Additionally, there is no contact between the sheet and mandrel wall under the three roller-traces during the first pass. The FE model

discussed in section 3.2.3 has been used and the working conditions of case B have been applied.

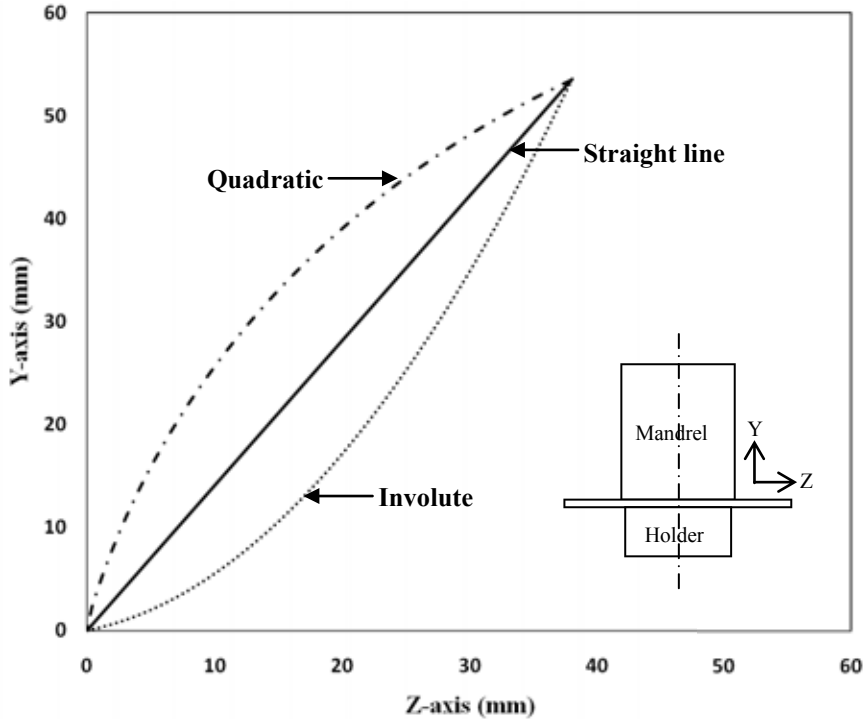

Figure 3.22: Schematic diagram for the three roller-traces curves used in the first pass.

3.4.2 Stress and strain distributions

Equivalent plastic strain and von Mises stress, in addition to strain distributions in the radial, hoop, and thickness directions, are used to examine the sheet thinning after the first and second pass of the spinning process. Figure 3.23 shows the equivalent plastic strain distribution after the first pass together with the cumulative equivalent plastic strain after the second pass. After the first pass, most of the plastic deformation occurs in a region that contacts the round corner of the mandrel at a sheet radius between 50mm and 60mm. After the second pass, most of the plastic deformation occurs along the cup wall with the highest value at the cup opening.

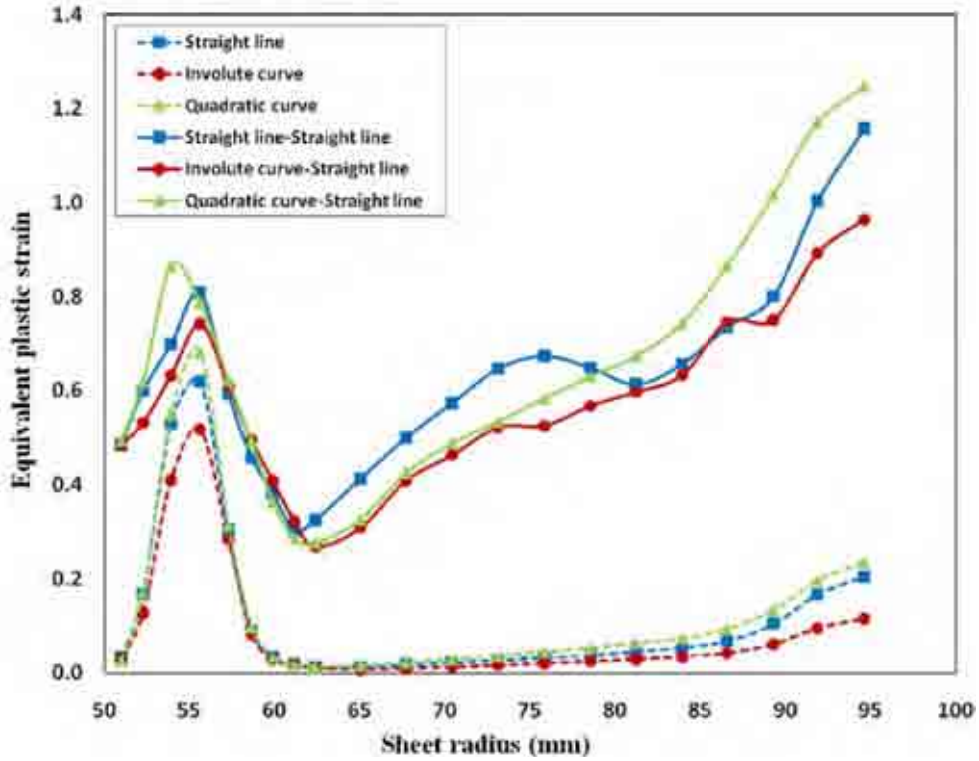

Figure 3.23: Equivalent plastic strain distributions after first and second pass.

The increase in plastic strain after the second pass at the cup wall is much higher than that at the round corner of the mandrel. The value of equivalent strain is the lowest under the involute curve-straight line strategy and highest under the quadratic curve-straight line strategy. There is good agreement between the trend of the results of the first pass and those obtained by Liu et al [22]. The von Mises stress distribution after the first and second pass is presented in Figure 3.24. A high level of stress is generated at the round corner of the mandrel compared to that at the cup wall after the first pass. However, after the second pass, a much more uniform level of stress is obtained along the sheet radius. This is because the increase of stress level at the cup wall is much higher than that at the round corner of the mandrel. A more uniform stress distribution is found using a roller-trace of involute curve during the first pass followed by a straight

line during the second pass. Greater variation in the stress distribution is found using a straight line roller-trace during the first and second passes.

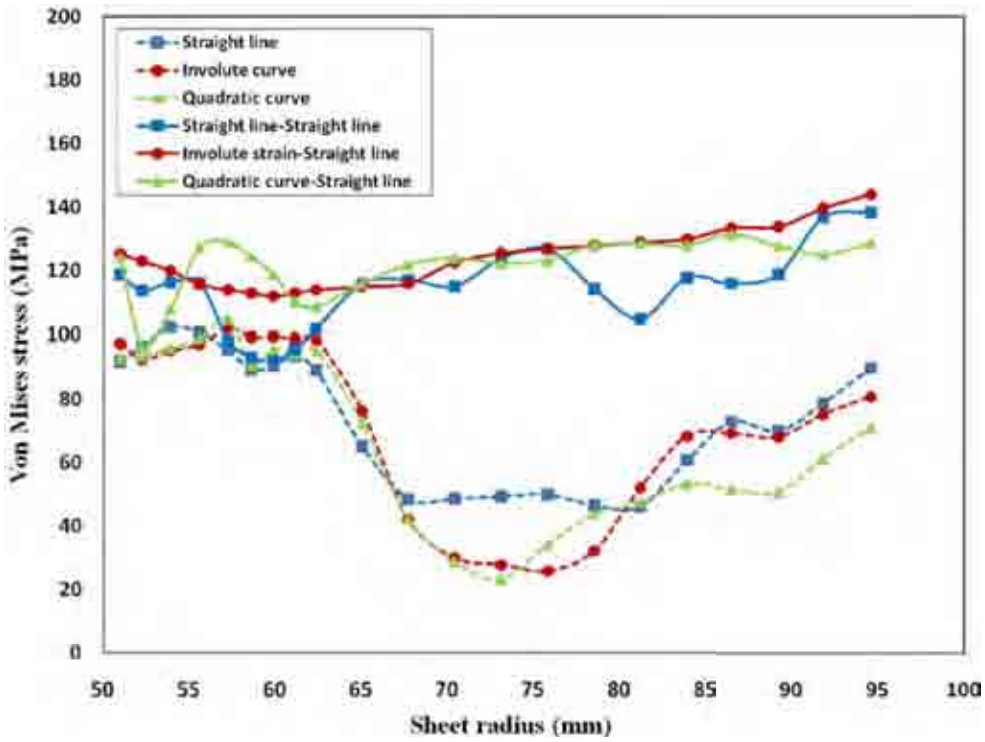

Figure 3.24: von Mises stress distributions after first and second pass.

Radial and circumferential cracks are the most common defects in conventional spinning practice. Since the equivalent plastic strain might hide the deformation behaviour in a specific direction, it is necessary to examine the strain components. Figure 3.25 shows the radial strain distribution after the first and second pass. After the first pass, a high positive (tensile) radial strain takes place at the region that contacts the round corner of the mandrel causing sheet thinning at this region. Then, the radial strain tends to be zero along the cup wall. The value of radial strain is lowest with an involute curve and highest with a quadratic curve, which agrees with the results obtained by Liu et al [22]. After the second pass, there is a slight increase in radial strain at the round corner of the mandrel followed by an increase to 0.38 at the middle of the cup wall.

Then, the radial strain decreases again toward the cup opening. The radial strain values after the second pass are lowest using an involute curve trace followed by a straight line trace.

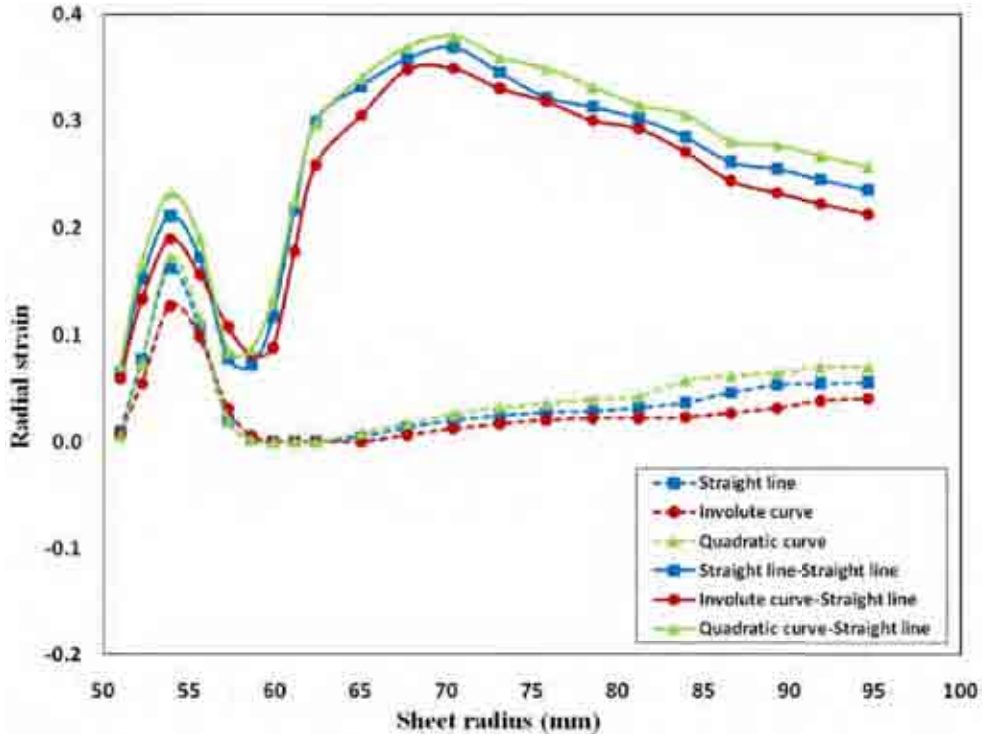

Figure 3.25: Radial strain distributions after first and second pass.

The distributions of hoop strain after the first and second pass are presented in Figure 3.26. The compressive hoop strain leads to sheet thickening which compensates for the sheet thinning that occurs due to tensile radial stresses. However, in a very recent study of multi pass conventional spinning by Wang and Long in 2011[204], it was concluded that the compressive hoop stresses at the open end should be recovered to a tensile state after roller contact to avoid wrinkling. High compressive hoop strain after the first pass is localised at the round corner of the mandrel. During the second pass, there is a slight increase in the compressive hoop strain at the round corner of the mandrel as compared with that quite increase toward the open end. Therefore, after the second pass, the sheet

thickness at the round corner of the mandrel is less than that at the open end as will be shown later. The values of hoop strain after the first pass are smallest with the involute curve and largest with the quadratic curve. The difference between the first and second pass hoop strain values are the smallest using an involute curve trace followed by a straight line trace which leads to a more uniform thickness distribution.

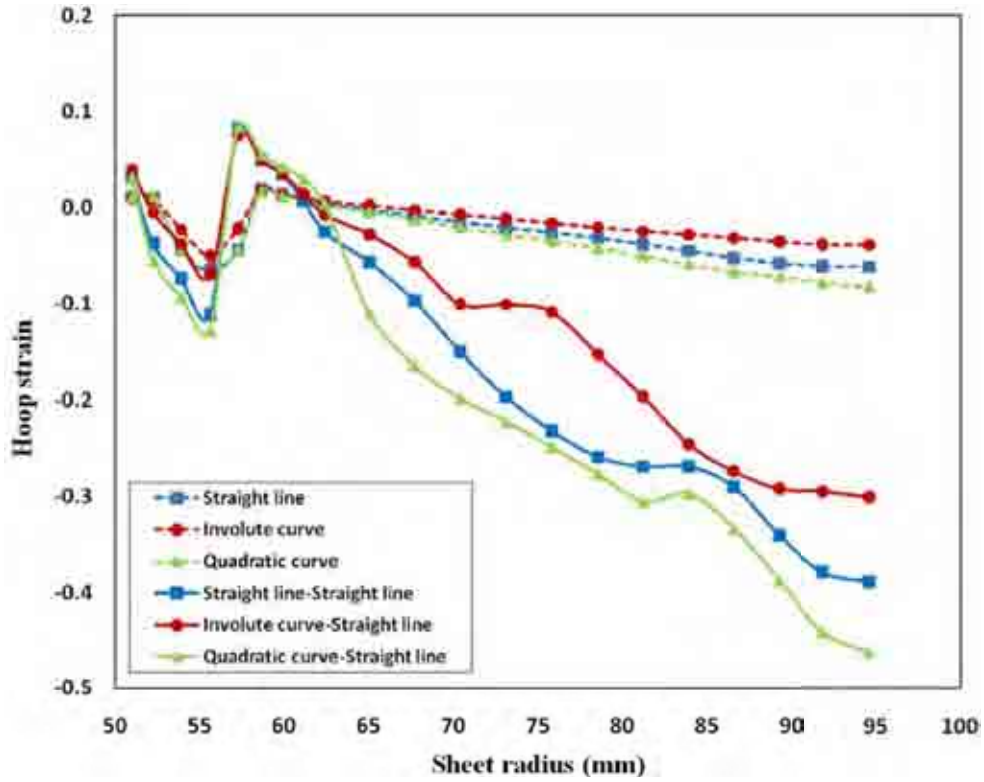

Figure 3.26: Hoop strain distributions after first and second pass.

Figure 3.27 shows the thickness strain after the first and second pass. A negative (compressive) thickness strain is located at the round corner of the mandrel after the first pass. A positive (tensile) thickness strain is located at the cup opening after the second pass. At the region that contacts the round corner of the mandrel (at a sheet radius between 50mm and 60mm), there is significant sheet thinning. This thinning decreases as the sheet radius increases and is followed by sheet thickening at the open

end. The thickness reduction at the round corner of the mandrel is lowest under the involute curve-straight line strategy and the thickening at the cup opening is highest under the quadratic curve-straight line strategy. The most uniform thickness strain distribution is under the involute curve-straight line strategy.

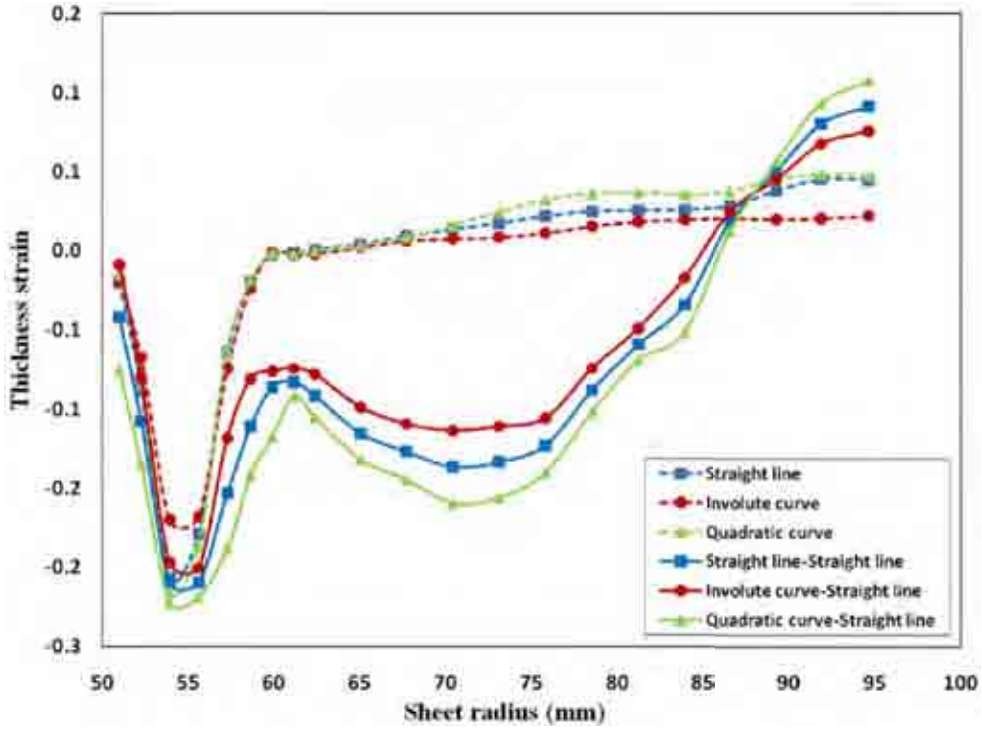

Figure 3.27: Thickness strain distributions after first and second pass.

This is confirmed by the thickness distribution shown in Figure 3.28. Less sheet thinning and a more uniform thickness distribution is obtained using an involute curve roller-trace during the first pass followed by a straight line roller-trace during the second pass. The highest sheet thinning at the round corner of the mandrel, highest sheet thickening at the cup opening and worst thickness uniformity is obtained using a quadratic curve roller-trace during the first pass followed by a straight line roller-trace during the second pass.

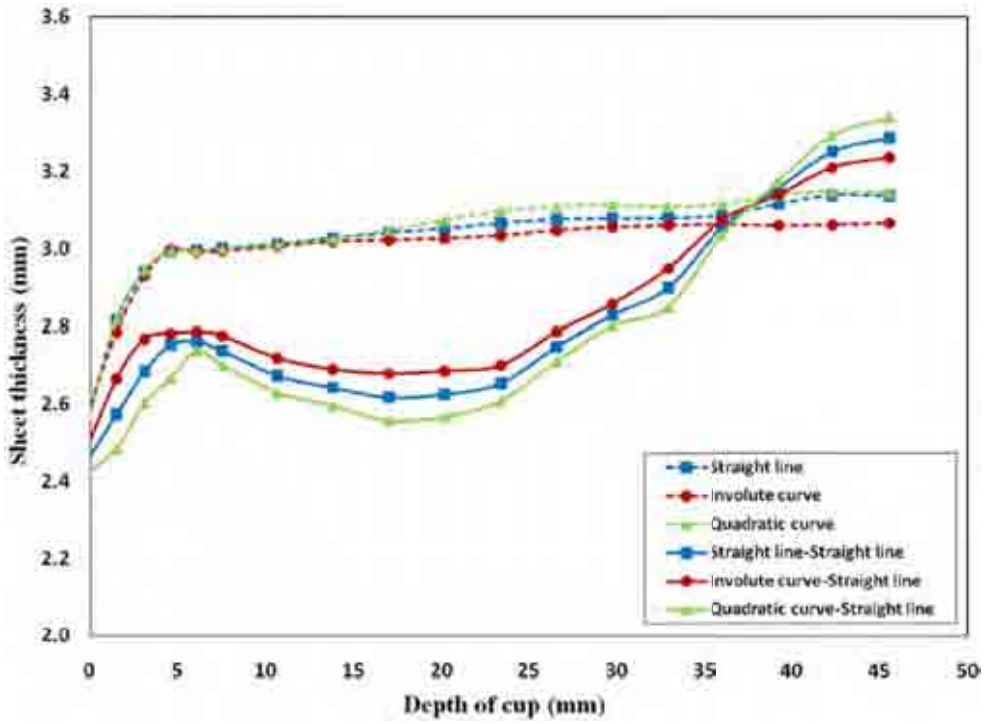

Figure 3.28: Thickness distributions after first and second pass.

3.5 Summary and Conclusions

Finite element modelling for single and dual pass conventional spinning processes has been used to simulate conventional spinning using ABAQUS/Explicit. Load rate scaling was used to reduce the simulation time. The initial model results were compared and validated against published experimental data and showed good agreement with axial force, radial force and thickness strain. The validated FE model was used to investigate the effect of subsequent roller passes and roller geometry. The effect of roller-trace and trace sequence on sheet thinning during dual-pass conventional spinning was also obtained. The simulated models show the ability for the dynamic explicit finite element code to simulate conventional spinning processes successfully. The study demonstrated the following,

- Using a load rate scale factor reduces the simulation time significantly, however, a reasonable value for this factor to achieve acceptable results should be selected.
- Increasing the roller feed rate will increase the axial and radial force.
- For the first 20 mm of roller displacement, the deformation state is similar to free bending. For the next 20 mm, the deformation state resembles deep drawing. After this, the deformation state displays the characteristics of compressed bending.
- Necking occurred at the round corner of the mandrel and as a result a thickening occurred at the open end.
- As feed rate increased, the axial force increased until the maximum plastic deformation, after which it reduced.
- After the maximum plastic deformation, the radial force increased further due to thickening near to the open end.
- The axial force in the second pass is larger than that in the first pass due to the material strengthening.
- As some plastic deformation took place in the first pass of conventional spinning, the maximum axial force in the second pass of dual-pass spinning is slightly less than that when using a single pass.
- The tool geometry has a significant effect on the axial force and thickness strain and thus, the roller dimension should be carefully selected.
- The stresses and strains generated in the second pass play an important role in the thinning of the final part. Therefore, not only the effect of the first pass is important but also the effect of subsequent roller passes.

- During the first pass, most of the plastic deformation takes place at the round corner of the mandrel. While, during the second pass, most of the plastic deformation occurs along the cup wall.
- Equivalent plastic strain, radial strain, hoop strain and thickness strain are smallest under the involute curve-straight line roller-trace strategy and highest under the quadratic curve-straight line roller-trace strategy.
- The uniformity of strain distribution is greater under the involute curve-straight line roller-trace strategy and worst under the quadratic curve-straight line roller-trace strategy.
- The least sheet thinning at the round corner of the mandrel and the most uniform thickness distribution are obtained using an involute curve roller-trace in the first pass.
- A more uniform stress distribution along the sheet radius is obtained using an involute curve roller-trace in the first pass.
- The sequence order of roller-traces controls the final part quality and thus, should be carefully designed.

CHAPTER 4:

OPTIMISATION OF CONVENTIONAL SPINNING PROCESS PARAMETERS BY MEANS OF NUMERICAL SIMULATION AND STATISTICAL ANALYSIS

4.1 Introduction and Scope of This Chapter

The conventional spinning process is affected by many process parameters such as roller feed rate, mandrel rotational speed, roller profile, number of passes and radius of mandrel. Although metal spinning was developed many years ago, much research is still conducted to optimise the process by identifying the appropriate combination of various parameters and to improve the final product quality. Not only are the stresses and strains under investigation, but also the thickness variation and other geometrical defects such as sheet thinning and wrinkling which remain as potential problems in conventional spinning practice. The key approach to avoid problems is through a careful control of relevant process parameters.

The large number of parameters that influence the conventional spinning process may be described either as machine or workpiece parameters. The machine parameters include rotational mandrel speed, roller feed rate, roller design (e.g. roller nose radius), tool surface quality and material. The workpiece parameters include sheet thickness, initial blank diameter and material properties. In addition, there are some common

measures, such as the relative clearance between the roller and mandrel, contact pressure, friction coefficient and sliding velocity [45]. It is therefore important to identify the individual parameters and also the combination of parameters that most directly affect the process performance. However, such a large number of parameters significantly increases the number of numerical experiments required to evaluate the effect of each one and their interaction. Additionally, if one factor at a time is considered, their interaction will be ignored. Statistical approaches can be used to reduce the required number of experiments and identify the important parameters and their interactions.

The use of design of experiments (DOE) and statistical analysis, for example, analysis of variance (ANOVA), have been shown to be useful approaches to study the effect of working parameters in sheet metal forming processes. Hussain et al [167], Ham and Jeswiet [169] and Filice et al [182] used Response Surface design of experiment and ANOVA techniques to investigate the effect of process variables such as feed rate, rotational speed and sheet thickness on formability in asymmetric incremental sheet forming. Using two design of experiments, Ham and Jeswiet [168] assessed the most critical variables for single point incremental forming in order to get successful deformation, i.e. no tearing or cracking. They then studied the effect of these significant variables on the process formability. Ambrogio et al [196] used statistical analysis methods by means of DOE and ANOVA to obtain an empirical model that related the process variables to the geometrical errors, i.e., springback in asymmetric incremental forming. Kleiner et al [205] used the same approaches to find the optimal working parameters to manufacture high voltage dividers by shear spinning. They concluded that

the implementation of these statistical methods was easy and an additional improvement of about 20% in process quality was gained.

The aim of much of the previous work was to investigate the individual effect of some of the process parameters on the forces generated and dimensional deviation. However, there was no justification why these particular parameters have been selected to be studied. Additionally, none of the previous work has discussed the optimisation of the process parameters in order to obtain defect-free products. In this chapter, a combination of design of experiment (DOE) and numerical simulation approaches were carried out to determine the most important working parameters in conventional spinning and to show how these parameters affect the average thickness, thickness variation, springback and axial force during the manufacture of a cylindrical cup. Additionally, using a min-max optimisation method, the optimum working parameter settings that allow the best quality characteristics to be obtained for this product are determined. The principal contributions of the research described here are:

- Determination of the most critical working parameters in conventional spinning.
- Examination of the effect of the critical working parameters on the final product quality characteristics, i.e. average thickness, thickness variation, springback and maximum axial force.
- Formation of an empirical model that relates the critical working parameters and the selected product quality characteristics.
- Determination of the optimum setting for working parameters that gives the best compromise between the mutually contradictory quality characteristics.

4.2 Plan of Investigation

In this study, two design of experiments are conducted. For the first DOE, the most important process parameters are included and the objective of this DOE is to define the most critical forming parameters in conventional spinning. The response for the first DOE is a qualitative measurement (either good, i.e. formed without defects, or a failed part). The objective of the second DOE is to show the effect of critical working parameters only on some of the process quality characteristics. The combination of the first DOE and the second DOE gives a comprehensive, in-depth analysis of the conventional spinning process and minimises the number of terms that will be used in the prediction of selected process quality characteristics. It is important to mention that in this investigation 'experiment' means an FE simulation. All simulations are performed using the FE model detailed in Chapter 3, Section 3.2.

4.3 Procedure of the Design of Experiments

To use the statistical approach in designing and analysing an experiment, it is necessary to have a clear idea of exactly what is to be studied, and how the data are to be collected and at least a qualitative understanding of how this data are to be analysed. The procedure of a 'Design of Experiment' approach is usually as follows [206]:

- Selection of the response variable
- Selection of the factors and levels
- Selection of the experimental design
- Performing the experiments
- Analysis of data
- Conclusions and recommendations

The aim of using Design of Experiments in these investigations is to investigate the conventional spinning process by determining the factors which significantly influence the process and the trend of changing the significant factors. This may lead to better control of the product quality characteristics through optimising the process factors.

The design of experiments (DOE) approach can be implemented through DESIGN EXPERT V.7, which is Windows compatible software that provides a highly efficient design of experiments procedure, and can identify the vital factors that affect the process or product. DESIGN EXPERT V.7 has many experimental design procedures such as factorial and response surface. Box-Behnken [206] is one of the response surface techniques available and has been used in this analysis. Using Box-Behnken design, each control factor is varied over three levels. Box-Behnken design was chosen as experimental runs do not need to be done at the limits of the process and the design has fewer runs than a 3-level full factorial. The design results are based on a second degree polynomial fitted by a least squares approach using Equation 4-1.

$$\hat{y} = b_0 + \sum_{i=1}^{k} b_i x_i + \sum_{i-1}^{k} \sum_{j=1}^{k} b_{ij} x_i x_j \quad \text{.....(4-1)}$$

Where b_o, b_i and b_{ij} are the model coefficients. Analysis of variance (ANOVA) is a powerful statistical tool which helps to determine whether observed differences among more than two sample means can be attributed to chance, or whether there are real differences among the means of the populations sampled. It is based upon a comparison of variance attributable to the independent variable relative to the variance within groups resulting from random chance. There are two types of ANOVA procedure, these are called One-way ANOVA (assesses the effect of one independent variable or factor)

and Two-way ANOVA (assess the effects of two (or more) independent variables or factors). The ANOVA procedure produces an *F* statistic, a value whose probability provides a means of rejecting or retaining the null hypothesis, i.e. to conclude whether or not the differences in the scores on the dependent variable are statistically significant or due to chance.

When the probability of occurrence of the *F* value is less than 0.05, we conclude that there are significant differences among groups, i.e., variation which cannot be attributed to chance. The concepts of one and two-way ANOVA are essentially the same, and the interpretation of the resulting *F*-values is also based on the same logic. The difference is that where one-way ANOVA only generates one *F*-value, two-way ANOVA generates one *F*-value for each factor and each interaction, i.e. the combined effect of the two factors.

The statistic *F* value is the ratio of treatment/factor mean square (MST) to the error mean square (MSE). If the null hypothesis is true, then the F ratio should be approximately one since MST and MSE should be about the same. If the ratio is much larger than one, then it is likely that MST is estimating a larger quantity than is MSE and that the null hypothesis is false. The procedure and methodology of one-way ANOVA is indicated in Table 4.1. As shown in Table 4.1, the sum of squares (SST) is calculated for each factor and for the error. Then, the degree of freedom DF is determined, which is equal to the number of levels minus one. It should be noticed that the error DF is equal to the total DF minus the factor/factors DF. The mean square (MS) is calculated for each factor by dividing the factor sum of squares (SST) by its DF and

for the error by dividing the error sum of squares (SSE) by its DF. Finally, the statistic *F*-value is the ratio between MST and MSE.

Table 4.1: The procedure of one-way ANOVA [206].

Source	**SS** *(Sum of Squares, the numerator of the variance)*	**DF** *(the denominator)*	**MS** *(Mean Square the variance)*	**F**
Treatment	$SST = \sum_{i=1}^{p}\sum_{j=1}^{n_i}(\bar{y}_i - \bar{y})^2$	*p - 1*	$MST = \frac{SST}{p-1}$	$F = \frac{MST}{MSE}$
Error	$SSE = \sum_{i=1}^{p}\sum_{j=1}^{n_i}(y_{ij} - \bar{y}_i)^2$	*n - p*	$MSE = \frac{SSE}{n-p}$	
Total	$TSS = \sum_{i=1}^{p}\sum_{j=1}^{n_i}(y_{ij} - \bar{y})^2$	*n - 1*		

4.4 First Design of Experiment

A selection DOE has not been used in previous investigations of spinning processes [8, 33-35, 39, 44] which would have provided a set of guidelines providing justification for the critical parameters chosen. Based on the use of a selection DOE, Box-Behnken design was used to generate a set of experiments for six process factors and each factor is varied over three levels, high level, intermediate level and low level.

4.4.1 Description of Factors, Levels and Response Variable

In conventional spinning processes, the factors that affect the product quality are feed rate, mandrel rotational speed, relative clearance between the roller and mandrel, friction coefficient, roller nose radius, sheet thickness and initial blank diameter. All these process parameters are considered in the first DOE. The levels of feed rate,

relative clearance between the roller and mandrel, sheet thickness and initial blank diameters are taken from experimental investigations by Xia et al [39]. In most previous investigations, the mandrel rotational speed is 200 rpm, and in the current study it is varied between 100 and 300 rpm, which provides a logical range. The roller nose radius used has been 10 mm whereas in this study, a further two levels at 15 and 20 mm are added. Finally, the previous published FE models used a friction coefficient of 0.05, a further two levels at zero (no friction) and at 0.1 (high friction) are used. Table 4.2 shows the different process factors and the corresponding levels.

Table 4.2: Process factors and corresponding levels.

Level / Factor	Low	Intermediate	High
Roller feed rate (mm/rev)	0.5	2.75	5.0
Mandrel revolution (rpm)	100	200	300
Relative clearance (%)	-20	0	20
Friction coefficient	0	0.05	0.1
Roller node radius (mm)	10	15	20
Sheet thickness (mm)	1	2	3
Initial blank diameter (mm)	192	198	204

The response variables are the Quality Characteristics (QC), which generally, refer to the measured results. The QC can be a single criterion (quantitative) such as pressure, temperature, efficiency, hardness, surface finish, etc. or a combination of several criteria together in a single index. The QC also refers to the nature of the performance objectives (qualitative) such as “bigger is better” or “smaller is better”. For the first DOE, a qualitative response, “amplitude of wrinkling or severe thinning” is used to

represent the forming quality or formability of the products. An index for different levels of the amplitude of wrinkling or severe thinning is shown in Table 4.3.

Table 4.3: An index for the different level of qualitative response.

Category / Response	0	1	2
Amplitude of wrinkling or severe thinning	None	Intermediate	Strong

The result of running the first Box-Behnken design is a table showing the order of implementation of the 62 experiments, which present different combinations of the previous factor levels. These combinations are assessed through the use of a 3-D FE model of the forming of a cylindrical cup by the conventional spinning process using the ABAQUS/ Explicit code. For each combination, an index for the amplitude of wrinkling or severe thinning is given. Typical results are shown in Figure 4.1.

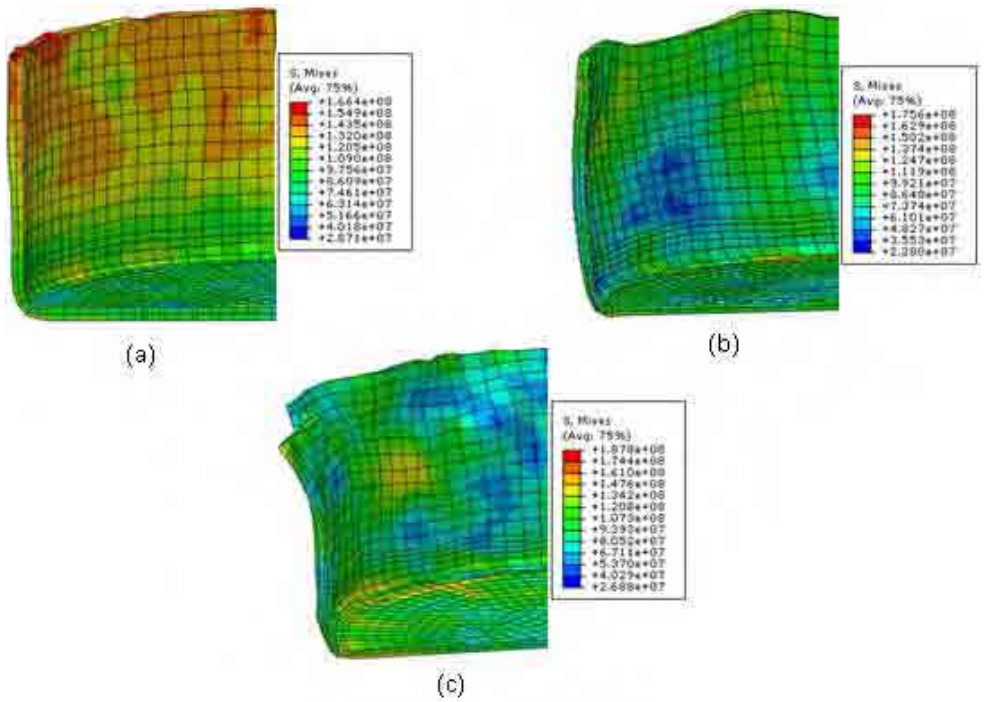

Figure 4.1: Typical results of wrinkling and severe thinning in the first DOE (a) None (index 0), (b) Intermediate (index 1), (c) Strong (index 2).

4.4.2 First DOE results

Based on the main effect model, the relationships between the process variables and response variable were estimated. The analysis of variance method was used to identify the most important factors. Values of the R-square and adjusted R-Square, a measure of model fit, showed that each of the models described the relationship between the factors and the quality characteristic reasonably, these were 92% and 90% respectively. The results of the first DOE are presented in Table 4.4 and shown in a standard factor plot (response diagram) in Figure 4.2.

The factor plot shows feed rate, relative clearance, roller nose radius and sheet thickness all have a critical effect upon product formability. The initial diameter is more likely to enhance the formability when the values are low. Mandrel rotational speed and coefficient of friction did not show any effect upon the formability.

Table 4.4: First DOE results for wrinkling and severe thinning.

Run	Feed rate (mm/rev)	Mandrel speed (rpm)	Relative clearance (%)	Friction coefficient	Roller nose radius (mm)	Sheet thickness (mm)	Initial blank diameter (mm)	Amplitude of wrinkling and severe thinning
1	0.5	200	-20	0.05	10	2	198	2
2	2.75	200	0	0.05	15	2	198	0
3	2.75	100	0	0.05	10	2	204	1
4	2.75	200	0	0	20	3	198	0
5	2.75	300	20	0.05	15	1	198	2
6	5	100	0	0	15	2	198	1
7	2.75	200	0	0.1	20	3	198	0
8	5	300	0	0.1	15	2	198	2
9	2.75	100	0	0.05	20	2	192	0

Run	Feed rate (mm/rev)	Mandrel speed (rpm)	Relative clearance (%)	Friction coefficient	Roller nose radius (mm)	Sheet thickness (mm)	Initial blank diameter (mm)	Amplitude of wrinkling and severe thinning
10	2.75	200	0	0.05	15	2	198	0
11	0.5	100	0	0.1	15	2	198	2
12	0.5	300	0	0	15	2	198	1
13	0.5	100	0	0	15	2	198	1
14	0.5	200	0	0.05	15	3	204	0
15	2.75	300	0	0.05	10	2	204	2
16	0.5	200	0	0.05	15	1	192	1
17	2.75	100	20	0.05	15	1	198	1
18	2.75	200	0	0	10	3	198	0
19	2.75	200	0	0.05	15	2	198	0
20	0.5	200	0	0.05	15	3	192	0
21	5	100	0	0.1	15	2	198	2
22	2.75	200	20	0	15	2	192	0
23	0.5	200	20	0.05	20	2	198	2
24	5	300	0	0	15	2	198	2
25	2.75	100	-20	0.05	15	1	198	1
26	2.75	200	0	0.1	20	1	198	2
27	2.75	200	0	0.1	10	3	198	0
28	2.75	200	20	0	15	2	204	0
29	2.75	300	0	0.05	20	2	204	2
30	5	200	0	0.05	15	3	192	0
31	2.75	200	20	0.1	15	2	204	1
32	2.75	200	0	0.1	10	1	198	1
33	5	200	20	0.05	20	2	198	0
34	2.75	200	0	0.05	15	2	198	0
35	5	200	0	0.05	15	3	204	0
36	2.75	200	0	0	10	1	198	2

Run	Feed rate (mm/rev)	Mandrel speed (rpm)	Relative clearance (%)	Friction coefficient	Roller nose radius (mm)	Sheet thickness (mm)	Initial blank diameter (mm)	Amplitude of wrinkling and severe thinning
37	2.75	200	0	0	20	1	198	1
38	0.5	200	-20	0.05	20	2	198	2
39	2.75	200	0	0.05	15	2	198	0
40	0.5	200	0	0.05	15	1	204	1
41	2.75	100	20	0.05	15	3	198	0
42	2.75	200	0	0.05	15	2	198	0
43	2.75	300	-20	0.05	15	3	198	0
44	5	200	-20	0.05	10	2	198	2
45	2.75	300	20	0.05	15	3	198	0
46	5	200	0	0.05	15	1	192	2
47	2.75	100	0	0.05	10	2	192	0
48	2.75	200	20	0.1	15	2	192	0
49	2.75	100	0	0.05	20	2	204	1
50	2.75	200	-20	0.1	15	2	204	0
51	2.75	300	-20	0.05	15	1	198	2
52	5	200	-20	0.05	20	2	198	1
53	0.5	300	0	0.1	15	2	198	2
54	5	200	0	0.05	15	1	204	2
55	2.75	100	-20	0.05	15	3	198	0
56	2.75	200	-20	0.1	15	2	192	1
57	5	200	20	0.05	10	2	198	1
58	0.5	200	20	0.05	10	2	198	2
59	2.75	200	-20	0	15	2	204	1
60	2.75	300	0	0.05	10	2	192	0
61	2.75	200	-20	0	15	2	192	0
62	2.75	300	0	0.05	20	2	192	0

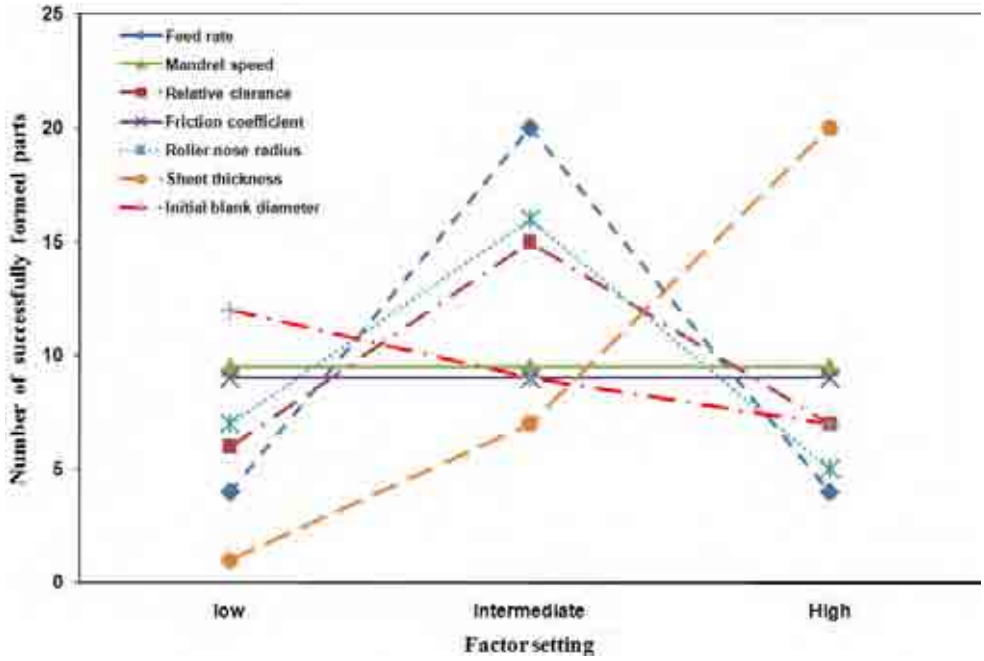

Figure 4.2: Factor comparison of working parameters used in the first DOE.

Using too low or too high axial feed rates leads to wrinkling defects. Using a too low feed rate allows the material to flow in the outer direction and using a too high feed rate causes excessive stresses in the radial and circumferential directions that lead to radial and circumferential cracking [2]. Accordingly, both results lead to wrinkling and severe thinning. Therefore, an optimum value of axial feed rate should be used to avoid this kind of defect.

The relative clearance between the roller and mandrel clearly plays an important role in the conventional spinning process. When using a relative clearance with a negative value, the distance between the roller and mandrel becomes less than the initial thickness which causes a reduction in the sheet thickness. As this negative value increases, the volume of the material to be reduced increases causing the material to build up in front of the roller. As a result, a large amplitude of wrinkling can be

observed. Using a high positive relative clearance tends to reduce the rigid contact between the roller and the sheet and allows the material to escape from beneath the roller causing dimensional and geometrical inaccuracy. Therefore, an optimum value for axial feed rate and relative clearance between the roller and mandrel should be selected in order to obtain defect-free products.

After the state of free bending deformation at the beginning of the process, the roller nose radius is completely responsible for the rest of the deformation characteristics. Using a large roller nose radius leads to an increase in the contact area between the roller and the sheet which provides forming stability [207]. However, a decrease in the contact pressure of the roller is expected and the generated stresses including the compressive tangential stress component will decrease [45]. On the other hand, it is known that compressive tangential stress will compensate the thinning caused by tensile radial stresses. Therefore, a too large roller nose radius is found to increase the severe thinning which is a result of the unfavourable large contact area between the roller and the sheet.

Sheet thickness plays a very important role in the process formability. It is known that the maximum axial force corresponds with the maximum plastic deformation that takes place near the round corner of the mandrel (cup bottom) [39]. After that, the force decreases as necking occurs at the corner of the mandrel under large axial tensile stresses. If the sheet thickness could not support these large axial tensile stresses, circumferential cracking and fracture at the cup bottom can be expected [39]. The results obtained agree with this, where only one cup is formed successfully for 1mm

sheet thickness and 5 for 2mm sheet thickness. Both results show a low formability index when compared to the 20 cups formed successfully for 3mm thick sheet.

In conventional spinning, the drawing ratio, m, is a relationship between the initial blank diameter, mandrel diameter and initial thickness as shown in Equation 4-2 [39].

$$m = \frac{D_s}{(D_m + t_0)} \quad \text{.....(4-2)}$$

Where m is the drawing ratio, D_s is the initial sheet diameter, D_m is the mandrel diameter and t_o is the sheet thickness. For a fixed sheet thickness and mandrel diameter, as the initial sheet diameter increases, the nominal drawing ratio will be increased as shown in Equation 4-2. When cups are spun with a large drawing ratio, large tensile forces are created in the cup wall and lead to an increase in the tensile stress. This results in a decrease in sheet thickness and large thinning can be observed at the cup bottom. Consequently, for the second DOE, the sheet thickness and initial blank diameter will be fixed at 3mm and 192 mm respectively in order to avoid forming defective parts and to optimise the process at fixed product dimensions.

The mandrel rotational speed and friction coefficient do not appear to influence the process formability. This agrees with the observations of previous investigations. Xia et al [39] concluded that mandrel rotational speed has no appreciable effect on the experimental results. Additionally, the friction coefficient did not show any effect on the results in previous FE models [33-35].

4.5 Second Design of Experiment

The objectives of the second DOE are to show the effect of feed rate, relative clearance and roller nose radius on the average thickness, thickness variation, springback and axial force. Additionally, to obtain an empirical model that can predict these responses for any combination of the working parameters. This will help to optimise the working parameters and obtain a final product with high quality. Box-Behnken design was used to generate a set of experiments for only these three factors.

4.5.1 Description of Factors, Levels and Response Variable

Each of the selected factors for the second DOE is varied over three levels as shown in Table 4.5. The levels of these factors are exactly the same as for the first DOE. The mandrel rotational speed, friction coefficient, sheet thickness and initial blank diameter are kept constant at 200 rpm, 0.05, 3mm and 192mm respectively. As mentioned above, the rotational mandrel speed and friction coefficient have very little effect. On the other hand, sheet thickness and initial blank diameter have been kept fixed at 3mm and 192mm respectively to avoid the production of defective parts and to optimise the process for specified product dimensions.

Table 4.5: Process factors and corresponding levels.

Level / Factor	Low	Intermediate	High
Roller feed rate (mm/rev)	0.5	2.75	5.0
Relative clearance (%)	-20	0	20
Roller node radius (mm)	10	15	20

In the second DOE, the QC's were selected to represent the product quality that involves only quantitative measurements. Quantitative quality characteristics include average thickness, thickness variation, diameter springback and maximum axial force. For each experiment, the thickness is recorded at eight points along the depth of the cup; the average thickness and standard deviation were then calculated. Standard deviation was used to indicate the thickness variation. The final inner diameter of the cup was also recorded at eight different points and the maximum deviation from the mandrel diameter was used to indicate the springback. Finally, the maximum value for the axial force was recorded for each combination.

The result of running the second Box-Behnken design is a table showing the order of implementation of the 17 experiments, which represent different combinations of the previous factor levels, as shown in Table 4.6. These combinations are used in the 3-D FE simulation of the formation of a cylindrical cup by the conventional spinning process.

4.5.2 Second DOE results

Table 4.6 shows the numerical results of the average thickness, thickness variation, springback and maximum axial force for 17 experiments. An analysis of variance (ANOVA) was performed on the design of experiments to identify the significant factors and interactions. A significance level of 5% was used.

Table 4.6: Quality characteristics for 17 experiments.

Run	Feed rate (mm/rev)	Relative Clearance (%)	Roller nose Radius (mm)	Average Thickness (mm)	Thickness Variation (mm)	Springback (mm)	Maximum axial force (N)
1	2.75	0	15	2.95	0.46	0.75	3153
2	2.75	-20	20	2.59	0.19	1.40	3716
3	0.50	-20	15	2.49	0.24	0.53	2499
4	2.75	20	20	3.04	0.58	0.80	3219
5	2.75	20	10	3.10	0.53	0.71	2861
6	5.00	20	15	3.08	0.54	1.11	3103
7	5.00	-20	15	2.74	0.33	2.06	3382
8	2.75	0	15	2.95	0.46	0.75	3153
9	2.75	0	15	2.95	0.46	0.75	3153
10	0.50	20	15	2.92	0.37	0.50	2179
11	2.75	0	15	2.95	0.46	0.75	3153
12	5.00	0	20	2.95	0.40	1.34	3748
13	2.75	-20	10	2.54	0.19	1.31	2933
14	0.50	0	10	2.86	0.28	0.44	2172
15	5.00	0	10	3.02	0.43	1.36	2912
16	2.75	0	15	2.95	0.46	0.75	3153
17	0.50	0	20	2.74	0.35	0.52	2589

In statistical hypothesis testing, the P-value is the probability of obtaining a result at least as extreme as the one that was actually observed, assuming that the null hypothesis is true [208]. The fact that P-values are based on this assumption is crucial to their correct interpretation. The smaller the P-value (less than 5%), the more important the factor. Table 4.7 shows the P-values for the significant factors and interactions. According to the value of R-Square and adjusted R-Square, the Box-Behnken statistical analysis highlighted that a quadratic model provides a very good description of the

evolution of the quality characteristics with respect to the working parameters. The R-Square and adjusted R-Square values for all responses did not go below 95%.

Table 4.7: Significant factors and corresponding P-value.

	Average Thickness	Thickness Variations	Springback	Maximum axial force
Feed rate (A)	0.002	0.016	0.001	0.001
Relative clearance (B)	0.001	0.001	0.132	0.001
Roller nose radius (C)	0.123	0.481	0.869	0.001
Significant interactions				(A*B) 0.001 (B*C) 0.001

The analysis of variance shows feed rate affects average thickness, thickness variation, springback and maximum axial force. Relative clearance affects average thickness, thickness variation and maximum axial force. The roller nose radius affects only the maximum axial force. The interactions between feed rate and relative clearance, relative clearance and roller nosed radius affect the maximum axial force. It is important to indicate that no defective products are observed and only very weak wrinkling is recognized for run numbers 3 and 7. This is a result of using a very high or very low feed rate with a large negative relative clearance. Wang et al in 2010 [209] conducted a similar study of single pass conventional spinning using Taguchi and finite element methods based on three factors only: feed rate, mandrel speed and relative clearance. It has been reported that the feed rate has a great influence on spun part dimensions which agrees with the results obtained here.

4.5.3 Average thickness

Figure 4.3 shows the effect of feed rate on the average thickness. Using a high feed rate leads to an increase in the compressive circumferential stress and accordingly, compressive circumferential deformation and an increase in thickness strain. The final average thickness will therefore deviate from the initial thickness. This agrees with results obtained by El-Khabeery et al [44]. Figure 4.4 shows the effect of relative clearance on the average thickness. It can be seen that the effect of relative clearance on the average thickness is more obvious. This is due to the fact that as relative clearance decreases (using a large negative value) large sheet thinning in the thickness direction takes place. However, decreasing the relative clearance between the roller and sheet results in a more uniform thickness distribution as will be shown later. This was also observed by Xia et al [39]. Therefore, a careful selection of the relative clearance should be taken into consideration.

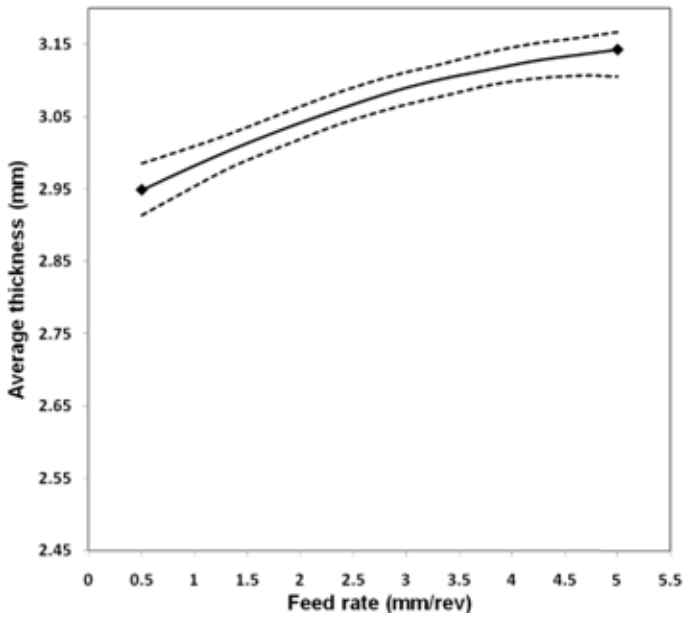

Figure 4.3: Effect of feed rate on the average thickness.

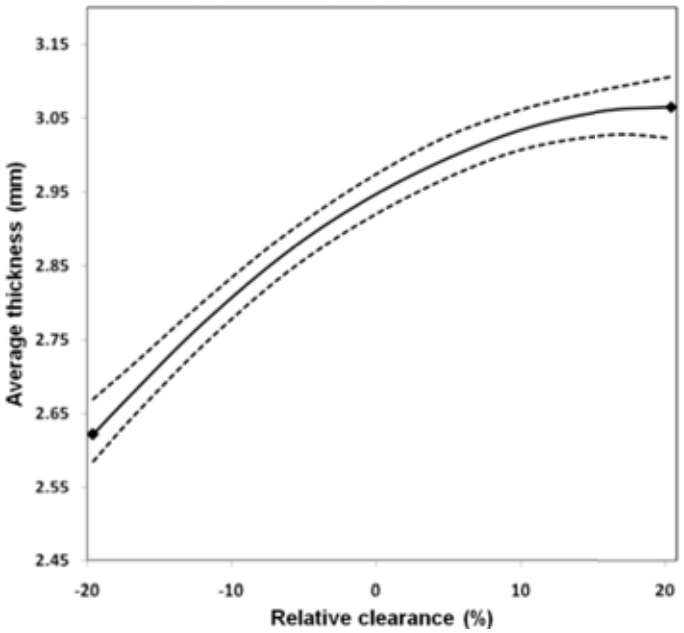

Figure 4.4: Effect of relative clearance on the average thickness.

4.5.4 Thickness variation

Figure 4.5 and Figure 4.6 show the effect of feed rate and relative clearance respectively on the thickness variation. It can be seen that both have a similar effect. In order to obtain a more uniform thickness distribution, a low feed rate and a negative relative clearance should be used. Low feed rates decrease the tensile radial stress and compressive circumferential stress and lead to more uniform distribution of these stress components along the cup wall. Therefore, a low thickness variation is found. By decreasing the relative clearance, additional plastic deformation is induced which results in the material work hardening, restricting any further thinning of the formed part. Accordingly, the differences between the earlier and later deformation decrease and thus, the thickness distribution becomes more uniform.

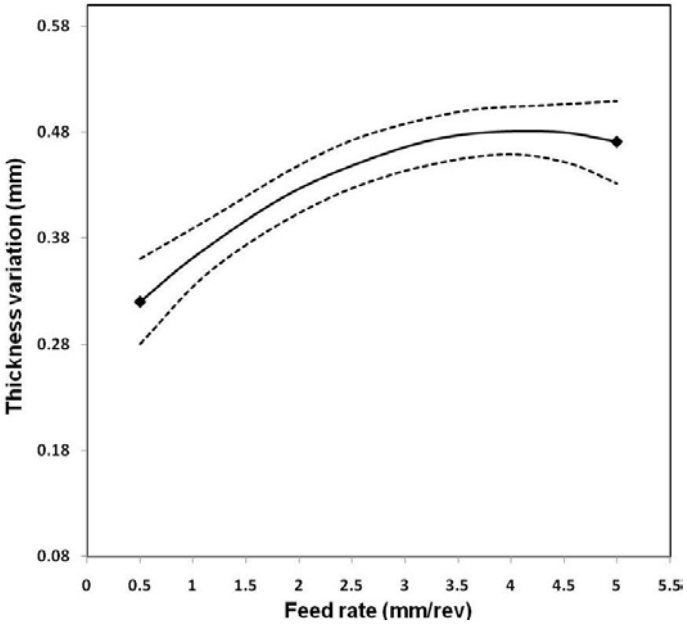

Figure 4.5: Effect of feed rate on the thickness variation.

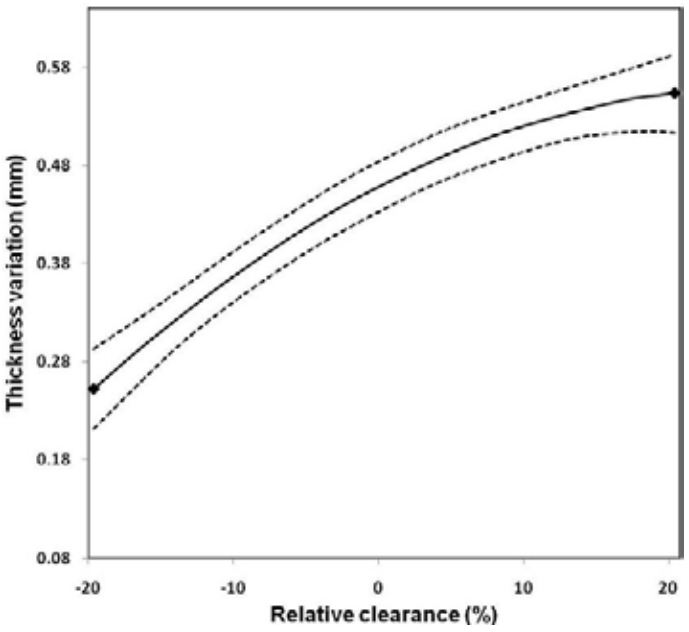

Figure 4.6: Effect of relative clearance on the thickness variation.

4.5.5 Springback

Figure 4.7 shows the effect of feed rate on the springback. As shown, increasing the axial feed rate has a significant impact on increasing springback and an increase in the inner diameter at the open end is found. It is known that a low feed rate is usually accompanied by an over-rolling between the roller and sheet material as suggested by El-Khabeery et al [44] which leads to an increase of the temperature in the deformation zone. This affects the material elasticity significantly and reduces the material recovery. El-Khabeery et al [44] reported that at a high feed rate this over-rolling does not occur and the generated temperature will be less than that at a low feed rate. Therefore, after removing the roller, springback will occur which leads to an increase in the inner diameter and bulging of the final cup. Kawai et al [210] studied the effect of feed rate on the springback in shear spinning and reported similar results. It is important to note that the maximum diameter develops near to the middle of the cup depth, which also agrees with the previous results obtained by El-Khabeery et al [44].

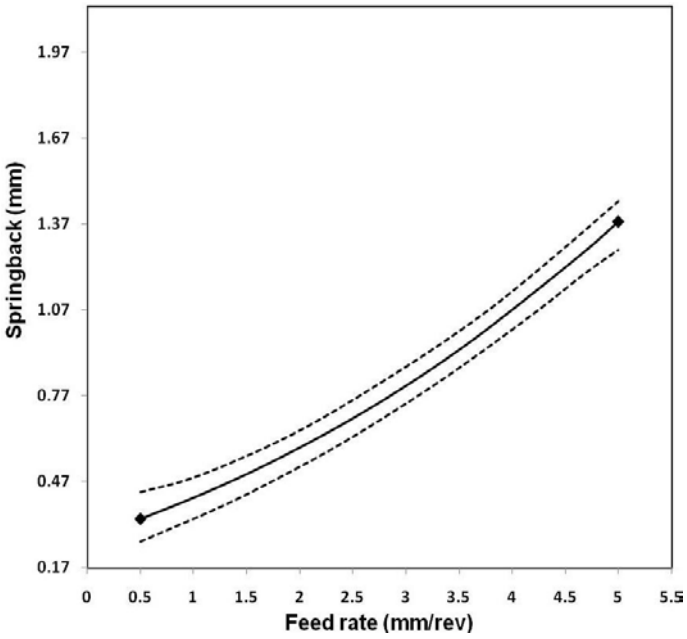

Figure 4.7: Effect of feed rate on the springback.

4.5.6 Maximum axial force

In the conventional spinning processes, the axial force is the main forming force. Figure 4.8 shows the effect of feed rate on the axial force. As the axial feed rate increases, the maximum axial force increases. An increasing axial feed rate leads to an increase in the volume of material underneath the roller per unit time. Hence a higher deformation power is required, therefore, an increase in the maximum axial force is observed. Figure 4.9 shows the effect of relative clearance on the maximum axial force. It shows that the maximum axial force increases with a decrease in the relative clearance. Consequently, a large thinning in the sheet thickness occurs and thus, the spinning forces increase. Figure 4.10 shows that as the roller nose radius increases, the maximum axial force increases. It is clear that as the roller nose radius increases, the contact area between the roller and sheet material also increases. Hence, the power, and the axial force, required to produce the cup, will be larger.

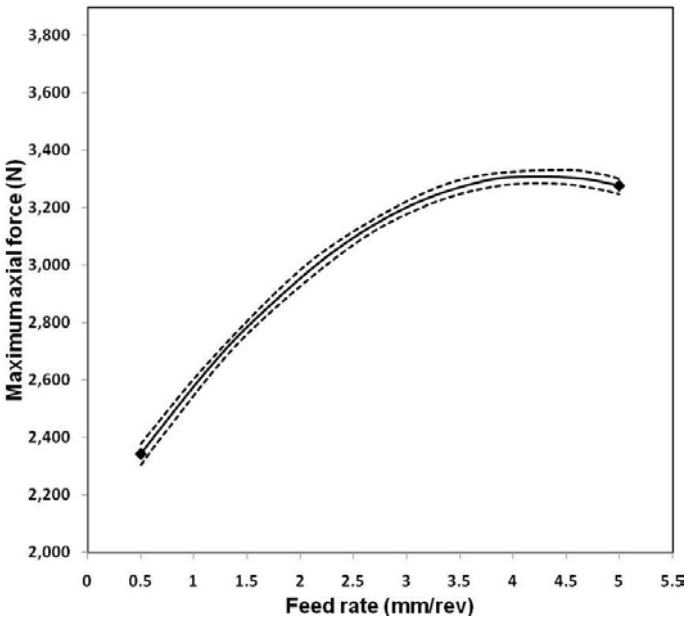

Figure 4.8: Effect of feed rate on the maximum axial force.

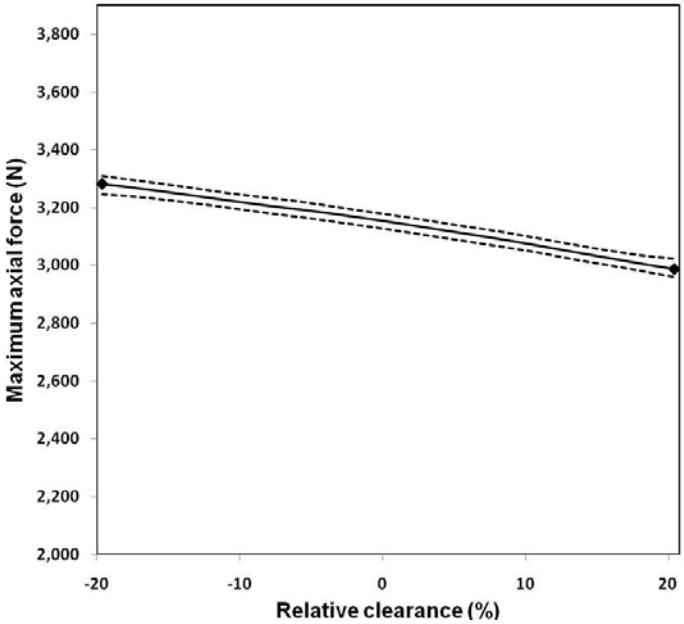

Figure 4.9: Effect of relative clearance on the maximum axial force.

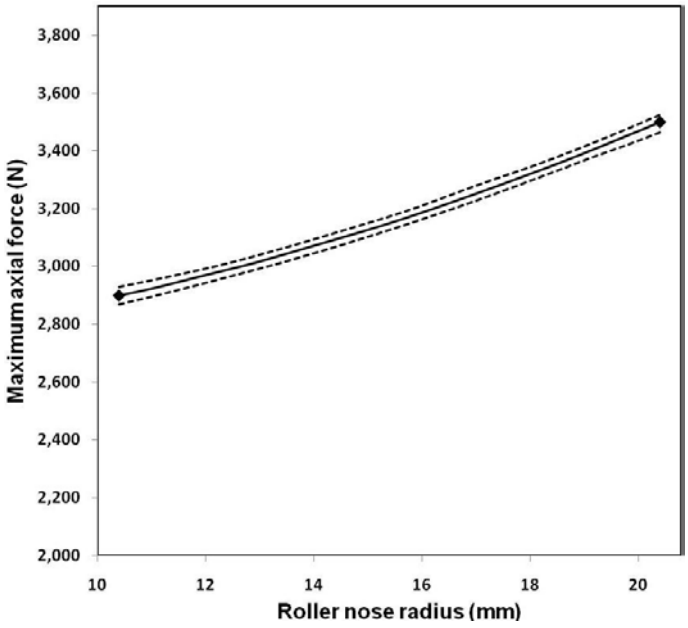

Figure 4.10: Effect of roller nose radius on the maximum axial force.

Figure 4.11 and Figure 4.12 show the effect of the interactions between feed rate and roller nose radius, relative clearance and roller nose radius on the maximum axial force. A high feed rate and large roller nose radius will increase the maximum axial force

significantly as shown in Figure 4.11. The large amount of material to be formed and large contact area that result from using high values of both factors lead to an increase the required deformation power and therefore the axial force increases. With a small roller nose radius, the relative clearance has no influence on the axial force as shown in Figure 4.12. Since the roller nose radius increases and a negative relative clearance has been used, the deformation power increases and axial force increases. This is due to an increase in the contact area between the roller and sheet material (resulting from using a large roller nose radius) in addition to a significant thickness reduction (resulting from the use of a negative relative clearance).

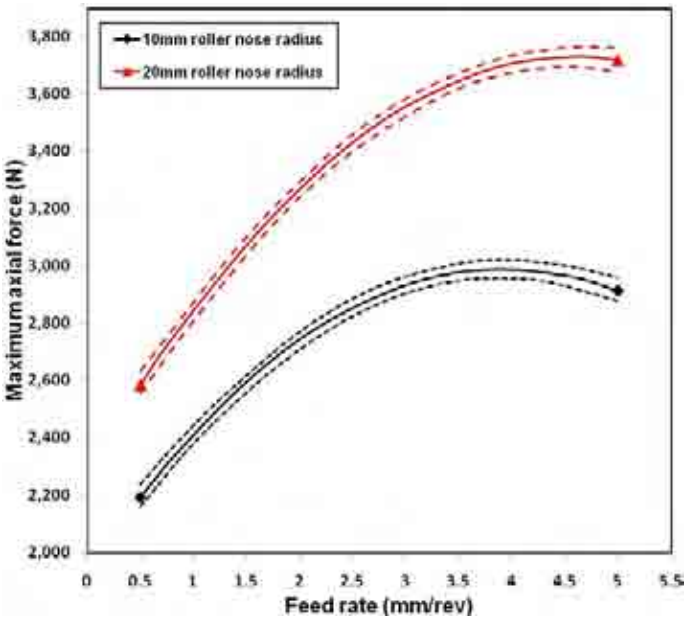

Figure 4.11: Effect of interactions between feed rate and roller nose radius on the maximum axial force.

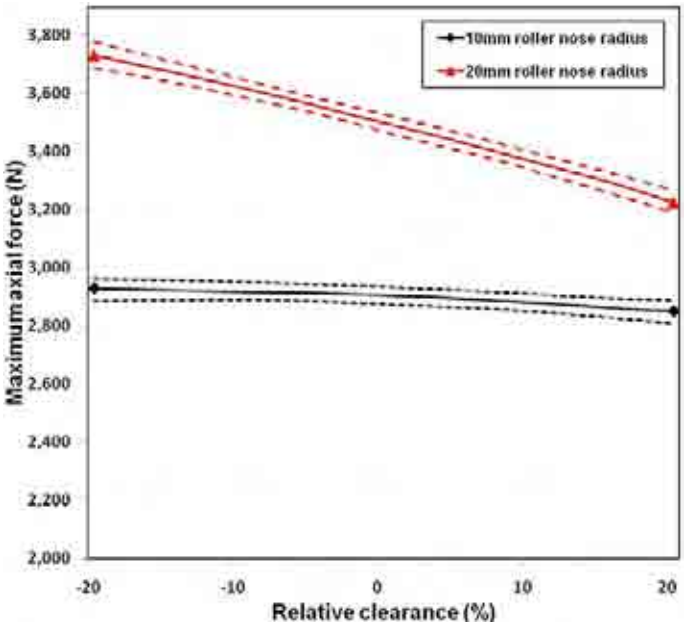

Figure 4.12: Effect of interactions between relative clearance and roller nose radius on the maximum axial force.

4.6 Prediction of Each Quality Characteristic

It is useful to develop an empirical model that allows the description and prediction of each of the selected quality characteristics under any combination of process parameters. As a result of using numerical factors in this study, it is possible to predict the equivalent quality characteristics at any value of each process parameter even if it was not one of the pre-selected levels. Using a general second order polynomial equation, an empirical model can be constructed based on the critical parameters, i.e. feed rate, relative clearance and roller nose radius and their interactions. Each process parameter and interaction is multiplied by a coefficient as shown in Equation 4-3. The value of each coefficient under each quality characteristic is displayed in Table 4.8. R-Square for all models did not go below 95%.

Quality characteristic =

$$\mathbf{X + x1*A + x2*B + x3*C + x4*A*B + x5*A*C + x6*B*C + x7*A^2 + x8*B^2 + x9*C^2} \quad \text{.....(4-3)}$$

Where, A is the feed rate, B is the relative clearance between the roller and mandrel, C is the roller nose radius and x_1: x_9 are the model coefficients indicated in Table 4.8.

Table 4.8: Coefficient values corresponding to each QC.

	Average thickness (mm)	Thickness variation (mm)	Springback (mm)	Maximum axial force (N)
Constant (X)	2.688E+00	-1.336E-01	1.027E+00	1.980E+03
x_1	6.333E-02	1.359E-01	2.303E-01	4.406E+02
x_2	1.663E-02	6.729E-03	4.306E-04	8.011E+00
x_3	2.044E-02	4.586E-02	-1.206E-01	-2.201E+01
x_4	-5.000E-04	-3.333E-04	-5.111E-03	2.278E-01
x_5	1.111E-03	-2.222E-03	-8.222E-03	9.311E+00
x_6	-2.750E-04	1.250E-04	7.286E-19	-1.063E+00
x_7	-6.667E-03	-1.259E-02	2.247E-02	-6.807E+01
x_8	-2.719E-04	-1.531E-04	4.656E-04	-4.406E-02
x_9	-9.500E-04	-1.250E-03	4.750E-03	1.875E+00

4.7 Optimisation of Working Process Parameters

In order to obtain a spun product with high dimensional accuracy and high surface quality, the optimal working conditions should be selected. In this study, the objective function is to obtain a final product that has a thickness closest to 3mm, minimum thickness variation, minimum springback and zero amplitude of wrinkling or severe thinning. Since there are no observed defective parts at 3mm sheet thickness, the last

objective function will be excluded. The objective function for the maximum axial force is ignored where it does not represent any dimensional or surface quality. All process parameters are constrained within their pre-selected levels and all quality characteristics given the same weight. Using a Min-Max optimisation method, the optimum working parameters that achieve all the objective functions are obtained as shown in Table 4.9. This is achieved by solving the three empirical equations of average thickness, thickness variation and springback together until the values of working variables that meet all objective functions (i.e., 3mm thickness, minimum thickness variation and minimum springback) are found.

Table 4.9: Optimal working parameters.

	Axial feed (mm/rev)	Relative clearance (%)	Roller nose radius (mm)
Optimal condition	0.62	-7.33	10

To validate this approach, a single numerical experiment using the optimal working parameters was performed using the same 3-D FE model. All quality characteristics were measured and compared to those predicted by the model as shown in Table 4.10. No amplitude of wrinkling or severe thinning has been observed. The desirability function, a function that shows how the different quality characteristics meet all the required objective functions is applied for all experimental runs and the optimal condition. For the spun components of the second Box-Behnken design, overall desirabilities between 0 and 66% are observed. For the optimal working setting, an overall desirability of 88% was observed as shown in Figure 4.12. Hence, compared to

the best spun component from the 17 experiments, an additional improvement of more than 22% could be gained as shown in Figure 4.12. It is important to notice that working parameters obtained are valid only under the preselected sheet dimensions. However, for different sheet dimensions, only the last 17 experiments are required to be conducted using these new dimensions rather than the whole procedure.

Table 4.10: Predicted and observed QC's at the optimal working parameters.

	Average thickness (mm)	Thickness variation (mm)	Springback (mm)	Maximum axial force (N)
Predicted	2.73	0.20	0.44	2266
Observed	2.74	0.22	0.46	2204

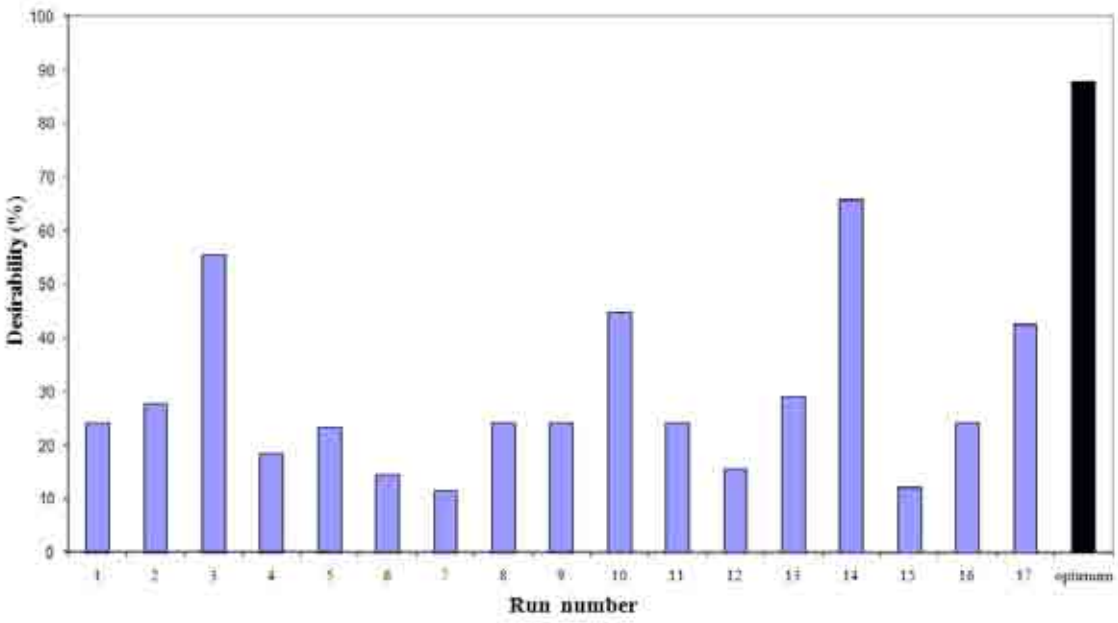

Figure 4.13: Comparison between the desirability of second DOE runs and optimal working condition.

4.8 Summary and Conclusions

- Using the design of experiments (DOE) approach, an experimental plan was generated and conducted through numerical simulation of the spinning process. The results were assessed using an analysis of variance (ANOVA) technique to identify the most critical working parameters.
- It was observed that the feed rate, relative clearance between the roller and mandrel, roller nose radius and sheet thickness were the most critical variables affecting the process formability, i.e. ability of forming without wrinkling or severe thinning. The initial sheet diameter, whilst important, had less effect. The rotational mandrel speed and friction coefficient had no observable effect upon the process formability.
- For each of the responses, i.e. average thickness, thickness variation, springback and maximum axial force, significant parameter interactions were identified and a mathematical model was fitted which described the influence of the machine factors reasonably well.
- As feed rate increased, the average thickness, thickness variation, springback and maximum axial force increased. A negative relative clearance decreased the average thickness, reduced the thickness variation and increased the maximum axial force. A large roller nose radius resulted in a large contact between the roller and sheet material which lead to an increase in the maximum axial force.
- The min-max optimisation method allowed the identification of a parameter setting which gave the best compromise between the mutually contradictory quality characteristics.

- The numerical models suggested that producing a cylindrical cup with this parameter setting resulted in an optimal component. An additional advantage of this optimisation approach is the flexibility with respect to customer requirements.
- This approach allowed an examination of components with the selected sheet dimensions without the need to perform additional numerical experiments. For new sheet dimensions, only a sub-set of the simulations would be required to be conducted.
- The statistical methods described in this chapter are easy to use and to implement. The proposed design of experiments, analysis of variance and min-max optimisation procedure is applicable to any forming process.

CHAPTER 5:

AN EVALUATION OF DEFORMATION MECHANISMS IN SPIF USING A DUAL-LEVEL FE MODEL

5.1 Introduction and Scope of This Chapter

In moving from a traditional process, single point incremental forming (SPIF) has been chosen as an example of a modern development in methods of incremental forming. Despite extensive research in single point incremental forming over the last decade, the deformation mechanics are not fully understood and accurate models to determine the behaviour through the thickness of the sheet have not been provided. At present, the phenomena associated with through-thickness modes of deformation and the existence of through-thickness shear, are not clear. An understanding of the deformation mechanism is important to allow accurate numerical models to be developed for tool path design and process control. Additionally, such information will help to develop an understanding of the increased forming limits observed in SPIF in comparison to conventional sheet metal forming processes. The nature of the process and the level of detail required makes SPIF a challenging process to simulate. The aim of this chapter is therefore to develop an accurate means of modelling the process and hence provide new insights into the deformation mechanics of sheet metals in SPIF.

5.2 State of the Art

Knowledge of the process mechanics is crucial to understand how the final properties of the part made by AISF develop and to identify the process forming limits. Many of the previous investigations have focused on an analysis of deformation mechanics through experimental investigations or by using the finite element (FE) method. The work however, is contradictory with different views on the detailed deformation modes. In the analysis of stress and strain history reported by Bambach et al [89], Hirt et al [155] and later Ambrogio et al [173], it was suggested that stretching and thinning are the dominant modes of deformation and all shear strain components through the thickness are negligible. Conversely, the experimental measurements of Allwood et al [118] indicated that high values of transverse shear are present through the thickness. Jackson and Allwood [161] also showed experimentally a significant value of through-thickness shear in two planes. One of these planes is perpendicular to the tool movement and the other is parallel to the tool direction. They suggested that this shear strain could be a major contribution to the increase in the forming limit of the material in this process. Analysis of crystallographic deformation texture and grain deformation by Eyckens [211] and Bosetti and Bruschi [212] provide a global overview of deformation texture and confirm the observation of Jackson and Allwood [161]. However, a quantification of through-thickness shear strain was very difficult and has not been attempted.

Several previous investigations were carried out to study the effect of process parameters on the final product geometry and accuracy, and to validate FE results. It is apparent that both the experimental and FE approaches do not provide sufficient detail of the through-thickness modes of deformation. For the published FE models, limitations are found in terms of the maximum number of elements through the

thickness. Most of the FE models used an explicit code with shell elements to reduce the simulation time with an inherent reduction in the accuracy of the results. In this chapter, a two-stage or dual-level approach is described which enables a more detailed description of the deformation mechanics to be provided. This is achieved initially through the use of a full 3-D FE model; in the example here the SPIF process is used to produce a truncated cone. The initial model of the complete sheet is performed using an implicit code (Abaqus) with two linear solid elements through the thickness. The objective of this is to predict the product geometry, normal strains and to provide general information on the process. The second stage of the modelling procedure is to interrupt the process simulation of the full model and create a more refined model of a smaller segment of the deforming sheet. This second model encompasses a region around the forming tool that includes deformed and un-deformed material. The geometry and boundary conditions of the new model are defined by the shape of the sheet at the point at which the process was interrupted. This is re-meshed with seven solid elements through the thickness and is designed to provide more detailed information on the through-thickness phenomena which cannot be obtained with the original full model. This approach allows a comprehensive study of the process behaviour with a higher level of accuracy. The following original contributions are made:

- The development of a more detailed finite element model for SPIF process.
- The provision of clear information about the deformation mechanism and the modes of deformation.
- A thorough description of the through-thickness shear strain.

5.3 Experimental Procedure

A part produced on the Cambridge AISF machine [76] is used to verify the sheet geometry indicated by the FE model described in the following sections. This is a three-axis computer numerically controlled (CNC) machine purpose-built for the AISF process, see Figure 5.1 (a). The test product, which is shown in Figure 5.1 (b), was formed using 5251-H22 aluminium alloy. Once the part had been supplied the profile of the truncated cone was measured using a 3-D coordinate measuring machine, the measuring setup is shown in Figure 5.2 (a). An electro-discharge cutting machine was used to cut the formed part along the central plane as shown in Figure 5.2 (b). A micrometer with a scale value of 0.01mm used to measure the sheet thickness. All the measurements were taken from the sheet flange to the centre of the part. The profile was measured before cutting to exclude the effect of additional springback resulting from the cutting process.

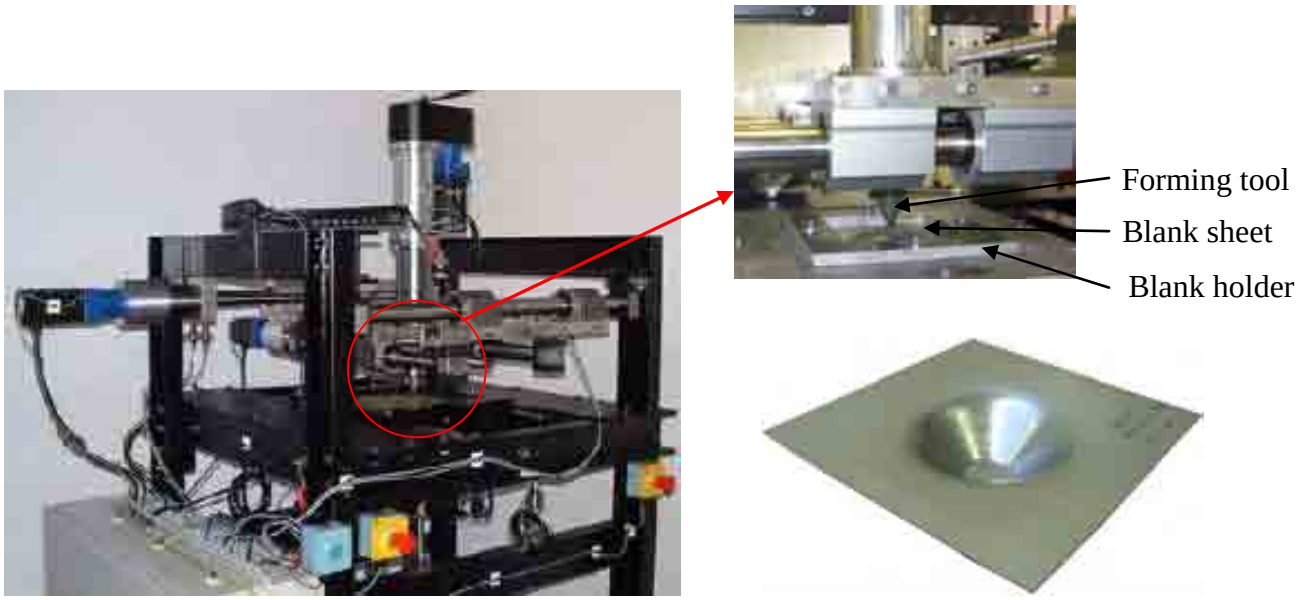

Figure 5.1: (a) AISF machine designed by Allwood et al [76] at the Cambridge University Institute for Manufacturing, (b) test product.

Figure 5.2: (a) The profile measuring setup, (b) the cutting process for the truncated cone along the central plane.

5.4 Implicit Finite Element Modelling

The word 'implicit' refers to the method by which the state of a finite element model is updated from time (*t)* to (*t*+Δ*t)*. A fully implicit procedure means that the state at (*t*+Δ*t)* is determined based on information at time (*t*+Δ*t)*, while the explicit method solves for (*t*+Δ*t)* based on information at time (*t)*. Therefore, in the implicit procedure a set of simultaneous equations are need to be solved. When solving a quasi-static boundary value problem, a set of non-linear equations is assembled as shown in Equation 5-1 [121].

$$G(u) = \int_v B^T \sigma(u) dV - \int_s N^T r dS = 0 \quad \text{.....(5-1)}$$

where (*G)* is a set of non-linear equations in (*u)*, and (*u)* is the vector of nodal displacements. *B* is the matrix relating the strain vector to displacement. The product of B^T and the stress vector σ are integrated over a volume *V*. *N* is the matrix of element

shape functions and is integrated over a surface *S*. The surface traction vector is denoted by *r*. Equation 5-1 is usually solved by incremental methods, where loads/displacements are applied in time steps (Δt), up to an ultimate time (t). The state of the analysis is updated incrementally from time (t) to time ($t+\Delta t$). ABAQUS/Implicit uses a form of a Newton–Raphson iterative solution method to solve for the incremental set of equations.

5.5 First-level Finite Element Model

The large plastic deformation and continuous change of tool-sheet contact location, inherent in SPIF provides a complex challenge for simulation. No conditions of symmetry may be assumed and thus, a full three dimensional FE model is required. The use of an implicit code will provide more reliable data on the stress and strain history but the simulation time is normally very long. In the example here the forming of an aluminium truncated cone is considered.

5.5.1 Sheet geometry and material properties

A rectangular sheet with an edge length of 170mm by 170mm and thickness of 1mm is used to produce a truncated cone that has a wall angle of 45° and a major diameter of 90mm. A hemispherical forming tool having a diameter of 15mm is used to produce the localised deformation. The initial configuration is shown in Figure 5.3. In the numerical simulation, the forming tool is modelled as a rigid body, while the blank sheet is represented as an elastic-plastic deformable body using the material properties of aluminium alloy, Al-5251-H22. The elastic part of the constitutive behaviour of the sheet material is defined by a Young's modulus of 70 GPa and a Poisson ratio of 0.34.

The plastic part of the material is assumed to be isotropic with the stress-strain curve described by, $\sigma=390\varepsilon^{0.19}$ MPa, and an initial yield stress of 165 MPa. Where, σ is the flow stress and ε is the plastic strain. The density of the sheet material is 2700kg/m^3. For simplicity, anisotropic, thermal and rate effects are not included in the present model. The material data are provided by the Institute for Manufacturing, Cambridge University, UK.

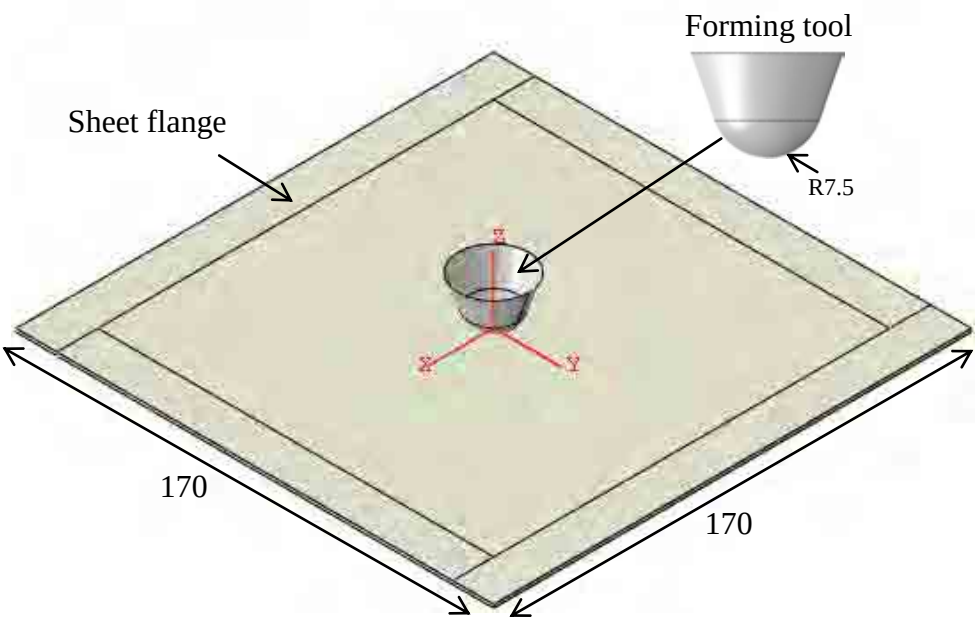

Figure 5.3: The configuration of the full, first-level, 3-D FE model of SPIF to produce a truncated cone (dimensions in mm).

5.5.2 Boundary conditions

The initial sheet blank is completely fixed at the sheet flange where it is constrained by displacement boundary conditions such that it cannot move in any of the XYZ directions. The flange is clamped around its periphery which results in a smaller region of 150mm x 150mm free to deform. These settings reproduce the experimental setup that is describing in the above section. The tool paths for the forming tool are generated

using Matlab software and applied in Abaqus/CAE. The forming tool is assigned to move at 30mm/s in the cartesian XYZ axes along the prescribed tool path and is free to rotate about its own axis. The tool path is principally a complete circular path through 360º followed by a downward translation of 1mm as shown in Figure 5.4. The radius of the circular path reduces each time the tool moves down, also by 1mm.

'Surface to surface' contact between the forming tool and sheet surface is assumed in the Abaqus model and coulomb friction is set with a low friction coefficient of 0.05. The tool does not rotate about its own axis in the FE model. At the end of the simulation, the forming tool moves freely to its original position and the boundary conditions of the sheet edges and clamped regions are removed. This allows springback to be assessed.

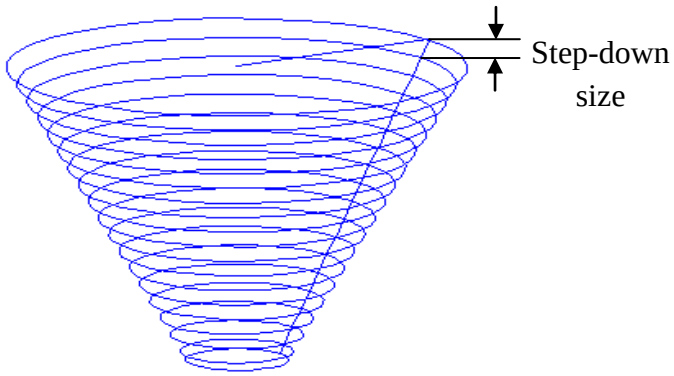

Figure 5.4: Schematic diagram for the designed tool path.

5.5.3 Finite element mesh

Several FE trials were performed using different element types including a 4-node shell element with reduced integration (S4R), an 8-node continuum shell element with reduced integration (SC8R), a fully integrated 8-node solid element (C3D8) and an 8-

node solid element with reduced integration and hourglass control (C3D8R). Figure 5.5 gives details of the performance regarding the prediction of the geometry and sheet thickness. The maximum deviation between the predicted and measured geometry $e_{g(max)}$ and between the predicted and measured thickness $e_{th(max)}$ were obtained as shown in Table 5.1.

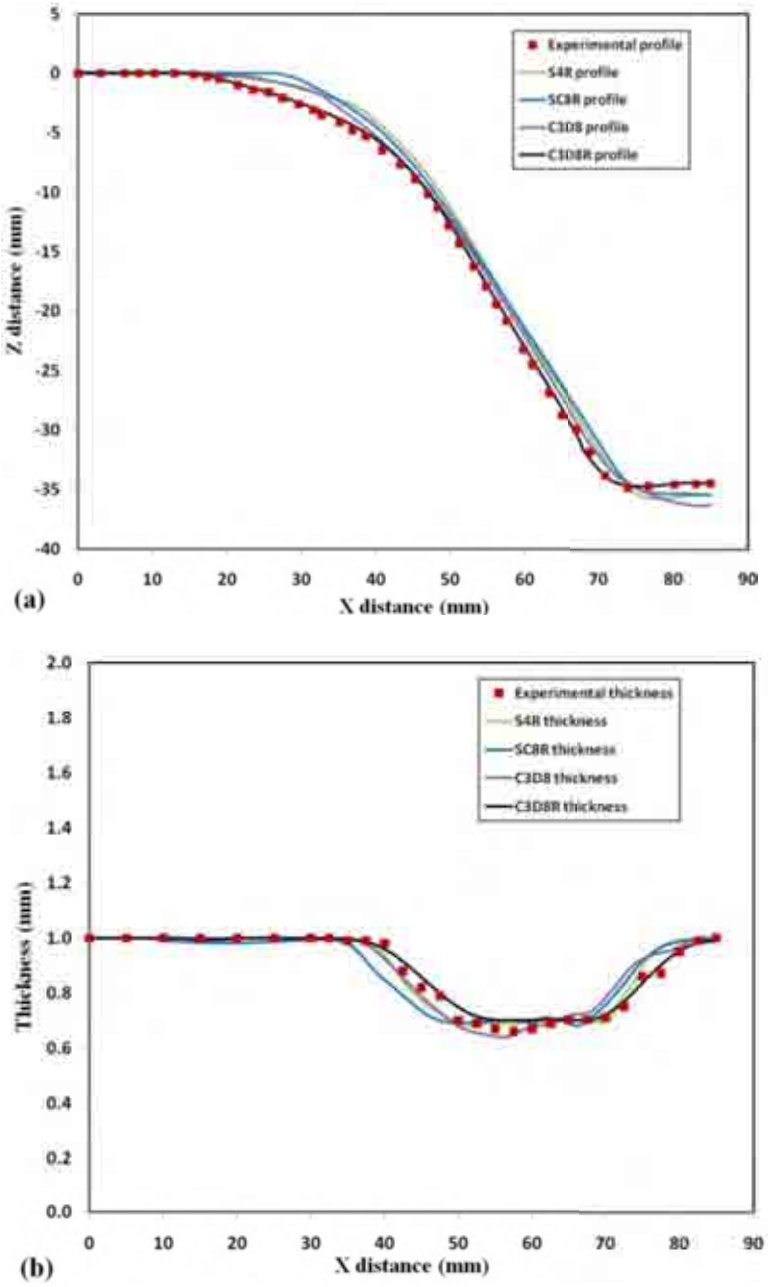

Figure 5.5: Effect of element type on the (a) profile plot, (b) thickness distribution.

The lowest simulation time was achieved using shell element S4R. But since an investigation of the deformation history through the thickness is required shell elements cannot be used. While all the FE analyses reproduced the general trend, Figure 5.5 confirms that the simulation conducted using the C3D8R elements most closely matched the experimental data and these elements were therefore used for all further analyses presented here. However, the use of solid elements results in a considerable increase in CPU time. The initial sheet was meshed with two elements only through the thickness and a total of 17298 C3D8R elements. All the simulations were performed using Abaqus/Implicit on an Intel® CoreTM Dual computer with a 3GHz CPU. The Implicit code has been used since it is expected to provide more accurate results than the explicit code as reported in the literature.

Table 5.1: Element performance.

Performance / Element	$e_{g(max)}$, %	$e_{th(max)}$, %	CPU time, hrs
S4R	4.3	18	18
SC8R	5.4	23	20
C3D8	5.3	21	31
C3D8R	1.8	10	34

5.6 Discussion and Validation of the FE Model Results

Figure 5.6 shows the truncated cone at the end of deformation and the corresponding von Mises stress distribution. Zero stress is indicated at the flange where the sheet is completely fixed. Adjacent to this region, a slight increase in the stress value can be

seen as a result of the global bending. A uniform distribution develops along the cone wall. Higher values of von Mises stress are found at the last tool path as a result of the materials decreasing ability to unload at the end of deformation.

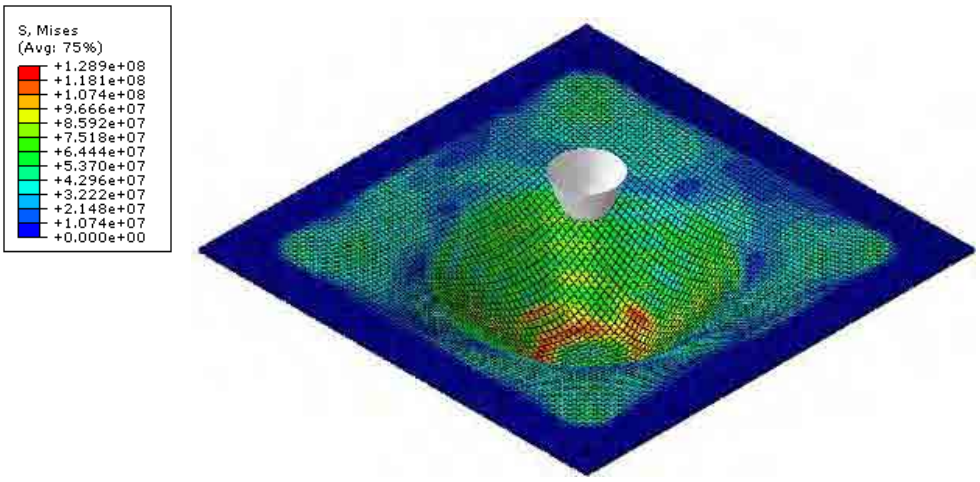

Figure 5.6: von Mises stress (Pa) distribution in the fully deformed truncated cone.

5.6.1 Profile and thickness distributions

Figure 5.7 shows the profile plots obtained by FE analysis and experimental measurement. For reference only, a theoretical profile of a 45º truncated cone is also shown. It can be seen that there is good agreement between the FE and experimental profiles. The FE model predicts the sheet bending close to the major diameter of the cone, the springback at the cone base and the pillow effect at the centre of the cone, a feature also observed by Micari et al [179]. The sheet bending is expected to be large since the deformation started at a large distance, i.e. 40mm, from the sheet flange.

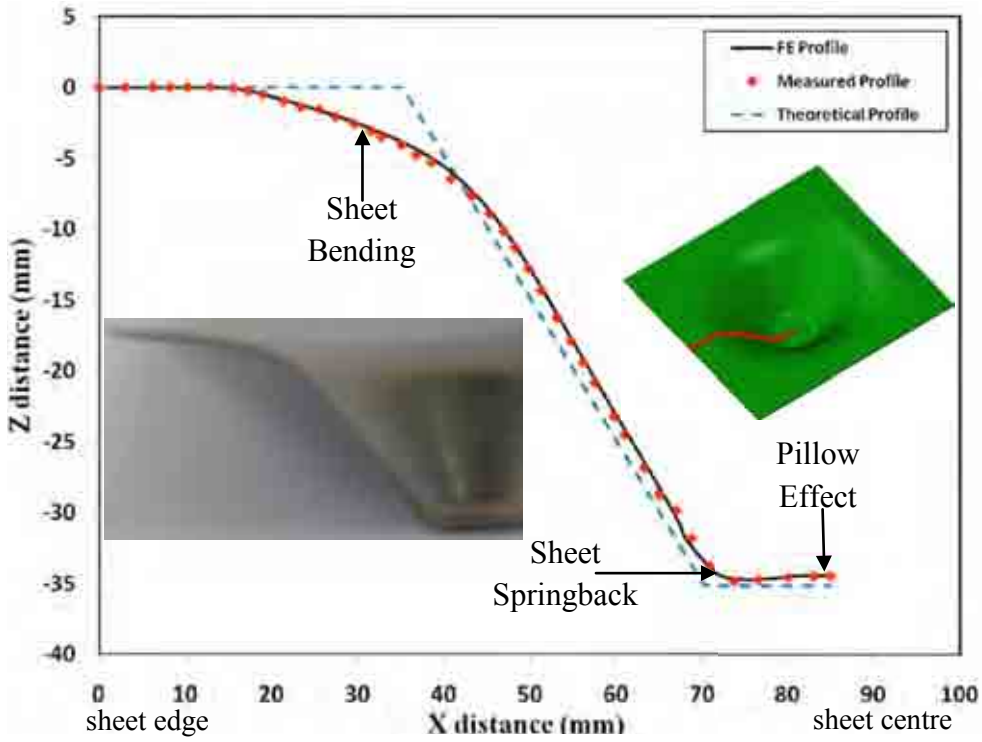

Figure 5.7: The profile plots of a 45° truncated cone.

The thickness distribution along the central plane of the deformed sheet is shown in Figure 5.8. This shows the thickness variation obtained by FE analysis, experimental measurements and for comparison, by an analytical technique. The latter was obtained by determining the tangent angle at a number of points along the measured profile and applying the sine law ($t_f = t_0 \sin\theta$) as reported by Hussain and Gao [163], a technique commonly applied in sheet forming to estimate the thickness of the formed sheet. It can be seen that the sheet thinning increases as the cone depth increases and near to the cone base, less thinning is apparent. From Figure 5.7, it is clear that the slope increases as the cone depth increases. For the final thickness predicted by the sine law, the sheet thickness will decrease as a result of increasing the slope angle. For a distance between 50mm and 70mm from the sheet edge, the wall angle is 45º as shown in Figure 5.7, and

therefore the sheet thickness remains almost constant at 0.70mm. As a result of sheet bending at the cone base, the slope begins to increase and accordingly, the sheet thickness is closer to its original value.

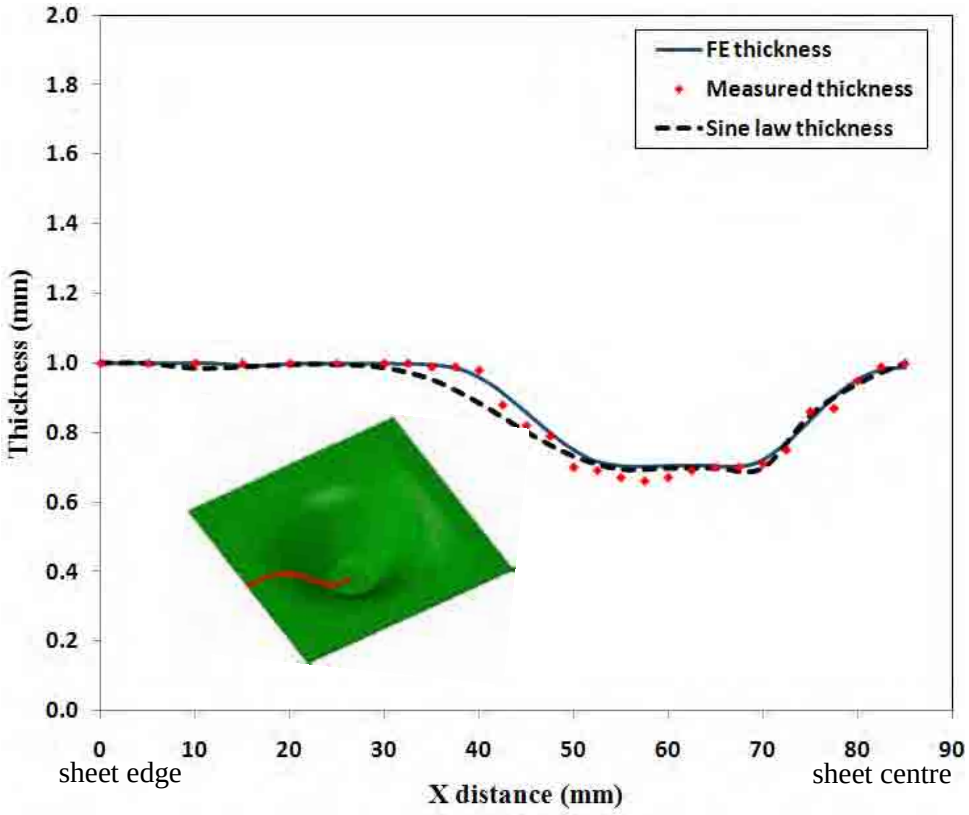

Figure 5.8: Thickness distribution along central plane of the 45^0 truncated cone.

5.6.2 Forming force components

During the forming process, three force components F_x, F_y and F_z are recorded as shown in Figure 5.9. F_x and F_y are those components in the plane of the tool's circular path while F_z is the tool force in the vertical direction. The experimentally measured force components were provided by the Institute for Manufacturing, Cambridge University, UK. The evolution of these forces can be explained as follows; in the first complete path, all forces are almost zero where the incremental step in this path is 0.1mm. For

any subsequent complete path, F_x and F_y have the same trend and reach their maximum and minimum values in a sinusoidal manner. F_x decreases for the first 90º of tool movement to reach its minimum value at this position. It then starts to increase and becomes zero again at 180º and continues to increase until its maximum value is reached at 270º, after which it decreases again and becomes zero when the tool returns to its original position. F_y has the opposite trend of F_x. F_z incrementally increases as the accumulated downward translation of the tool increases with much higher peak values than F_x and F_y.

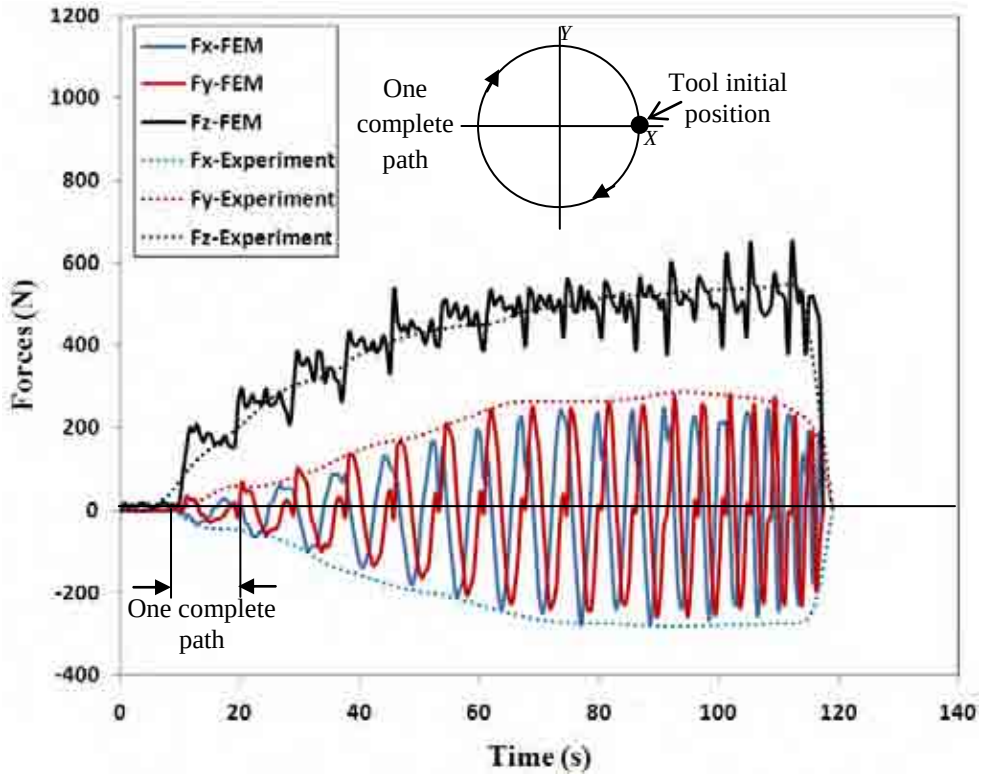

Figure 5.9: Development of the three force components.

In order to simplify the graph, the average amplitude of the experimental force F_z and the maximum amplitude of the experimental forces F_x, F_y (the averages being zero) are displayed. As the cone depth increases, the peak values of F_x, F_y and F_z increase until

maximum plastic deformation after which the forces stabilise at approximately 280N and 630N respectively. There is very good agreement between the FE and measured forces. Similar trends between the FE and experimental forces have been observed by Duflou et al [108].

5.6.3 Stress and strain distributions

In order to display the stress and strain data shown in Figure 5.10, Figure 5.11 and Figure 5.13, the deformation history is divided into three regions; (a) the commencement of deformation, (b) mid-way through the process and (c) at the end of the forming process. Figure 5.10 shows the von Mises stress distribution for these three stages. After initial tool contact, Figure 5.10(a), the stress is localised principally beneath the tool while the rest of the sheet deforms elastically. Due to the evolution of deformation induced by the tool movement, out-of-plane distortion develops as the sheet adopts a more three-dimensional geometry. This, together with further plastic deformation, provides a more rigid behaviour and restricts the elastic recovery of the material away from the contact region.

The localised peak stress areas are clearly defined by the annular regions shown in Figure 5.10(b) and Figure 5.10(c) which develop along the tool path that has just completed. The final stress distribution varies over the sheet surface as shown in Figure 5.10(c). At the end of the process there is a small variation from the inner edge of the flange region to the highly localised region at the last tool path. Across the cone base only low levels of stress develop. Rotation of the cone base with low stress is apparent.

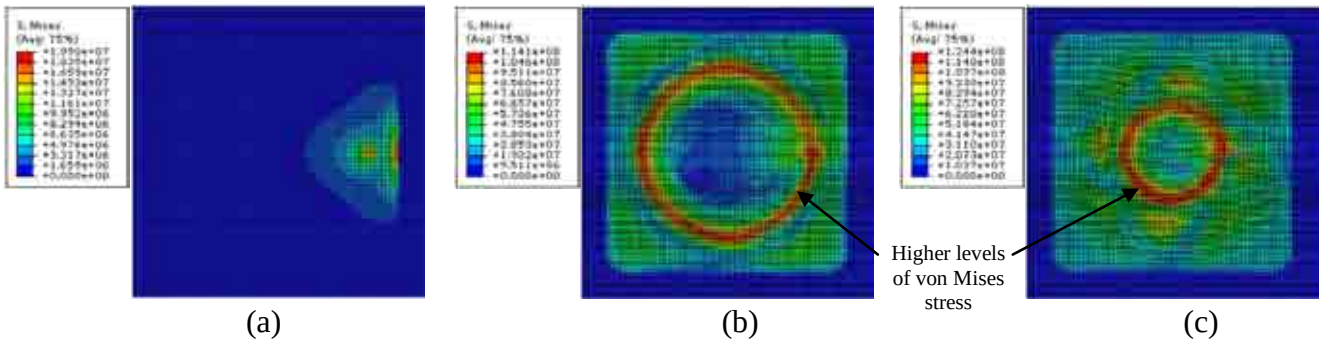

(a) (b) (c)

Figure 5.10: von Mises stress (Pa) distributions, at (a) the commencement of deformation, (b) mid-way through the process and (c) at the end of the forming process.

Figure 5.11 shows the evolution of equivalent plastic strain through the deformation process. There is clearly no plastic deformation at the beginning of deformation as shown in Figure 5.11(a). Plastic strain is generated as the tool moves across the sheet, associated with the combined stretching and bending behaviour, Figure 5.11(b). As a result of increasing the deformation depth, the plastic strain gradually increases over the cone wall and attains its maximum value near to the cone base. It decreases again after the location of maximum sheet thinning and reduces to zero at the cone base as shown in Figure 5.11(c).

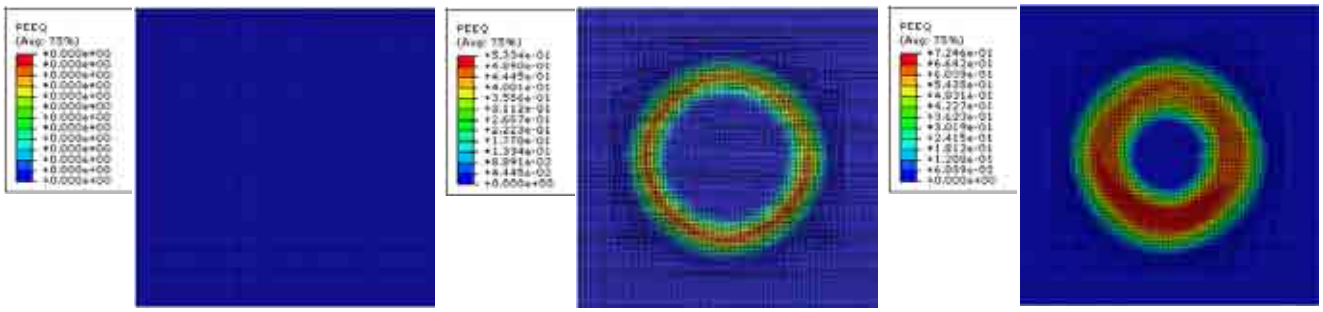

(a) (b) (c)

Figure 5.11: Evolution of plastic strain, at (a) the commencement of deformation, (b) mid-way through the process and (c) at the end of the forming process.

This can be confirmed from the plastic strain distribution along the central plane of the cone shown in Figure 5.12. At the sheet flange, the plastic deformation is zero where the sheet is completely fixed. The plastic deformation then starts to increase and the maximum corresponds to the maximum sheet thinning which takes place along the 45º wall angle (see Figure 5.7 and Figure 5.8). After this peak, the plastic deformation decreases towards the centre of the sheet.

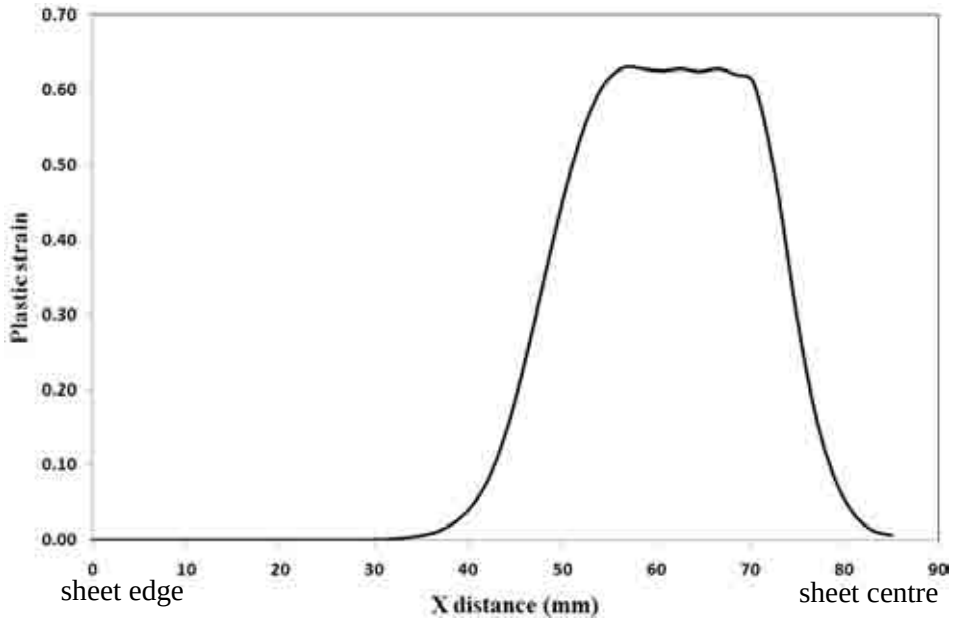

Figure 5.12: Plastic strain distribution along central plane of the 45º truncated cone.

In this type of process, the deformation transforms very quickly from a broad elastic region to a highly localised region of plastic deformation beneath the forming tool. From the total strain rate distribution shown in Figure 5.13(a), there is a wide area of deformation around the tool at the beginning of deformation. This area is the main cause of sheet bending that occurs next to the sheet flange. As the process progresses, the deformation becomes more localised at the contact region beneath the forming tool which clearly demonstrates the incremental nature of the process as shown in Figure

5.13(b) and Figure 5.13(c). This small area of deformation is the main cause for the increase in the vertical force F_z and agrees with the observations reported by Jackson and Allwood [161].

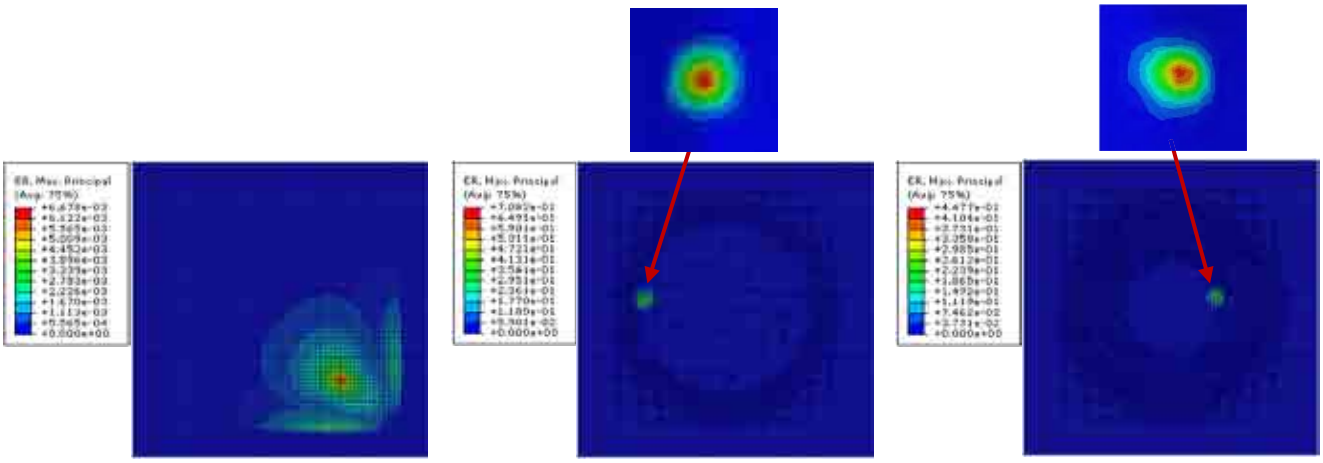

(a) (b) (c)

Figure 5.13: Evolution of strain rate (s^{-1}), at (a) the commencement of deformation, (b) mid-way through the process and (c) at the end of the forming process.

5.6.4 History of strain components

To demonstrate the strain component history through the process, two control elements on the upper surface of the cone are selected (Figure 5.14a). One is located at the middle upper region of the cone wall and the other at the lower region near to the cone base. The strain components are measured with respect to a local coordinate system. ε_{11}, ε_{22} and ε_{33} are the strain components equivalent to directions 1, 2 and 3 respectively as shown in Figure 5.14(a). Only the components in the 1-3 plane, ε_{11}, ε_{33} have significant values while ε_{22} is almost zero as shown in Figure 5.14(b), which indicates near plane-strain deformation.

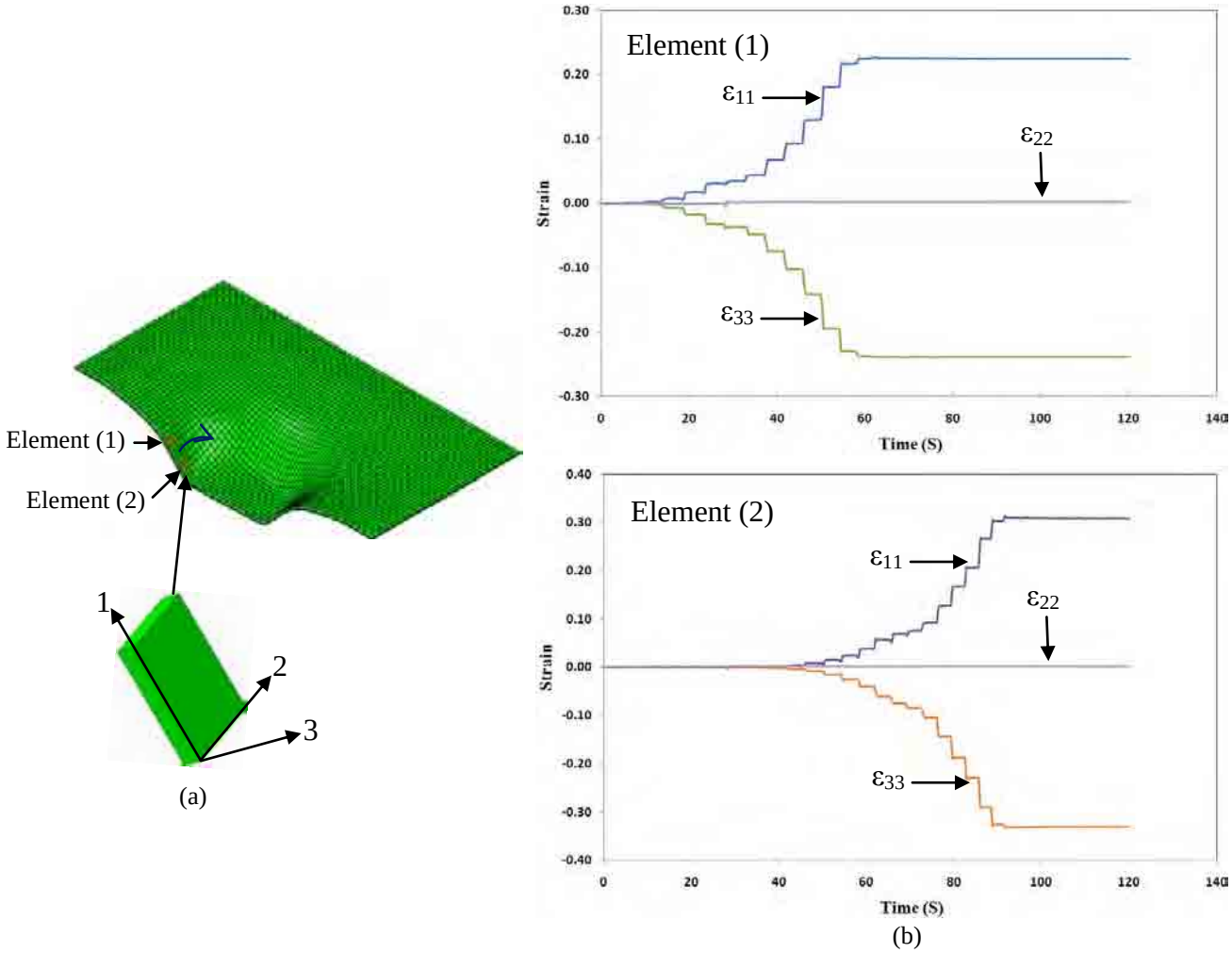

Figure 5.14: (a) Two control elements along the cone wall, (b) strain history on the control elements.

The strain increases incrementally each time the forming tool deforms the elements. It can be seen that the sheet stretching associated with ε_{11} and sheet thinning associated with ε_{33} (see Figure 5.15), combined with sheet bending next to the sheet flange, are the dominant modes of deformation in SPIF. The values of ε_{11} and ε_{33} components clearly increase as the forming progresses. No further strain is imposed once the forming tool moves out of contact with the element and on to a subsequent path. The significant strain components and their trends agree with the observations by Bamback et al [89], Hirt et al [155] and Ambrogio et al [173]. However, while the full model predicts the

history of the normal strain components, the use of two elements through the sheet is not sufficient to obtain accurate data on through-thickness shear strains.

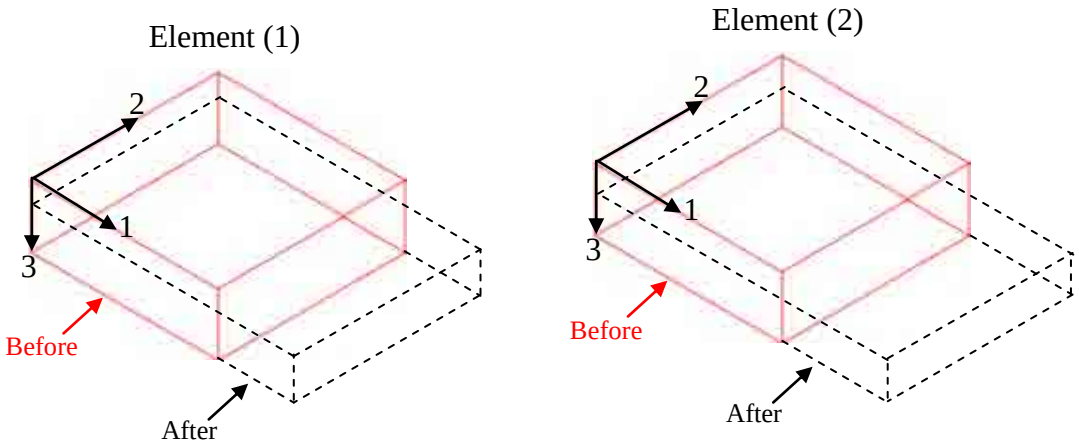

Figure 5.15: Deformation of control elements, element 2 shows larger stretching and more sheet thinning.

5.7 Methodology for the Dual-level Finite Element Model

In order to predict the through-thickness shear strains which are believed to be the main contribution to the high forming limits typical of this process, a model with a sufficient number of elements through the thickness must be constructed. For the full FE model presented above, a large number of elements, i.e. more than three, will result in very long, unrealistic simulation times, of the order of several days or more for each simulation. Therefore, it is necessary to use a dual-level approach. In this technique the full model is run only until sufficient deformation, typical of the whole process, has occurred. A second-level FE model is then created in which a large number of elements can be assigned through the thickness. Since the required model should have the same characteristics and performance of the full model, a simplified model such as that constructed by Ma and Mo [135] would not be suitable.

These requirements can be fulfilled through the following procedure: The full model is to be simulated for a number of successive loops of tool movement until a sufficient amount of plastic strain is generated. This could be established qualitatively. A segment of the sheet that surrounds the forming tool and includes deformed and un-deformed regions is then extracted. For this second-level FE model, the geometry of the full model including the last position of the forming tool is applied and a larger number of elements through the thickness is assigned. In the second-level FE model, the deformation process should continue exactly as in the full model.

5.7.1 Example of dual-level approach

This procedure can be demonstrated with a simple generic example, which is used also to determine the minimum number of elements required through the sheet thickness. An FE model for the SPIF process was constructed using a sheet strip of 80mm length, 50mm width and 1mm thickness. The material properties of the truncated cone are used for the sheet strip. The sheet end faces are constrained by displacement boundary conditions such that they cannot move in the X-direction and the side faces cannot move in the Y-direction (Figure 5.16). The tool is free to move corresponding to the tool path. The tool movement is principally a complete linear path along the Y-direction followed by a downward translation along the X-Z plane, after which the Y-translation is repeated. The sheet was meshed with 2 elements through the thickness and a total of 3102 solid elements, type C3D8R. The process of constructing the second-level FE model is shown in Figure 5.16. After three successive tool paths, a partially deformed 30mm x 15mm segment of sheet was extracted as shown in Figure 5.16(a) and Figure 5.16(b). The current nodal coordinate points of the selected piece were extracted from the model data and used to define the bounding surfaces within which a new body, as

shown in Figure 5.16(c), could be created. A new second-level FE model using this geometry was then constructed (Figure 5.16d) and meshed with solid elements.

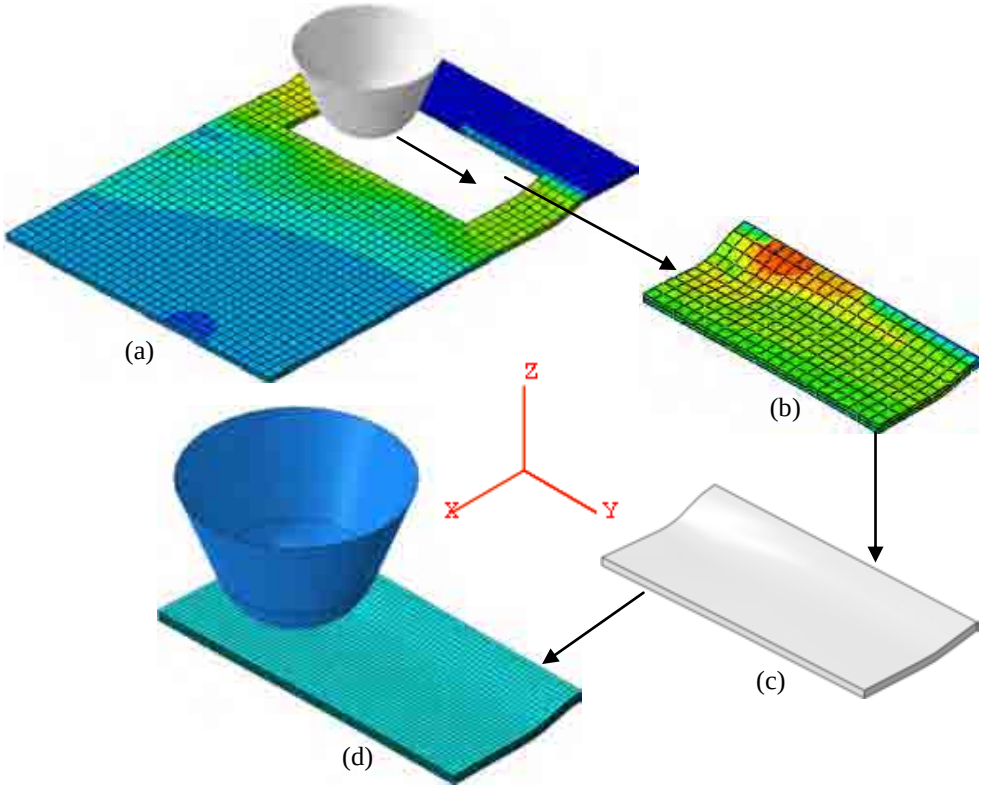

Figure 5.16: The process of constructing the second, lower level, FE model.

The forming tool was modelled as a rigid body with a 15mm diameter hemisphere and placed at the last position attained in the original model. The tool is again prescribed to move parallel to the sheet in the Y-direction. The same boundary conditions of the strip model are applied to the new FE model. Since the segment was removed near to the beginning of deformation, the amount of generated stresses and strains are very small compared to those at the end of deformation, and any initial stresses or strains were therefore ignored.

5.7.2 Influence of number of through-thickness elements

In order to assess the influence of changing the number of elements through the sheet thickness the maximum value of shear strain γ_{23} was selected as the main criterion. This was expected to show the most significant contribution of the strain components. As the number of through-thickness elements increased, the maximum value of the shear strain γ_{23} also increased as shown in Figure 5.17. However, increasing the number of elements beyond seven showed very little effect as the value began to stabilise. Seven elements through the thickness and a total of 15190 elements were therefore used in all subsequent analyses. It is important to mention that decreasing the element size through the thickness should be associated with a corresponding decrease in the elements size in the plane of the sheet to keep a proper aspect ratio for all elements. Figure 5.17 also shows the significant increase in simulation time for each model.

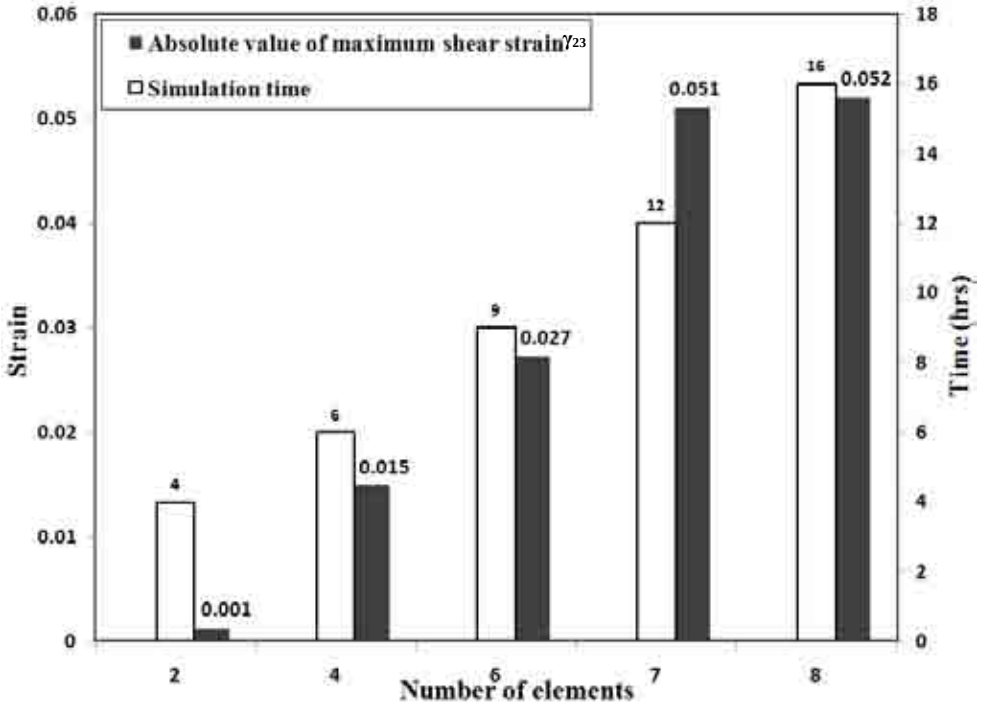

Figure 5.17: Effect of number of elements through the sheet thickness on the maximum value of shear strain γ_{23} and simulation time.

The need to use a sufficient number of elements is confirmed by an examination of the strain components for an element in the centre of the sheet, originally under the tool at the beginning of the process. Figure 5.18 shows the strain history obtained at the end of deformation with two elements through the sheet, while Figure 5.19 shows the strain history obtained from the more refined second-level FE model. The strain components ε_{11}, ε_{22} and ε_{33} are similar in both cases, but there are clear differences in the shear strain components γ_{13} and γ_{23}.

Strain γ_{13} is the shear component in the plane perpendicular to the tool movement and results from pushing the forming tool across the material along the wall angle. This component increases incrementally until it reaches a steady value and then remains

constant. Strain γ_{23} is the shear component in the plane parallel to the tool movement and is principally a result of the friction between the forming tool and the sheet surface. The maximum value of this shear strain is much higher than the other components, which could contribute to a higher forming limit. Shear strain component γ_{12} has no contribution.

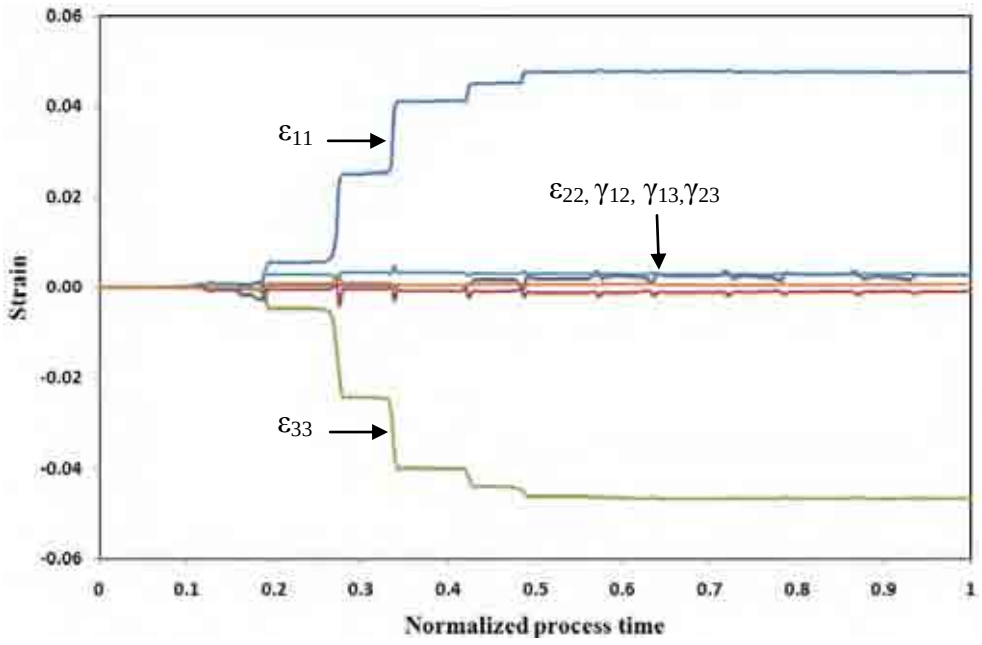

Figure 5.18: Strain history obtained from the simple case at the end of deformation with 2 elements through the sheet thickness.

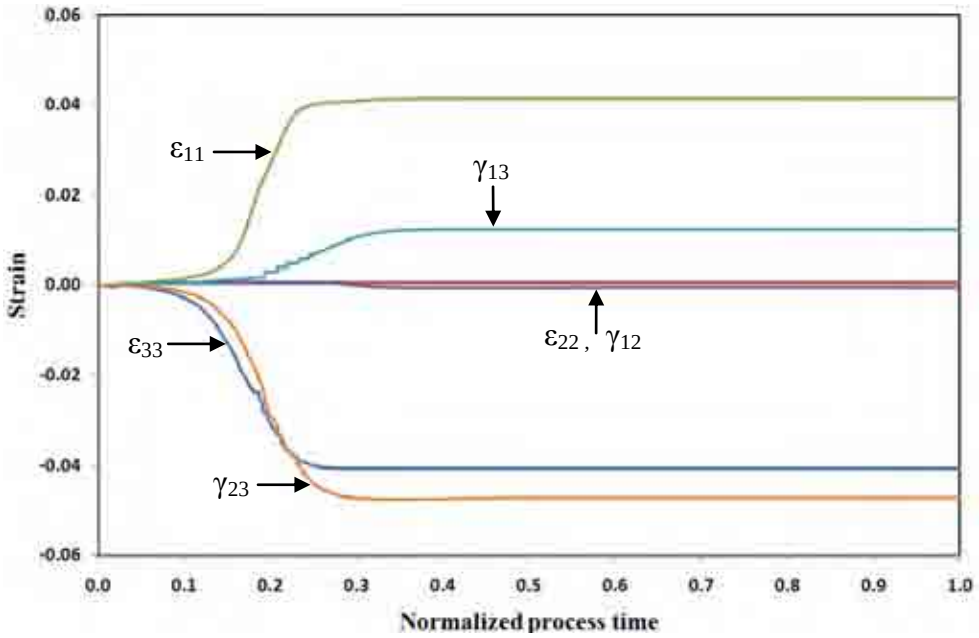

Figure 5.19: Strain history on an element in the middle of the sheet thickness of the second-level FE model with 7 elements through the sheet thickness.

5.8 A Refined Second-level FE Model for a Truncated Cone

Having demonstrated the effectiveness of the two-level FE strategy for a simple case, the same approach is now applied to the forming of the truncated cone. The process is illustrated in Figure 5.20. After three successive paths of deformation in the full model, a 30mm x 30mm segment of the sheet was extracted. The nodal coordinate points of the segment extracted from the full model defined the boundary surfaces of the new model, as shown in Figure 5.20(c), within which the second-level FE mesh was created. This model was meshed with 7 elements (type C3D8R) through the thickness, with a total of 25137 elements, as shown in Figure 5.20(d). The forming tool is set to move a distance of 25mm along an arc at the same speed as in the full model.

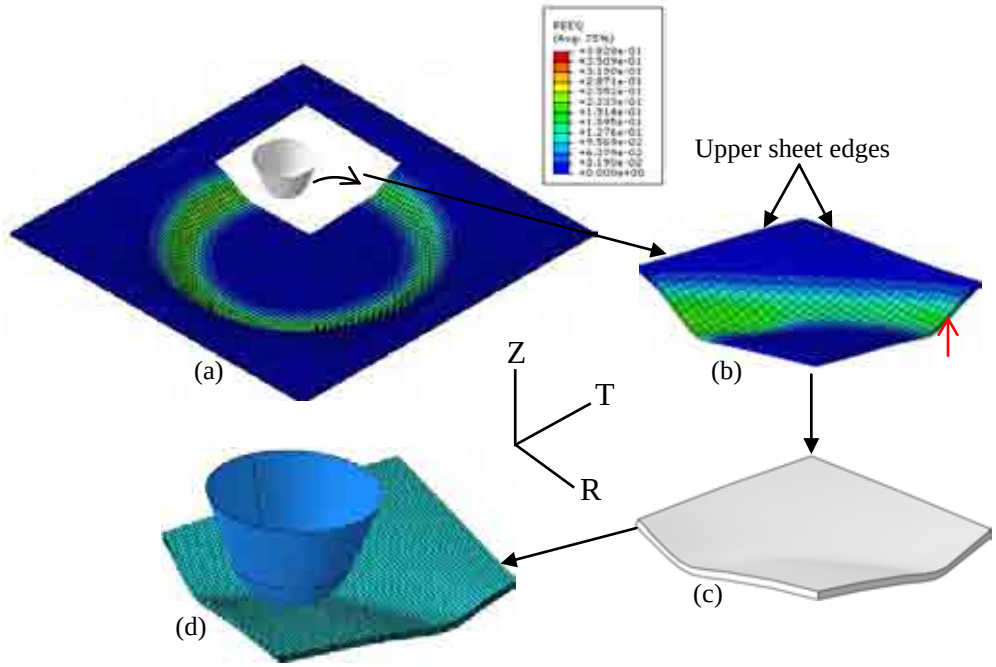

Figure 5.20: The four stages in the process of constructing the second level FE model for a truncated cone.

The boundary conditions in the smaller segment must reproduce, as close as possible, the sheet behaviour in the full model. The size of the segment was chosen after preliminary trials to ensure that the tool trajectory and the elements selected for a more detailed examination were sufficiently far from the segment edges to minimise any minor differences in boundary effects. The two outer edges of the segment near to the original outer edges of the sheet were selected to coincide with the limits of the mesh in the full model beneath the clamped region. The nodes on these edges, in both the full (first-level) and in the segment (second-level) were constrained so that there was no movement in the vertical, Z-direction. The experimental measurements showed no reduction in thickness in this region of the sheet. If the edges of the segment were not coincident with the edges of the clamped region then different boundary conditions, consistent with any local displacement would be required. The other two side edges of

the segment are constrained so that any nodal displacement occurs either in the R-Z or T-Z planes as appropriate. In order to establish the suitability of these constraints, the displacements of nodal points on the two faces in the reduced segment, and at the corresponding locations in the full model were checked. One example for a node (indicated by the arrow in Figure 5.20) is given in Figure 5.21, which shows a typical correlation between the edge displacements and demonstrates the suitability of the boundary conditions imposed.

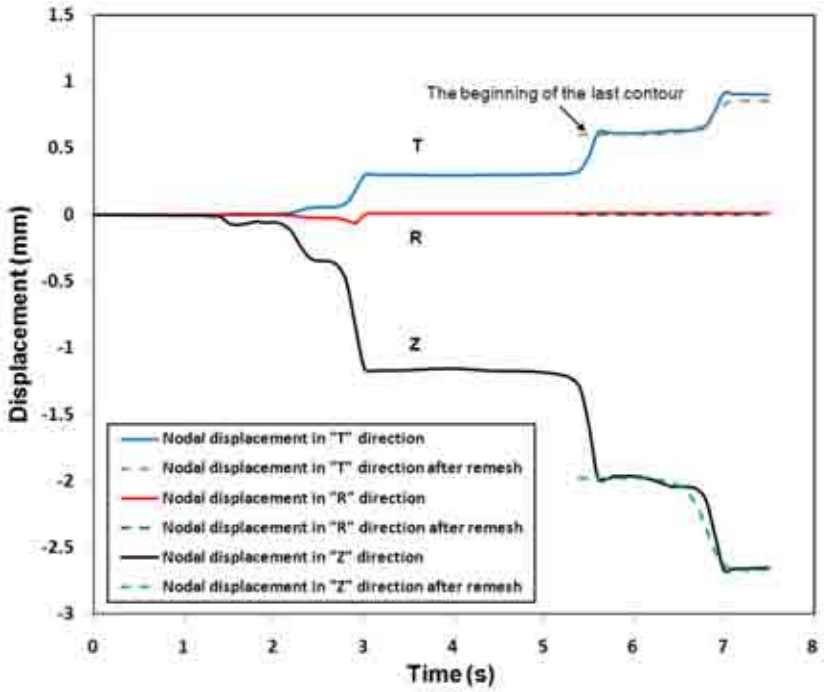

Figure 5.21: Comparison of node displacements in the first and second level models for a selected nodal point, the selected node is from the region indicated by the arrow in Figure 5.20.

5.9 Stress and strain in the cone forming process

The von Mises stress distribution in the second-level model, is shown in Figure 5.22(a), with the distinct annulus of high localised stresses developing and very little

deformation in the remainder of the sheet, consistent with the full model. A cross-section along the T-Z plane, located near to the initial tool position, shown in Figure 5.22(b), illustrates the shear deformation through the thickness. The enlarged view in Figure 5.22(c) highlights the significant shear deformation compared to the elements in the un-deformed region. Figure 5.22(c) shows the shear deformation in the 1-3 plane, γ_{13}, and in the 2-3 plane, γ_{23} for this set of elements. A control element in the middle of this set, as shown in Figure 5.22(c), is selected from which to extract the strain history.

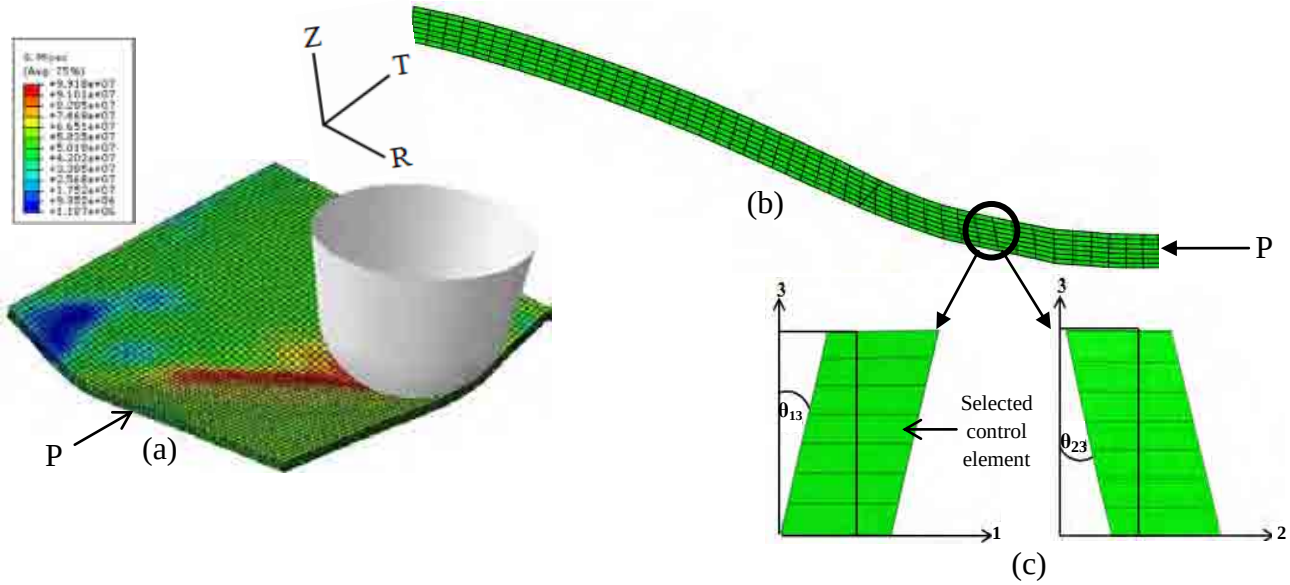

Figure 5.22: (a) von Mises stress (Pa) distribution, (b) edge view in the T-Z (1-3) plane near the initial tool position and (c) illustration of shear deformation.

The strain history of the selected element (see Figure 5.22c) is shown in Figure 5.23. Two shear strain components γ_{13} and γ_{23}, in addition to the normal strain components ε_{11} and ε_{33}, are clearly revealed as a result of increasing the number of elements through the thickness. The shear strain γ_{23} has the greatest magnitude with no contribution from the normal strain component ε_{22} and shear strain component γ_{12}. The distributions of the shear strains γ_{13} and γ_{23} through the thickness are shown in Figure 5.24. The maxima are

found at the top surface in contact with the tool, reducing to small values at the opposing surface. These findings agree with the experimental results obtained by Allwood et al [118] and Jackson et al [161].

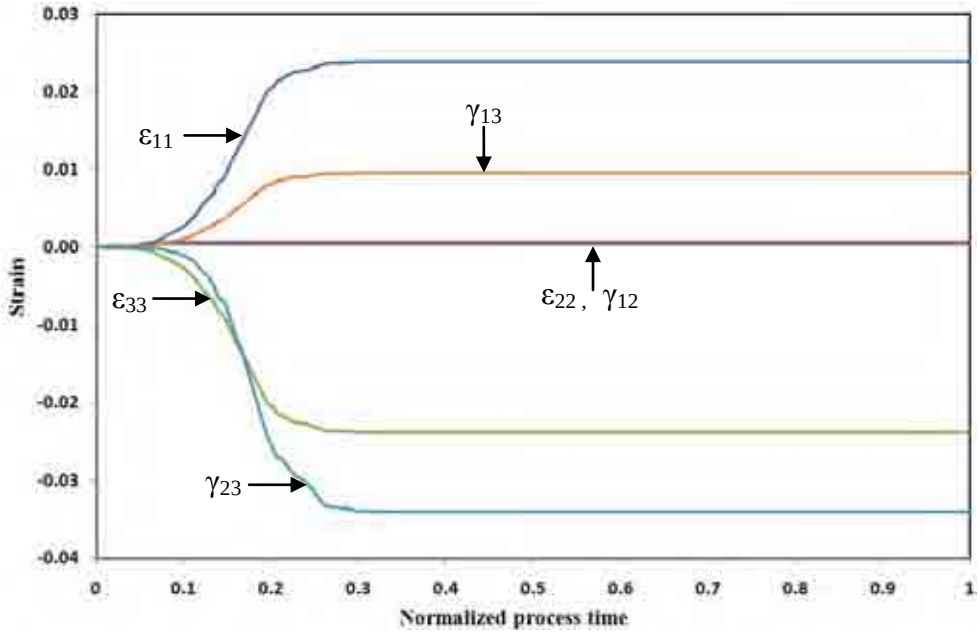

Figure 5.23: Strain history of the second-level FE model of the truncated cone.

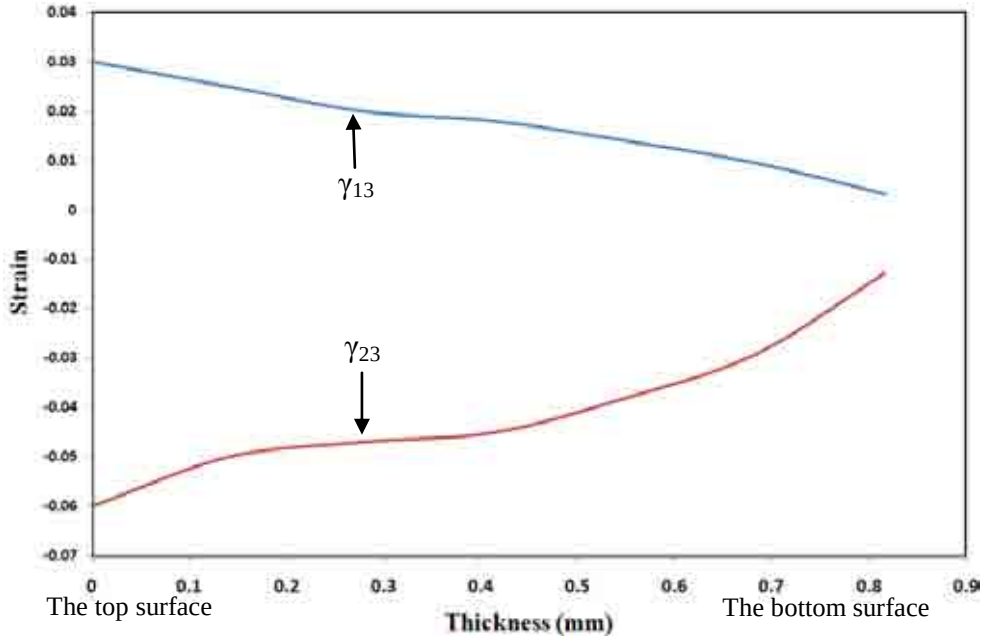

Figure 5.24: Shear strain distribution along the sheet thickness of the second-level FE model of the truncated cone.

5.10 Influence of Friction and Tool Diameter on Shear Strain

The development of the dual-level methodology provided the opportunity to assess the influence of process parameters on the shear strain distribution through the sheet. In the cone forming process the interface friction and tool diameter were considered as they are expected to have a significant influence on the deformation mechanics in SPIF. In the case of friction, three coefficients of 0.05, 0.26 and 0.5 were used (each with a tool diameter of 15mm). Tool diameters of 10, 15 and 20mm were assessed (each with a friction coefficient of 0.26). Allwood et al [118] and Jackson and Allwood [161] reported that the process formability is strongly influenced by the through-thickness shear strains, and these could be increased by increasing the friction between the forming tool and sheet surface. The influence of friction in the present model is shown in Figure 5.25. With a low value of friction, 0.05, the variation in shear strain γ_{23}, across the sheet is greater than the variation in γ_{13}.

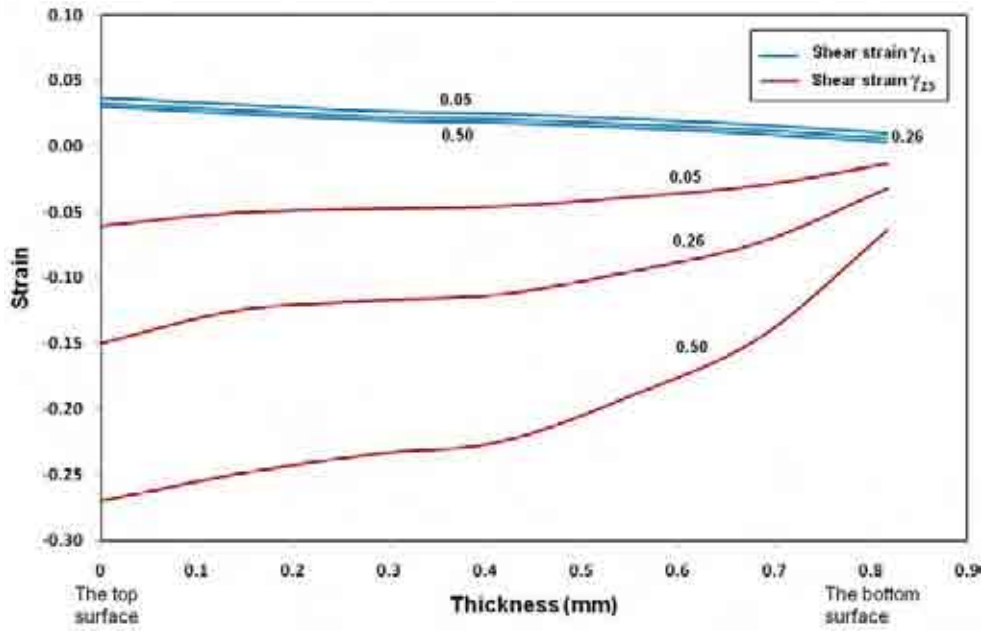

Figure 5.25: Effect of friction coefficient on the through-thickness shear strain.

When the friction is increased, the γ_{13} component changes very little and a similar variation is observed, but at a slightly lower magnitude. The effect of friction on the γ_{23} component is much more pronounced. Not only does the gradient across the sheet increase, but also the magnitude significantly increases. For example, at the upper surface in contact with the tool, it is 0.06 for a coefficient of 0.05, 0.15 for a coefficient of 0.26 and 0.27 for the higher coefficient of 0.5. This confirms that increasing friction will increase shear strain. A disadvantage of this however, has been shown by Hussain et al [166], who demonstrated that high friction will result in an undesirable surface roughness, so clearly, care must be exercised when increasing friction.

Using a small diameter tool tends to localise the deformation underneath the tool and increase the strains. As the tool diameter increases, the contact area increases and hence the contact pressure decreases. As a result of increasing the contact area, the deformation becomes more distributed and hence the forming forces decrease which leads to a decrease in the strains that are generated. Figure 5.26 shows clearly that the magnitude of the shear strain reduces as the tool diameter is increased, although the gradient across the sheet remains unchanged. A similar result is implied by Hussain et al [138], Le et al [140] and Ham and Jeswiet [168] who reported that as the tool diameter decreases the process formability increases, consistent with an increase in shear deformation.

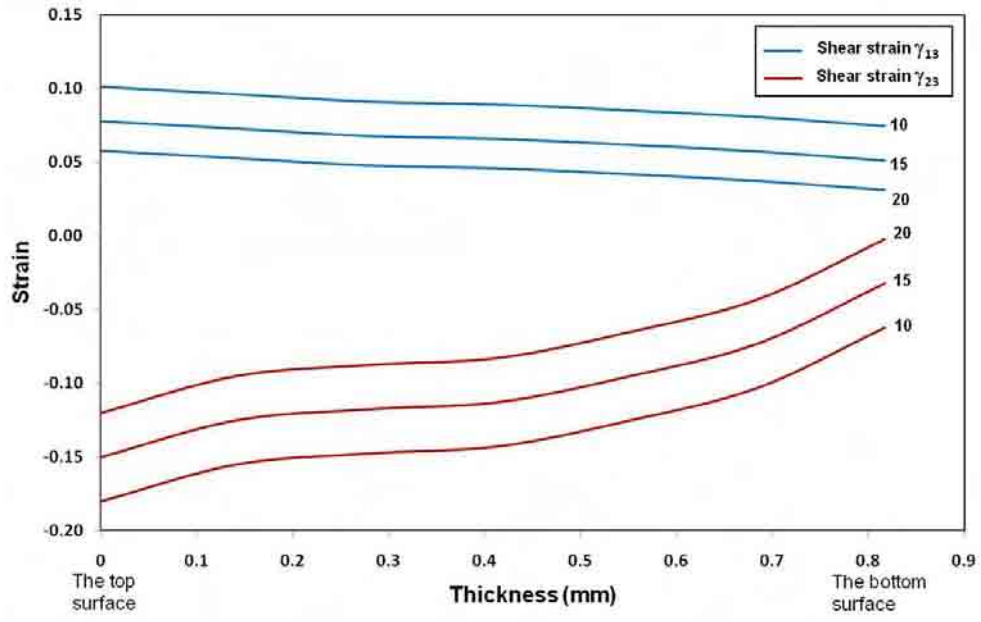

Figure 5.26: Effect of tool diameter on the through-thickness shear strain.

5.11 Through-thickness Shear Strain as a Stabilisation Mechanism in SPIF

Continuous inelastic deformation for any material will finally lead to failure. The deformation created increases the number of dislocations that move through the material; these act together and create voids that finally result in a fracture. The limit strain before failure is called the fracture limit. Under a certain state of stress such as hydrostatic compressive stress, these voids can be suppressed which leads to a delay in development of the fracture. For this reason, rolling and wire drawing along with forming processes that are largely compressive in nature can develop large levels of strain without failure. For forming processes that operate largely in tension, such as stamping, the deformation is limited by instabilities or necking instead of fracture. Instabilities create a situation in which the deformation is concentrated into a small region (the neck) while the remainder of the product suffers little or no further

deformation. Because of the small size of the neck, even small extra displacements will generate large additional strains and the material will soon reach the fracture limit and fail. For most ductile metals, the necking limit is much lower than the fracture limit. This leads to an important conclusion: the formability of a material in a forming operation can be increased significantly if the necking instability can be avoided or postponed or the growth rate of a neck is reduced [171].

In classical sheet forming, localisation is synonymous with necking and instability because a low force will be enough to elongate the necking zone. Once a neck is initiated it will remain the weakest point. Therefore, the incremental nature and the localised deformation by themselves do not explain the enhanced formability in AISF. Another aspect of AISF is that the zone of localised deformation moves with the tool over the sheet. One might argue that high deformations in AISF are obtained because the neck cannot grow into a crack, since the tool is already in another location before the fracture limit can be reached. This explanation is not completely satisfactory, because it does not explain why a neck once generated will not keep growing, if it is still under tensile stresses as reported by Emmens and Boogaard [171]. To successfully deform a sheet using AISF the deformation must be localised into a small zone and in that zone a special condition that delays necking must exist. Simultaneously, outside that zone the condition must be such that if a neck is generated inside the zone it will not grow. This effect of stabilisation can be achieved if the stress at the location of the neck is below the level that is required for further growth.

In the literature, a number of mechanisms have been proposed to explain the enhanced formability associated with AISF processes, as discussed in Chapter 2. One of these

theories which had not previously been numerically predicted is based on the existence of an enhanced through-thickness shear strain. In this chapter, a dual-level FE modelling technique has been used to predict this deformation mechanism. The principle of shear as a stabilising mechanism and hence its ability to improve the forming limit can be explained as follows. In terms of stability, simple shear would completely avoid necking, because no tensile force is applied in the plane of the sheet. However of more relevance is shear superposed on stretching of the sheet as in SPIF. An additional shear stress will lower the normal stresses as graphically presented in Figure 5.27. This follows the von Mises yield criterion shown below.

$$\sigma_f = \sqrt{0.5[(\sigma_{11}-\sigma_{22})^2+(\sigma_{22}-\sigma_{33})^2+(\sigma_{11}-\sigma_{33})^2+6*(\tau_{12}^2+\tau_{23}^2+\tau_{13}^2)]} \quad \text{.....(5-2)}$$

Where: σ_f is the flow stress, σ_{11}, σ_{22} are normal stresses parallel to the sheet surface, σ_{33} is the normal stress perpendicular to the sheet surface, and τ_{ij} are the shear stresses.

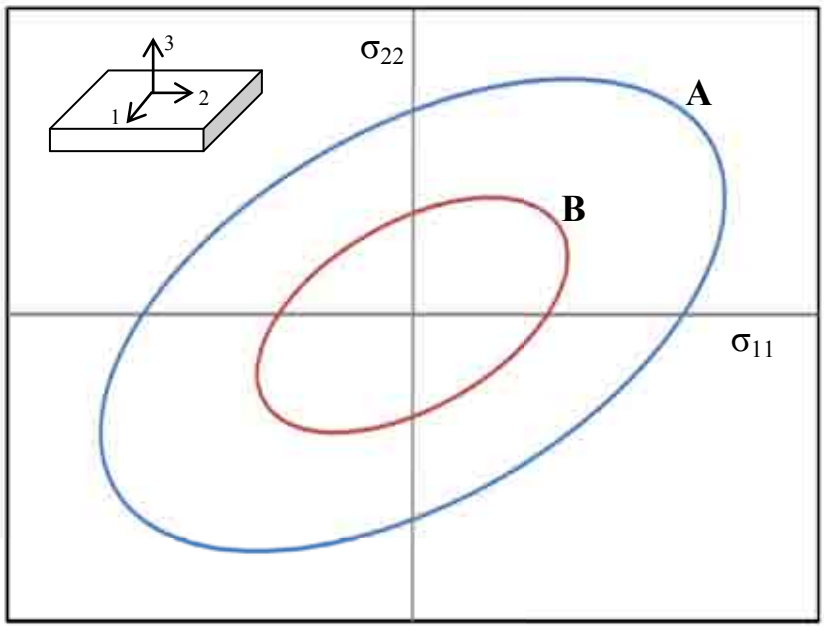

Figure 5.27: Effect on the von Mises yield locus, (A) standard locus (σ_{33}=0, τ_{ij}=0) and (B) effect of shear stress (σ_{33}=0, $\tau_{ij} \neq 0$).

This means that if a sheet is stretched to a level below the flow stress, a relatively small amount of additional shear stress will be sufficient to start plastic deformation. If the shear stress is caused by a tangential displacement, e.g. by tool movement, or friction, the shear stress cannot be continued if a neck starts to grow. Without a shear stress, the in-plane yield stress increases again and the deformation mechanism is stable, even without additional shear stress, until the in-plane stress is high enough to deform the sheet plastically. The result of this stabilising effect is that it raises the necking limit.

Based on the results obtained from the first-level FE model, it can be concluded that in SPIF the product is made by stretching and that the material is elongated and thinned. In the literature shown in Chapter 2, it has been suggested that this stretching is done mainly by pure shear. This suggestion was not based on experimental analysis, but intuitively by drawing a parallel with shear spinning. However, the results obtained from the second-level FE model reveal a significant magnitude of the through-thickness shear strains on planes perpendicular to and parallel to the tool movement in addition to the stretching. This contradicts the earlier suggestion. It can be concluded that this through-thickness shear works as a stabilisation mechanism and hence improves the formability compared with conventional sheet forming processes. Emmens and Boogaard [171] reported that the traditional forming curve FLC is only valid under certain restrictions and one of these is that the through-thickness shear is negligible. Based on this conclusion, the results of the second-level FE model suggest that the FLC cannot be used to evaluate the formability in AISF which agrees with the conclusion reported by Bambach et al [176].

In order to show the effect of through-thickness shear on the necking strain, the extended MK model proposed by Eyckens [119, 120] (see Section 2.4.5.2) is applied to the SPIF process. It serves to illustrate how a formability prediction can be made based on an overall deformation that includes in-plane stretching and through-thickness shear. The through-thickness shear strain can be predicted with a validated dual-level FE model, as illustrated in this chapter. The results presented hereafter may not be considered as quantitative formability predictions, but rather show that through-thickness shear strain is a contributing factor to the high formability in SPIF.

The SPIF investigation presented in this chapter has shown that the deformation of the sheet surface corresponds to plane strain, the direction with negligible elongation being the local tool movement direction, corresponding to the 2-axis of the local sheet frame. The 1-axis (along the cone wall) thus corresponds to the major in-plane strain direction. Figure 5.28 shows the total deformation that includes the through-thickness shear γ_{13} and γ_{23} of an element deformed by SPIF. Based on the extended MK model proposed by Eyckens, material vectors **X** along the three reference axes in the undeformed state, Figure 5.28(a), are transformed into material vectors **x** at the end of process as shown in Figure 5.28(b). The overall deformation in a SPIF cone can be described by the total deformation gradient **F**, which satisfies $\mathbf{x}=\mathbf{F}.\mathbf{X}$ under the assumption of homogeneous straining. The expression of **F** in the 1-2-3 reference frame can thus be constructed from Figure 5.28 as shown in Equation 5-3 [119, 120]:

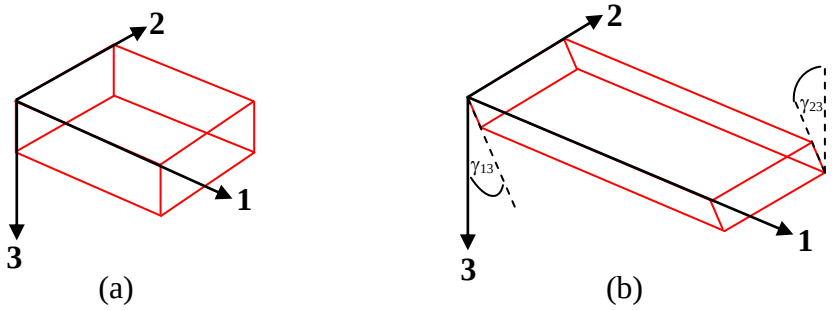

Figure 5.28: (a) an element in the undeformed state, (b) In the fully formed state, the element is elongated along the 1-direction, un-stretched along the 2-direction, thinned along the 3-direction and shows through-thickness shear in the 1-3- and 2-3-planes.

$$[\mathbf{F}]=\begin{vmatrix} t_0/t_f & 0 & \tan(\gamma_{13})\,t_0/t_f \\ 0 & 1 & \tan(\gamma_{23})\,t_0/t_f \\ 0 & 0 & t_f/t_0 \end{vmatrix} \quad \text{.....(5-3)}$$

Where, t_o is the initial sheet thickness, t_f is the final sheet thickness, γ_{13} and γ_{23} are the shear strains in the 1-3 and 2-3 planes respectively. It is assumed that volume is conserved by imposing that $F_{11}F_{22}F_{33}=1$. Then, assuming that the velocity gradient **L** is constant throughout the process, it can be calculated from the tensorial differential equation:

$$\mathbf{L}=\frac{d\mathbf{F}}{dt}\mathbf{F}^{-1}=constant \quad \text{.....(5-4)}$$

which has the solution:

$$\mathbf{L}=\frac{\ln(\mathbf{F})}{T} \quad \text{.....(5-5)}$$

in which 'ln' represents the tensorial logarithm, and T is the total time of the deformation process. The velocity gradient **L,** obtained by applying equation 5.3 to 5.5, is compared to the symmetric part of matrix velocity gradient L^a, i.e. D^a equation 5.6. The strain mode ratio's ρ_{11} ρ_{22} ρ_{33} ρ_{13} and ρ_{23} are then retrieved, which together describe the *monotonic* strain mode to reach the deformation from Figure 5.28 (a) to (b). The in-plane strain mode ρ_{22} found in this way equals 0 (plane strain surface deformation), ρ_{11} and ρ_{33} are therefore 1 and -1 respectively, while ρ_{13} is non-zero for a non-zero γ_{13}, and ρ_{23} is non-zero for a non-zero γ_{23}.

$$\mathbf{[D^a]}=\begin{vmatrix} 1 & 0 & \rho_{13} \\ 0 & \rho_{22} & \rho_{23} \\ \rho_{13} & \rho_{23} & -(1+\rho_{22}) \end{vmatrix} D_{11}^a \quad \text{.....(5-6)}$$

Where,

$$\rho_{22}=\frac{D_{22}^a}{D_{11}^a}, \qquad \rho_{13}=\frac{D_{13}^a}{D_{11}^a}, \qquad \rho_{23}=\frac{D_{23}^a}{D_{11}^a} \quad \text{.....(5-7)}$$

The SPIF aluminum cone of 45° wall angle shown in this chapter is taken as an example. The through-thickness shears γ_{13} and γ_{23} have been predicted through the dual-level FE model at the top surface and the final thickness is also measured. Hardening is assumed to be isotropic with strain hardening exponent of 0.19 and strength coefficient of 390MPa.Three different deformation gradients **F** are selected, the first represents zero through-thickness shear case. The second and third deformation gradients correspond to the measured total deformation that includes through-thickness shear strains γ_{13} and γ_{23}. These three cases are considered in order to illustrate the influence of

through-thickness shear deformation on the onset of localized necking in SPIF as shown in Table 5.2.

Table 5.2: Three deformation cases of aluminium cone of 45°.

Case	γ_{13}	γ_{23}
1	0	0
2	0.03	- 0.06
3	0.07	- 0.14

The extended MK model is implemented in Fortran 95 Standard code. Running on an Intel PC with two 3.0GHz processors (Core™ Q6850), the calculation time for a single point is about 40 minutes. In these calculations, a total of 90 initial groove orientations Φ_0 in the range of -90° to +90° with steps of 2°are tested to obtain the necking strains ε_{11}. However, the minimum of the necking strains ε_{11} is found at initial groove directions Φ_0 between -2° to +26° as shown in Figure 5.29. The calculation procedure are detailed in Eyckens et al [120].

Figure 5.29 presents the MK necking strain results from the different deformations of Table 5.2, for different initial groove normal directions Φ_0. The necking strain, i.e. forming limit ε_{11}, is higher for the cases 2 and 3 compared to case 1. For case 1 that includes zero through-thickness shear, the predicted major in-plane limit strain, i.e. the curve minimum, is found to be 0.169 at approximately 0^o initial groove angle. This is reasonable since the value of the necking strain is very close to the strain hardening exponent 0.19 when the through-thickness shear is not considered as reported by Eyckens et al [120].

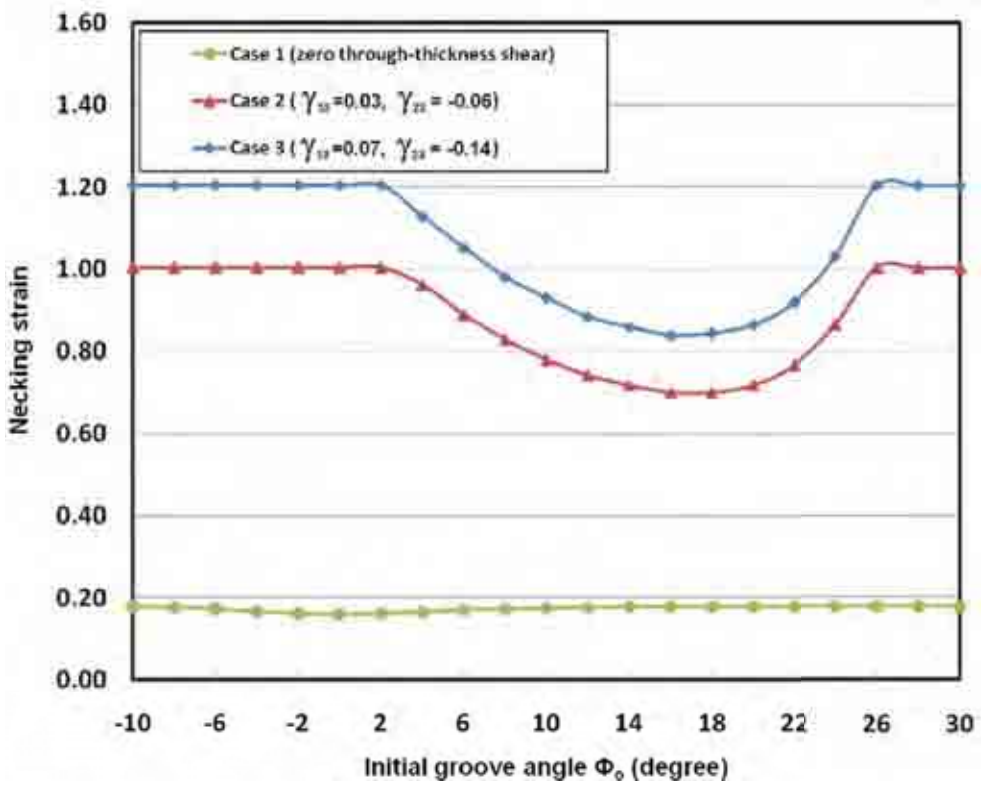

Figure 5.29: Predicted necking strain as a function of the initial groove directions.

For cases 2 and 3, higher necking strain has been achieved as a result of including the through-thickness shear in the deformation gradient. The necking strain or the forming limit is significantly affected with γ_{13} and/or γ_{23}. The larger the through-thickness shear, the higher the necking limits are raised compared to the deformation without through-thickness shear. This means that a large amount of deformation can be obtained without reaching the necking limit i.e. higher formability. For the calculated total deformation in the 45° wall angle cone, case 2 and case 3 predicted that the major in-plane limit strain is found to be 0.701 and 0.838 respectively at an initial groove angle between 16^o and 18^o, while it is only 0.169 if through-thickness shear strain is not considered in the MK model (case 1). The relative increase in formability is thus significant.

The new results gain insight into the mechanics of SPIF and provide some information about the reason for the enhanced formability of the process, i.e. the through-thickness shear, which could be used as an indicator of the process formability instead of the FLC.

5.12 Summary and Conclusions

A dual-level finite element model for single point incremental forming processes has been developed and implemented using the Abaqus/Implicit code. The full, first-level, FE model results were compared to and validated against experimental data. The FE results showed good correlation with the profile, thickness distribution and force history from experimental measurements. The second-level FE model based on a segment of the original model, showed the importance of assigning a sufficient number of elements through the thickness to provide a more comprehensive study on shear effects in the SPIF process. This study demonstrated the following,

- The full FE model was capable of predicting the final part geometries and dimensions in addition to the force history and normal strain evolution.
- The full model showed that stretching, thinning and bending were the dominant modes of deformation in SPIF.
- All components of strain generally increase on successive laps.
- In order to explore through-thickness modes of deformation, a large number of elements through the thickness were required and thus, the full model was not suitable.

- The second-level FE model revealed a significant magnitude of the through-thickness shear strains on planes perpendicular to and parallel to the tool movement, the greatest shear appearing on the former.
- Strain γ_{13} increases with the deformation progress until it reaches a maximum value and then remains constant. The shear strain γ_{23} is a reflection of γ_{13} where it increases with a negative sign, then remains constant.
- The maximum value of this shear strain γ_{23} is much higher than the other components, which could contribute to a higher forming limit.
- Through-thickness shear increases the necking limit and hence improves formability.
- The development of the dual-level FE model will permit further research on the influence of various process parameters on through-thickness shear deformation.

CHAPTER 6:

PROCESS PARAMETERS AND THROUGH-THICKNESS SHEAR STRAIN IN SPIF

6.1 Introduction and Scope of This Chapter

The through-thickness shear strains have been examined using FE modelling but sufficient accuracy is provided only when the models contained a sufficient number of through-thickness elements, as demonstrated in the previous chapter. The current chapter focuses on how process parameters influence the through-thickness shear strain, as this has been shown to be a likely indicator of formability in the SPIF process. An evaluation is conducted of five process parameters in SPIF of a truncated cone; these are step-down size, sheet thickness, tool diameter, friction coefficient and strength coefficient. The dual-level FE approach is used in conjunction with a statistical analysis of the results. The results are analysed using the DOE and ANOVA method to identify the most critical working parameters. Additionally, using a min-max optimisation method, the optimum working parameter setting that allows the maximum shear strain is determined.

Most of the previous work used either the maximum wall angle or the forming limit FLC_0 as an indicator of formability in single point incremental forming. High levels of through-thickness shear strain are suggested to be the reason for the increased forming limits of SPIF as verified in the previous chapter. The aim here is to obtain the most

critical working parameters and their effects on the through-thickness shear deformation. The principal contributions of the research described here are:

- Determination of the most critical working parameters that affect the shear deformation through the thickness.
- Establishing an empirical model that relates the critical working parameters and the through-thickness shear strains.
- Examination of the effects of the critical working parameters on the through thickness shear strains.
- Determination of the optimum setting of the working parameters that give maximum through-thickness shear deformation.

6.2 Parametric Investigation

In single point incremental forming there is a number of parameters that affect the process mechanics. These could be classified into process parameters (tool feed rate, tool diameter, incremental step-down and lubrication), material parameters (strength coefficient, strain hardening, anisotropy and Young's modulus) and design parameters (sheet thickness and final product geometry). Based on a preliminary study, the feed rate was excluded from the investigation as it did not show any significant effect on the shear deformation for the example shown here. Except for the feed rate, all process parameters are included in the present plan while the strength coefficient is chosen to represent the material parameters. Since the analysis will be conducted for a fixed product geometry, i.e. a truncated cone, the sheet thickness is chosen to represent the design parameters. A design of experiment (DOE) approach requires a range of each

parameter to be selected. These cover most of the experimental investigations appearing in the literature. Table 6.1 shows the different process factors and their corresponding levels.

Table 6.1: Process factors and corresponding levels.

Level / Factor	Low level	Intermediate level	High level
Step-down size (mm)	0.2	1.1	2
Friction coefficient	0.02	0.26	0.5
Tool diameter (mm)	10	15	20
Sheet thickness (mm)	0.4	1.7	3
Strength coefficient (MPa)	170	400	670

Response variables are also required; these are the Quality Characteristics (QC), which generally refer to the measured results. In the present investigation, the response variables are the shear strain in a plane normal to the tool movement i.e., γ_{13} and the shear strain in a plane parallel to the tool movement i.e., γ_{23},. These were chosen as values representative of the shear deformation through the thickness. Based on the use of a design of experiment (DOE approach), the Box-Behnken design technique [169] was used to generate a set of experiments for combinations of the five process factors which are varied over the three levels, i.e. low level, intermediate level and high level as shown in Table 6.1. The result of running the Box-Behnken design produced 46 different combinations of these factors as shown in Table 6.2. Each of these combinations is assessed through the use of a separate dual-level FE simulation. In each case the through-thickness shear strain γ_{13} and γ_{23} are recorded at the top surface.

Table 6.2: Through-thickness shear strains for 46 experiments.

Run	Step-down size (mm)	Friction coefficient	Tool diameter (mm)	Sheet thickness (mm)	Strength coefficient (MPa)	Shear strain γ_{13}	Shear strain γ_{23}
1	2.0	0.26	15	1.7	170	0.100	0.033
2	1.1	0.26	10	3.0	420	0.349	0.740
3	0.2	0.5	15	1.7	420	0.096	0.374
4	0.2	0.26	10	1.7	420	0.129	0.244
5	1.1	0.02	15	1.7	170	0.080	0.068
6	2.0	0.26	15	1.7	670	0.083	0.023
7	0.2	0.26	15	1.7	170	0.071	0.129
8	1.1	0.26	20	1.7	670	0.053	0.108
9	0.2	0.26	15	0.4	420	0.033	0.018
10	1.1	0.50	10	1.7	420	0.289	0.730
11	1.1	0.26	20	3.0	420	0.118	0.295
12	1.1	0.50	20	1.7	420	0.078	0.375
13	1.1	0.26	10	1.7	670	0.127	0.208
14	0.2	0.26	15	1.7	670	0.058	0.106
15	1.1	0.50	15	1.7	170	0.083	0.308
16	2.0	0.02	15	1.7	420	0.092	0.029
17	1.1	0.26	10	0.4	420	0.056	0.045
18	1.1	0.26	15	1.7	420	0.068	0.102
19	1.1	0.26	15	3.0	170	0.254	0.504
20	1.1	0.02	20	1.7	420	0.065	0.071
21	0.2	0.02	15	1.7	420	0.067	0.089
22	1.1	0.02	15	3.0	420	0.178	0.107
23	1.1	0.26	15	0.4	170	0.033	0.019
24	2.0	0.26	15	3.0	420	0.173	0.035
25	1.1	0.26	20	1.7	170	0.066	0.126
26	0.2	0.26	15	3.0	420	0.135	0.386
27	2.0	0.26	15	0.4	420	0.026	0.011
28	1.1	0.50	15	3.0	420	0.400	0.605
29	1.1	0.26	15	1.7	420	0.068	0.102
30	2.0	0.50	15	1.7	420	0.092	0.014
31	1.1	0.26	10	1.7	170	0.138	0.327
32	2.0	0.26	20	1.7	420	0.071	0.011
33	0.2	0.26	20	1.7	420	0.051	0.090
34	2.0	0.26	10	1.7	420	0.138	0.034
35	1.1	0.26	15	3.0	670	0.194	0.370
36	1.1	0.26	15	1.7	420	0.068	0.102
37	1.1	0.26	20	0.4	420	0.022	0.009
38	1.1	0.02	10	1.7	420	0.129	0.103
39	1.1	0.26	15	0.4	670	0.032	0.014
40	1.1	0.50	15	1.7	670	0.065	0.211
41	1.1	0.26	15	1.7	420	0.068	0.102
42	1.1	0.26	15	1.7	420	0.068	0.102
43	1.1	0.50	15	0.4	420	0.047	0.027
44	1.1	0.02	15	1.7	670	0.065	0.053
45	1.1	0.02	15	0.4	420	0.036	0.011
46	1.1	0.26	15	1.7	420	0.068	0.102

An analysis of variance (ANOVA) was performed on the design of experiments to identify the significant factors and interactions. A significance level of 5% was used. A smaller P-value (less than 5%) is associated with increased importance of the factor. Table 6.3 shows the P-values for the significant factors and interactions. According to the R-Square and adjusted R-Square values, the Box-Behnken statistical analysis highlighted that a quadratic model provides a very good description of the evolution of the quality characteristics with respect to the working parameters. The R-Square and adjusted R-Square values for all responses did not fall below 89%.

Table 6.3: Significant factors and corresponding P-values.

	P Values	
	Shear strain γ_{13}	Shear strain γ_{23}
Step-down size **(A)**	0.0622	0.01
Friction coefficient **(B)**	0.0776	0.0001
Tool diameter **(C)**	0.0003	0.001
Sheet thickness **(D)**	0.0001	0.0001
Strength coefficient **(E)**	0.594	0.351
Significant interactions	(C*D) 0.001	(B*C) 0.028 (B*D) 0.0002 (C*D) 0.032

The analysis of variance shows that the shear strain γ_{13} is affected by tool diameter, sheet thickness and the interaction between the tool diameter and sheet thickness.

While, the shear strain γ_{23} is affected by step-down size, friction coefficient, tool diameter and sheet thickness. Additionally, it is affected by the following interactions; friction coefficient and tool diameter, friction coefficient and sheet thickness, tool diameter and sheet thickness. On the other hand, the strength coefficient seems to have no significant effect upon the shear deformation and hence the formability, confirming the observations of Fratini et al [97] and Hussain et al [165].

6.3 Shear Strain γ_{13}

Figure 6.1 shows the effect of tool diameter on the through-thickness shear strain γ_{13}. The solid line represents the quadratic model while the dotted lines represent the maximum variation of the actual results. The results show that as tool diameter increases the shear strain γ_{13} decreases. Using a small diameter tool tends to localise the deformation underneath the tool and increase the local strains. As the tool diameter increases, the contact area increases and hence the contact pressure decreases. As a result of increasing the contact area, the deformation becomes more distributed and hence the forming forces decrease which leads to a decrease in the generated strains. The shear strain γ_{13} increases from 0.043 to 0.067 by decreasing the tool diameter from 20mm to 15mm and increases significantly to 0.184 by using a tool diameter of 10mm. Similar results are found by Ham and Jeswiet [168] and Le et al [140], although not related directly to shear strain.

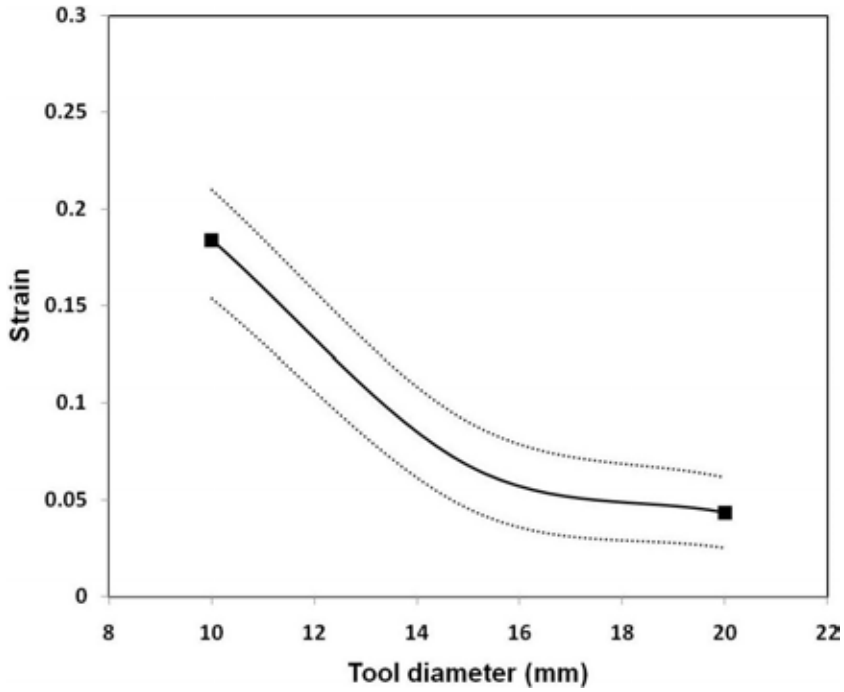

Figure 6.1: Effect of tool diameter on the shear strain γ_{13}.

The effect of sheet thickness on the shear strain γ_{13} is shown in Figure 6.2. It can be seen that the shear strain γ_{13} increases by increasing the sheet thickness. γ_{13} is the shear strain in the plane perpendicular to the tool movement and results from pushing the forming tool across the material along the wall angle. Additionally, as the sheet thickness increases, the maximum radial and thickness strains that the sheet can support without fracture and hence the maximum wall angle increase [168]. Therefore, increasing the sheet thickness will result in a significant increase in the shear strain γ_{13}.

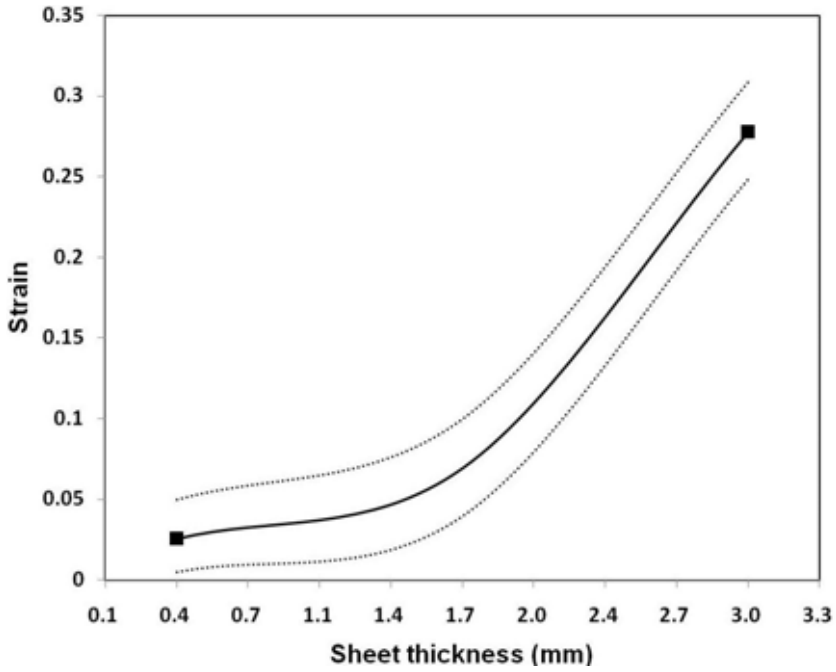

Figure 6.2: Effect of sheet thickness on the shear strain γ_{13}.

The interaction between the sheet thickness and tool diameter has a significant effect on the shear strain γ_{13} as shown in Figure 6.3. The contribution resulting from increasing the sheet thickness upon the shear strain γ_{13} becomes more significant by decreasing the tool diameter. Using a 3mm sheet thickness and 20mm tool diameter, the maximum shear strain achieved is 0.124. For the same sheet thickness, the shear strain γ_{13} could be increased to 0.515 by decreasing the tool diameter to 10mm. This suggests that to increase the shear strain γ_{13} and hence the formability, it is recommended to minimise the tool diameter and maximise the sheet thickness. Similar findings have also been reported [168], although not related directly to shear strain.

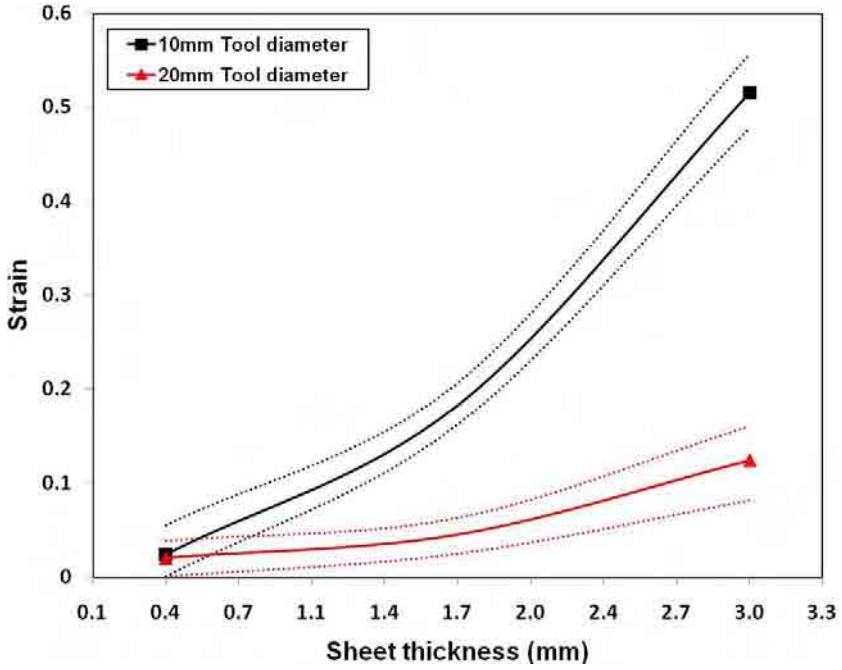

Figure 6.3: Effect of the interaction between tool diameter and sheet thickness on the shear strain γ_{13}.

6.4 Shear Strain γ_{23}

Figure 6.4 shows the effect of the step-down size on the shear strain γ_{23}. A decrease in the incremental step results in an increase in the shear strain. As the step-down size increases, the normal stresses in the sheet material at the forming tool increases and thus the sheet fracture may take place earlier. Additionally, a large step-down size results in a large loss in the material thickness i.e., sheet thinning, which leads to a reduction in the shear deformation that takes place along the sheet thickness. An alternative explanation for decreasing the shear strain γ_{23} could be the following; as a result of using a large incremental step-down size, the material is partially deformed by pulling/stretching instead of shear induced by the forming tool. This leads to a decrease in the localised deformation and thus the shear strain γ_{23} decreases. This agrees with the results reported by Ham and Jeswiet [168], although not related directly to shear strain.

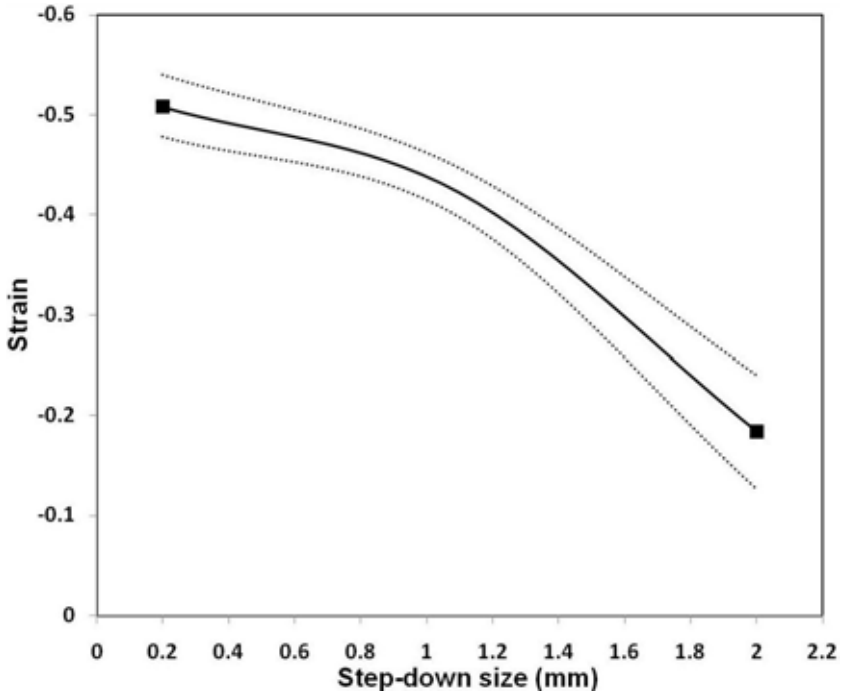

Figure 6.4: Effect of step-down size on the shear strain γ_{23}.

It can be seen that the friction coefficient has a significant impact on the shear strain γ_{23} as shown in Figure 6.5. This is the shear strain in a plane parallel to the tool movement and results from the friction between the forming tool and sheet surface. Therefore, as the friction coefficient increases, the through-thickness shear strain γ_{23} increases. This agrees with previous results found by Allwood et al [118], Jackson and Allwood [161]. They reported that the formability in SPIF could be increased by increasing the friction between the forming tool and sheet surface. In a recent study on the frictional effects on the deformation behaviour by Yamashita et al in 2010 [213], it was concluded that a higher friction coefficient produced a higher and more uniform strain distribution. More recent, Eyckens et al in 2011 [214] reported that friction between the forming tool and sheet surface is most likely playing a key role in through-thickness shearing in AISF. However, Hussain et al [166] suggested that if the friction is too high, an unacceptable surface roughness will develop. The effect of the tool diameter on the shear strain γ_{23} is

shown in Figure 6.6. Similar to the effect of tool diameter on the shear strain γ_{13}, shear strain γ_{23} increases by decreasing the tool diameter.

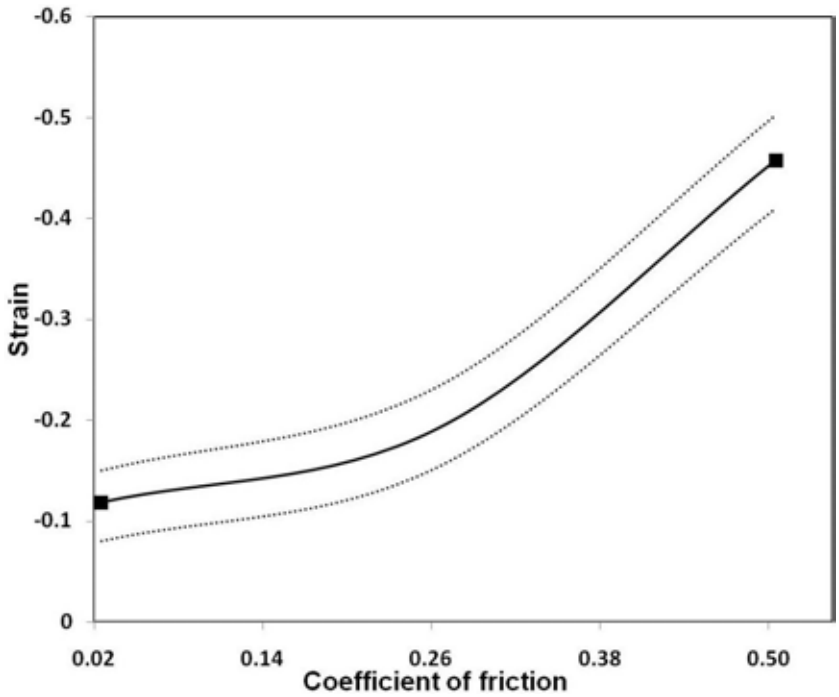

Figure 6.5: Effect of coefficient of friction on the shear strain γ_{23}.

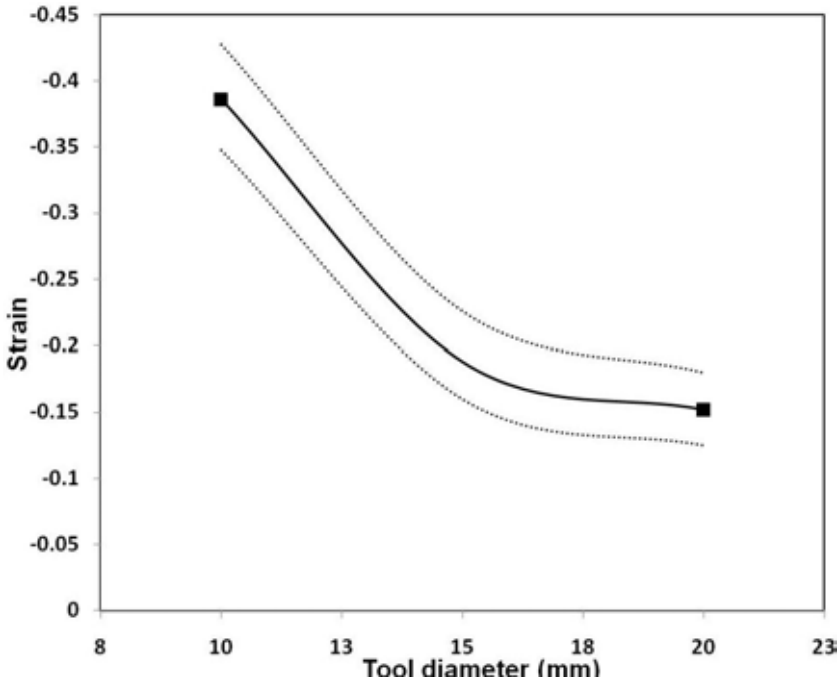

Figure 6.6: Effect of tool diameter on the shear strain γ_{23}.

Figure 6.7 shows the effect of the sheet thickness on the shear strain γ_{23}. This shows that an increase in the shear strain γ_{23} is associated with an increase in the sheet thickness. In the results reported by Jackson and Allwood [161], it was concluded that the shear strain γ_{23} increases as a result of overlapping the contact area of the tool on successive passes. This overlapping effect is expected to increase as a result of decreasing the step-down size and increasing the sheet thickness, where large sheet thickness will delay the onset of instability and fracture. Therefore, a large sheet thickness has a significant effect on increasing the shear strain γ_{23}.

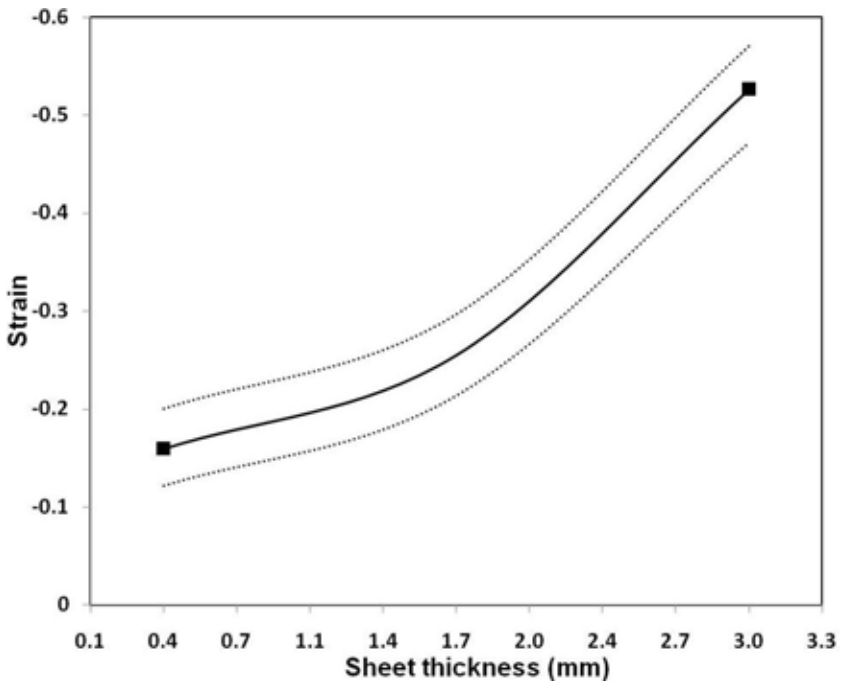

Figure 6.7: Effect of sheet thickness on the shear strain γ_{23}.

The effect of the interaction between tool diameter and coefficient of friction on the shear strain γ_{23} is shown in Figure 6.8. At a low coefficient of friction (0.02), the effect of the tool diameter on the shear strain γ_{23} is not clear. However, at a high coefficient of friction (0.5), the absolute value of the shear strain γ_{23} reduced by approximately half by

increasing the tool diameter from 10mm to 20mm. It means that the impact of the tool diameter upon the shear deformation becomes highly significant at higher values of the coefficient of friction. This suggests that the shear strain γ_{23} could be further increased by using a small tool diameter and a large coefficient of friction.

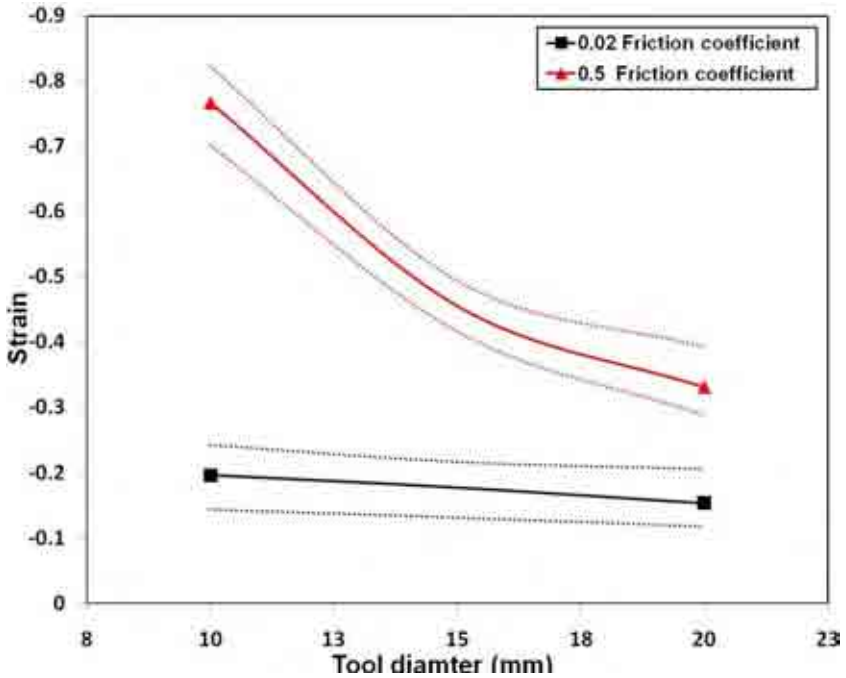

Figure 6.8: Effect of the interaction between tool diameter and coefficient of friction on the shear strain γ_{23}.

Figure 6.9 shows the effect of the interaction between sheet thickness and coefficient of friction on the shear strain γ_{23}. At 0.4mm sheet thickness and 0.02 coefficient of friction, the absolute value of shear strain γ_{23} is 0.238. This represents a small amount of shear strain compared to that of 1.433 at a 3mm sheet thickness and 0.5 coefficient of friction. This suggests that using a large value of sheet thickness combined with a large value of coefficient of friction would increase the through-thickness shear strain γ_{23}.

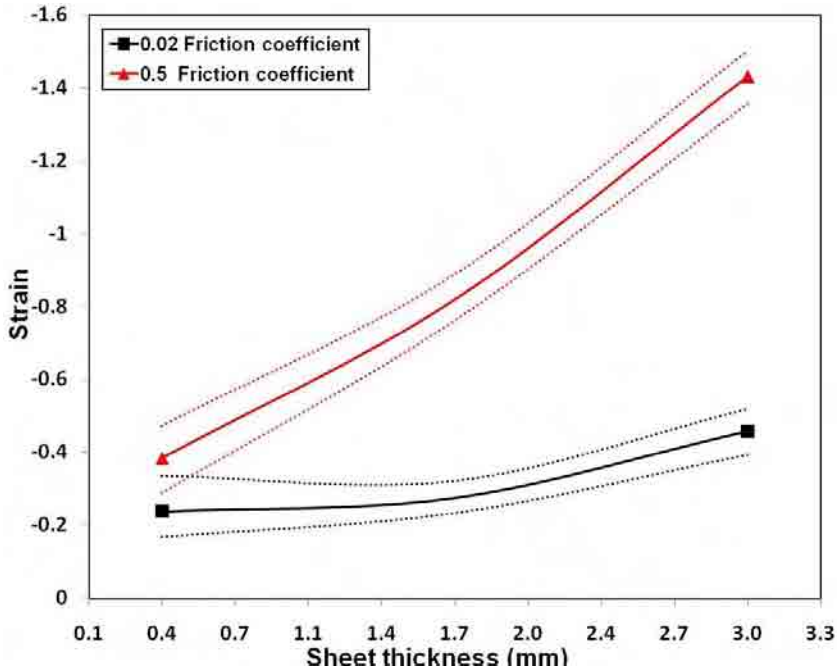

Figure 6.9: Effect of the interaction between sheet thickness and coefficient of friction on the shear strain γ_{23}.

Figure 6.10 shows the effect of the interaction between sheet thickness and tool diameter on the shear strain γ_{23}. As a result of using a large tool diameter and small sheet thickness the generated shear strain γ_{23} reduces. On the other hand, using a small tool diameter and large sheet thickness leads to a localisation of the deformation underneath the tool and an increase in the overlapping contact area of the tool on successive passes. Thus, the generated shear strain γ_{23} increases. Based on the previous results, the through-thickness shear strains and hence the process formability could be improved by increasing the sheet thickness and the coefficient of friction and decreasing the tool diameter and step-down size. With a better control of these parameters, a large amount of through-thickness shear deformation could be generated and further improvement of the process formability would be expected.

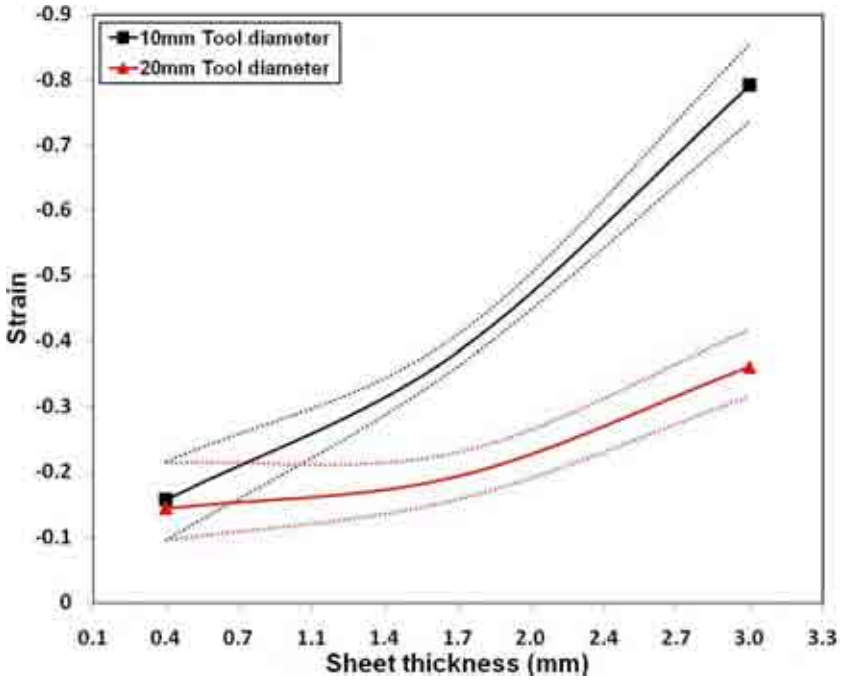

Figure 6.10: Effect of the interaction between sheet thickness and tool diameter on the shear strain γ_{23}.

6.5 Prediction and Optimisation of the Through-thickness Shear Strain

It is useful to develop an empirical model that can predict the value of each of the through-thickness shear strain components for any combination of the working parameters. As a result of using numerical factors in this study, it is possible to predict the resulting shear strain components for any value of each parameter within the range studied even if it was not one of the pre-selected levels. Using a general second order polynomial equation, an empirical model can be developed based on the working parameters, i.e. step-down size, coefficient of friction, tool diameter, sheet thickness, strength coefficient and their interactions. Each parameter and interaction is multiplied by a coefficient as shown in Equations 6-1 and 6-2. These empirical models determine the generated through-thickness shear strains at the end of the second level FE model.

γ_{13} = 0.134287 + 0.041008***A*** - 0.21807***B*** - 0.02944***C*** + 0.145754***D*** + 0.000195***E*** - 0.03227***A*B** + 0.000671***A*C*** + 0.009768***A*D*** - 4.8E-06***A*E*** - 0.03076***B*C*** + 0.32892***B*D*** - 1.1E-05***B*E*** - 0.01911***C*D*** - 4E-07***C*E*** - 4.6E-05***D*E*** - 0.02174*$\mathbf{A^2}$ + 0.628904*$\mathbf{B^2}$ + 0.001841*$\mathbf{C^2}$ + 0.04736*$\mathbf{D^2}$ - 1.7E-07*$\mathbf{E^2}$

……..…..……(6-1)

γ_{23} = 0.523286 + 0.229111***A*** + 0.579018***B*** - 0.17483***C*** + 0.17483***D*** - 0.0002***E*** - 0.34656***A*B*** + 0.007258***A*C*** - 0.07342***A*D*** + 1.4E-05***A*E*** - 0.10893***B*C*** + 0.786695***B*D*** - 0.00034***B*E*** - 0.01955***C*D*** + 2E-05***C*E*** - 9.9E-05***D*E*** - 0.09806*$\mathbf{A^2}$ + 1.874758*$\mathbf{B^2}$ + 0.004124*$\mathbf{C^2}$ + 0.059989*$\mathbf{D^2}$ + 3.81E08*$\mathbf{E^2}$……..……...……(6-2)

Where, **A** is the step-down size, **B** is the coefficient of friction, **C** is the tool diameter, **D** is the sheet thickness and **E** is the strength coefficient.

R-Square, multiple correlation coefficients that indicate the model fit did not go below 89% for both models. This suggests a very good fit for the data points. The normal distribution of the residuals is one of the measures that used to check the efficiency of an empirical model. It has been used here to verify the above empirical models as shown in Figure 6.11. The residual plot should have a linear spread close to the normal distribution in order to accept the model results. The normal plots for γ_{13} and γ_{23} show a satisfactory deviation from normality and acceptable variance distribution. The results suggest that the models can be used to explore the design space of the working parameters.

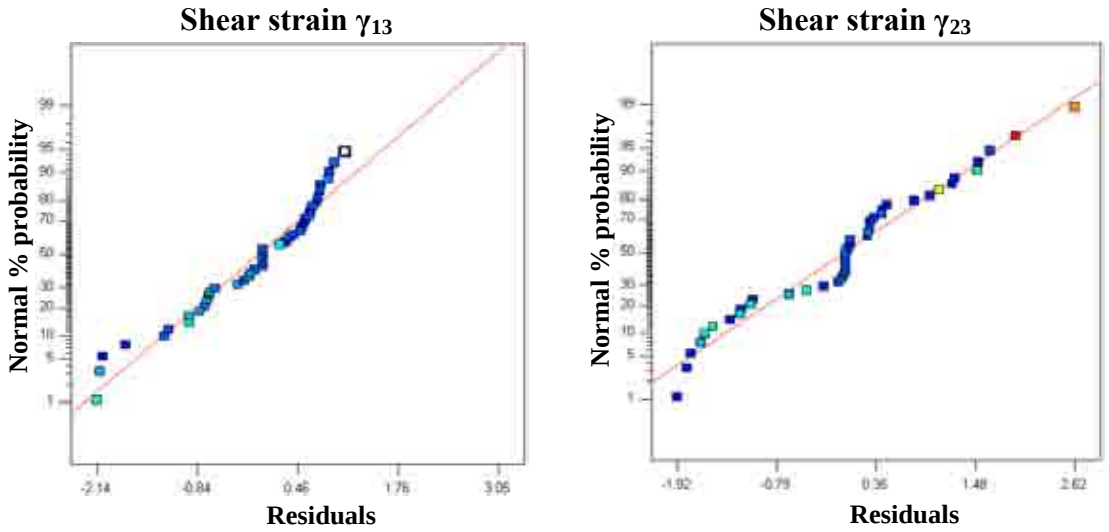

(a) (b)

Figure 6.11: Normal plots of the residual for the empirical models of (a) γ_{13} and (b) γ_{23}.

Using a Min-Max optimisation method, Equations 6-1 and 6-2 are solved together to obtain the optimal setting of the working parameters that maximise the through-thickness shear deformation. The objective function is to maximise the response variables, i.e. γ_{13} and γ_{23} for a minimum coefficient of friction. This objective function helps to identify the process conditions that lead to an increase in the through-thickness shear deformation and hence the formability at minimum surface roughness. All working parameters are constrained within their design space, i.e. their pre-selected levels, and all strain components given the same weight, i.e. same priority and importance. The optimal setting obtained is shown in Table 6.4 while the corresponding through-thickness strains are presented in Table 6.5. In order to validate the results, a single process simulation using the optimal working parameters is performed through the dual-level FE modelling approach. The through-thickness shear strains γ_{13} and γ_{23} are measured (observed strains) and compared to those predicted by the empirical

models. The results show very good agreement between predicted and observed strains which provides another check on the efficiency of the empirical models.

Table 6.4: Optimal setting of the involved working parameters.

	Step-down size (mm)	Coefficient of friction	Tool diameter (mm)	Sheet thickness (mm)	Strength coefficient (MPa)
Optimal setting	0.41	0.3	10	3	170

Table 6.5: Predicted and observed shear strains.

	shear strain γ_{13}	shear strain γ_{23}
Predicted strains	0.535	0.855
Observed strains	0.531	0.821

6.6 Summary and Conclusions

A dual-level FE model for single point incremental forming has been used to explore the shear deformation through the sheet thickness in the forming of a truncated cone. DOE and ANOVA approaches were adopted to study the effect of process, design and material parameters on the through-thickness shear strains. This shear strain can be used as a direct indicator of formability in the SPIF process.

This study demonstrated the following;

- Tool diameter and sheet thickness are the most critical parameters that influence the through-thickness shear strain, γ_{13} and γ_{23}. Coefficient of friction and step-

down size have a significant effect on the through-thickness shear strain, γ_{23} only. Strength coefficient did not show any influence on the shear deformation.

- A significant increase in the shear strain γ_{13} was observed by decreasing the tool diameter and increasing the sheet thickness.
- A higher shear strain γ_{23} was achieved by increasing the coefficient of friction and sheet thickness and decreasing the step-down size and tool diameter.
- An empirical model was developed to describe the through-thickness shear strains for any combination of working parameters.
- The min-max optimisation method allowed the optimal setting of the working parameters at a minimum coefficient of friction that maximised the through-thickness shear deformation to be obtained**.**

CHAPTER 7:

STRATEGIES FOR IMPROVING PRECISION IN SPIF

7.1 Introduction and Scope of This Chapter

Large elastic springback resulting from the die-less nature of the SPIF process can cause problems if high levels of accuracy are required. In this chapter, the first-level FE model of the forming of a truncated cone, discussed in chapter 5, is used to investigate springback with various process strategies to improve the product accuracy. These strategies involve the introduction of a backing plate, a supporting kinematic tool and a modification of the tool path. The accumulated effect of these modifications on the final geometrical precision is also investigated.

The aim of this chapter is to improve precision in SPIF through reducing the most common geometrical errors. The chapter focuses on an investigation of the following four strategies:

1. This is based on the traditional method of SPIF and is provided as a benchmark. The results have previously been validated as shown in chapter 5.
2. Strategy 2 incorporates the use of an annular backing plate located beneath the sheet.
3. In this strategy a supporting kinematic tool is used in addition to the backing plate.

4. The final strategy is based on the same setup as strategy 3 but incorporates modifications to the tool path so that the pillow effect at the sheet centre can be eliminated.

The principal contributions of the research described here are:

- Clarification of the improvements in geometrical accuracy by using simple modifications to the SPIF process.
- An illustration of the accumulated effects of the process modifications on the final profile, stress, plastic strain and thickness distributions.

7.2 Geometrical Errors in SPIF

Although single point incremental forming can be performed using a simple forming tool without a dedicated die, the process suffers from a lack in precision as a result of minimal clamping, especially when the deformation starts at a large distance from the clamping frame, and significant springback. The first strategy represents the traditional setup of SPIF with a single forming tool that follows the contour of the part through a number of step-down levels (see chapter 5, section 5.3). Figure 7.1 shows the profile plots obtained from the first-level FE model, strategy 1 compared to the theoretical profile. The comparison demonstrates the geometrical deviations in SPIF which were due to the sheet bending close to the major diameter of the cone, the springback at the cone base and the pillow effect at the centre of the cone [179].

The geometrical errors are evaluated as the distance between the theoretical and FE profiles [179]. According to this definition, three measures e_b, e_s and e_p are used to

represent the different geometrical errors as shown in Figure 7.1. The deviation at the major diameter is given by e_b which represents the geometrical error resulting from the sheet bending. The deviation at the minor base is shown by e_s which represents the sheet lifting resulting from springback. The deviation at the sheet centre is given by e_p which represents the geometrical error resulting from the pillow effect. The values of e_b, e_s and e_p obtained from strategy 1 are 3.99mm, 1.52 and 0.63mm respectively.

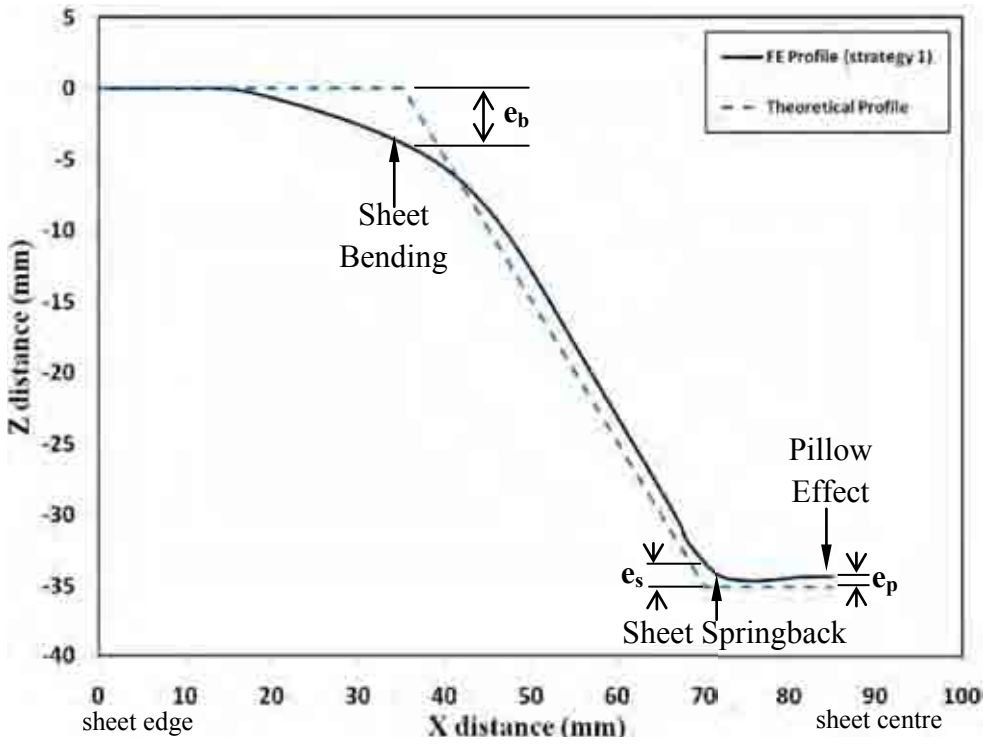

Figure 7.1: The profile plots of a 45° truncated cone.

7.3 Strategies to Improve the Geometrical Accuracy in SPIF

Strategies 2, 3 and 4 are investigated to assess their potential for improving the geometrical accuracy in SPIF processes. All models/strategies are performed using the first-level Implicit FE model detailed in chapter 5.

7.3.1 Strategy No 2

In the SPIF process, the distance between the forming area and sheet flange is recommended to be as small as possible to reduce the bending effect at the major diameter [179]. Elastic springback will occur locally during deformation and globally after the forming process. Springback that results from post-processing such as trimming is not considered in the present model. The local springback could be reduced by using static dies [191]. These static dies could provide partial support or re-create the final product shape. The partial dies reduce springback in particular areas of deformation, while the full dies are much better but can be used for specific products only and increase the tooling cost. The introduction of an annular backing plate in strategy 2, located beneath the sheet, extends the supporting structure and minimises this distance. Strategy 2 therefore aims to investigate the effect of the backing plate on geometrical deviations, in particular the sheet bending at the major diameter. Figure 7.2 shows the geometry and dimensions of the backing plate used for the truncated cone. The inner geometry of the plate is a circular profile that has a fillet curvature of 4mm radius in order to allow smooth contact with the deformed material. The backing plate is modelled as a rigid body and fixed concentrically under the sheet so that it cannot move in any direction. The FE model for strategy 2 is shown in Figure 7.3.

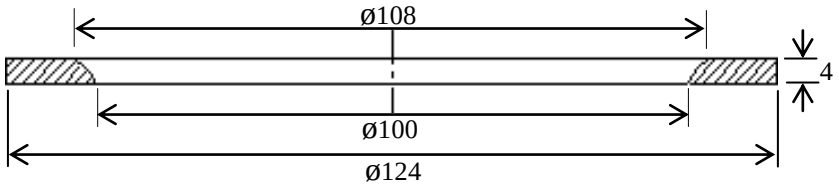

Figure 7.2: Dimensions (mm) and geometries of the designed backing plate.

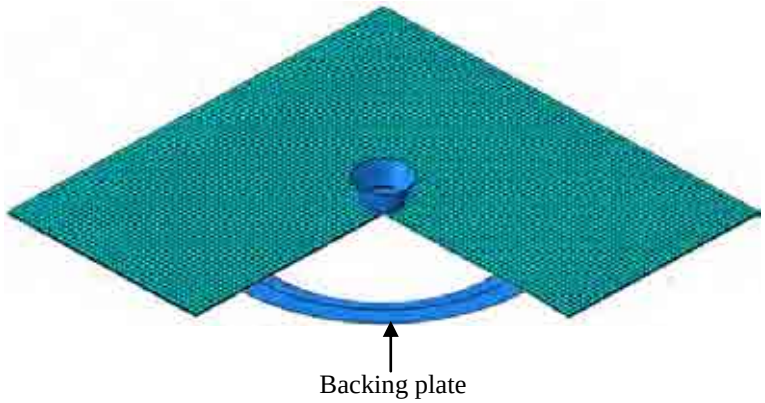

Figure 7.3: The configuration of the FE model of strategy 2.

7.3.2 Strategy No 3

In this strategy a supporting kinematic tool is used in addition to the backing plate. The forming tool and the kinematic supporting tool move in a synchronized motion and incrementally form the blank sheet into the required shape as shown in Figure 7.4. The supporting tool has the same dimensions and geometry as the forming tool. The new tool is modelled as a rigid body and its boundary condition is defined so that it moves in a synchronized motion with the forming tool in the XY plane and is always in contact with the bottom surface of the sheet. Surface to surface contact between the new tool and the bottom surface of the sheet is defined and coulomb friction is set with a friction coefficient of 0.05. Figure 7.5 shows the FE model for strategy 3.

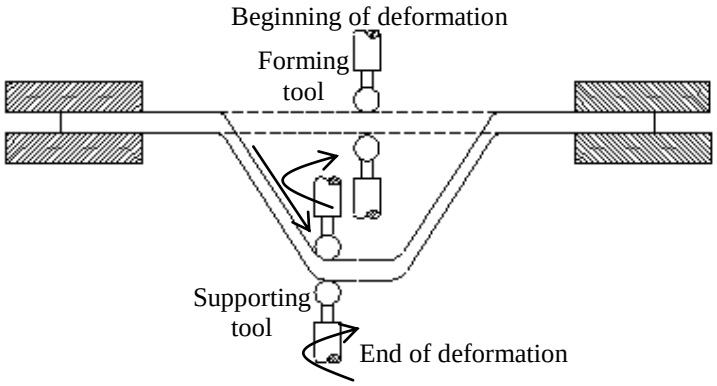

Figure 7.4: The full kinematic setup.

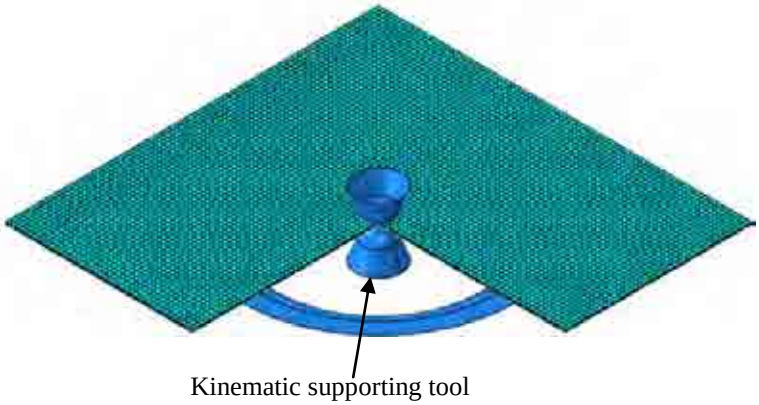

Figure 7.5: The configuration of the FE model of strategy 3.

7.3.3 Strategy No 4

The final strategy is based on the same setup as strategy 3 but incorporates modifications to the tool path so that the pillow effect at the sheet centre can be eliminated. The pillow effect occurs when the final height at the sheet centre is less than that at the last tool position. If the required product geometry contains an area in which there is no deformation imposed by the forming tool, such an effect is to be expected. In the example here the minor base of the truncated cone represents such an area. It is clear that this defect, at the end of the forming process, is a result of the product geometry, tool path and lack of support at the sheet centre. The tool path is extended so that at the end of deformation, the forming tool and the kinematic supporting tool continue circular paths on a horizontal plane toward the sheet centre. This concept allows small plastic deformation that leads to a flat surface instead of the curved profile previously observed, so that the height at the sheet centre will be close to the desired height. Figure 7.6 shows a schematic diagram for the modified tool path.

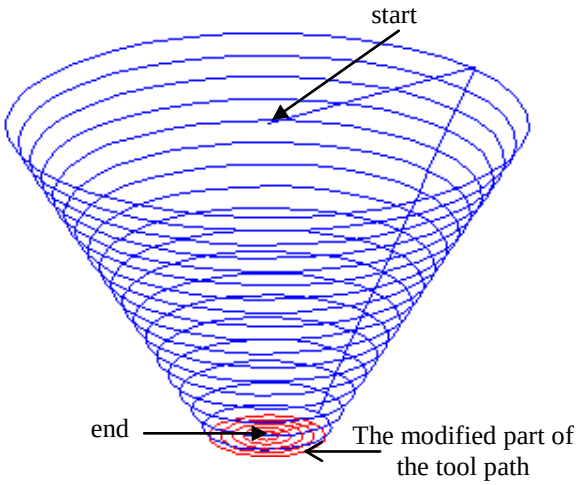

Figure 7.6: Schematic diagram for the modified tool path, strategy 4.

7.4 Results Analysis and Discussion

Figure 7.7 shows a comparison between strategy 1 and 2 to illustrate the effect of the backing plate on the final profile. The theoretical profile is also plotted to show by how much the geometrical errors are reduced. Using strategy 2, a significant reduction in the sheet bending at the major diameter is achieved. The backing plate clearly increases the sheet rigidity by introducing additional support nearer to the deformation zone. However, there is no significant change to the final profile either at the minor diameter or at the cone centre. The results show that e_b is reduced from 3.99mm to 1.62mm while e_s and e_p are found to be 1.50mm and 0.63mm respectively. This suggests that the backing plate could only reduce the deviation resulting from the bending effect and it does not influence the deviation resulting from the sheet springback and the pillow effect.

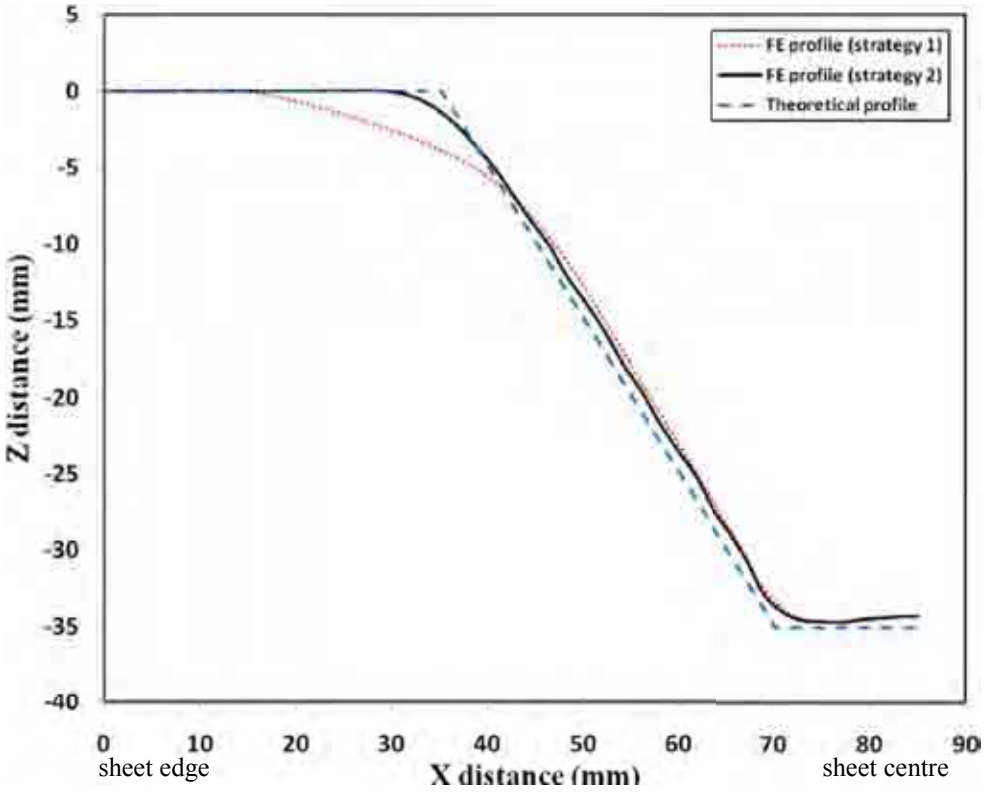

Figure 7.7: Effect of the backing plate on the final profile.

In order to illustrate the effect of the kinematic supporting tool on the geometrical errors, a comparison between strategy 2 and 3 is shown in Figure 7.8. At the major diameter and sheet centre of the truncated cone, there is no difference between strategy 2 and 3 which means that the kinematic supporting tool does not affect either the sheet bending or the pillow effect. Along the cone wall until the minor diameter, there is a significant reduction in sheet springback as a result of adding a new kinematic tool. The results show that only e_s is reduced from 1.50mm by strategy 2 to 0.60mm by strategy 3. The kinematic supporting tool leads to a greater localisation of the deformation underneath the forming tool and a reduction of the local springback. Therefore, the cone wall obtained from strategy 3 is very close to that of the theoretical profile and thus, the sheet lifting of the minor diameter of the cone is less than that in strategy 2.

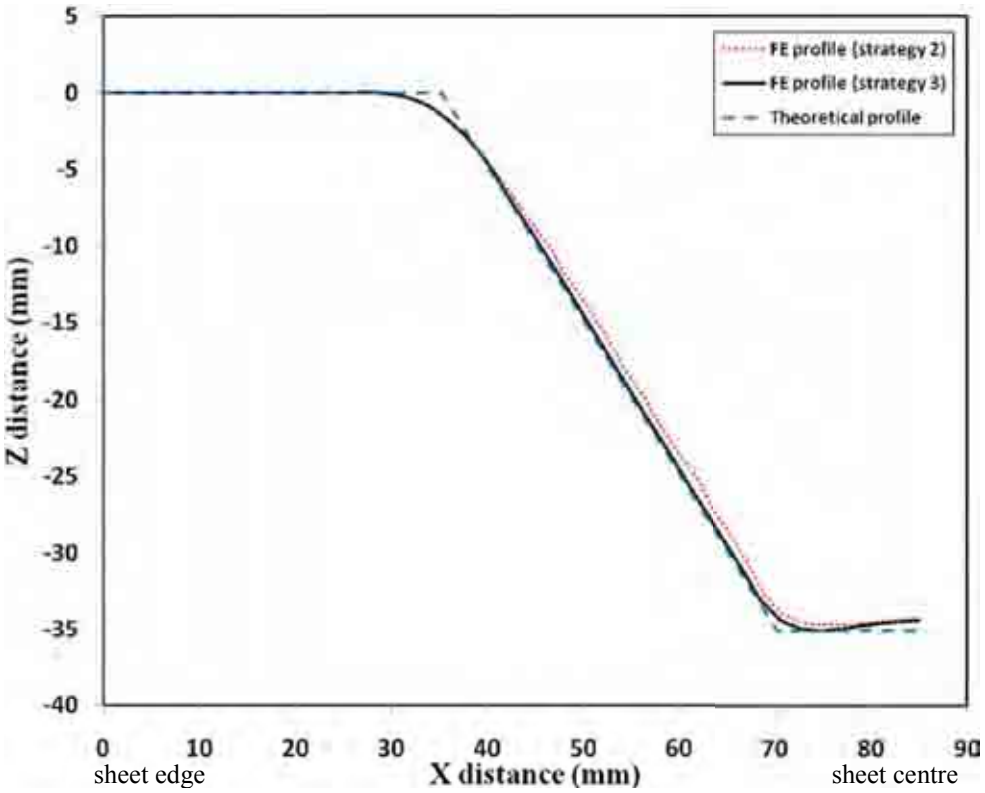

Figure 7.8: Effect of the kinematic supporting tool on the final profile.

Figure 7.9 and Figure 7.10 show the profile plot during the deformation process for strategies 1 and 3 respectively in order to illustrate the effect of the kinematic tool on the local springback. Six profiles are plotted, at 2, 4, 6, 8 and 10 mm step-down positions and at the final deformation i.e., 35mm step-down size. In Figure 7.9, the elastic springback and the sheet lifting in conventional SPIF setup can clearly be seen after every tool path, especially below the tool location. At the beginning of deformation, the elastic springback is large. As a result of the sheet lifting after the tool moves across its path, the FE profile deviates from the theoretical one. As the deformation progresses, the local elastic springback decreases as a result of increasing the amount of plastic deformation. At the end of deformation, the deviation between the

FE profile and the theoretical one represents the cumulative effect of the sheet springback that took place during the deformation process.

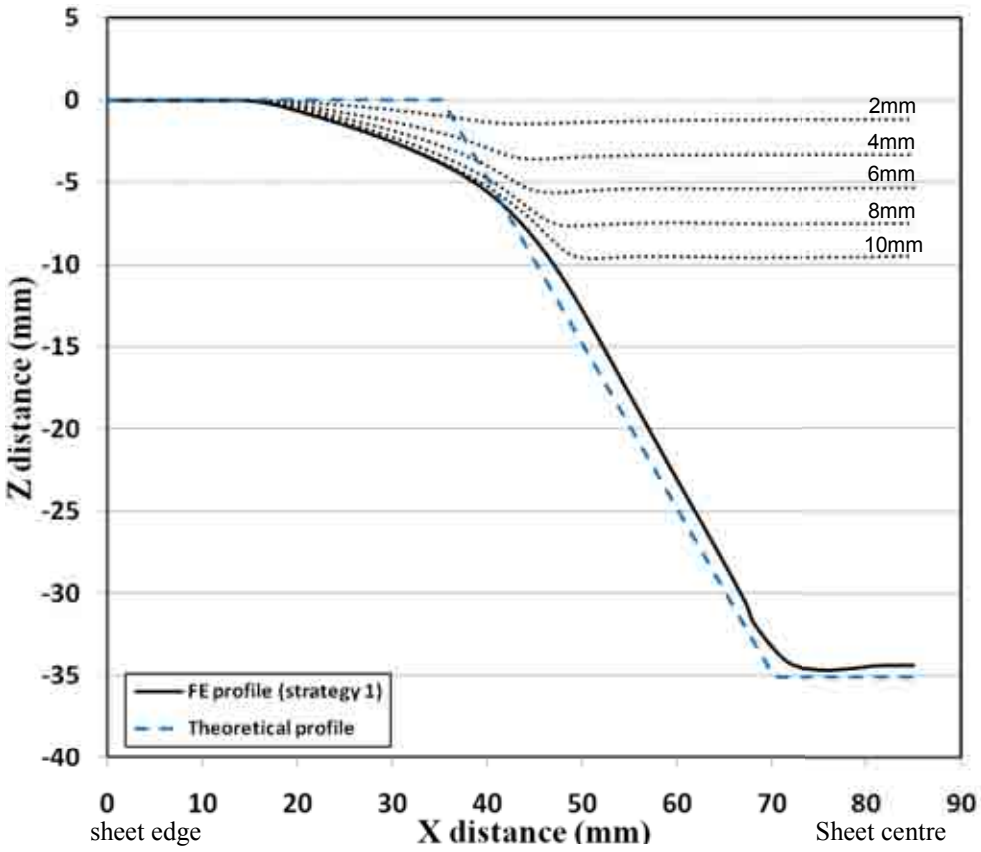

Figure 7.9: Deformation history using strategy 1.

As a result of adding another kinematic tool on the bottom surface of the sheet, the deformation becomes more localised beneath the tool which leads to an increase in local plastic deformation and a decrease in the elastic springback, as shown in Figure 7.10. During the initial stages of the process, plastic deformation increases and the FE profile becomes very close to the theoretical profile along the cone wall. At the end of deformation, the cumulative local springback is less than that for strategy 1.

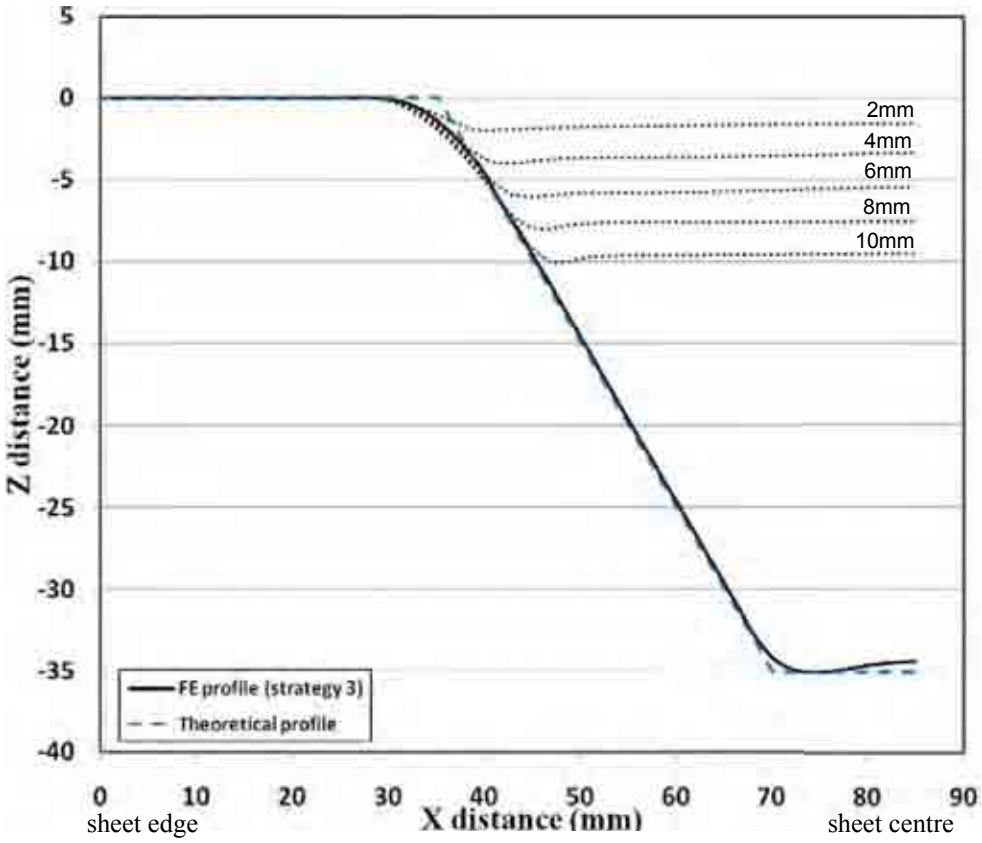

Figure 7.10: Deformation history using strategy 3.

Figure 7.11 shows a comparison of the profile obtained from strategy 3 and from strategy 4 to show only the effect of the new tool path. The results confirm that the modified tool path affects only the region at the cone base. It leads to a decrease in the deviation resulting from the pillow effect at the sheet centre but it does not have any effect on the geometrical accuracy either at the major or the minor diameters. The results show that e_p is reduced from 0.63mm to 0.01mm while e_b and e_s are found to be 1.62 mm and 0.60mm respectively. The modified tool path allows the forming tool to produce a small amount of plastic deformation at the cone base which helps this surface to become flat and thus the pillow effect at the sheet centre can be eliminated.

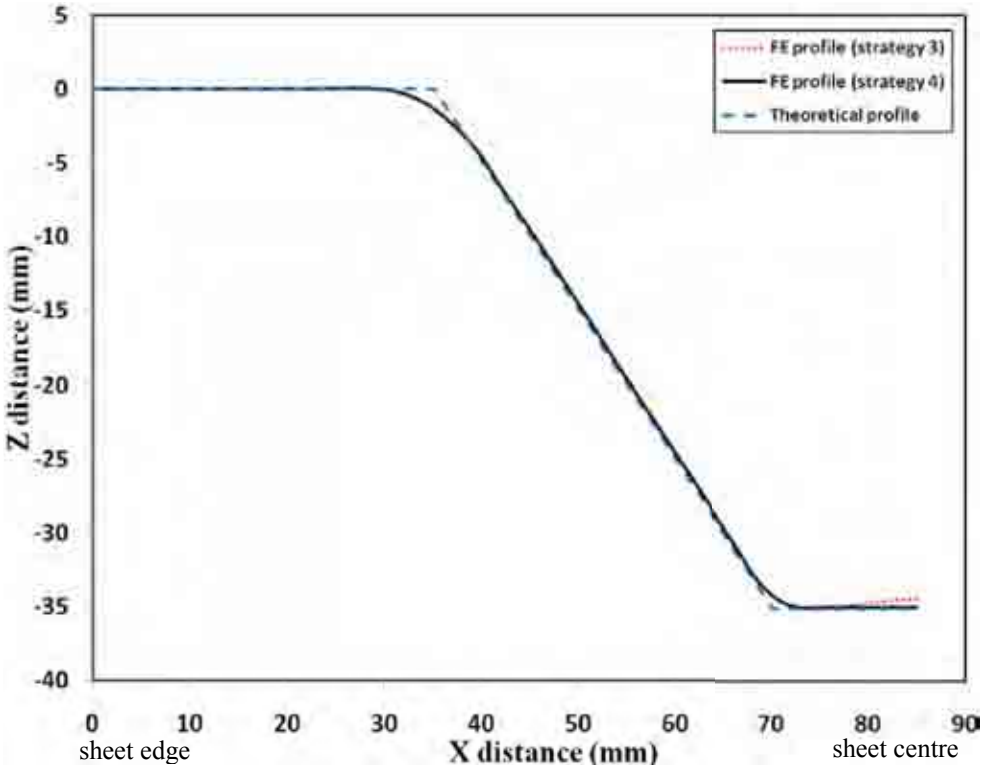

Figure 7.11: Effect of the modified tool path on the final profile.

Figure 7.12 shows the typical values for the different deviation measures obtained from the four strategies. The best geometrical accuracy is obtained using strategy 4 which includes adding a backing plate, kinematic supporting tool and a modified tool path.

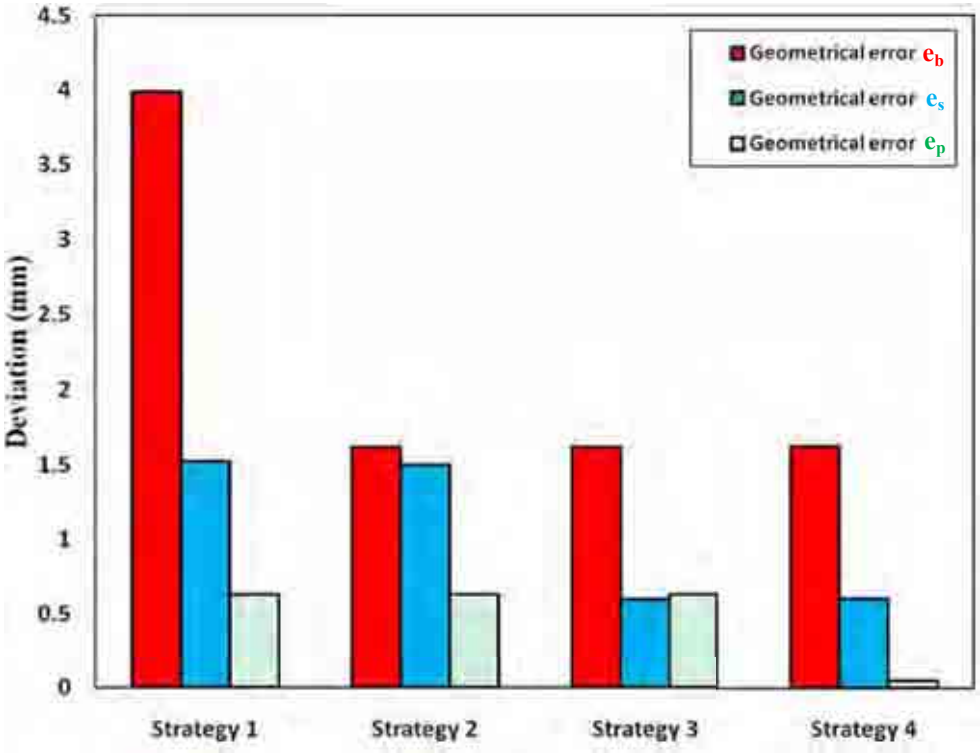

Figure 7.12: Summary of deviations obtained from the four strategies.

Figure 7.13 shows a comparison between strategy 1 and strategy 4 for the von Mises stress distribution at the start of the process, mid-way and when the forming tool reaches the base of the cone. For strategy 1, Figure 7.13 (a) after initial tool contact, the stress is localised principally beneath the tool, which at this initial point is only elastic. Immediately after this stage, as the tool begins to traverse the sheet, plastic deformation is induced in the sheet. The narrow annular region of plastic stress displayed mid-way through is typical of the process. Elastic stresses in the sheet bending region next to the clamped flanges and further towards the base are clearly visible. The three-dimensional geometry developed in the sheet provides a restriction to the elastic recovery of the material away from the contact region. The addition of a backing plate and kinematic supporting tool results in noticeable differences in the stress distribution, as shown in Figure 7.13 (b). At the start of deformation, the backing plate restricts the deformation

area and hence the stress is more localised beneath the forming tool compared with that in strategy 1. As the deformation progresses, negligible stress can be found in the region that surrounds the forming area as a result of using the backing plate and thus, the stress localises only in the area of deformation. The higher level of von Mises stress takes place underneath the forming tool i.e., at the last tool position as a result of the kinematic supporting tool.

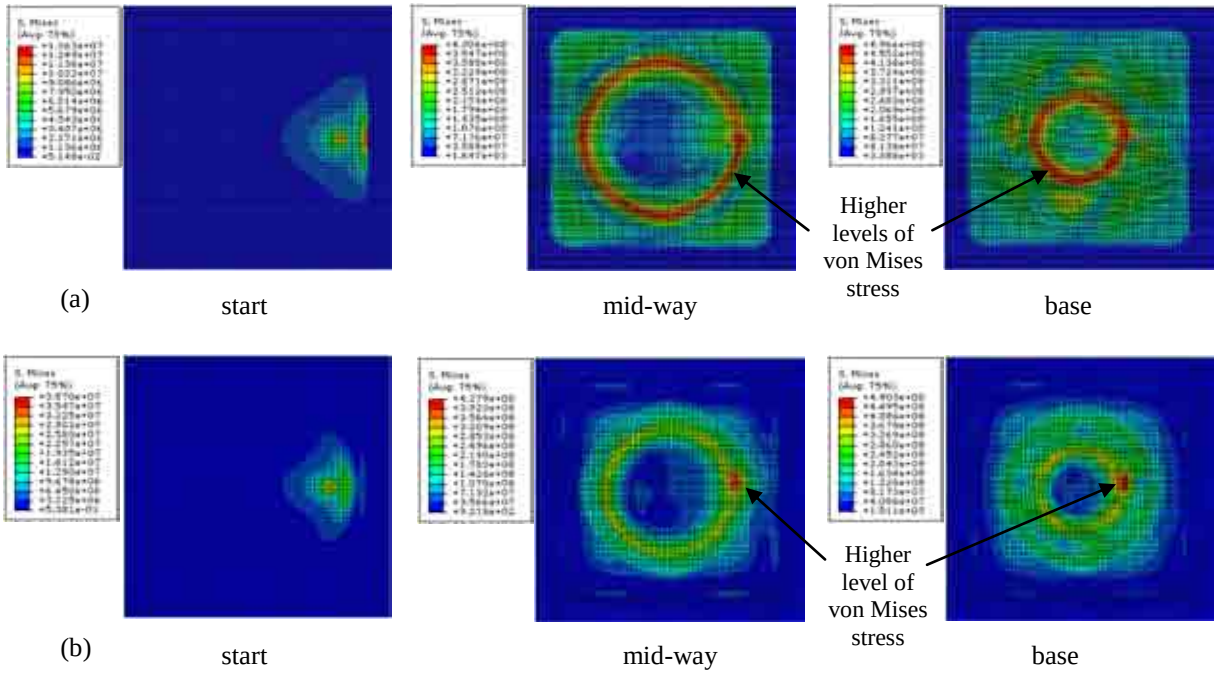

Figure 7.13: Effect of the new strategies on the von Mises distribution (a) strategy 1, (b) strategy 4.

Figure 7.14 shows the plastic strain distribution obtained from strategy 1 and strategy 4. For strategy 1, there cannot be any plastic strain at the sheet flange where the sheet is completely fixed. It develops at the start of the deformation area i.e., approximately 35mm from the sheet edge. The maximum value of the plastic strain occurs in a position corresponding to the location of maximum sheet thinning which takes place along the

45º wall angle. After this peak, the plastic deformation decreases towards the centre of the sheet. For strategy 4, the plastic strain starts earlier, near the inner edge of the backing plate. The maximum plastic strain is approximately uniform along the cone wall (between 45mm and 70mm). It then decreases toward the sheet centre. The plastic strain at the sheet centre is higher than that for strategy 1 as a result of the modified tool path and elimination of the pillow effect.

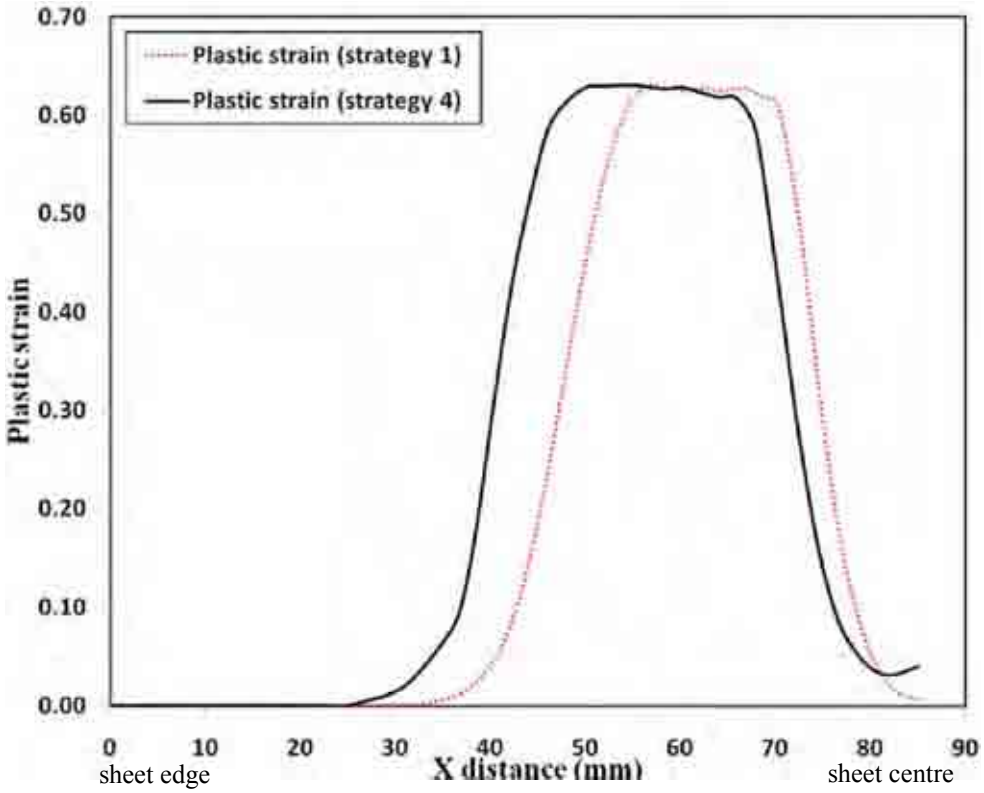

Figure 7.14: Effect of the new strategies on the plastic strain distribution.

The thickness distributions obtained from strategy 1 and from strategy 4 are illustrated in Figure 7.15. The theoretical thickness obtained from applying the sine law [163] to the theoretical profile is also given. As a result of using the backing plate the region of sheet bending is reduced and the FE thickness is closer to the theoretical one at the

major diameter. As a result of adding the kinematic supporting tool which reduced the local springback, the thickness distribution along the cone wall is more uniform than that obtained from strategy 1. As a result of modifying the tool path, the pillow effect is eliminated and the FE thickness is closer to the theoretical variation along the cone base.

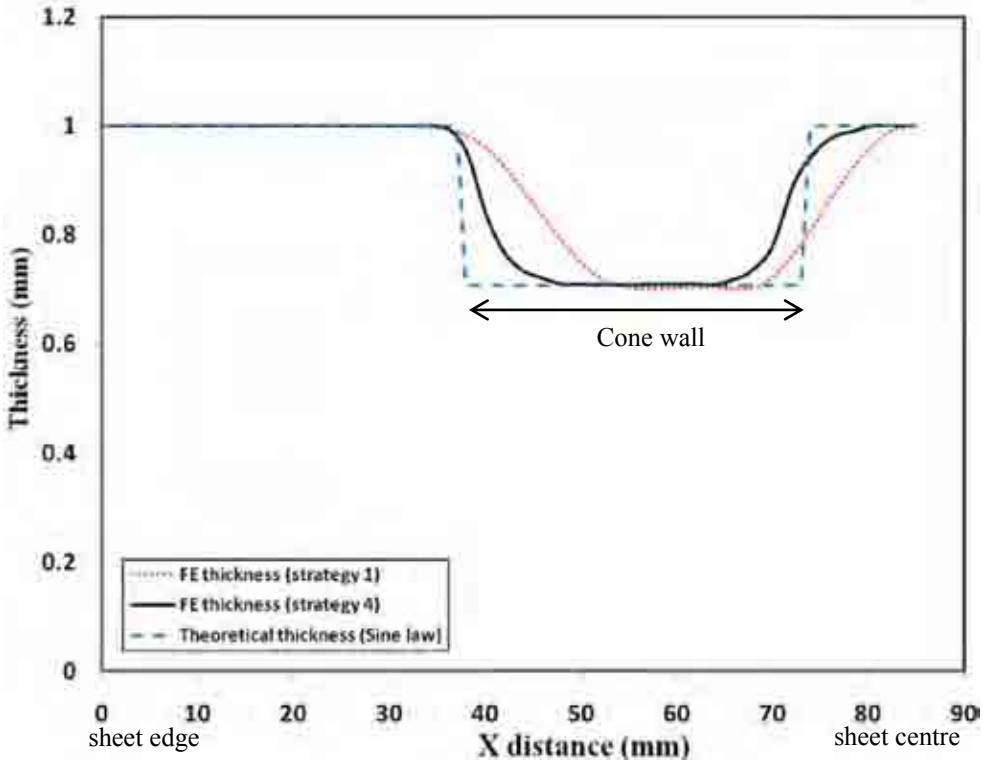

Figure 7.15: Effect of the new strategies on the thickness distribution.

7.5 Summary and Conclusions

A 3-D finite element model for single point incremental forming processes has been developed and implemented using the Abaqus/Implicit code. For the forming of a truncated cone, the effect of different process strategies, i.e. the addition of a backing

plate, kinematic supporting tool and a modification of the final part of the tool path, on the geometrical accuracy were investigated.

This study demonstrated the following,

- Adding a backing plate permitted a reduction in the region of sheet bending in an area closer to the major diameter.
- Adding a kinematic supporting tool reduced the local springback.
- An extension of the tool path across the cone base eliminated the pillow effect at the sheet centre.
- The addition of a backing plate and kinematic supporting tool restricts the deformation area i.e., negligible stress can be found in the region that surrounds the forming area, and localises the stress underneath the forming tool respectively.
- A combination of adding a backing plate, kinematic tool and extended tool path provided the most accurate product profile.
- For the simple case study of a truncated cone, the geometrical deviations could be reduced from 3.99, 1.52 and 0.63mm to 1.62, 0.60 and 0.01mm at the major diameter, minor diameter and sheet centre respectively.

CHAPTER 8:

SUMMARY AND FUTURE WORK

8.1 Summary

This thesis deals with two incremental sheet forming processes, one is the traditional method of conventional spinning and the second is the more recently developed method of single point incremental forming. Conventional spinning is a process in which a sheet metal blank is gradually shaped over a rotating mandrel through a roller that produces a localised pressure and thus axisymmetric parts can be formed. A finite element analysis of forces, stresses and strain in single and dual pass conventional spinning was carried out. The effects of different roller-traces in dual pass spinning on the stress and strain distributions were investigated. The application of statistical methods in combination with the finite element analysis was used in conventional spinning in order to identify the most critical working parameters and determine the optimal setting of these parameters to achieve optimal quality characteristics and produce defect-free products.

For an aluminium sheet formed by conventional spinning into a cylindrical cup, the principal conclusions can be summarised as follows:

- In dual pass conventional spinning, some plastic deformation took place in the first pass and thus, the maximum axial force in the second pass is less than that when using a single pass.
- During the first pass, most of the plastic deformation takes place at the round corner of the mandrel. While, during the second pass, most of the plastic deformation occurs along the cup wall.

- The least sheet thinning at the round corner of the mandrel, a more uniform thickness distribution and a more uniform stress distribution along the sheet radius are obtained using an involute curve roller-trace in the first pass followed by a straight line roller-trace in the second pass.
- In combination with finite element analysis FEA, analysis of variance ANOVA was used to obtain the most critical working parameters that affect the final product quality characteristics. The critical working parameters are feed rate, relative clearance between the roller and mandrel, roller nose radius and sheet thickness.
- As feed rate increased, the average thickness, thickness variation, springback, and maximum axial force increased. A negative relative clearance decreased the average thickness, reduced the thickness variation, and increased the maximum axial force. A large roller nose radius resulted in a large contact between the roller and sheet material which led to an increase in the maximum axial force.
- The min-max optimisation method allowed the identification of a parameter setting which gave the best compromise between the mutually contradictory quality characteristics. This setting is 0.62 mm/rev feed rate, -7.33% relative clearance, 10 mm roller nose radius and 3 mm sheet thickness. This setting results in an additional improvement of more than 22%.

Single point incremental forming is one of Asymmetric incremental sheet forming processes in which a sheet metal blank is formed by a progressive, localised plastic deformation induced by a numerically controlled forming tool and thus, a variety of complex 3-D shapes can be created. Using dual-level FE modelling, the deformation mechanisms, in particular through-thickness shear, were predicted. The Marciniak-

Kuczynski (MK) model framework was used to show the effect of the predicted through-thickness shear on the necking strain. The results obtained addressed the contradiction found in the literature for the deformation mechanics, in particular the through-thickness shear deformation and explained the reason for the higher forming limit that associated with SPIF. An investigation on the effect of different process parameters on the through-thickness shear was conducted. The optimal setting of different working parameters to maximize the through-thickness shear was identified. A lack of accuracy in the process due to its die-less nature was improved through simple strategies that improve the geometrical accuracy without affecting the process flexibility.

For an aluminium plate formed by SPIF into a truncated cone of wall angle of 45^0, the principal conclusions can be summarised as follows:

- The dual-level FE modelling technique is capable of predicting the complex deformation mechanism of SPIF.
- An important component in the deformation mechanism of SPIF is shear, both perpendicular and parallel to the tool plane, in addition to stretching, thinning and bending.
- All components of strain generally increase on successive laps.
- The maximum shear strains are found at the top surface in contact with the tool, reducing to smaller values at the opposing surface.
- Through-thickness shear increases the necking limit and hence improves formability.

- Through-thickness shear strains increase by decreasing the tool diameter and step-down size and increasing the sheet thickness and coefficient of friction.
- Through-thickness shear strains can be used as an indicator for the process formability.
- Using 0.41 mm step-down size, 0.3 coefficient of friction, 10 mm tool diameter and 3 mm sheet thickness results in a maximum through-thickness strain both perpendicular and parallel to the tool plan.
- The geometrical errors in terms of the undesired bending at the major diameter, local springback and pillow effect at the sheet centre are reduced by using simple strategies such as adding a backing plate, using a kinematic supporting tool and tool path modification. Using these strategies the geometrical errors that resulted from the sheet bending, springback and pillow effect reduced from 3.99 mm, 1.5 mm, 0.63 mm to 1.62 mm, 0.6 mm 0.01 mm respectively.

8.2 Future Work

Compared to shear spinning, conventional spinning has been the subject of much less research. There are some gaps in the present knowledge which were highlighted in the review in Chapter 2. In this thesis, a number of open questions regarding conventional spinning were analysed. For future work, some interesting points need to be investigated. In this thesis, the process mechanics for a dual-pass process were investigated. Future work on the effect of process parameters during the subsequent roller passes needs to be established. This would provide a clear understanding of the deformation behaviour in multi-pass spinning and hence provide better control to the process parameters. The effect of roller-trace on the stress and strain distributions needs

to be extended to a variety of product shapes so that the subsequent roller-trace could be any quadratic or involute shape. The effects of residual stresses and the development of microstructure in metal spinning have largely been neglected, and further research would help in improving the geometrical accuracy of the final product.

Despite extensive research over the last decade and strong potential industrial and economic benefits, AISF is still not widely applied in industry. The outlook for future research into AISF should be focussed on developing the process in the most advantageous ways to make it suitable for wide industrial application. The main shortcomings of the process or gaps in the present knowledge were highlighted in the review in Chapter 2. This thesis addresses some of these shortcomings by researching the deformation mechanics of the SPIF, investigating the effect of process parameters on the through-thickness shear strains and developing simple strategies to overcome the geometrical inaccuracy. To build on the research that has been presented in this thesis, some directions for future research are suggested below.

- The prediction of the through-thickness shear strain has been undertaken for a truncated cone of 45^0 wall angle formed by SPIF, future work to predict the shear strain through the thickness for different wall angles and different shapes is required. Additionally, it would be very useful to apply the multi-level FE modelling to explore the shear deformation through the sheet thickness in TPIF. Hence, to compare the deformation mechanics of both processes.
- SPIF shows a higher formability as a result of through-thickness shear. The results obtained could be used as a basis to test the applicability of the process to deform

low formability sheets such as titanium and the more recently developed materials such as composite materials.

- A suggestion for future research is to carry out an investigation of the evolution of deformation during the process, and hence to determine why the tool forces and strains follow an increasing trend. It was suggested by Jackson and Allwood [161] that this increasing trend may be a result of the progressive localisation of the deformation as the sheet becomes more rigid as it is formed. Verification of the reason for increasing forces and strains is therefore required.

REFERENCES

[1] Slater, R.A.C., 1979. *A review of analytical and experimental investigations of the spinforging of sheet metal cones*. In: 1st International Conference on Rotary Metal-working Processes. UK. pp. 33-60.

[2] Lange, K., 1985. *Handbook of Metal Forming*: SME publications.

[3] Hagan, E. and Jeswiet, J., 2003. *A review of conventional and modern single-point sheet metal forming methods.* Proceedings of the Institution of Mechanical Engineers, Part B: Journal of Engineering Manufacture. **217(2)**: pp. 213-225.

[4] Wong, C.C., Dean, T.A., and Lin, J., 2003. *A review of spinning, shear forming and flow forming processes.* International Journal of Machine Tools and Manufacture. **43(14)**: pp. 1419-1435.

[5] Music, O., Allwood, J.M., and Kawai, K., 2009. *A review of the mechanics of metal spinning.* Journal of Materials Processing Technology. **210(1)**: pp. 3-23.

[6] Kalpakjian, S. and Schmid, S., 2001. *Manufacturing Engineering and Technology*. London, : Prentice Hall Intern.

[7] Gur, M. and Tirosh, J., 1982. *Plastic flow instability under compressive loading during shear spinning process.* Journal of Engineering for Industry-Transactions of the ASME. **104(1)**: pp. 17-22.

[8] Bai, Q., Yang, H., and Zhan, M., 2008. *Finite element modeling of power spinning of thin-walled shell with hoop inner rib.* Transactions of Nonferrous Metals Society of China. **18(1)**: pp. 6-13.

[9] Brown, J., 1998. *Advanced Machinning Technology Handbook*: McGraw-Hill.

[10] LEIFELD. *Spinning Applications*. Website: http://www.leifeldms.de/en/home/.

[11] Library, C.M. *Metal Spinning*. Website: http://cltad.arts.ac.uk/groups/camberwellmateriallibrary/wiki/36c10/Metal_Spinning.html.

[12] Metspin. *Metal Spinning Gallery*. Website: http://www.metspincc.co.za/page.php?5.

[13] Runge, M., 1994. *Spinning and Flow forming*: Leifeld GmbH.

[14] SPINDUSTRIES, M.S.F. *About the Metal Spinning Process*. Website: http://www.lgspin.com/about_process.html.

[15] Avitzur, B. and Yang, C.T., 1960. *Analysis of Power Spinning of Cones.* Trans. ASME, Ser. B, Journal of Engineering for Industry. **82**: pp. 231-245.

[16] Kalpakcioglu, S., 1961. *On the Mechanics of Shear Spinning.* Journal of Engineering for Industry-Transactions of the ASME. **83(Series B)**: pp. 125-130.

[17] Quigley, E. and Monaghan, J., 2000. *Metal forming: an analysis of spinning processes.* Journal of Materials Processing Technology. **103(1)**: pp. 114-119.

[18] Kim, C., Jung, S.Y., and Choi, J.C., 2003. *A lower upper-bound solution for shear spinning of cones.* International Journal of Mechanical Sciences. **45(11)**: pp. 1893-1911.

[19] Kim, J.H., Park, J.H., and Kim, C., 2006. *A study on the mechanics of shear spinning of cones.* Journal of Mechanical Science and Technology. **20(6)**: pp. 806-818.

[20] Joorabchian, A. and Slater, R.A.C., 1979. *Spin forging of sheet metal cones having various cone angles and an upper bound estimate for the tangential component force exerted at the workpiece-roller interfaces*. In: Proceedings of the 20th International Machine Tool Design and Research Conference. Birmingham, UK. 512-529.

[21] Alberti, N., Cannizzaro, L., Lo Valvo, E., and Micari, F., 1989. *Analysis of metal spinning processes by the ADINA code.* Computers & Structures. **32(3-4)**: pp. 517-525.

[22] Liu, J.H., Yang, H., and Li, Y.Q., 2002. *A study of the stress and strain distributions of first-pass conventional spinning under different roller-traces.* Journal of Materials Processing Technology. **129(1-3)**: pp. 326-329.

[23] Quigley, E. and Monaghan, J., 2001. *Using a Finite Element model to study plastic strains in Metal Spinning*. In: 9th International Conference on Sheet Metal. Leuven Belgium. 255-262.

[24] Quigley, E. and Monaghan, J., 2002. *The finite element modelling of conventional spinning using multi-domain models.* Journal of Materials Processing Technology. **124(3)**: pp. 360-365.

[25] Klocke, F. and Wehrmeister, T., 2003. *Laser-assisted metal spinning of advanced materials*. In: 4th Lane Conference. Erlangen, Germany.

[26] Lu, X.Y., Zhang, S.H., Hou, H.L., Li, J.Z., and Zhou, L.X., 2006. *Three dimensional FE analysis on flange bending for TC4 alloy during shear spinning.* Journal of Materials Science and Technology. **22(6)**: pp. 855-859.

[27] Alberti, N. and Fratini, L., 2004. *Innovative sheet metal forming processes: numerical simulations and experimental tests.* Journal of Materials Processing Technology. **150(1-2)**: pp. 2-9.

[28] Kleiner, M., Gbel, R., Kantz, H., Klimmek, C., and Homberg, W., 2002. *Combined Methods for the Prediction of Dynamic Instabilities in Sheet Metal Spinning.* CIRP Annals - Manufacturing Technology. **51(1)**: pp. 209-214.

[29] Klimmek, C., K., , Gobel, R., and Homberg, K., 2003. *Finite Element Analysis of Sheet Metal Forming by Spinning.* Journal of Japan Society for Technology of Plasticity. **44(507)**: pp. 372-374.

[30] Zhan, M., Zhanga, J.H., Xua Y.L., and Ma, F., 2006. *Research on variation of stress and straing field and wall thickness during cone spinning* In: Materials Science Forum pp. 149-152.

[31] Zhan, M., Yang, H., Zhang, J.H., Xu, Y.L., and Ma, F., 2007. *3D FEM analysis of influence of roller feed rate on forming force and quality of cone spinning.* Journal of Materials Processing Technology. **187-188**: pp. 486-491.

[32] Sebastiani, G., Brosius, A., Homberg, W., and Kleiner, M., 2007. *Process characterization of Sheet Metal Spinning by Means of Finite Elements*. In: Key Engineering Materials (Shemet 2007). 637-644.

[33] Liu, C.H., 2007. *The simulation of the multi-pass and die-less spinning process.* Journal of Materials Processing Technology. **192-193**: pp. 518-524.

[34] Long, H. and Hamilton, S., 2008. *Simulation of effects of material deformation on thickness variation in conventional spinning*. In: 9th International Conference on Technology of Plasticity. Gyeongju, South Korea.

[35] Hamilton, S. and Long, H., 2008. *Analysis of Conventional Spinning Process of a Cylindrical Part using Finite Element Methods.* Steel Research International **79(1)**: pp. 632-639.

[36] Dröge, K.H., 1954. *Forces and material flow in spinning*. In: Technische Universität Dortmund. Germany.

[37] Liu, C.H., 2007. *Dynamic Finite Element Modeling for the Conventional Spinning Process.* Journal of the Chinese Institute of Engineers. **30(5)**: pp. 911-916.

[38] Sebastiani, G., Brosius, A., Ewers, R., Kleiner, M., and Klimmek, C., 2006. *Numerical investigation on dynamic effects during sheet metal spinning by explicit finite-element-analysis.* Journal of Materials Processing Technology. **177(1-3)**: pp. 401-403.

[39] Xia, Q.X., Shima, S., Kotera, H., and Yasuhuku, D., 2005. *A study of the one-path deep drawing spinning of cups.* Journal of Materials Processing Technology. **159(3)**: pp. 397-400.

[40] Singhal, R.P., Das, S.R., and Prakash, R., 1987. *Some experimental observations in the shear spinning of long tubes.* Journal of Mechanical Working Technology. **14(2)**: pp. 149-157.

[41] Mori, K., Ishiguro, M., and Isomura, Y., 2009. *Hot shear spinning of cast aluminium alloy parts.* Journal of Materials Processing Technology. **209(7)**: pp. 3621-3627.

[42] Hayama, M., 1971. *Study of lubrication in shear spinning*. In: Bulletin of the Faculty of Engineering. Yokohama National University. pp. 61-69.

[43] Chen, M.D., Hsu, R.Q., and Fuh, K.H., 2005. *Effects of over-roll thickness on cone surface roughness in shear spinning.* Journal of Materials Processing Technology. **159(1)**: pp. 1-8.

[44] El-Khabeery, M.M., Fattouh, M., El-Sheikh, M.N., and Hamed, O.A., 1991. *On the conventional simple spinning of cylindrical aluminium cups.* International Journal of Machine Tools and Manufacture. **31(2)**: pp. 203-219.

[45] Groche, P. and Schäfer, R., 2003. *Analysis of the geometrical tolerances and surface roughness of the spinning process*. Process Scaling. Vol. 24. Bremen: BIAS. 8.

[46] Chen, M.D., Hsu, R.Q., and Fuh, K.H., 2001. *Forecast of shear spinning force and surface roughness of spun cones by employing regression analysis.* International Journal of Machine Tools and Manufacture. **41(12)**: pp. 1721-1734.

[47] Hayama, M., Murota, T., and Kudo, H., 1965. *Experimental study of shear spinning* In: Bulleting of JSME. pp. 453-460.

[48] Huang, L., Yang, H., Zhan, M., and Liu, Y., 2008. *Analysis of splitting spinning force by the principal stress method.* Journal of Materials Processing Technology. **201(1-3)**: pp. 267-272.

[49] Liang, H., He, Y., Mei, Z., and Li-Jin, H., 2008. *Numerical simulation of influence of material parameters on splitting spinning of aluminum alloy.* Transactions of Nonferrous Metals Society of China. **18(3)**: pp. 674-681.

[50] Hayama, M. and Murota, T., 1963. *On the study of metal spinning* In: Bulletin of the Faculty of Engineering Yokohama National University. pp. 53-88.

[51] Wang, Q., Wang, T., and Wang, Z.R., 1989. *A study of the working force in conventional spinning*. In: Proceedings of the 4th International Conference of Rotary Forming. pp. 103-108.

[52] Quigley, E. and Monaghan, J., 2002. *Enhanced finite element models of metal spinning.* Journal of Materials Processing Technology. **121(1)**: pp. 43-49.

[53] Kalpakcioglu, S., 1961. *A Study of Shear-Spinability of Metals* Journal of Engineering for Industry-Transactions of the ASME **83(Series B)**: pp. 478-484.

[54] Kegg, R.L., 1961. *A New Test Method for Determination of Spinnability of Metals* Journal of Engineering for Industry-Transactions of the ASME. **83(Series B)**: pp. 118-125.

[55] Kobayashi, S., 1963. *Instability in Conventional Spinning of Cones* Journal of Engineering for Industry-Transactions of the ASME **85(Series B)**: pp. 44-48.

[56] Hayama, M., Kudo, H., and Shinokura, T., 1970. *Study of the pass schedule in conventional simple spinning* Bulletin of the JSME. **13(65)**: pp. 1358-1365.

[57] Kang, D., Gao, X., Meng, X., and Wang, Z., 1999. *Study on the deformation mode of conventional spinning of plates.* Journal of Materials Processing Technology. **91(1-3)**: pp. 226-230.

[58] Roy, M.J., Klassen, R.J., and Wood, J.T., 2009. *Evolution of plastic strain during a flow forming process.* Journal of Materials Processing Technology. **209(2)**: pp. 1018-1025.

[59] Kawai, K., Yang, L.N., and Kudo, H., 2001. *A flexible shear spinning of truncated conical shells with a general-purpose mandrel.* Journal of Materials Processing Technology. **113(1-3)**: pp. 28-33.

[60] Shima, S., 2001. *State of the art - Incremental forming*. In: 3rd International Conference on Intelligent Processing and Manufacturing of Materials. Vancouver, Canada.

[61] Jeswiet, J., Micari, F., Hirt, G., Bramley, A., Duflou, J., and Allwood, J., 2005. *Asymmetric Single Point Incremental Forming of Sheet Metal.* CIRP Annals - Manufacturing Technology. **54(2)**: pp. 88-114.

[62] Jeswiet, J., Geiger, M., Engel, U., Kleiner, M., Schikorra, M., Duflou, J., Neugebauer, R., Bariani, P., and Bruschi, S., 2008. *Metal forming progress since 2000.* CIRP Journal of Manufacturing Science and Technology. **1(1)**: pp. 2-17.

[63] Jeswiet, J. and Hagan, E., 2001. *Rapid Proto-typing of a Headlight with Sheet Metal*. In: 9th International Conference on Sheet Metal. Leuven. pp. 165-170.

[64] Kleiner, M., Geiger, M., and Klaus, A., 2003. *Manufacturing of Lightweight Components by Metal Forming.* CIRP Annals - Manufacturing Technology. **52(2)**: pp. 521-542.

[65] Jeswiet, J., 2004. *Single PointI ncremental Forming: recent results*. In: Seminar on Incremental Forming. Cambridge University.

[66] Ambrogio, G., De Napoli, L., Filice, L., Gagliardi, F., and Muzzupappa, M., 2005. *Application of Incremental Forming process for high customised medical*

product manufacturing. Journal of Materials Processing Technology. **162-163**: pp. 156-162.

[67] Tanaka, S., Nakamura, T., Hayakawa, K., Nakamura, H., and Motomura K., 2005. *Incremental Sheet Metal Forming Process for Pure Titanium Denture Plate* In: 8th International Conference on Technology of Plasticity - ICTP. pp. 135-136.

[68] Allwood, J., Bramley, A., Ridgman, T., and Mileham, A., 2006. *A Novel Method for the Rapid Production of Inexpensive Dies and Moulds with Surfaces Made by Incremental Sheet Forming.* Proceedings of the Institution of Mechanical Engineers, Part B: Journal of Engineering Manufacture. **220(2)**: pp. 323-327.

[69] Smith, S., Woody, B., Ziegert, J., and Huang, Y., 2007. *Deformation Machining - A New Hybrid Process.* CIRP Annals - Manufacturing Technology. **56(1)**: pp. 281-284.

[70] Silva, M.B., Skjoedt, M., Vilaça, P., Bay, N., and Martins, P.A.F., 2009. *Single point incremental forming of tailored blanks produced by friction stir welding.* Journal of Materials Processing Technology. **209(2)**: pp. 811-820.

[71] Kopp, R.a.S., J., 2002. *Flexible Sheet Forming Technology by Double-sided Simultaneous Shot Peen Forming.* Annals of CIRP. **Vol.51/1/2002**.

[72] Petek, A., Jurisevic, B., Kuzman, K., and Junkar, M., 2009. *Comparison of alternative approaches of single point incremental forming processes.* Journal of Materials Processing Technology. **209(4)**: pp. 1810-1815.

[73] Hirt, G., 2004. *Tools and Equipment used in Incremental Forming*. In: 1st Incremental Forming Workshop, University of Saarbrucken. On Cdrom.

[74] Iseki, H., Kato, K., and Sakamoto, S., 1992. *Flexible and incremental sheet metal bulging using a path-controlled spherical roller*. Trans. JSME Ser. C. **58(554)**: pp. 279-287.

[75] Maki, T., 2006. *Presentation: 'Dieless NC Forming'*. In: International Seminar on Novel Sheet Metal Forming Technologies. Jvyäskylä, Finland.

[76] Allwood, J., Houghton, N.E., and Jackson, K., 2005. *The design of an incremental forming machine*. In: SheMet '05 International Conference on Sheet Metal. Erlangen, Germany. pp. 471-478.

[77] Meier, H., Dewald, O., and Zhang, J., 2005. *A new robot-based sheet metal forming process*. In: SheMet '05 International Conference on Sheet Metal. Erlangen, Germany. pp. 465-470.

[78] Lamminen, L., 2005. *Incremental sheet forming with an industrial robot - Forming limits and their effect on component design*. In: SheMet '05 International Conference on Sheet Metal. Erlangen, Germany. pp. 457-464.

[79] Maidagan, E., Zettler, J., Bambach, M., Rodriguez, P.P., and Hirt, G., 2007. *A new incremental sheet forming process based on a flexible supporting die system*. In: SheMet '07 International Conference on Sheet Metal. Palermo, Sicily. pp. 607-614.

[80] Callegari, M., Gabrielli, A., Palpacelli, M.C., and Principi, M., 2008. *Incremental Forming of Sheet Metal by Means of Parallel Kinematics Machines.* Journal of Manufacturing Science and Engineering. **130(5)**: pp. 1-5.

[81] Vihtonen, L., Puzik, A., and Katajarinne, T., 2008. *Comparing two robot assisted incremental forming methods: incremental forming by pressing and incremental hammering.* International Journal of Material Forming. **1**: pp. 1207-1210.

[82] Leach, D., Green, A.J., and Bramley, A.N., 2001. *A new incremental sheet forming process for small batch and prototype parts*. In: 9th International Conference on Sheet Metal. Leuven. pp. 211-218.

[83] Hirt, G., Bambach, M., Junk, S., and Chouvalova, I., 2003. *FEM modelling and optimisation of geometric accuracy in incremental CNC sheet forming, Developments in Equipment Based Accuracy*. In: CIRP international conference on accuracy in forming technology (ICAFT/10). Chemnitz. pp. 293-304.

[84] Ambrogio, G., Costantino, I., De Napoli, L., Filice, L., Fratini, L., and Muzzupappa, M., 2004. *Influence of some relevant process parameters on the dimensional accuracy in incremental forming: a numerical and experimental investigation.* Journal of Materials Processing Technology. **153-154**: pp. 501-507.

[85] Ambrogio, G., Filice, L., Gagliardi, F., Micari, F., and Umbrello, D., 2005. *Application of the neural network technique for reducing springback in incremental forming processes*. In: 8th ESAFORM Conference. Cluj-Napoca, Romania. pp. 699-702.

[86] Duflou, J., Lauwers, B., Verbert, J., Tunckol, Y., and De Baerdemaeker, H., 2005. *Achievable accuracy in single point incremental forming: Case studies*. In: 8th ESAFORM Conference. Cluj-Napoca, Romania. pp. 675-678.

[87] Filice, L., Fratini, L., and Micari, F., 2002. *Analysis of Material Formability in Incremental Forming.* CIRP Annals - Manufacturing Technology. **51(1)**: pp. 199-202.

[88] Iseki, H. and Naganawa, T., 2002. *Vertical wall surface forming of rectangular shell using multistage incremental forming with spherical and cylindrical rollers.* Journal of Materials Processing Technology. **130-131**: pp. 675-679.

[89] Bambach, M., Hirt, G., and Junk, S., 2003. *Modelling and experimental evaluation of the incremental CNC sheet metal forming process*. In: Proceedings of the 7th International Conference on Computational Plasticity. Barcelona, Spain. pp. 1-17.

[90] Hirt, G., Ames, J., and Bambach, M., 2005. *A new forming strategy to realise parts designed for deep-drawing by incremental CNC sheet forming.* Steel Research. **76(2005)**: pp. 2-3.

[91] Jeswiet, J., Young, D., and Ham, M., 2005. *Non-traditional forming limit diagrams for incremental forming*. In: SheMet '05 International Conference on Sheet Metal. Erlangen, Germany. pp. 409-416.

[92] Dai, K., Wang, Z.R., and Fang, Y., 2000. *CNC incremental sheet forming of an axially symmetric specimen and the locus of optimization.* Journal of Materials Processing Technology. **102(1-3)**: pp. 164-167.

[93] Kim, T.J. and Yang, D.Y., 2000. *Improvement of formability for the incremental sheet metal forming process.* International Journal of Mechanical Sciences. **42(7)**: pp. 1271-1286.

[94] Young, D. and Jeswiet, J., 2004. *Wall thickness variations in single-point incremental forming.* Proceedings of the Institution of Mechanical Engineers, Part B: Journal of Engineering Manufacture. **218(11)**: pp. 1453-1459.

[95] Ambrogio, G., Filice, L., Gagliardi, F., and Micari, F., 2005. *Sheet thinning prediction in single point incremental forming*. In: SheMet '05 International Conference on Sheet Metal. Erlangen, Germany. pp. 479-486.

[96] Bambach, M., Ames, J., Azaouzi, M., Campagne, L., Hirt, G., and Batoz, J.L., 2005. *Initial experimental and numerical investigations into a class of new strategies for single point incremental sheet forming (SPIF)*. In: 8th ESAFORM Conference. Cluj-Napoca, Romania. pp. 671-674.

[97] Fratini, L., Ambrogio, G., Di Lorenzo, R., Filice, L., and Micari, F., 2004. *Influence of mechanical properties of the sheet material on formability in single point incremental forming.* CIRP Annals - Manufacturing Technology. **53(1)**: pp. 207-210.

[98] Ceretti, E., Giardini, C., and Attanasio, A., 2004. *Experimental and simulative results in sheet incremental forming on CNC machines.* Journal of Materials Processing Technology. **152(2)**: pp. 176-184.

[99] Ambrogio, G., Filice, L., De Napoli, L., and Muzzupappa, M., 2005. *A simple approach for reducing profile diverting in a single point incremental forming process.* Proceedings of the Institution of Mechanical Engineers, Part B: Journal of Engineering Manufacture. **219(11)**: pp. 823-830.

[100] Robert, C., Dal Santo, P., Delamézière, A., Potiron, A., and Batoz, J.L., 2008. *On some computational aspects for incremental sheet metal forming simulations.* International Journal of Material Forming. **1**: pp. 1195-1198.

[101] Nguyen, D.T., Park, J.G., Lee, H.J., and Kim, Y.S., 2009. *Finite element method study of incremental sheet forming for complex shape and its improvement.*

Proceedings of the Institution of Mechanical Engineers, Part B: Journal of Engineering Manufacture. **224(6)**: pp. 913-924.

[102] Watzeels, K., Tunckol, Y., Henrard, C., Gu, J., Sol, H., Duflou, J., and Habraken, A.M., 2005. *Experimental validation of the finite element simulation of the first stroke in single point incremental forming*. In: 8th ESAFORM Conference. Cluj-Napoca, Romania. pp. 703-706.

[103] Kitazawa, K., 1993. *Incremental sheet metal stretch-expanding with CNC machine tools*. In: Proceedings of the 4th International Conference on Technology of Plasticity. pp. 1899-1904.

[104] Iseki, H., 2001. *Flexible and Incremental Bulging of Sheet Metal Using a High-Speed Water Jet.* JSME International Journal, Series C. **44(2)**: pp. 486-493.

[105] Shim, M. and Park, J.J., 2001. *The formability of aluminum sheet in incremental forming.* Journal of Materials Processing Technology. **113(1-3)**: pp. 654-658.

[106] Kim, Y.H. and Park, J.J., 2002. *Effect of process parameters on formability in incremental forming of sheet metal.* Journal of Materials Processing Technology. **130-131**: pp. 42-46.

[107] Duflou, J., Szekeres, A., and VanHerck, P., 2005. *Force Measurements for Single Point Incremental Forming: and experimental study*. In: SheMet '05 International Conference on Sheet Metal. Erlangen, Germany. pp. 441-448.

[108] Duflou, J., Tunçkol, Y., Szekeres, A., and Vanherck, P., 2007. *Experimental study on force measurements for single point incremental forming.* Journal of Materials Processing Technology. **189(1-3)**: pp. 65-72.

[109] Bologa, O., Oleksik, V., and Racz, G., 2005. *Experimental research for determining the forces on incremental sheet forming process*. In: 8th ESAFORM Conference. Cluj-Napoca, Romania. pp. 317-320.

[110] Jeswiet, J., Duflou, J., and Szekeres, A., 2005. *Forces in Single Point and Two point Incremental Forming*. In: SheMet '05 International Conference on Sheet Metal. Erlangen, Germany. pp. 449-456.

[111] Ambrogio, G., Filice, L., Gagliardi, F., and Micari, F., 2005. *Three-dimensional FE simulation of single point incremental forming: experimental evidences and process design improving*. In: 8th International Conference on Computational Plasticity. Barcelona. pp. 1-4.

[112] Dejardin, S., Gelin, J., and Thibaud, S., 2010. *On-Line Thickness Measurement in Incremental Sheet Forming Process.* Steel Research International. **81(9)**: pp. 938-941.

[113] Hagan, E. and Jeswiet, J., 2004. *Analysis of surface roughness for parts formed by computer numerical controlled incremental forming.* Proceedings of the

Institution of Mechanical Engineers, Part B: Journal of Engineering Manufacture. **218(10)**: pp. 1307-1312.

[114] Martins, P.A.F., Bay, N., Skjoedt, M., and Silva, M.B., 2008. *Theory of single point incremental forming.* CIRP Annals - Manufacturing Technology. **57(1)**: pp. 247-252.

[115] Silva, M.B., Skjoedt, M., Atkins, A.G., Bay, N., and Martins, P.A.F., 2008. *Single point incremental forming and formability–failure diagrams.* The Journal of Strain Analysis for Engineering Design. **43(1)**: pp. 15-35.

[116] Silva, M.B., Skjoedt, M., Martins, P.A.F., and Bay, N., 2008. *Revisiting the fundamentals of single point incremental forming by means of membrane analysis.* International Journal of Machine Tools and Manufacture. **48(1)**: pp. 73-83.

[117] Marciniak, Z. and Kuczynski, K., 1967. *Limit Strains in the Processes of Stretch-forming Sheet Metal.* International Journal of Mechanical Sciences. **9**: pp. 609-620.

[118] Allwood, J., Shouler, D.R., and Tekkany, A.E., 2007. *The increased forming limits of incremental sheet forming processes*. In: SheMet '07 International Conference on Sheet Metal. Palermo, Italy. pp. 621-628.

[119] Eyckens, P., Del-lero Moreau, J., Duflou, J., Van Bael, A., and Van Houtte, P., 2009. *MK modelling of sheet formability in the incremental sheet forming process, taking into account through-thickness shear.* International Journal of Material Forming. **2**: pp. 379-382.

[120] Eyckens, P., Van Bael, A., and Van Houtte, P., 2009. *Marciniak-Kuczynski type modelling of the effect of Through-Thickness Shear on the forming limits of sheet metal.* International Journal of Plasticity. **25(12)**: pp. 2249-2268.

[121] ABAQUS, I., 2007. *ABAQUS User Manuals, Version 6.7*. United State of America.

[122] Ambrogio, G., Filice, L., and Manco, G., 2008. *Considerations on the Incremental Forming of Deep Geometries.* International Journal of Material Forming. **1**: pp. 1143-1146.

[123] Hirt, G., Junk, S., and Witulsky, N., 2002. *Incremental sheet forming: Quality evaluation and process simulation*. In: 7th International Conference on Technology of Plasticity-ICTP Yokohama, Japan. pp. 925-930.

[124] Qin, Q., Masuku, E.S., Bramley, A.N., Mileham, A.R., and Owen, G.W., 2005. *Incremental sheet forming simulation and accuracy*. In: 8th International Conference on Technology of Plasticity-ICTP. Verona, Italy.

[125] He, S., Van Bael, A., Van Houtte, P., Tunckol, Y., Duflou, J., Henrard, C., Bouffioux, C., and Habraken, A.M., 2005. *Effect of FEM choices in the*

modelling of incremental forming of aluminium sheets. In: 8th ESAFORM Conference. Cluj-Napoca, Romania. pp. 711-714.

[126] Decultot, N., Velay, V., Robert, L., Bernhart, G., and Massoni, E., 2008. *Behaviour modelling of aluminium alloy sheet for single point incremental forming.* International Journal of Material Forming. **1**: pp. 1151-1154.

[127] Bambach, M., 2007. *Process Strategies and Modelling Approaches for Asymmetric Incremental Sheet Forming.* PhD Thesis, Materials Technology/Precision Forming, Saarland University, Saarbrücken, Germany.

[128] Bambach, M. and Hirt, G., 2007. *Error analysis in explicit finite element analysis of incremental sheet forming*. In: Numiform '07.

[129] Hadoush, A. and van den Boogaard, A.H., 2008. *Time reduction in implicit single point incremental sheet forming simulation by refinement - derefinement.* International Journal of Material Forming. **1**: pp. 1167-1170.

[130] Hadoush, A. and van den Boogaard, A., 2009. *Substructuring in the implicit simulation of single point incremental sheet forming.* International Journal of Material Forming. **2(3)**: pp. 181-189.

[131] Lasunon, O. and Knight, W., 2007. *Comparative investigation of single-point and double-point incremental sheet metal forming processes.* Proceedings of the Institution of Mechanical Engineers, Part B: Journal of Engineering Manufacture. **221(12)**: pp. 1725-1732.

[132] Dejardin, S., Thibaud, S., and Gelin, J., 2008. *Finite element analysis and experimental investigations for improving precision in single point incremental sheet forming process.* International Journal of Material Forming. **1**: pp. 121-124.

[133] Eyckens, P., He, S., Van Bael, A., Van Houtte, P., and Duflou, J., 2007. *Forming Limit Predictions for the Serrated Strain Paths in Single Point Incremental Sheet Forming.* AIP Conference Proceedings. **908(1)**: pp. 141-146.

[134] Tanaka, S., Nakamura, T., Hayakawa, K., Nakamura, H., and Motomura, K., 2007. *Residual Stress In Sheet Metal Parts Made By Incremental Forming Process.* AIP Conference Proceedings. **908(1)**: pp. 775-780.

[135] Ma, L.W. and Mo, J.H., 2008. *Three-dimensional finite element method simulation of sheet metal single-point incremental forming and the deformation pattern analysis.* Proceedings of the Institution of Mechanical Engineers, Part B: Journal of Engineering Manufacture. **222(3)**: pp. 373-380.

[136] Matsubara, S., 2001. *A computer numerically controlled dieless incremental forming of a sheet metal.* Proceedings of the Institution of Mechanical Engineers, Part B: Journal of Engineering Manufacture. **215(7)**: pp. 959-966.

[137] Hirt, G., Junk, S., Bambach, M., and Chouvalova, I., 2003. *Process limits and material behaviour in incremental sheet forming with CNC-Tools.* In: THERMEC 2003 International Conference on Processing & Manufacturing of Advanced Materials-Fabrication, Properties, Applications. Institute of Materials Technology/Precision Forming (LWP). Madrid, Spain. pp. 3825-3830.

[138] Hussain, G., Hayat, N., and Gao, L., 2008. *An experimental study on the effect of thinning band on the sheet formability in negative incremental forming.* International Journal of Machine Tools and Manufacture. **48(10)**: pp. 1170-1178.

[139] Landert, M., 2006. *Forming behaviour of metal sandwich sheets.* PhD Thesis, Department of Materials Science and Metallurgy, Cambridge University.

[140] Le, V., Ghiotti, A., and Lucchetta, G., 2008. *Preliminary Studies on Single Point Incremental Forming for Thermoplastic Materials.* International Journal of Material Forming. **1**: pp. 1179-1182.

[141] Franzen, V., Kwiatkowski, L., Martins, P.A.F., and Tekkaya, A.E., 2009. *Single point incremental forming of PVC.* Journal of Materials Processing Technology. **209(1)**: pp. 462-469.

[142] Martins, P.A.F., Kwiatkowski, L., Franzen, V., Tekkaya, A.E., and Kleiner, M., 2009. *Single point incremental forming of polymers.* CIRP Annals - Manufacturing Technology. **58(1)**: pp. 229-232.

[143] Allwood, J., King, G.P., and Duflou, J., 2005. *A structured search for applications of the incremental sheet-forming process by product segmentation.* Proceedings of the Institution of Mechanical Engineers, Part B: Journal of Engineering Manufacture. **219(2)**: pp. 239-244.

[144] Tanaka, S., Nakamura, T., and Hayakawa, K., 2002. *Minature incremental forming of millimetre-sized thin shell structures.* Advanced Technology of Plasticity (Proceedings of the 7th International Conference on Technology of Plasticity-ICTP, Yokohama, Japan). pp. 403-408.

[145] Jyllilä, M., 2006. *Presentation: 'Incremental sheet forming as a part of a sheet metal business'.* In: International Seminar on Novel Sheet Metal Forming Technologies. Jvyäskylä, Finland.

[146] Junk, S., Hirt, G., and Chouvalova, I., 2003. *Forming Strategies and Tools in Incremental Sheet Forming*. In: SheMet '03 International Conference on Sheet Metal. University of Ulster, Ireland. Institute of Materials Technology/Precision Forming (LWP). pp. 57-64.

[147] Wang, Y., Xiao, X., Yuan, Z., and Wu, W., 2010. *Incremental Sheet Metal Forming with Multiple-Head Tools.* Steel Research International. **81(9)**: pp. 922-925.

[148] He, S., Bael, A.V., Houtte, P.V., Szekeres, A., Duflou, J.R., Henrard, C., and Habraken, A.M., 2005. *Finite element modelling of incremental forming of aluminium sheets*. In: SheMet '05 International Conference on Sheet Metal. Erlangen, Germany. pp. 525-532.

[149] Iseki, H., 2001. *An approximate deformation analysis and FEM analysis for the incremental bulging of sheet metal using a spherical roller.* Journal of Materials Processing Technology. **111(1-3)**: pp. 150-154.

[150] Duflou, J., Tunckol, Y., and Aerens, R., 2007. *Force analysis for single point incremental forming*. In: SheMet '07 International Conference on Sheet Metal. Palermo, Sicily. pp. 543-550.

[151] Bouffioux, C., Eyckens, P., Henrard, C., Aerens, R., Van Bael, A., Sol, H., Duflou, J.R., and Habraken, A.M., 2008. *Identification of material parameters to predict Single Point Incremental Forming forces.* International Journal of Material Forming. **1**: pp. 1147-1150.

[152] Durante, M., Formisano, A., Langella, A., and Capece Minutolo, F.M., 2009. *The influence of tool rotation on an incremental forming process.* Journal of Materials Processing Technology. **209(9)**: pp. 4621-4626.

[153] Katajarinne, T., Komulainen, A., and Kivivuori, S., 2010. *Force and Frictional Conditions in Incremental Forming.* Steel Research International. **81(9)**: pp. 934-937.

[154] Iseki, H., Kato, K., and Sakamoto, S., 1993. *Forming limit of flexible and incremental sheet metal bulging with a spherical roller*. In: Proceedings of the 4th International Conference on Technology of Plasticity. pp. 1635-1904.

[155] Hirt, G., Bambach, M., and Junk, S., 2003. *Modelling of the incremental CNC sheet metal forming process*. In: Proceeding of the 10th International Conference on Sheet Metal. Leuven.

[156] Park, J.-J. and Kim, Y.-H., 2003. *Fundamental studies on the incremental sheet metal forming technique.* Journal of Materials Processing Technology. **140(1-3)**: pp. 447-453.

[157] Jeswiet, J. and Young, D., 2005. *Forming limit diagrams for single-point incremental forming of aluminium sheet.* Proceedings of the Institution of Mechanical Engineers, Part B: Journal of Engineering Manufacture. **219(4)**: pp. 359-364.

[158] Matsubara, S., 1994. *Incremental backward bulge forming of a sheet metal with a hemispherical head tool - A study of a numerically controlled forming system.* Journal of the Japanese Society of Technology of Plasticity (Plasticity and Processing). **35(406)**: pp. 1311-1321.

[159] Shankar, R., Jadhav, S., Goebel, R., Homberg, W., and Kleiner, M., 2005. *Incremental sheet metal forming of preformed sheets*. In: 8th International Conference on Technology of Plasticity-ICTP. Verona, Italy.

[160] Hirt, G., Junk, S., Bambach, M., Chouvalouva, I., and Ames, J., 2003. *Flexible CNC incremental sheet forming: Process evaluation and simulation*. In: 6th National Conference on Sheet Metal Forming. Porto Alegre/RS, Brasilien. pp. 30-38.

[161] Jackson, K. and Allwood, J., 2009. *The mechanics of incremental sheet forming.* Journal of Materials Processing Technology. **209(3)**: pp. 1158-1174.

[162] Hussain, G., Dar, N.U., Gao, L., and Chen, M.H., 2007. *A comparative study on the forming limits of an aluminum sheet-metal in negative incremental forming.* Journal of Materials Processing Technology. **187-188**: pp. 94-98.

[163] Hussain, G. and Gao, L., 2007. *A novel method to test the thinning limits of sheet metals in negative incremental forming.* International Journal of Machine Tools and Manufacture. **47(3-4)**: pp. 419-435.

[164] Hussain, G., Gao, L., and Dar, N.U., 2007. *An experimental study on some formability evaluation methods in negative incremental forming.* Journal of Materials Processing Technology. **186(1-3)**: pp. 45-53.

[165] Hussain, G., Gao, L., Hayat, N., and Ziran, X., 2009. *A new formability indicator in single point incremental forming.* Journal of Materials Processing Technology. **209(9)**: pp. 4237-4242.

[166] Hussain, G., Gao, L., and Zhang, Z., 2008. *Formability evaluation of a pure titanium sheet in the cold incremental forming process.* The International Journal of Advanced Manufacturing Technology. **37(9)**: pp. 920-926.

[167] Hussain, G., Gao, L., and Hayat, N., 2009. *Empirical modelling of the influence of operating parameters on the spifability of a titanium sheet using response surface methodology.* Proceedings of the Institution of Mechanical Engineers, Part B: Journal of Engineering Manufacture. **223(1)**: pp. 073-081.

[168] Ham, M. and Jeswiet, J., 2006. *Single Point Incremental Forming and the Forming Criteria for AA3003.* CIRP Annals - Manufacturing Technology. **55(1)**: pp. 241-244.

[169] Ham, M. and Jeswiet, J., 2007. *Forming Limit Curves in Single Point Incremental Forming.* CIRP Annals - Manufacturing Technology. **56(1)**: pp. 277-280.

[170] Jeswiet, J., Hagan, E., and Szekeres, A., 2002. *Forming parameters for incremental forming of aluminium alloy sheet metal.* Proceedings of the Institution of Mechanical Engineers, Part B: Journal of Engineering Manufacture. **216(10)**: pp. 1367-1371.

[171] Emmens, W.C. and Van Den Boogaard, A.H., 2009. *An overview of stabilizing deformation mechanisms in incremental sheet forming.* Journal of Materials Processing Technology. **209(8)**: pp. 3688-3695.

[172] Micari, F., 2005. *Some remarks on material formability in single point incremental forming of sheet metal*. In: 8th International Conference on Technology of Plasticity-ICTP. Verona, Italy.

[173] Ambrogio, G., Filice, L., Fratini, L., and Micari, F., 2004. *Process Mechanics analysis in single point incremental forming*. In: NUMIFORM 2004-Proceedings of the 8th International Conference on Numerical Methods in Industrial Forming Processes. Columbus, Ohio. pp. 922-927.

[174] Emmens, W.C. and Van Den Boogaard, A.H., 2008. *Tensile tests with bending: a mechanism for incremental forming.* International Journal of Material Forming. **1**: pp. 1155-1158.

[175] Allwood, J. and Shouler, D.R., 2009. *Generalised forming limit diagrams showing increased forming limits with non-planar stress states.* International Journal of Plasticity. **25(7)**: pp. 1207-1230.

[176] Bambach, M., Todorova, M., and Hirt, G., 2007. *Experimental and numerical analysis of forming limits in CNC incremental sheet forming*. In: SheMet '07 International Conference on Sheet Metal. Palermo, Sicily. pp. 511-518.

[177] Emmens, W.C., 2007. *Strain in shear, and material behaviour in incremental forming*. In: SheMet '07 International Conference on Sheet Metal. Palermo, Sicily. pp. 519-526.

[178] Fiorentino, A., Ceretti, E., Attanasio, A., Mazzoni, L., and Giardini, C., 2009. *Analysis of forces, accuracy and formability in positive die sheet incremental forming.* International Journal of Material Forming. **2**: pp. 805-808.

[179] Micari, F., Ambrogio, G., and Filice, L., 2007. *Shape and dimensional accuracy in Single Point Incremental Forming: State of the art and future trends.* Journal of Materials Processing Technology. **191(1-3)**: pp. 390-395.

[180] Hirt, G., Ames, J., Bambach, M., and Kopp, R., 2004. *Forming strategies and Process Modelling for CNC Incremental Sheet Forming.* CIRP Annals - Manufacturing Technology. **53(1)**: pp. 203-206.

[181] Rauch, M., Hascoet, J., Hamann, J., and Plennel, Y., 2008. *A new approach for toolpath programming in Incremental Sheet Forming.* International Journal of Material Forming. **1**: pp. 1191-1194.

[182] Filice, L., Ambrogio, G., and Micari, F., 2006. *On-Line Control of Single Point Incremental Forming Operations through Punch Force Monitoring.* CIRP Annals - Manufacturing Technology. **55(1)**: pp. 245-248.

[183] Attanasio, A., Ceretti, E., and Giardini, C., 2006. *Optimization of tool path in two points incremental forming.* Journal of Materials Processing Technology. **177(1-3)**: pp. 409-412.

[184] Attanasio, A., Ceretti, E., Giardini, C., and Mazzoni, L., 2008. *Asymmetric two points incremental forming: Improving surface quality and geometric accuracy by tool path optimization.* Journal of Materials Processing Technology. **197(1-3)**: pp. 59-67.

[185] Bambach, M., Cannamela, M., Azaouzi, M., Hirt, G., and Batoz, J.L., 2007. *Computer-aided tool path optimization for single point incremental sheet forming.* Advanced Methods in Material Forming. pp. 233-250.

[186] Oleksik, V., Bologa, O., Breaz, R., and Racz, G., 2008. *Comparison between the numerical simulations of incremental sheet forming and conventional stretch forming process.* International Journal of Material Forming. **1**: pp. 1187-1190.

[187] Duflou, J.R., Verbert, J., Belkassem, B., Gu, J., Sol, H., Henrard, C., and Habraken, A.M., 2008. *Process window enhancement for single point incremental forming through multi-step toolpaths.* CIRP Annals - Manufacturing Technology. **57(1)**: pp. 253-256.

[188] Verbert, J., Belkassem, B., Henrard, C., Habraken, A., Gu, J., Sol, H., Lauwers, B., and Duflou, J., 2008. *Multi-Step toolpath approach to overcome forming limitations in single point incremental forming.* International Journal of Material Forming. **1**: pp. 1203-1206.

[189] Skjoedt, M., Bay, N., Endelt, B., and Ingarao, G., 2008. *Multi Stage Strategies for Single Point Incremental Forming of a Cup.* International Journal of Material Forming. **1**: pp. 1199-1202.

[190] Bambach, M., Taleb Araghi, B., and Hirt, G., 2009. *Strategies to improve the geometric accuracy in asymmetric single point incremental forming.* Production Engineering. **3(2)**: pp. 145-156.

[191] Franzen, V., Kwiatkowski, L., Sebastiani, G., Shankar, R., Tekkaya, A., and Kleiner, M., 2008. *Dyna-Die: Towards Full Kinematic Incremental Forming.* International Journal of Material Forming. **1**: pp. 1163-1166.

[192] Duflou, J.R., Callebaut, B., Verbert, J., and De Baerdemaeker, H., 2007. *Laser Assisted Incremental Forming: Formability and Accuracy Improvement.* CIRP Annals - Manufacturing Technology. **56(1)**: pp. 273-276.

[193] Duflou, J.R., Callebaut, B., Verbert, J., and De Baerdemaeker, H., 2008. *Improved SPIF performance through dynamic local heating.* International Journal of Machine Tools and Manufacture. **48(5)**: pp. 543-549.

[194] Hino, R., Nagaishi, N., Yamamoto, Y., Naka, T., and Yoshida, F., 2010. *Incremental Forming with Local Heating for Aluminum-Magnesium Alloy Sheet.* Steel Research International. **81(9)**: pp. 946-949.

[195] Ghiotti, A. and Bruschi, S., 2010. *A Novel Experimental Set-Up for Warm Incremental Forming of AZ31B Magnesium Alloy Sheets.* Steel Research International. **81(9)**: pp. 950-953.

[196] Ambrogio, G., Cozza, V., Filice, L., and Micari, F., 2007. *An analytical model for improving precision in single point incremental forming.* Journal of Materials Processing Technology. **191(1-3)**: pp. 92-95.

[197] Filice, L., 2006. *A phenomenology-based approach for modelling material thinning and formability in incremental forming of cylindrical parts.* Proceedings of the Institution of Mechanical Engineers, Part B: Journal of Engineering Manufacture. **220(9)**: pp. 1449-1455.

[198] Ambrogio, G., De Napoli, L., and Filice, L., 2009. *A novel approach based on multiple back-drawing incremental forming to reduce geometry deviation.* International Journal of Material Forming. **2**: pp. 9-12.

[199] Kim, J., Kang, Y.H., Choi, H.H., Hwang, S.M., and Kang, B.S., 2002. *Comparison of Implicit and Explicit Finite-Element Methods for the Hydro-forming process of an Automobile Lower Arm* The International Journal of Advanced Manufacturing Technology. **20**: pp. 407-713.

[200] Wong, C.C., Dean, T.A., and Lin, J., 2004. *Incremental forming of solid cylindrical components using flow forming principles.* Journal of Materials Processing Technology. **153-154**: pp. 60-66.

[201] Plancak, M., Vilotic, D., and Vujovic, V., 1992. *Technology of Plasticity in Mechanical Engineering*. Second Ed. Novi Sad: University of Novi Sad, Faculty of Technical Science.

[202] Jurković, M., Jurković, Z., and Mahmić, M., 2006. *An Analysis and Modelling of Spinning Process without Wall-Thickness Reduction.* Metalurgija. **45(4)**: pp. 307-312.

[203] Akkus, N. and Kawahara, M., 2006. *An experimental and analytical study on dome forming of seamless Al tube by spinning process.* Journal of Materials Processing Technology. **173(2)**: pp. 145-150.

[204] Wang, L. and Long, H., 2011. *Investigation of material deformation in multi-pass conventional metal spinning.* Materials & Design. **32(5)**: pp. 2891-2899.

[205] Kleiner, M., Ewers, R., Kunert, J., Henkenjohann, N., and Auer, C., 2005. *Optimisation of the Shear Forming Process by Means of multivariate Statistical Methods*. In: Technical Report 23/2005, SFB475. Universität Dortmund, Germany.

[206] Robert, L., Richard, F., and James, L., 2003. *Statistical Design and Analysis of Experiments: with Applications to Engineering and Science*. Second Ed. Canada: John Wiley & sons, Inc.

[207] Lexian, H. and Dariani, B.M., 2009. *Effect of roller nose radius and release angle on the forming quality of a hot-spinning process using a non-linear finite element shell analysis.* Proceedings of the Institution of Mechanical Engineers, Part B: Journal of Engineering Manufacture. **223(6)**: pp. 713-722.

[208] Lind, D.A., Marchal, W.G., and Wathen, S.A., 2005. *Statistical Techniques in Business and Economics*. 12th Ed. Boston: McGraw Hill Irwin.

[209] Wang, L., Long, H., Ashley, D., Roberts, M., and White, P., 2010. *Analysis of single-pass conventional spinning by Taguchi and Finite Element methods.* Steel Research International. **81(9)**: pp. 974-977.

[210] Kawai, K., Yang, L.N., and Kudo, H., 2007. *A flexible shear spinning of axi-symmetrical shells with a general-purpose mandrel.* Journal of Materials Processing Technology. **192-193**: pp. 13-17.

[211] Eyckens, P., 2010. *Formability in Incremental Sheet Forming: Gneralization of the Marciniak-Kuczynski Model.* PhD Thesis, Department MTM, Faculty of Engineering, Katholieke Universiteit Leuven, Belgium.

[212] Bosetti, P. and Bruschi, S., 2010. *Some Remarks on Formability and Microstructural Features of Incrementally Formed Sheets as a Function of Geometrical Parameters.* Steel Research International. **81(9)**: pp. 914-917.

[213] Yamashita, M., Hattori, T., Yamada, K., and Nishimura, N., 2010. *Frictional Effect on Deformation Behavior in Incremental Sheet Forming.* Steel Research International. **81(9)**: pp. 926-929.

[214] Eyckens, P., Belkassem, B., Henrard, C., Gu, J., Sol, H., Habraken, A., Duflou, J., Van Bael, A., and Van Houtte, P., 2011. *Strain evolution in the single point incremental forming process: digital image correlation measurement and finite element prediction.* International Journal of Material Forming. **4(1)**: pp. 55-71.